

Hydrogen-bonding ferrocene derivatives for molecular recognition and organocatalysis

by

Michel-Franck Boissonnet



UNIVERSITY OF
BIRMINGHAM

A thesis submitted to

The University Of Birmingham

For the degree of

DOCTOR OF PHILOSOPHY

School Of Chemistry

College of Engineering and Physical Sciences

University of Birmingham

June 2015

UNIVERSITY OF
BIRMINGHAM

University of Birmingham Research Archive

e-theses repository

This unpublished thesis/dissertation is copyright of the author and/or third parties. The intellectual property rights of the author or third parties in respect of this work are as defined by The Copyright Designs and Patents Act 1988 or as modified by any successor legislation.

Any use made of information contained in this thesis/dissertation must be in accordance with that legislation and must be properly acknowledged. Further distribution or reproduction in any format is prohibited without the permission of the copyright holder.

Abstract

The study and applications of non-covalent interactions within an assembly of distinct molecules have attracted much attention over the past few decades. The energy range of these interactions such as hydrogen-bonding (H-bonding) makes them a subtle phenomenon to investigate. The aim of this project was to prepare novel ferrocene-based H-bonding receptors and to study them in the electrochemical sensing of neutral compounds and in organocatalysed transformations. The synthesis and characterisation of 2-ferrocenyl oxazoles via gold chemistry to access a new H-bonding motif for electrochemical sensing was successfully achieved. However the targeted structure bearing a secondary amine at the 4-position of the oxazole, was found to be highly unstable and unsuitable for sensing applications. Further studies on ferrocene-based H-bonding systems towards their application in asymmetric organocatalysis were also carried out. Different chiral and achiral ferrocene-(thio)ureas were prepared and tested in four organic reactions. Their performances in the Henry and in the Morita-Baylis-Hillman reactions gave acceptable yields but did not show significant enantioselectivities. A bi-functional ferrocene-thiourea was found to be effective in the enamine co-catalysed aldol reaction of acetone and *trans*- β -nitrostyrene, and in the double Michael cycloaddition of ω -nitropentenoate methyl and *trans*- β -nitrostyrene, leading to a tetrasubstituted cyclopentane. The H-bonding properties of the ferrocene-(thio)ureas with carboxylates was also studied by ^1H NMR spectroscopy. Finally, approaches towards the preparation of ferrocene-based boronate-ureas were investigated.

Table of Contents

Table of contents.....	i
Acknowledgements.....	v
List of abbreviations.....	vi
1. General introduction	1
1.1. Supramolecular chemistry / H-bonding.....	1
1.2. Types of HBD	2
1.3. Strategies for activating HBDs	4
1.4. Chiral Scaffolds	6
1.5. Organocatalysis: screened reactions	9
1.5.1. The Henry reaction	9
1.5.2. The Morita-Baylis-Hillman reaction.....	11
1.5.3. HBD / Enamine co-catalysis.....	13
1.5.4. Formation of tetrasubstituted cyclopentane.....	14
1.6. HBD for recognition purposes: ferrocene-containing sensors.....	17
1.7. Thesis outline.....	19
1.8. References.....	21
2. Ferrocenyl amino oxazoles as H-bonding receptors.....	25
2.1. Introduction.....	25
2.1.1. Oxazoles in weak interaction / coordination chemistry.....	25

2.1.2.	Project – Aims.....	26
2.1.3.	Preparation of oxazoles.....	28
2.2.	Results and discussion	30
2.2.1.	Synthesis of <i>N</i> -nosyl-protected ferrocene oxazole	30
2.2.2.	Electrochemistry	40
2.2.3.	Deprotection of 4- <i>N</i> -Nosylamine oxazole	44
2.3.	Conclusion and future work.....	50
2.4.	References.....	51
3.	Ferrocenyl-(thio)ureas as organocatalysts	53
3.1.	Introduction.....	53
3.1.1.	Ferrocene-containing organocatalysts	53
3.1.2.	Project - Design.....	55
3.2.	Results and discussion	56
3.2.1.	Synthesis	56
3.2.1.1.	Preparation of achiral ferrocenyl thiourea	56
3.2.1.2.	Preparation of achiral ferrocene-methylene thiourea	57
3.2.1.3.	Preparation of central chiral thiourea	57
3.2.1.4.	Preparation of planar chiral thiourea	59
3.2.1.5.	Preparation of bi-functional thiourea.....	62
3.2.2.	NMR studies	63
3.2.2.1.	Achiral and bi-functional Fc-(thio)urea.....	63

3.2.2.2.	H-bonding study by ¹ H-NMR spectroscopy.....	65
3.2.3.	Application of Fc-(thio)urea in organocatalysis	72
3.2.3.1.	The Henry reaction	72
3.2.3.2.	The MBH reaction	75
3.2.3.3.	HBD / Enamine catalysis.....	76
3.2.3.4.	Formation of tetrasubstituted cyclopentane.....	77
3.2.4.	Boron-containing Fc thiourea	83
3.2.4.1.	Preparation of 1-urea-2-boronate ferrocene	84
3.2.4.2.	Preparation of 1-methyleneurea-2-boronate ferrocene.....	88
3.2.4.3.	Synthesis of 1-methyleneurea-1'-boronate ferrocene.....	90
3.3.	Conclusions and future work	91
3.4.	References.....	93
4.	Experimental section.....	95
4.1.	General.....	95
4.2.	Synthesis	95
4.2.1.	Ferrocene Oxazoles.....	95
4.2.1.1.	Synthesis of Fc-oxazoles	95
4.2.1.2.	Synthesis of ylides	98
4.2.1.3.	Synthesis of ynamides	100
4.2.1.4.	Deprotection of nosyl	101
4.2.2.	Ferrocene (thio)ureas	103

4.2.2.1.	General procedure for preparation of (thio)urea.....	103
4.2.2.2.	Precursors for achiral ferrocene (thio)ureas	110
4.2.2.3.	Precursors central chiral ferrocene (thio)ureas.....	112
4.2.2.4.	Precursors for planar chiral ferrocene (thio)urea.....	117
4.2.2.5.	Precursors for the bi-functional ferrocene-thiourea.....	120
4.2.2.6.	Ferrocene Boronate-Urea	124
4.3.	Electrochemistry	134
4.4.	¹ H-NMR binding studies.....	134
4.5.	Procedures for Organocatalysis	135
4.5.1.	General procedure for the Henry Reaction	135
4.5.2.	General procedure for the Morita-Baylis-Hillman	135
4.5.3.	General procedure for the HBD/Enamine catalysis.....	136
4.5.4.	General procedure for the formation of tetrasubstituted cyclopentane.....	136
4.6.	References.....	139
	Appendix.....	140

Acknowledgements:

Acknowledgements go to my supervisors Prof. Jim Tucker and Dr. Paul Davies who accepted me in their groups and offered me advice, suggestions and encouragements during these four years. Past and present group members of the two groups are also to be acknowledged for their help, support and laughter, especially Holly, Pete, Antoine and Andrea. More generally other postgraduate students within the School Of Chemistry for the “social” side they maintained in my life: Carlotta, Chris, Manu, Mark, Jack, Alex, Yanouk, Miguel, Elli, and more... I would like to thank Dr. Neil Spencer for his work in the NMR facility and his help, Mr. Chi Tsang for his very much appreciated help with the HPLC, Mr Peter Ashton and Mr Nick May for the Mass Spectroscopy and Dr. Mateusz B. Pitak for the resolution of the crystal structures. The School Of Chemistry is acknowledged for the funding of my PhD. I am grateful for all the good people I met in Birmingham, who participated to the precious memories I will have from this period. Finally, I want to thank my friends and family from France, who supported me despite the distance. 27.

List of Abbreviations:

<i>A</i>	Electrode Surface Area (cm ²)
A	Hydrogen Bond Acceptor Atom
AcO	Acetate
app	Apparent
Ar	Aromatic
Bn	Benzyl
Boc	Butoxycarbamate
br s	Broad Singlet
Bu	Butyl
C	Concentration (mol.cm ⁻³)
CBS	Corey-Bakshi-Shibata Catalyst
Cp	Cyclopentadienyl
CV	Cyclic Voltammetry
δ	Chemical Shift (ppm)
d	Doublet
<i>D</i>	Diffusion Coefficient of Solution Species (cm ² .s ⁻¹)
D	Hydrogen Bond Donor Atom
DABCO	1,4-diazabicyclo[2.2.2]octane
DBU	Diazabicyclo[2.2.2]octane
DEAD	Diethyl Azodicarboxylate
DMAP	Dimethylaminopyridine
DMF	Dimethylformamide
DMSO	Dimethylsulfoxide
DNA	Deoxyribonucleic Acid

E	Potential (V)
ee	Enantiomeric Excess
EI	Electron Impact
E_{pa}	Anodic Potential (V)
E_{pc}	Cathodic Potential (V)
eq.	Molar Equivalent
ES	Electrospray
Fc	Ferrocene
HBD	Hydrogen Bond Donor
HBD / A	Hydrogen Bond Donor / Acceptor
HPLC	High Performance Liquid Chromatography
HR-MS	High Resolution Mass Spectroscopy
<i>i</i>	Intensity of current (A)
IPA	Isopropyl Alcohol
i_{pa}	Anodic Peak Current (A)
i_{pc}	Cathodic Peak Current (A)
IR	Infrared Spectroscopy
<i>J</i>	Coupling Constant (Hz)
<i>K</i>	Association constant
m	Multiplet
Me	Methyl
MeCN	Acetonitrile
mp	Melting Point
MS	Mass Spectroscopy
ν	Wave Number (cm^{-1})

ν	Scan Rate ($V.s^{-1}$)
n	Number of Electron
NMR	Nuclear Magnetic Resonance
Ph	Phenyl
pin	Pinacol
pK_a	Acidity Constant
ppm	Parts per Million
PTSA	<i>para</i> -Toluene Sulfonic Acid
q	Quadruplet
rt.	Room Temperature
s	Singlet
t	Triplet
TFA	Trifluoroacetic Acid
THF	Tetrahydrofuran
TLC	Thin Layer Chromatography
vs	Versus

1. General introduction

1.1. Supramolecular chemistry / H-bonding

Supramolecular chemistry is the study of well-defined and highly organised structures formed by non-covalently bound molecules. It involves weaker types of bonding arising from electrostatic interactions, such as hydrogen bonding (H-bonding), ion pairing (stronger in the solid state) or π -stacking, and hydrophobic interactions. Depending on the features of the bound molecules (polar groups, aromatic, alkyl chain, polarizability...) all of these interactions can play a role, with different intensities, and combine to offer new interactions (for example cation- and anion- π interactions, ion-dipole...).¹ An important concept of the supramolecular field is the specific affinity of a given host (receptor) towards its guest (substrate). The best illustration of the potential of these weak interactions is found in the evolution of Nature, which gave rise to the very fine utilisation of these dynamic interactions in biological systems. Early studies in supramolecular chemistry led Donald Cram (cancerands encaging Cl^- anion),² Jean-Marie Lehn and Charles Pedersen (polycyclic ethers chelating K^+ cation)³ to the Nobel Prize in 1987 "for their development and use of molecules with structure-specific interactions of high selectivity".⁴

H-bond interactions (Figure 1) have received much attention for their potential in binding strength and substrate recognition, due to their directionality and cooperativity.⁵

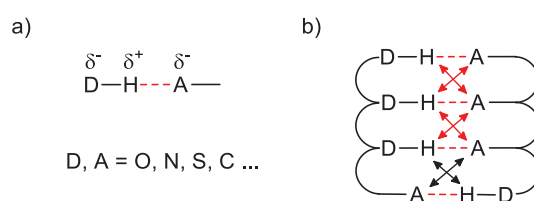


Figure 1: a) Hydrogen-bonding interaction between the electronegative donor D and acceptor A. b) Cooperativity of multiple H-bonds, and secondary interactions between adjacent H-bonds (attractive: red, repulsive: black)

A vast number of synthetic receptors, neutral or charged, have now been designed around simpler Hydrogen Bond Donor (HBD) units, among them amides, ureas, hydroxyl, amines and N-heterocycles (Figure 2).

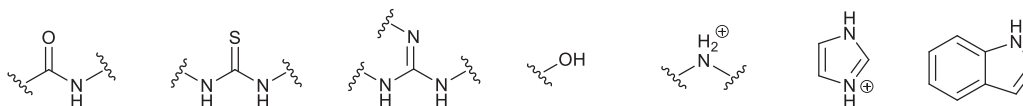


Figure 2: simple HBD

To be specific to a substrate, the different H-bonding sites of a receptor also need to be spatially localised, via their backbone, to adopt a complementary shape that optimises the binding affinity (lock and key model).⁶

1.2. Types of HBD

An important feature in H-bond assisted catalysis is primarily the type of Hydrogen Bond Donor (HBD), in which the number and the directionality of the H-bond(s) as well as the width between them can be tuned to ensure the best geometry for a given transformation. The focus of this discussion is on the most developed dual HBD, which possesses two anchoring points for the substrate(s). The most common strategy to access a polarised D-H bond (D = Donor) is the use of nitrogen as D, and to a lesser extent oxygen. Due to its trivalency, the geometry of the N-H bond can be more easily controlled than with divalent oxygen (in the case of O-H bonds). Among the different types of dual HBD, the earliest examples were made using urea or thiourea (Figure 3).

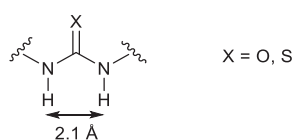


Figure 3: Model of (thio)urea

The potential for urea to selectively bind to a guest (nitro, phosphine oxide, ketone, aldehyde, ether) was discovered through solid-state studies.⁷ Soon after, this potential was successfully

applied in solution-state chemistry in the radical allylation of cyclic α -sulfinyl radicals.⁸ Since then the scope of (thio)urea catalysed transformations has widened immensely and tremendous levels of yield and enantio-selectivity have been achieved when used in organocatalysts.⁹

With a very similar structure, guanidine derivatives have also been investigated by Takemoto's group (Figure 4).¹⁰

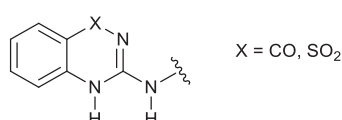


Figure 4: Guanidine derivatives

They offer access to more rigid HBD as it is possible to lock the conformation through covalent bonds linking the imine with one of the amine moieties. Furthermore, the substitution of the imine nitrogen by an electron withdrawing group (CO or SO₂) allows for further acidification of the hydrogens. These types of guanidine exhibit a slightly longer distance ($\approx + 0.2$ Å) between the two hydrogens.

From an understanding of the active sites of some enzymes, which exhibit ionic interactions, a new type of ionic HBD has emerged based on protonated pyridine.¹¹ Work by Takenaka and co-workers led to the preparation of dual HBD based on 2-aminopyridinium (Figure 5).¹²

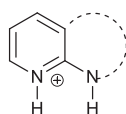


Figure 5: Model of 2-aminopyridinium

They developed a chiral version by merging their 2-aminopyridinium catalytic unit into the framework of helicenes.¹³

All the afore-mentioned HBD exhibit the same directionality regarding H-bond donation (parallel). A new class of dual HBD has been studied during the past decade, namely squaramide (Figure 6). Squaramides present a number of differences with thioureas: rigidity

(through more delocalisation possible), non-zero polar moment, distance between hydrogens (typically 2.7 Å) and a notably different directionality of the two H-bonding sites.

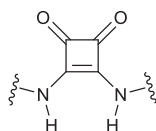


Figure 6: Model of squaramide

Squaramides have proven to be reliable and powerful dual HBD catalysts in many different transformations.¹⁴

As with ureas, sulfamides have been considered as potential HBD in organocatalysis after H-bonding interaction were first established in the solid state (Figure 7).¹⁵

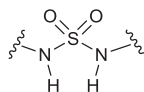


Figure 7: Model of sulfamide

Their NH protons are more acidic due to the higher electron-withdrawing effect of the sulfonyl group. The geometry of the sulfur atom, tetrahedral as opposed to the planar carbone sp^2 in (thio)ureas, also modifies the directionality of the H-bonds. Sulfamides have been successful catalysts in the addition of aldehydes and acetone to β -aryl-nitroethenes and (*E*)-methyl 2-oxo-4-phenylbut-3-enoate.¹⁶

1.3. Strategies for activating HBDs

Besides the geometry of the D-H bonds mainly addressed by the type of HBD (directionality, relative position), their strength has to be tuned to match the requirement of a particular transformation. Although factors other than pK_a are at play, it is generally the case that an increased acidity of the protons tends to have a beneficial effect on both selectivity and yield. pK_a values for simple neutral (thio)urea HBD can vary from 18.7 for diphenyl urea to 13.4 for diphenyl thiourea in DMSO.¹⁷ Due to the difference in p orbitals (2p in O and N, and 3p in S) overlapping with the carbon's 2p orbital, the character of the CO, CN and CS bonds (simple or

double) can be described through the predominance of one of the mesomeric forms (Scheme 1).



Scheme 1: Mesomeric forms of urea and thiourea. Predominant forms in red

From this it appears that the carbonyl/amine form of the urea and the iminium/thiolate form of the thiourea are the most favoured, explaining the greater acidity of the thiourea over urea.

Many strategies have been developed to enhance and modulate the pK_a , the earliest of them using electron-withdrawing phenyl substituents. In 2002, Schreiner and co-workers successfully used the 3,5-bis(CF_3)phenyl substituent (Figure 8),¹⁸ which proved to be a standard reference due to its reliability and efficiency in many cases.¹⁹

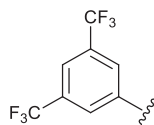


Figure 8: Electron-withdrawing 3,5-bis(trifluoromethyl)phenyl substituent

The electron-withdrawing, hence acidifying, trifluoromethyl groups can also help to maintain a stabilised conformation of the catalyst by introducing more H-bonds into the system (Figure 9).²⁰

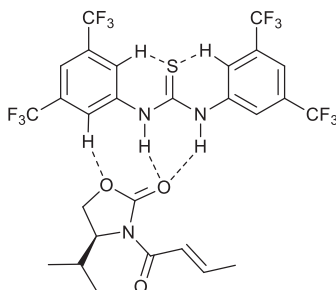
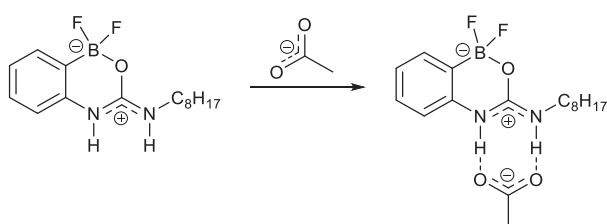


Figure 9: Example of substituent assistance, offering higher HBD acidity, planarity, and substrate organisation

The acidity is increased by the electron-withdrawing character of the CF_3 groups which also induce intramolecular H-bonding between the *meta*-hydrogens (acting as a Lewis acid) and the sulfur (acting as a Lewis base). The concept of activation by Lewis acid was put forward by Smith and co-workers in 1996 with their work on boronate-urea receptors.²¹ They studied the binding to acetate in DMSO and calculated an equilibrium constant of $6 \times 10^4 \text{ M}^{-1}$ compared to $4 \times 10^2 \text{ M}^{-1}$ for the corresponding phenyl analogue (Scheme 2).



Scheme 2: Difluoroboronate enhancing the H-bonding strength

This elegant difluoroboronate-urea strategy has been successfully employed in the activation of nitrocyclopropane ester and α -nitrodiazo esters, and in the enantioselective addition of indoles to nitrostyrene.²² Sulfoxides have also been incorporated into the design of HBD as they provide a convenient acidifying effect, decreasing the $\text{p}K_{\text{a}}$ by 2 – 3 units compared to the 3,5-bis(CF_3)phenyl substituted equivalent, and at the same time, giving the opportunity to add a chiral element to the structure (Figure 10).²³

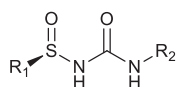
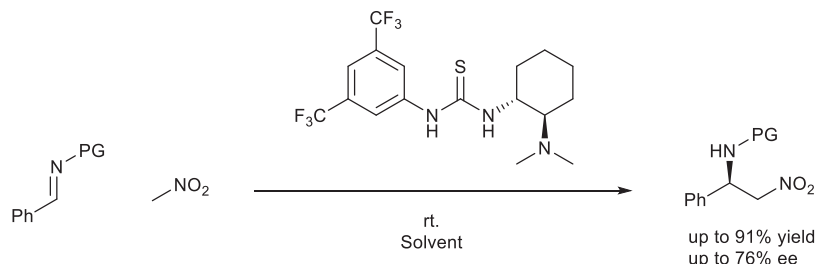


Figure 10: Sulfoxide activating substituent bringing chirality

1.4. Chiral Scaffolds

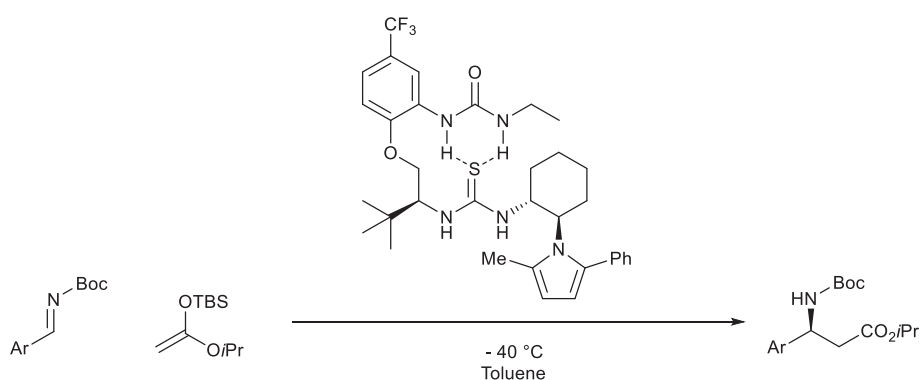
As discussed above, sulfoxides are a chiral acidifying substituents and offer a good opportunity for enantioselectivity.²⁴ Incorporated a decade earlier, the 1,2-*trans*-substituted cyclohexane scaffold gave the highly enantioselective hydrocyanation of *N*-allyl or *N*-benzyl aldimines,²⁵

ketoimines,²⁶ and Mannich reactions.²⁷ The Takemoto group designed a bi-functional catalyst featuring a HBD thiourea moiety and a tertiary amine linked by cyclohexyl (Scheme 3) capable of achieving the aza-Henry reaction with good enantiomeric ratios.²⁸



Scheme 3: 1,2-*trans*-substituted cyclohexane scaffold in the aza-Henry reaction

Notably, a recent study showed the presence of four different conformers in solution, which exhibited deactivating inter- or intra-molecular H-bonding interactions.²⁹ The active conformation happened to be the least populated conformation. Smith and co-workers addressed this issue with the efficient design of the catalyst depicted in Scheme 4.³⁰ Their work on non-peptidic reverse turn linkers allowed them to elaborate a highly populated state of pre-organised active conformations.³¹ This bio-mimetic structure gave astonishing results in terms of enantio-selectivity (>99% ee) and catalyst-loading (5% down to 0.1%) in the Mannich reaction between N-Boc aldimines and silyl ketene acetals.



Scheme 4: Flexible well-defined bi-functional catalyst for the Mannich reaction between N-Boc aldimines and silyl ketene acetals

Nature provides a myriad of available complex chiral molecules; one of them, cinchona, has attracted many researchers' attention. The cinchona-based skeleton (Figure 11) offers many

derivatisation options and as a consequence is now widely found in the literature regarding multifunctional HBD organocatalysis.³²

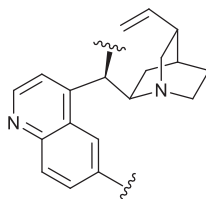


Figure 11: Model of cinchona

Cinchona-based catalysts also give an easy access to an array of different weak interactions: H-bonding (HBD), ionic interactions (protonated tertiary amine), π -stacking (quinoline) and hydrophobic (3-vinylquinuclidine).

More recently, paracyclophane-based catalysts have emerged as a new unexplored area that uses planar chirality (Figure 12).

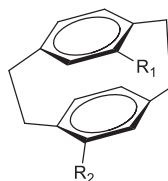


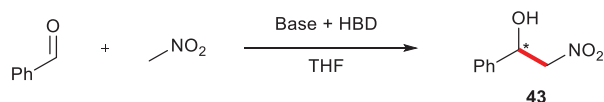
Figure 12: Model of paracyclophane

This simple scaffold was used in the thiourea (R_1 = thiourea, R_2 = OH) catalysed Friedel-Crafts alkylation of indole with nitro-styrene and the hydrogenation of nitro-olefins in moderate to good yields but low levels of enantioselectivity.³³ The aldol reaction of acetone with isatin mediated by a proline-thiourea paracyclophane catalyst (R_1 = thiourea, R_2 = *N*-Boc-prolinamido) was achieved with consistently good yields and moderate to good enantioselectivity.³⁴ Finally, Kitagaki and co-workers reported in 2013 the efficient bis-thiourea paracyclophane-catalysed Henry reaction of nitromethane and nitro-ethane with aromatic aldehydes.³⁵ Good enantiomeric excesses were obtained (typically more than 90%), confirming the potential of planar chirality in being investigated when designing new chiral HBD catalysts.

1.5. Organocatalysis: screened reactions

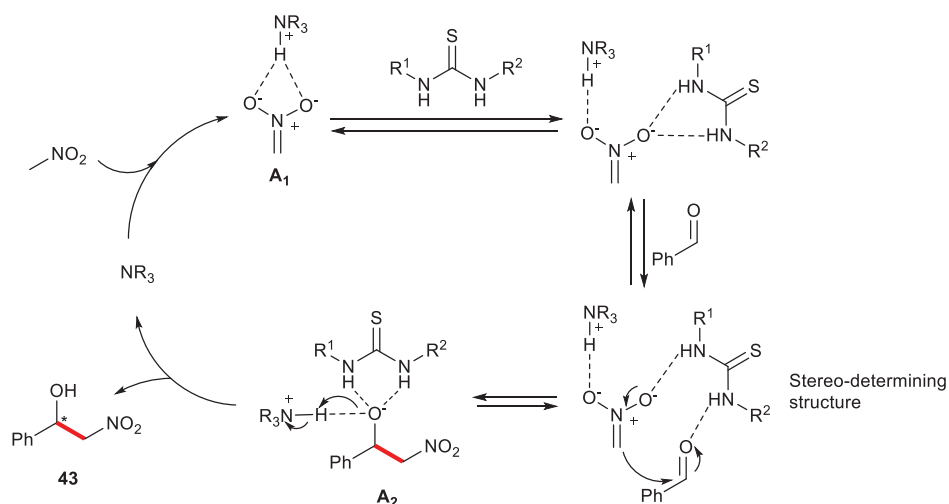
1.5.1. The Henry reaction

Discovered in 1895, the Henry reaction provides an efficient way of forming a C-C bond from nitroalkanes and aldehydes or ketones (Scheme 5).



Scheme 5: The Henry reaction catalysed by a base and a HBD

A sub-stoichiometric amount of base is required to deprotonate the α -proton of the nitroalkane, generating nitronate **A1** (Scheme 6). Nitronate **A1** is stabilised by H-bonding with the protonated base, and can also be further stabilised by the HBD (thiourea in Scheme 6). Upon approaching of the aldehyde, the weakest H-bond between nitronate **A1** and the thiourea breaks to allow for the aldehyde to bind to the thiourea.³⁶ If the conformation of the resulting structure is constrained (low degree of freedom) then the relative position of the nitronate and the aldehyde remains constant, which consequently sets the stereo-outcome of the reaction. Subsequent nucleophilic attack of nitronate **A1** onto the activated carbonyl leads to β -nitro alcoholate **A2** which gives the Henry product **43** upon reprotonation.



Scheme 6: General mechanism for the HDB catalysed Henry reaction

Among the most efficient organocatalysts for the Henry reaction, a bi-functional tertiary amine-thiourea derived from cinchona gave high yields and enantioselectivities (typically 90% ee) with a variety of aromatic aldehydes (Figure 13).³⁷

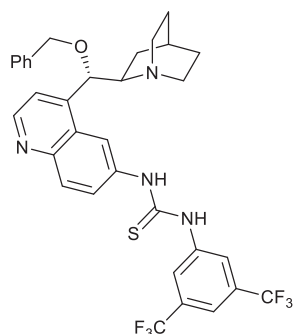
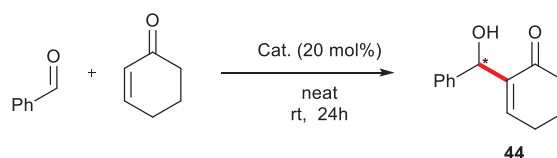


Figure 13: Highly stereoselective organocatalyst for the Henry reaction of aromatic aldehydes and nitromethane

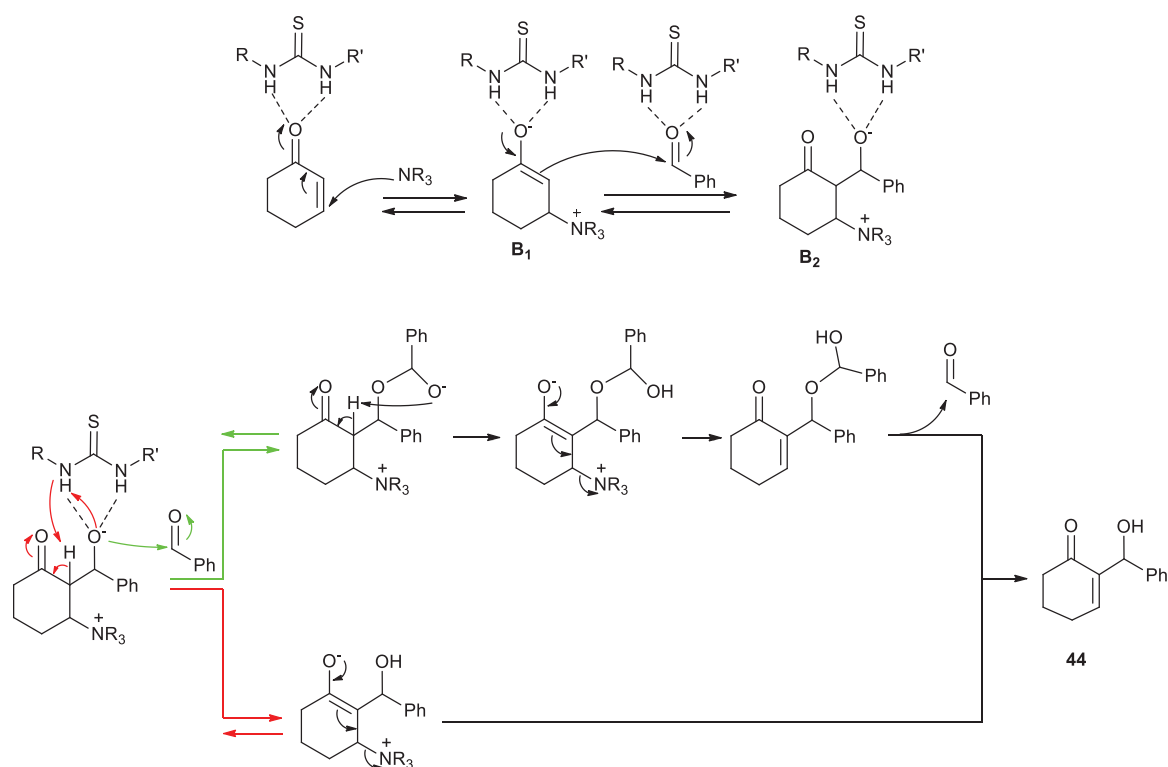
1.5.2. The Morita-Baylis-Hillman reaction

The Morita-Baylis-Hillman (MBH) reaction is another powerful C-C bond forming process between a Michael acceptor and an aldehyde or ketone, catalysed by a tertiary amine (Scheme 7).



Scheme 7: The Morita-Baylis-Hillman reaction between benzaldehyde and cyclohexen-1-one

The general accepted mechanism of the HBD assisted MBH reaction between cyclohexenone and benzaldehyde involves the aza-Michael addition of the tertiary amine onto the enone to form zwitterion **B₁** which can be stabilised by the HBD (Scheme 8).³⁸ The HBD activated aldehyde is then attacked by **B₁** to give the aldol adduct **B₂**. It is still under debate whether the proton-transfer conducting to product **44** is initiated by a proton source (HBD in this case, red arrow) or involves the *O*-addition to another molecule of aldehyde (green arrow) followed by a six-membered conformation able to ensure the proton-transfer.³⁹



Scheme 8: General mechanism for the HDB catalysed MBH reaction

The stereo-determining step is the attack of **B₁** onto the aldehyde. Consequently, their approach towards each other must be organised to achieve any enantioselectivity. The first example of bi-functional (hydroxyl HBD / tertiary amine) cinchona-based catalysts (Figure 14) was reported in 1999 for the reaction of various aromatic and aliphatic aldehydes with the very reactive 1,1,1,3,3,3-hexafluoroisopropyl-acrylate.⁴⁰ Enantiomeric excesses as high as 99% were observed.

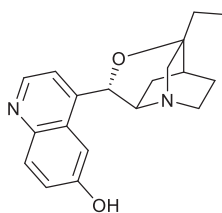
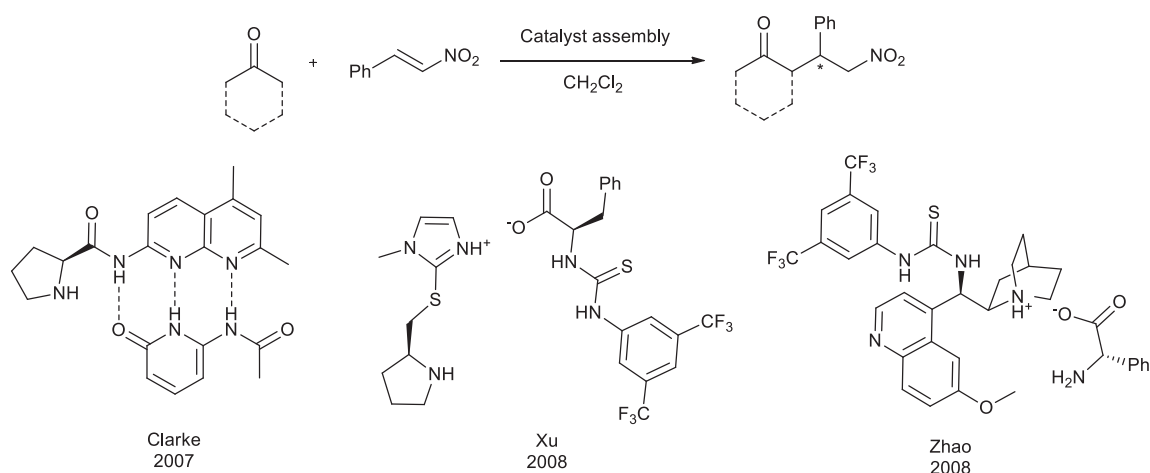


Figure 14: Efficient organocatalyst in the asymmetric MBH reaction

1.5.3. HBD / Enamine co-catalysis

The organocatalysed enamine type reaction of ketones with nitroolefins was described in 2001 with *L*-proline.⁴¹ Despite the very good yields obtained, the transformation suffered from a lack of enantioselectivity, reaching 7% ee for the reaction between acetone and *trans*- β -nitrostyrene. In 2007, Clarke and co-worker reported a new approach for this reaction by creating a multi-component catalytic system that self-assembles through H-bonding (Scheme 9), giving 67% ee with cyclohexanone and *trans*- β -nitrostyrene.⁴²



Scheme 9: Enamine/HBD organocatalysis via self-assembled catalysts

This catalytic system was developed with the desire to improve the enantioselectivity of the process by adding a bulky stereo-controlling element to the *L*-proline. To create an organised chiral environment and at the same time speed up the screening of catalysts, a non-covalent bond between the catalytic site and the stereo-controlling part of the catalysts was introduced. This non-covalent interaction can be hydrogen-bonding or ionic as reported in the more recent study carried out by Xu and co-workers in 2008.⁴³ They combined a phenylalanine (exhibiting a carboxylic acid functionality) derived thiourea with a modified proline bearing an imidazole thio-ether (exhibiting basic sp^2 nitrogen) in place of the original carboxylic acid moiety (Figure 15). They reported the efficient asymmetric conjugate addition of acetone to *trans*- β -

nitrostyrene (95% yield, 64% ee). The same year another study was published by Zhao and co-workers using an amino acid and a chiral tertiary amine bearing a thiourea unit (based on cinchona) to catalyse the same reaction.⁴⁴ The self-assembled catalytic system was held together by ionic interaction (acid/base) and achieved moderate to good enantio-selectivity, and an excellent 95% ee (*R* enantiomer) when *L*-phenylglycine was used in place of *L*-proline (Figure 15). The proposed mechanism involves the condensation of the ketone and the amino-acid catalyst forming the enamine intermediate as a first step. The nitroalkene then binds to the HBD enabling it to be attacked by the enamine. The authors suggested the following transition-state prior to C-C bond formation:

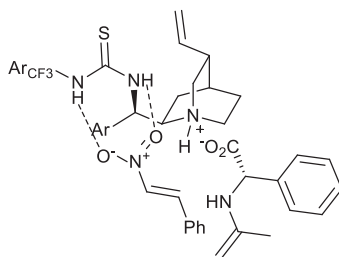
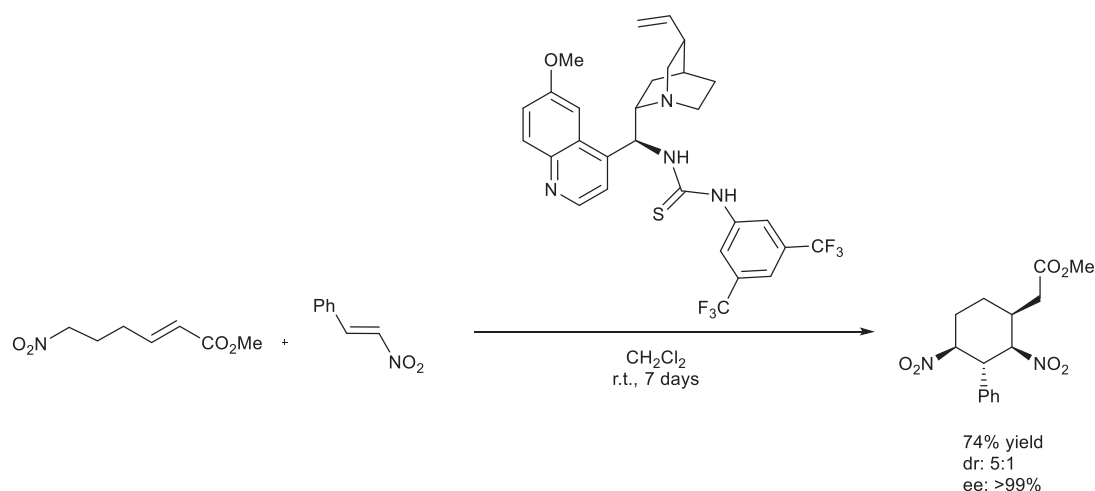


Figure 15: Transition state of nitrostyrene with an assembly of cinchona-based thiourea and *L*-phenylglycine

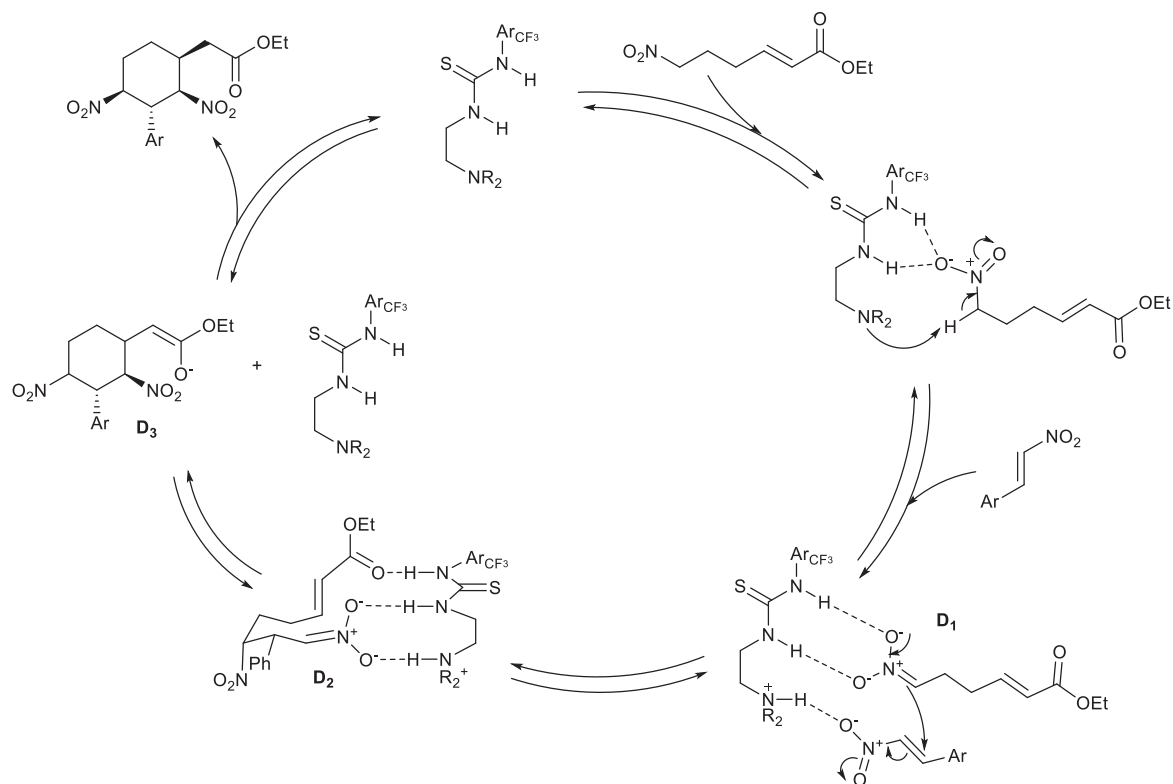
1.5.4. Formation of tetrasubstituted cyclopentane

The generation of a contiguous multi-stereocenter-containing cyclic product from achiral substrates is also possible using organocatalysis.⁴⁵ While proline derived catalysts have been widely employed to prepare optically active poly-substituted cyclohexanes and cyclopentane, the use of HBD catalysts remains largely unexplored.⁴⁶ Very recently Cobb and co-workers designed an asymmetric domino Michael-Michael reaction between ω -nitro-hexenoate and *trans*- β -nitrostyrene catalysed by a cinchona-based thiourea (Scheme 10).⁴⁷



Scheme 10: HBD catalysed cycloaddition of ω -nitro-hexenoate and *trans*- β -nitrostyrene by Cobb and co-workers

The reaction scope was explored by varying the substituent of the nitroalkene, including pentafluorophenyl, furan, thiofuran, and *para*-methyl, -methoxy, -fluoro and -chlorophenyl. All of these gave the corresponding cyclohexanes with high enantiomeric excess (from 87% to >99% ee). They noted that the enantiomeric excess was time-dependent and that the minor diastereoisomers were converted to the major diastereoisomer when subjected to the same reaction conditions, so the major diastereoisomer was the thermodynamic product. They proposed the mechanism depicted in Scheme 11.



Scheme 11: Proposed mechanism for the domino Michael-Michael reaction leading to thermodynamic cyclohexane product

The coordination of ω -nitro-hexenoate to the thiourea catalyst allows for the deprotonation in α - of the bound nitro group to form azinate **D1**. Upon binding of **D1** and *trans*- β -nitrostyrene to the catalyst, the stereocontrolled intermolecular nucleophilic attack takes place to give a second azinate **D2**. The subsequent cyclisation of **D2** gives four cyclohexane products **D3**. This is thought to be a fast process relative to the protonation of the azinate as no protonated **D2** was observed. The four diastereoisomers **D3** are then equilibrated to the most stable diastereoisomer. It is interesting to note that while the formation of cyclohexane was highly promoted, the cyclopentane analogue could not be produced with this catalyst.

1.6. HBD for recognition purposes: ferrocene-containing sensors

Due to its reliable redox properties, ferrocene has been incorporated into a number of supramolecular receptors that can sense the binding of a guest species due to a change in its oxidation potential (Fc/Fc^+).⁴⁸ Some examples of H-bonding systems containing urea and related motifs are here described. In 2002, Alonso and co-workers successfully detected the presence of submillimolar hydrogenphosphate anion using dendrimers of poly(propyleneimine) backbones and peripheral ferrocenyl-urea groups.⁴⁹ Similar work on ferrocenyl-ureas showed the selective binding to hydrogenphosphate or chloride (Figure 16).⁵⁰

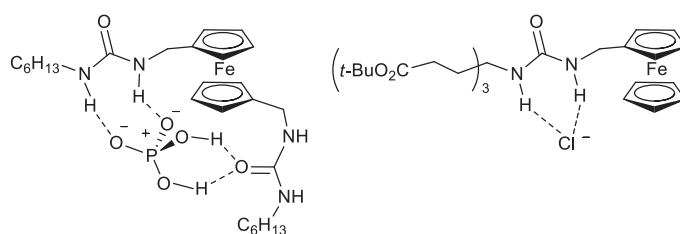


Figure 16: Electrochemical detection of H_2PO_4^- (left, $K = 1.2 \times 10^3 \text{ M}^{-1}$) and Cl^- (right, $K = 8.8 \times 10^2 \text{ M}^{-1}$)

Molina and co-workers added 18-crown-6 ether to the urea and found that only H_2PO_4^- formed a complex, over Cl^- , Br^- , HSO_4^- and NO_3^- .⁵¹ A slight change in the redox potential of the ferrocene was observed upon chelation of the potassium cation into the crown ether (Figure 17).

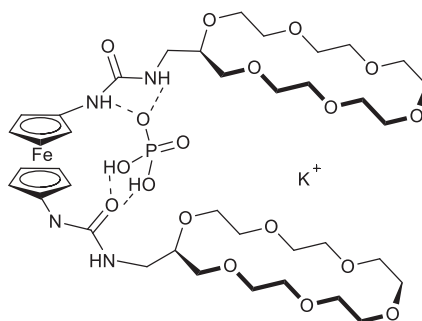


Figure 17: Ferrocenyl-urea crown ether for the electrochemical sensing of KH_2PO_4

A series of calixarene-containing ferrocenyl-ureas have been developed by Beer and co-workers (Figure 18), showing high affinity for benzoate and hydrogenphosphate anions ($K = 2.1$ and $1.1 \times 10^3 \text{ M}^{-1}$ respectively in CD_3CN at 293 K and 1.5 mM).⁵²

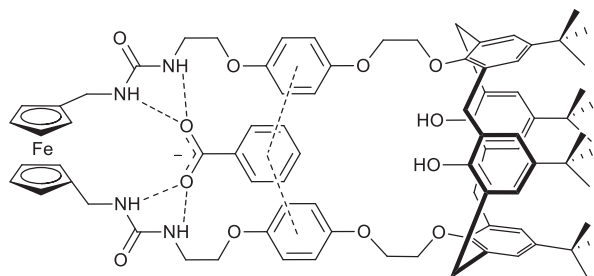


Figure 18: Calix[4]arene-containing ferrocenyl-urea for privileged hosting of benzoate anion

Neutral molecules have also been investigated as guests, such as barbital compounds. A 1,3-disubstituted ferrocene was prepared by Collinson and co-workers to selectively bind to neutral di-ethyl barbital, over ethylene urea and trimethylene urea, via six H-bonds (Figure 19).⁵³ The binding constant was established as $K = 3.2 \times 10^3 \text{ M}^{-1}$ in CDCl_3 at 5 mM at 293 K.

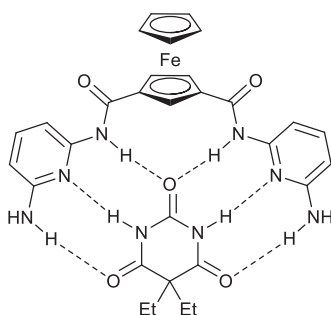


Figure 19: 1,3-di-substituted ferrocene receptor for the selective binding to barbital

In 2008, the Tucker group reported the efficient asymmetric preparation of chiral ferrocene ureas (Figure 20) and their electrochemical properties concerning the chiral recognition of carboxylate guests (tetrabutylammonium salts of 2-phenyl butyrate, mandelate and *N*-benzenesulfonyl proline).⁵⁴ The redox potential of the ferrocene moiety upon guest binding moved towards lower values. However the values were the same for each enantiomer of each guest used. Nevertheless a degree of enantioselectivity was observed in the recognition of the enantiomers of *N*-benzenesulfonyl proline guest ($K_{(S)} = 1778 \text{ M}^{-1}$, $K_{(R)} = 1071 \text{ M}^{-1}$).

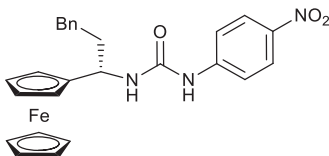


Figure 20: Chiral ferrocene-based urea receptor

Two years later, the same group published their work on the electrochemical determination of the enantiomeric excess of a mixture of (*R*)- and (*S*)-binol using a chiral ferrocene imine (Figure 21).⁵⁵ They found the binding constant with (*R*)-binol to be 19 times higher than with (*S*)-binol.

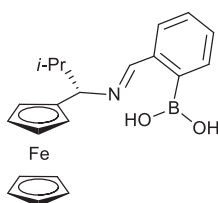


Figure 21: Chiral ferrocene-based boronic acid receptor

1.7. Thesis outline

This thesis concerns the study of supramolecular ferrocene systems for molecular recognition and organocatalysis.

Chapter 2 explores the feasibility of building new hydrogen bond donor / acceptor sensors based on the gold-catalysed formation of ferrocene oxazoles. The preparation of 2-ferrocenyl-4-*N*-sulfonamide-5-alkyloxazole via gold chemistry and their electrochemistry (cyclic voltammetry) are reported. Further deprotection of the sulfonamide to the corresponding secondary amine using a simpler model is also discussed. Finally, a number of X-ray structures are analysed.

Chapter 3 focuses on the application of ferrocene systems to the well-studied area of asymmetric catalysis using ureas and thioureas. A series of ferrocene-tethered (thio)urea

catalysts were prepared, containing either central or planar chirality, or both within a bifunctional catalyst. An NMR study of their hydrogen bonding properties is presented and their performances in selected asymmetric catalytic reactions are assessed. An evolution of their design and the resulting preparations are also described and discussed.

1.8. References

-
- ¹ a) H-J. Schneider, *Angew. Chem. Int. Ed.*, **2009**, *48*, 3924-3977; b) R. K. Castellano, F. Diederich, E. A. Meyer, *Angew. Chem. Int. Ed.*, **2003**, *42*, 1210-1250; c) S. Scheiner, *Acc. Chem. Res.*, **2013**, *46*, 280–288.
- ² a) D. J. Cram, K. D. Stewart, I. Goldberg, K. N. Trueblood, *J. Am. Chem. Soc.*, **1985**, *107*, 2574-2575; b) D. J. Cram, S. Karbach, Y. H. Kim, L. Baczynskyj, G. W. Kallemeyn, *J. Am. Chem. Soc.*, **1985**, *107*, 2575-2576.
- ³ a) J. M. Lehn, *Angew. Chem. Int. Ed. Engl.*, **1988**, *27*, 89-112; b) C. J. Pedersen, *J. Am. Chem. Soc.* **1967**, *89*, 7017-7036.
- ⁴ "The Nobel Prize in Chemistry 1987". *Nobelprize.org*. Nobel Media AB 2014.
- ⁵ L. J. Prins, D. N. Reinhoudt, P. Timmerman, *Angew. Chem. Int. Ed.*, **2001**, *40*, 2382-2426.
- ⁶ D. E. Koshland Jr., *Angew. Chem. Int. Ed. Engl.*, **1994**, *33*, 2375-2378.
- ⁷ M. C. Etter, Z. Urbańczyk-Lipkowska, M. Zia-Ebrahimi, T. W. Panunto, *J. Am. Chem. Soc.*, **1990**, *112*, 8415-8426.
- ⁸ D. P. Curran, L. H. Kuo, *J. Org. Chem.*, **1994**, *59*, 3259-3261.
- ⁹ a) Y. Takemoto, *Chem. Pharm. Bull.*, **2010**, *58*, 593-601; b) Z. Zhang, P. R. Schreiner, *Chem. Soc. Rev.*, **2009**, *38*, 1187-1198; c) Y. Takemoto, *Org. Biomol. Chem.*, **2008**, *3*, 4299-4306.
- ¹⁰ T. Inokuma, M. Furukawa, T. Uno, Y. Suzuki, K. Yoshida, Y. Yano, K. Matsuzaki, Y. Takemoto, *Chem. Eur. J.*, **2011**, *17*, 10470-10477.
- ¹¹ a) B. M. Nugent, R. A. Yoder, J. N. Johnston, *J. Am. Chem. Soc.*, **2004**, *126*, 3418-3419; b) A. Singh, R. A. Yoder, B. Shen, J. N. Johnston, *J. Am. Chem. Soc.*, **2007**, *129*, 3466-3467; c) A. Singh, J. N. Johnston, *J. Am. Chem. Soc.*, **2008**, *130*, 5866-5867; d) T. A. Davis, J. C. Wilt, J. N. Johnston, *J. Am. Chem. Soc.*, **2010**, *132*, 2880-2882; e) M. Ganesh, D. Seidel, *J. Am. Chem. Soc.*, **2008**, *130*, 16464-16465.
- ¹² N. Takenaka, R. S. Sarangthem, S. K. Seerla, *Org. Lett.*, **2007**, *9*, 2819-2822.
- ¹³ N. Takenaka, J. Chen, B. Captain, R. S. Sarangthem, A. Chandrakumar, *J. Am. Chem. Soc.*, **2010**, *132*, 4536-4537.
- ¹⁴ a) J. P. Malerich, K. Hagihara, V. H. Rawal, *J. Am. Chem. Soc.*, **2008**, *130*, 14416-14417; b) Y. Qian, G. Ma, A. Lv, H.-L. Zhu, J. Zhao, V. H. Rawal, *Chem. Commun.*, **2010**, *46*, 3004-3006; c) H. Konishi, T. Y. Lam, J. P. Malerich, V. H. Rawal, *Org. Lett.*, **2010**, *12*, 2028-2031; d) J. Alemán, A. Parra, H. Jiang, K. A. Jørgensen, *Chem. Eur. J.*, **2011**, *17*, 6890-6899.

- ¹⁵ a) B. Gong, C. Zheng, E. Skrzypczak-Jankun, Y. F. Yan, J. H. Zhang, *J. Am. Chem. Soc.*, **1998**, *120*, 11194-11195; b) B. Gong, C. Zheng, E. Skrzypczak-Jankun, J. Zhu, *Org. Lett.*, **2000**, *2*, 3273-3275.
- ¹⁶ X-J. Zhang, S-P. Liu, X-M. Li, M. Yan, A. S. C. Chan, *Chem. Commun.*, **2009**, 833-835; b) J-H. Lao, X-J. Zhang, J-J. Wang, X-M. Li, M. Yan, H-B. Luo, *Tetrahedron: Asymmetry*, **2009**, *20*, 2818-2822; c) S. Tortoioli, S. Bacchi, C. Tortoreto, J. B. Strachan, A. Perboni, *Tetrahedron Lett.*, **2012**, *53*, 1878-1881.
- ¹⁷ G. Jakab, C. Tancon, Z. Zhang, K. M. Lippert, P. R. Schreiner, *Org. Lett.*, **2012**, *14*, 1724-1727.
- ¹⁸ P. R. Schreiner, A. Wittkopp, *Org. Lett.*, **2002**, *4*, 217-220.
- ¹⁹ a) A. Wittkopp, P. R. Schreiner, *Chem. Eur. J.* **2003**, *9*, 407-414; b) T. Okino, Y. Hoashi, Y. Takemoto, *J. Am. Chem. Soc.*, **2003**, *125*, 12672-12673; c) T. Ooi, T. Miki, M. Taniguchi, M. Shiraishi, M. Takeuchi, K. Maruoka, *Angew. Chem. Int. Ed.*, **2003**, *42*, 3796-3798; d) Y. Sohtome, A. Tanatani, Y. Hashimoto, K. Nagasawa, *Tetrahedron Lett.*, **2004**, *45*, 5589-5592; e) R. P. Herrera, V. Sgarzani, L. Bernardi, A. Ricci, *Angew. Chem. Int. Ed.*, **2005**, *44*, 6576-6579; f) T. Honjo, S. Sano, M. Shiro, Y. Nagao, *Angew. Chem. Int. Ed.*, **2005**, *44*, 5838-5841; g) J. Wang, H. Li, X. Yu, L. Zu, W. Wang, *Org. Lett.*, **2005**, *7*, 4293-4296; h) B. Vakulya, S. Varga, A. Csámpai, T. Soós, *Org. Lett.*, **2005**, *7*, 1967-1969; i) Q. Lan, X. Wang, K. Maruoka, *Tetrahedron Lett.*, **2007**, *48*, 4675-4678; j) R. S. Klausen, E. N. Jacobsen, *Org. Lett.*, **2009**, *11*, 887-890; k) Z. Zhang, K. M. Lippert, H. Hausmann, M. Kotke, P. R. Schreiner, *J. Org. Chem.*, **2011**, *76*, 9764-9776.
- ²⁰ K. M. Lippert, K. Hof, D. Gerbig, D. Ley, H. Hausmann, S. Guenther, P. R. Schreiner, *Eur. J. Org. Chem.*, **2012**, 5919-5927.
- ²¹ a) M. P. Hughes, B. D. Smith, *J. Org. Chem.*, **1997**, *62*, 4402-4499; b) M. P. Hughes, M. Y. Shang, B. D. Smith, *J. Org. Chem.*, **1996**, *61*, 4510-4511.
- ²² a) S. S. So, J. A. Burkett, A. E. Mattson, *Org. Lett.* **2011**, *13*, 716-719; b) S. S. So, A. E. Mattson, *J. Am. Chem. Soc.*, **2012**, *14*, 8798-8801; c) S. S. So, T. J. Auvil, V. J. Garza, A. E. Mattson, *Org. Lett.*, **2011**, *13*, 444-447.
- ²³ M. T. Robak, M. Trincado, J. A. Ellman, *J. Am. Chem. Soc.*, **2007**, *129*, 15110-15111.
- ²⁴ K. L. Kimmel, M. T. Robak, J. A. Ellman, *J. Am. Chem. Soc.*, **2009**, *131*, 8754-8755.
- ²⁵ a) M. S. Sigman, E. N. Jacobsen, *J. Am. Chem. Soc.*, **1998**, *120*, 4901-4902; b) M. S. Sigman, P. Vachal, E. N. Jacobsen, *Angew. Chem., Int. Ed.*, **2000**, *39*, 1279-1281.
- ²⁶ P. Vachal, E. N. Jacobsen, *Org. Lett.*, **2000**, *2*, 867-870.
- ²⁷ A. G. Wenzel, E. N. Jacobsen, *J. Am. Chem. Soc.*, **2002**, *124*, 12964-12965.

- ²⁸ T. Okino, S. Nakamura, T. Furukawa, Y. Takemoto, *Org. Lett.*, **2004**, *6*, 625-627.
- ²⁹ G. Tárkányi, P. Király, T. Soós, S. Varga, *Chem. Eur. J.*, **2012**, *18*, 1918-1922.
- ³⁰ C. R. Jones, G. Dan Pantoş, A. J. Morrison, M. D. Smith, *Angew. Chem. Int. Ed.*, **2009**, *48*, 7391-7394.
- ³¹ C. R. Jones, M. K. N. Qureshi, F. R. Truscott, S-T. D. Hsu, *Angew. Chem. Int. Ed.*, **2008**, *47*, 7099-7102.
- ³² a) B. Vakulya, S. Varga, A. Csámpai, T. Soós, *Org. Lett.*, **2005**, *7*, 1967-1969; b) S. H. McCooney, S. J. Connon, *Angew. Chem. Int. Ed.*, **2005**, *44*, 6367-6370; c) A. Russo, G. Galdi, G. Croce, A. Lattanzi, *Chem. Eur. J.*, **2012**, *18*, 6152-6157; d) X-F. Huang, Y-F. Zhang, Z-H. Qi, N-K. Li, Z-C. Geng, K. Li, X-W. Wang, *Org. Biomol. Chem.*, **2014**, *12*, 4372-4385; e) Y. Arakawa, S. P. Fritz, H. Wennemers, *J. Org. Chem.*, **2014**, *79*, 3937-3945; f) G. Rassu, V. Zambrano, L. Pinna, C. Curti, L. Battistini, A. Sartori, G. Pelosi, G. Casiraghi, F. Zanardi, *Adv. Synth. Catal.*, **2014**, *356*, 2330-2336.
- ³³ J. F. Schneider, F. C. Falk, R. Fröhlich, J. Paradies, *Eur. J. Org. Chem.*, **2010**, 2265-2269.
- ³⁴ Y. Lu, Y. Ma, S. Yang, M. Ma, H. Chu, C. Song, *Tetrahedron : Asymmetry*, **2013**, *24*, 1082-1088.
- ³⁵ S. Kitagaki, T. Ueda, C. Mukai, *Chem. Commun.*, **2013**, *49*, 4030-4032.
- ³⁶ a) P. Hammar, T. Marcelli, H. Hiemstra, F. Himo, *Adv. Synth. Catal.*, **2007**, *349*, 2537-2548; b) M. Heshmat, A. Kazaryan, E. J. Baerends, *Phys. Chem. Chem. Phys.*, **2014**, *16*, 7315-7323.
- ³⁷ T. Marcelli, R. N. S. van der Haas, J. H. van Maarseveen, H. Hiemstra, *Angew. Chem. Int. Ed.*, **2006**, *45*, 929-931.
- ³⁸ Y. Wei, M. Shi, *Chem. Rev.*, **2013**, *113*, 6659-6690.
- ³⁹ a) K. E. Price, S. J. Broadwater, H. M. Jung, D. T. McQuade, *Org. Lett.*, **2005**, *7*, 147-150; b) K. E. Price, S. J. Broadwater, B. J. Walker, D. T. McQuade, *J. Org. Chem.*, **2005**, *70*, 3980-3987; c) V. K. Aggarwal, S. Y. Fulford, G. C. Lloyd-Jones, *Angew. Chem., Int. Ed.*, **2005**, *44*, 1706-1708; d) G. W. Amarante, H. M. S. Milagre, B. G. Vaz, B. R. Vilachã Ferreira, M. N. Eberlin, F. Coelho, *J. Org. Chem.* **2009**, *74*, 3031-3037.
- ⁴⁰ Y. Iwabuchi, M. Nakatani, N. Yokoyama, S. Hatakeyama, *J. Am. Chem. Soc.*, **1999**, *121*, 10219-10220.
- ⁴¹ B. List, P. Pojarliev, H. J. Martin, *Org. Lett.*, **2001**, *3*, 2423-2425.
- ⁴² M. L. Clarke, J. A. Fuentes, *Angew. Chem. Int. Ed.*, **2007**, *46*, 930-933.
- ⁴³ D-Q. Xu, H-D. Yue, S-P. Luo, A-B. Xia, S. Zhang, Z-Y. Xu, *Org. Biomol. Chem.*, **2008**, *6*, 2054-2057.
- ⁴⁴ T. Mandal, C-G. Zhao, *Angew. Chem. Int. Ed.*, **2008**, *47*, 7714-7717.

- ⁴⁵ a) E. Reyes, H. Jiang, A. Milelli, P. Elsner, R. G. Hazell, K. A. Jørgensen, *Angew. Chem. Int. Ed.*, **2007**, *46*, 9202-9205; b) Z-X. Jia, Y-C. Luo, X-N. Cheng, P-F. Xu, Y-C. Gu, *J. Org. Chem.*, **2013**, *78*, 6488-6494; c) S. Wang, Y. Zhang, G. Dong, S. Wu, K. Fang, Z. Li, Z. Miao, J. Yao, H. Li, J. Li, W. Zhang, W. Wang, C. Sheng, *Org. Lett.*, **2014**, *16*, 692-695.
- ⁴⁶ a) S. Gouedranche, W. Raimondi, X. Bugaut, T. Constantieux, D. Bonne, J. Rodriguez, *Synthesis*, **2013**, *45*, 1909-1930; b) X-F. Wang, J. An, X-X. Zhang, F. Tan, J-R. Chen, W-J. Xiao, *Org. Lett.*, **2011**, *13*, 808-811.
- ⁴⁷ S. Rajkumar, K. Shankland, G. D. Brown, A. J. A. Cobb, *Chem. Sci.*, **2012**, *3*, 584-588.
- ⁴⁸ J. H. R. Tucker, **2012**, Molecular redox sensors. *Supramolecular chemistry: from molecules to nanomaterials*. J.W. Steed and P.A. Gale (eds), page 2523 (John Wiley & Sons Ltd, Chichester, UK)"
- ⁴⁹ B. Alonso, C. M. Casado, I. Cuadrado, M. Morán, A. Kaifer, *Chem. Commun.*, **2002**, 1778-1779.
- ⁵⁰ M. D. Pratt, P. D. Beer, *Polyhedron*, **2003**, *22*, 649-653.
- ⁵¹ a) F. Oton, A. Tarraga, M. D. Velasco, P. Molina, *Dalton Trans.*, **2005**, 1159-1161; b) F. Otón, A. Tarraga, A. Espinosa, M. D. Velasco, P. Molina, *J. Chem. Soc. Dalton Trans.*, **2006**, 3685-3692.
- ⁵² N. H. Evans, C. J. Serpell, K. E. Christensen, P. D. Beer, *Eur. J. Inorg. Chem.*, **2012**, 939-944.
- ⁵³ S. R. Collinson, T. Gelbrich, M. B. Hursthouse, J. H. R. Tucker, *Chem. Commun.*, **2001**, 555-556.
- ⁵⁴ Willener, Y.; Joly, K. M.; Moody, C. J.; Tucker, J. H. R., *J. Org. Chem.*, **2008**, *73*, 1225-1233
- ⁵⁵ G. Mirri, S. D. Bull, P. N. Horton, T. D. James, L. Male, J. H. R. Tucker, *J. Am. Chem. Soc.*, **2010**, *132*, 8903-8905.

2. Ferrocenyl amino oxazoles as H-bonding receptors

2.1. Introduction

2.1.1. Oxazoles in weak interaction / coordination chemistry

Prior to the 1980's oxazoles were thought to be a type of heterocycle rarely encountered in biologically active compounds. Since then, a myriad of oxazole-containing molecules, such as Ulapualide A (Figure 22), have been discovered, their pharmaceutical properties have been studied (anti-tumour, anti-fungal, anti-bacterial, anti-malaria, anti-viral),⁵⁶ and synthetic methodologies have been developed towards their preparation.⁵⁷

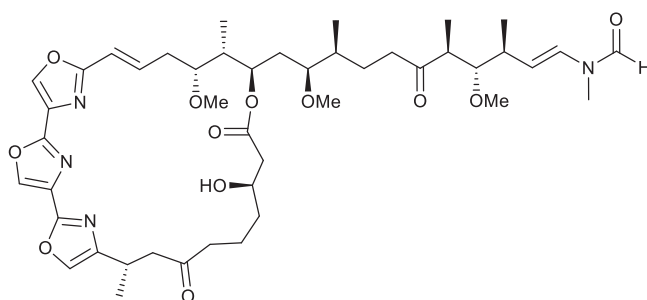


Figure 22: (-)-Ulapualide A extracted from *Hexabranhus sanguineus*, a nudibranch from the Indo-Pacific

Although the sp^2 nitrogen within the ring is a rather weak Lewis base, oxazoles may coordinate to a metal and form a complex. Hence, many oxazole-containing ligands have been designed and successfully incorporated in metallic complexes, of iridium,⁵⁸ copper,⁵⁹ zinc,⁶⁰ nickel,⁶¹ or palladium (Figure 23).⁶²

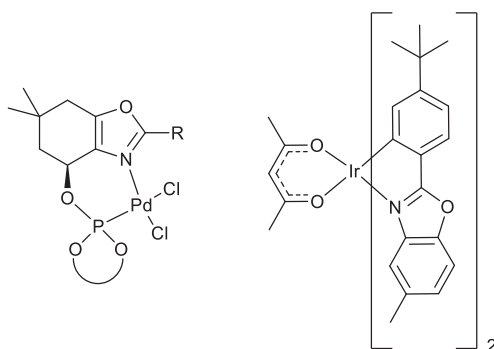


Figure 23: Oxazole ligands in palladium and iridium complexes

Furthermore, chiral polyoxazole macrocycles (tris-, hexa-, septa-oxazole, telomestatin) showed the ability to selectively bind to G-quadruplex DNA through weak interactions such as π -stacking and/or hydrogen bonding.⁶³

2.1.2. Project – Aims

Previous work in the Tucker group showed that amidopyridine ferrocene (Figure 24) binds to carboxylic acids through hydrogen-bonding interactions.⁶⁴ The electrochemical potential of the ferrocene unit was then shifted towards less positive values by *ca.* 20 mV upon addition of one equivalent of the neutral guest, allowing for the detection of aliphatic carboxylic acids.

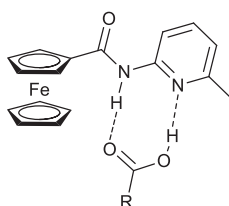
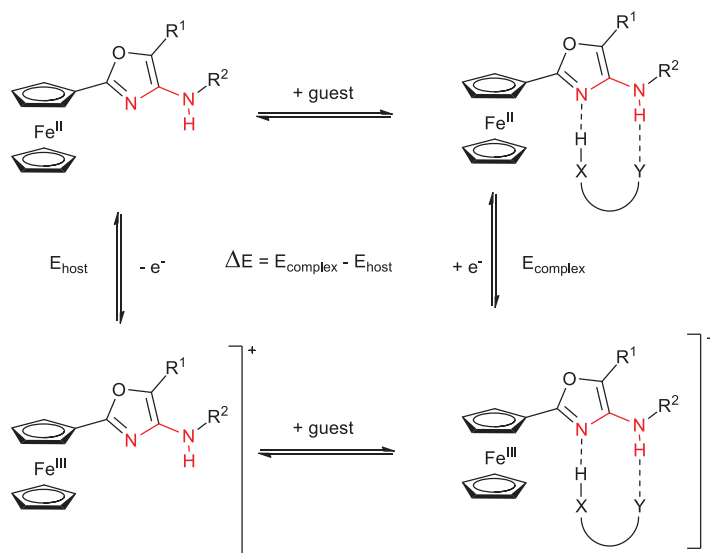


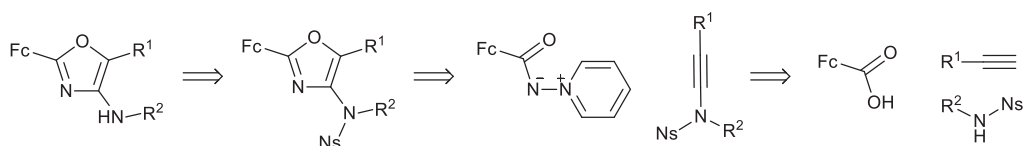
Figure 24: Amidopyridine ferrocene binding to carboxylic acid (R = alkyl)

The aim of the work presented here was to create a new oxazole-based motif for recognition of neutral guests and incorporate it within the ferrocene sensing unit (Scheme 12).



Scheme 12: 2-Ferrocenyl-4-aminoxazole for electrochemical recognition of a matching guest

This two-point motif was to be generated using gold chemistry developed in the Davies group;⁶⁵ via the addition of a pyridinium-*N*-aminide onto a nosyl-protected (4-nitrobenzylsulfonyl) ynamide to form a 4-*N*-trisubstituted oxazole and subsequent deprotection of the sulfonamide (Scheme 13).



Scheme 13: Retro-synthetic analysis of gold-mediated 4-*N*-substituted oxazole formation (Fc = Ferrocene)

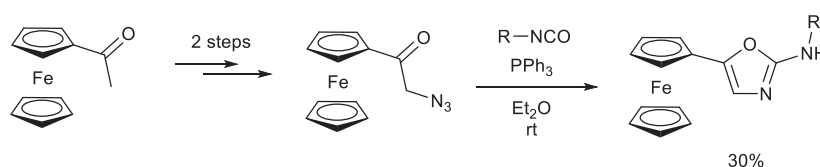
The resulting motif presents a hydrogen bond donor, as a secondary amine substituted to the 4-position of the oxazole ring, and a hydrogen bond acceptor, as the sp^2 nitrogen belonging to the oxazole ring. The tethering of a ferrocenyl unit on the 2-position of the oxazole would allow for sensing and reporting the presence (or absence) of a guest binding to the 4-amino oxazole moiety by electrochemical methods. This guest should possess a complementary H-bonding motif such as carboxylic acid for example. The redox potential of the ferrocenyl unit should change upon addition of a guest. Ideally, the change in potential would be dependent of the

specific detected guest. In addition, such an organometallic compound might be a candidate for drug discovery, as it is composed of the bio-interactive moieties oxazole and ferrocene.⁶⁶

2.1.3. Preparation of oxazoles

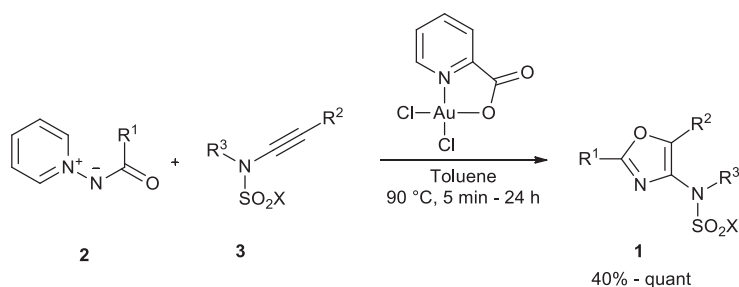
Numerous synthetic methods have been developed to build this heterocycle, offering milder and milder reaction conditions and increasing flexibility regarding to the substituent scope.⁶⁷ Multi-component reactions were designed to yield fully substituted oxazoles from readily available starting materials,⁶⁸ as well as metal free procedures using iodine,⁶⁹ hypervalent iodine,⁷⁰ brønsted acid catalysis,⁷¹ one-pot cyclisation/reduction of β -hydroxy amides.⁷² Investigations on metal-catalysed processes also provided many methodologies to achieve the formation of highly substituted oxazoles using, among others, propargylic alcohols,⁷³ propargylic amides,⁷⁴ α -diazocarbonyl compounds,⁷⁵ or alkynes.⁷⁶

In 1999, Tárraga and co-workers developed an aza-Wittig methodology to prepare the disubstituted 2-amino-5-ferrocenyloxazole from β -azido acetylferrocene (Scheme 14). They also reported its electrochemistry, which will be discussed later.⁷⁷



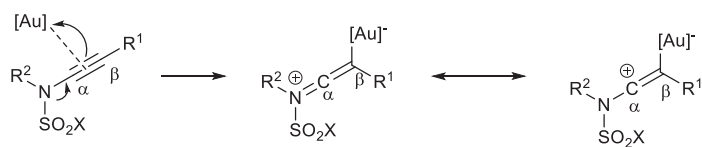
Scheme 14: Tárraga's synthesis of 2-amino-5-ferrocenyloxazole

In 2011 the Davies group reported the efficient gold (III) mediated formation of 4-aminoxazoles from ynamide and pyridinium-*N*-aminides, through a formal [3+2] dipolar cycloaddition (Scheme 15).⁶⁵



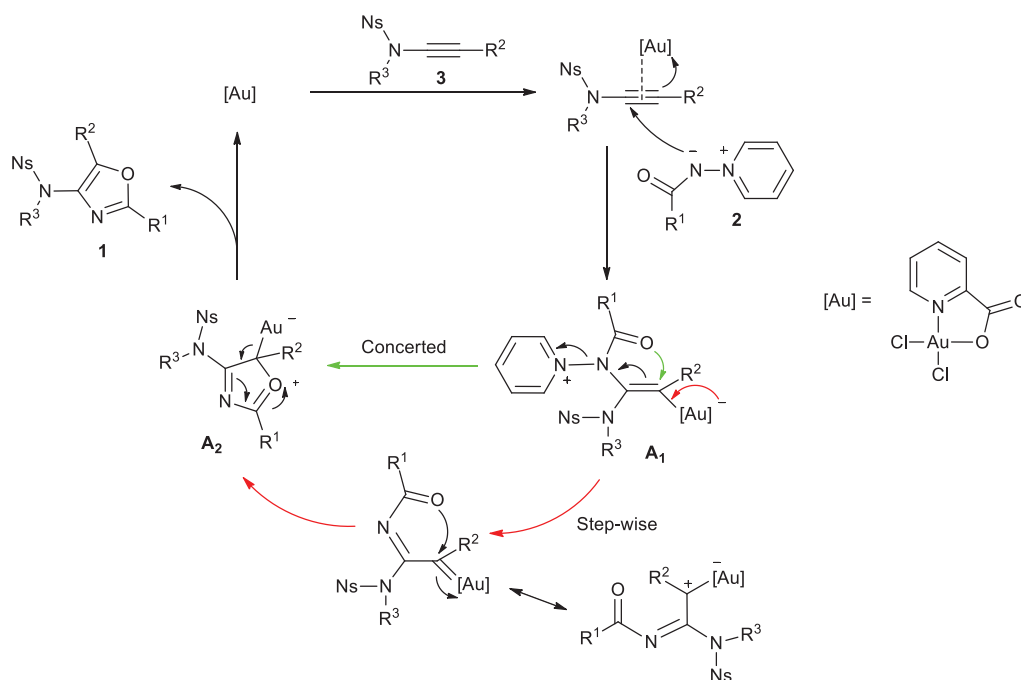
Scheme 15: Formal [3+2] cycloaddition of pyridine *N*-aminide onto ynamides catalysed by gold

The scope of this reaction allows for a wide variety of substituents at all positions, such as alkyl, allyl, aryl, halo-aryl, heterocycles, ethers or silyl alkynyl groups. In addition, the use of an ynamide instead of a simple alkyne ensures an exceedingly high level of chemo- and regio-selectivity, due to the increased electrophilicity centred on the α carbon of the triple bond (Scheme 16).⁷⁸



Scheme 16: Origin of the chemo- and regio-selectivity of nucleophilic attack onto activated ynamide

The proposed mechanism (Scheme 17) involves the coordination of gold(III) onto the triple bond of ynamide **3**, enhancing the electrophilic character on the carbon adjacent to the nitrogen. The aminide **2** then attacks the alkyne regioselectively forming intermediate **A1**. The next step can be the concerted cyclisation / loss of pyridine (green arrow) or the step-wise loss of pyridine then cyclisation (red arrow). Deauration of **A2** inducing aromatisation leads to the desired oxazole **1** and regeneration of the gold catalyst.



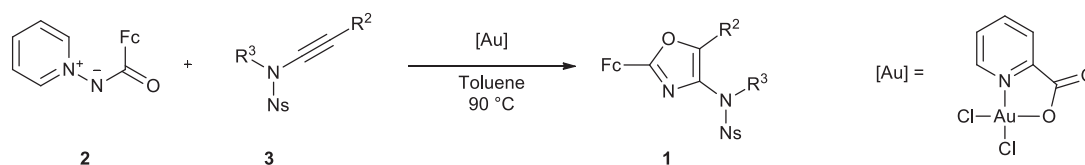
Scheme 17: Proposed mechanism for the gold mediated [3+2] dipolar cycloaddition of aminide **2** to ynamide **3**

To date, no organometallic oxazoles have been prepared via this route, and 2-ferrocenyl-4-*N*-aminoalkyl-5-alkyl or -aryl oxazoles have not been synthesised in general. The challenges here are to determine whether this structure **1**) can be made via a gold catalysed [3+2] dipolar cycloaddition / nosyl deprotection sequence, **2**) possesses the ability to engage in hydrogen bonding with selected partners, and **3**) can report the bound/unbound state of the ferrocene unit.

2.2. Results and discussion

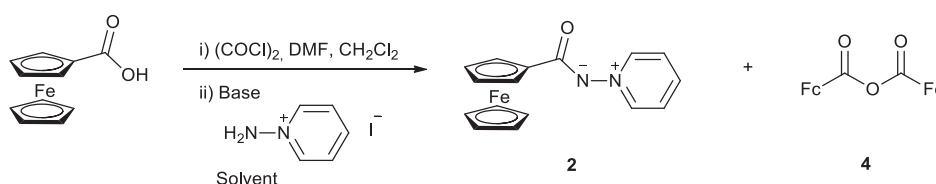
2.2.1. Synthesis of *N*-nosyl-protected ferrocene oxazole

Ferrocene oxazole **1** was to be prepared via gold-catalysed formal [3+2] dipolar cycloaddition of pyridinium ylide **2** and ynamide **3** in a regioselective fashion to offer the 4-*N*-(4-nitrobenzene)sulfonylamide ring substitution (Scheme 18).



Scheme 18: Gold-mediated formation of oxazole **1** (Fc = Ferrocene)

To achieve this, ylide **2** and ynamides **3** needed to be prepared. The ferrocene derived ylide **2** was synthesised from commercially available ferrocenecarboxylic acid, which was subjected to oxalyl chloride in dichloromethane to generate the acyl chloride, then to aminopyridinium iodide (Scheme 19).



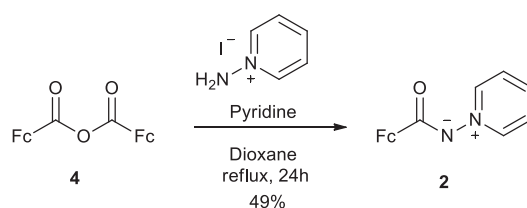
Scheme 19: Preparation of ylide **2**

Unlike its phenyl equivalent, ferrocene ylide **2** could not be successfully prepared in sodium hydroxide / water system (Table 1, Entry 1).⁶⁵ Switching to toluene as solvent, several bases were tried, potassium carbonate revealed to be the best choice ahead of cesium carbonate or pyridine (Table 1, Entry 2, 3 and 5). Although a good yield was obtained when triethylamine was used (Table 1, Entry 4), it could not be removed.

Entry	Solvent	Base	Temp (°C)	Yield 2	Yield 4
1	Water	NaOH	rt	12	0
2	Toluene	Pyridine	rt	9	50
3	Toluene	Pyridine	90	7	30
4	Toluene	Et ₃ N	rt	62 (a)	0
5	Toluene	K ₂ CO ₃	90	35	28
6	MeCN	K ₂ CO ₃	80	24	0
7	CH ₂ Cl ₂	K ₂ CO ₃	rt	65	0
8	CH ₂ Cl ₂	K ₂ CO ₃	40	60	0
9	CH ₂ Cl ₂	Cs ₂ CO ₃	rt	50	0

Table 1: Optimisation of the preparation of ylide **2**. Isolated yields (%). (a) NMR yield

A solvent study showed that dichloromethane was more suitable than toluene or acetonitrile (Table 1, Entry 5, 6 and 7). After 5 days at room temperature, the desired compound was obtained in 65% yield (Table 1, Entry 7). Increasing the temperature did not have a beneficial effect on the reaction outcome (Table 1, Entry 7 and 8). Up to half of the starting carboxylic acid self-condensed to give anhydride **4** when toluene was the solvent (Table 1, Entry 2). Conversion of **4** to the desired ylide **2** was achieved by reaction of aminopyridinium iodide in presence of pyridine (Scheme 20).



Scheme 20: Conversion of anhydride **4** into ylide **2**

Crystals of ylide **2** suitable for X-ray diffraction were obtained by slow evaporation of chloroform. They crystallised in a monoclinic system, along with water in a 1:1 ratio. The Cp rings of ferrocene were only 3° away from eclipsed. The dihedral angle between O1, C6, N2 and N1 was nil, indicating the full conjugation of the π orbital of the carbonyl with the p_z of the nitrogen. As shown in Figure 25 and 26, both of the hydrogen atoms of the water molecule participate in the resulting four member ring structure by H-bonding with the lone pairs of the oxygen of the carbonyl with a distance $d_{\text{H-O}} = 2.00 \text{ \AA}$ (Table 2).

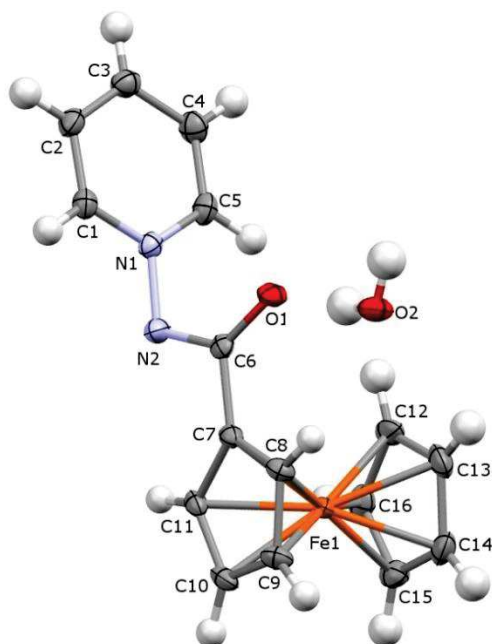


Figure 25: Crystallographic structures of ylide **2**, along with a molecule of water. Displacement ellipsoids – 50% probability. (Data collection and structure resolution by Dr. Mateusz B. Pitak)

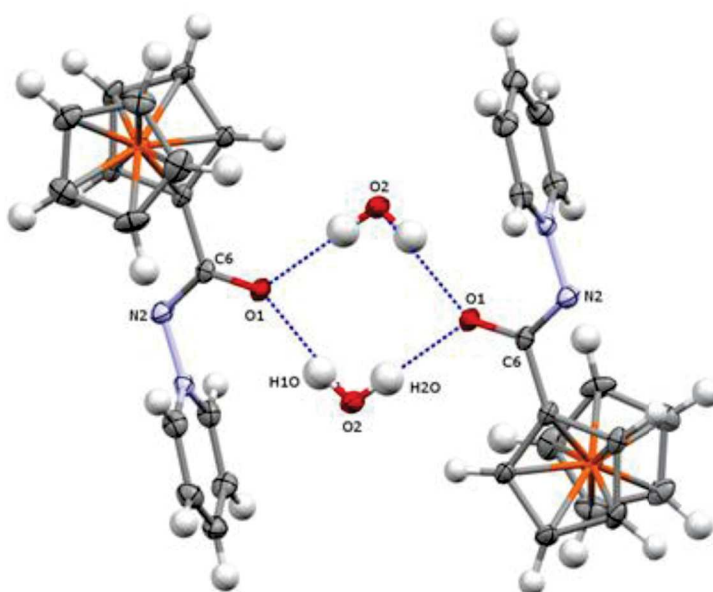


Figure 26: Hydrogen-bonds between water and the carbonyl of ylide **2** within the crystal structure. Displacement ellipsoids – 50% probability. (Data collection and structure resolution by Dr. Mateusz B. Pitak)

DHA	d(DH)	d(HA)	d(DA)	<(DHA)
O2–H10...O1 ⁱ	0.839(15)	1.998(17)	2.8171(16)	165(2)
O2–H20...O1	0.816(16)	2.001(16)	2.8174(16)	178(2)

Table 2: Distances and angles of Hydrogen bonds between ylide **2** and water (Å and °)

Each molecule of water is also engaged, by the oxygen atom this time, in 3 other hydrogen bonds which are almost orthogonal to each other (Figure 27). They involve the *para* hydrogen of the pyridinium moiety of a 2nd aminide molecule (distance $d_{O-H} = 2.52$ Å, Table 3, Entry 4), the *ortho* and *meta* hydrogens of the pyridinium moiety of a 3rd aminide molecule (distance $d_{O-H} = 2.31$ and 3.21 Å, Table 3, Entry 2 and 3 respectively) and the proton at the 2-position of the Cp ring of the 1st aminide bound (distance $d_{O-H} = 2.47$ Å, Table 3, Entry 5).

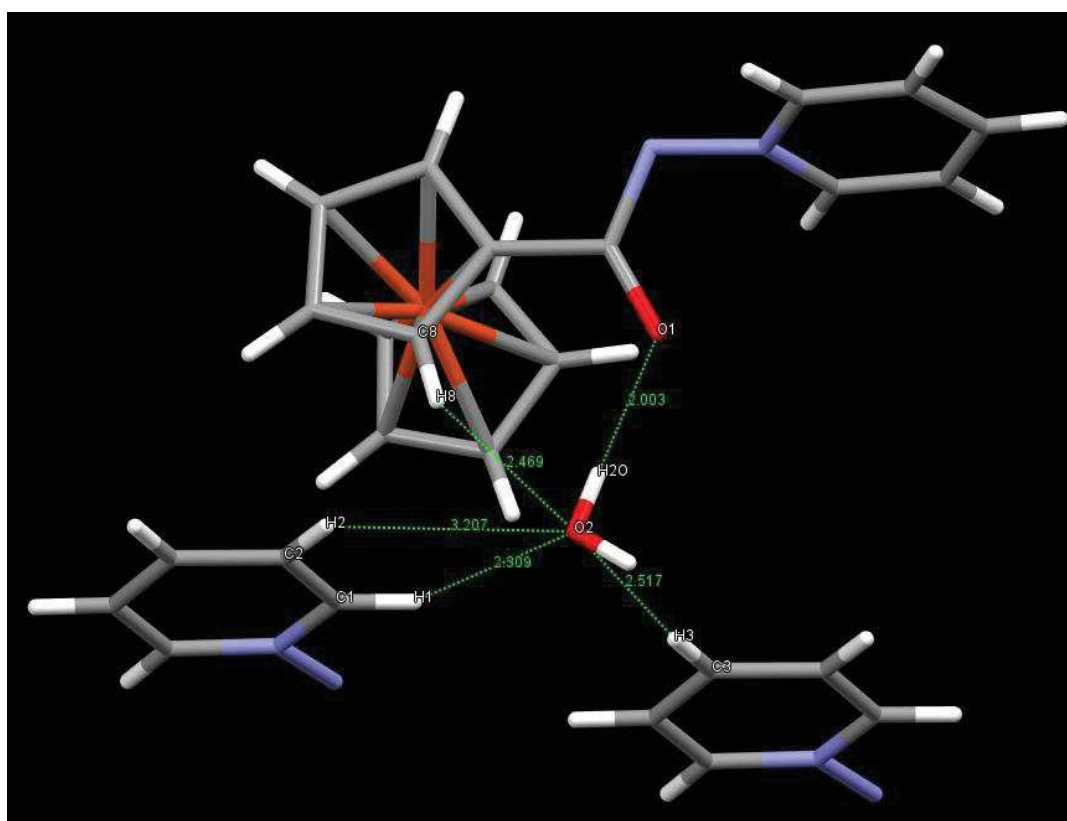
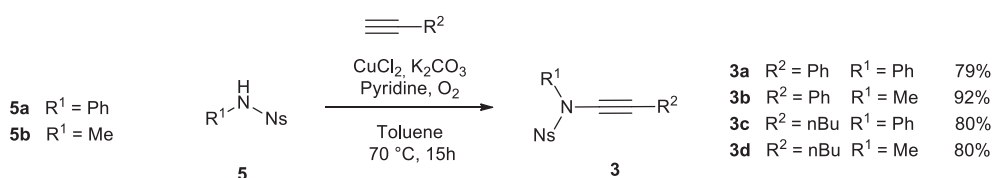


Figure 27: Crystallographic structure of ylide **2** exhibiting hydrogen bonds with molecules of water. (Some ferrocenyl units are omitted for clarity). (Data collection and structure resolution by Dr. Mateusz B. Pitak)

Entry	DHA	d(DHA)	d(HA)	d(DH)	<(DHA)
1	O1-H2O-O2	2,817	2,003	0,815	178
2	C1-H1-O2	3,446	2,309	0,951	147
3	C2-H2-O2	3,581	3,207	0,95	106
4	C3-H3-O2	3,458	2,517	0,95	171
5	C8-H8-O2	3,331	2,469	0,95	151

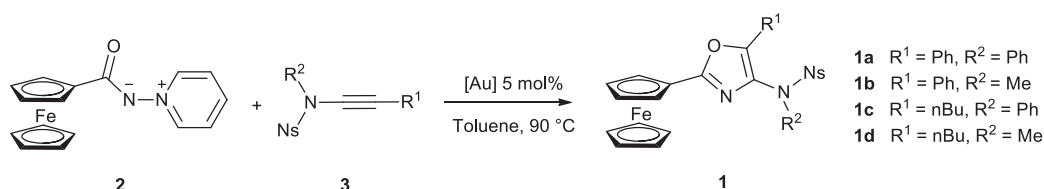
Table 3: Hydrogen bonds in the crystal structure of ylide **2** (Å and °, determined from the crystallographic data with the software Mercury 2.4)

In 2008, Stahl and co-workers reported the preparation of ynamides from different types of secondary amines: cyclic carbonates or carbamates, indoles and sulfonamides.⁷⁹ The latter was hoped to allow deprotection to give direct access to the desired secondary amine in the target oxazoles **1**. To offer the mildest deprotection conditions, *p*-nitrobenzenesulfonamide (nosyl, Ns) was chosen as it requires the least aggressive conditions to be removed.⁸⁰ Consequently ynamides **3** were prepared from the corresponding protected amine **5** reacted with the appropriate terminal alkyne in the presence of copper (II) chloride catalyst (Scheme 21: Copper-mediated oxidative coupling of protected amine **5** and terminal alkyne to form ynamides 3a-d). Good to high yields were obtained.



Scheme 21: Copper-mediated oxidative coupling of protected amine **5** and terminal alkyne to form ynamides 3a-d

With the ylide **2** and the ynamides **3** in hand, the formation of ferrocene oxazole **1** was catalysed by dichloro(pyridine-2-carboxylato)gold(III) ([Au]) in toluene at 90 °C (Scheme 22).



Scheme 22: Gold catalysed formation of oxazoles **1a-d**

Compound **1c** was obtained in 15% yield after one day, and in 51% when left for six days (Table 4, Entry 4 and 5). The bulkier 2-ferrocenyl-4-*N*-(*N*-phenyl)nosylamide-5-phenyloxazole **1a** required two days with 2.5 equivalents of ylide **2** to yield 46% of product (Table 4, Entry 1), and gave only 10% yield with 1.5 equivalents after 24 hours (Table 4, Entry 2). Compounds **1b** and **1d** gave 37% and 10% yields respectively (Table 4, Entry 3 and 6).

Entry	Compound	R ¹ , R ²	Time (d)	Yield
1	1a	Ph, Ph	2	46 ^a
2	1a	Ph, Ph	1	10
3	1b	Ph, Me	6	37 ^b
4	1c	<i>n</i> -Bu, Ph	1	15
5	1c	<i>n</i> -Bu, Ph	6	51
6	1d	<i>n</i> -Bu, Me	1	10

Table 4: Gold catalysed formation of oxazole with various substituents. Isolated yields (%).

Equivalents of ylide **2** used: 1.5 in all cases, except for a) 2.5 and b) 2

2-Phenyl-oxazole **6** was also synthesised (Figure 28) in a much greater yield (80%) from ynamide **3b** and *N*-benzoylpyridinium ylide to be used as a model in the deprotection step (see section 2.2.3).

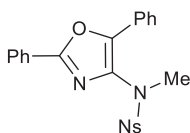


Figure 28: Phenyl oxazole **6**

Crystallographic structures of oxazole **1a** and **1c** were obtained (Figure 29 and Figure 30). The Cp rings of ferrocene were only 5° away from eclipsed for both **1a** and **1c**. The carbon substituted on the Cp (C21) ring was not in the Cp ring plane, with a dihedral angle (C21-C22-

C26-C25 in Figure 29 and C19-C20-C24-C23 in Figure 30) of 9.8° and 10.5° for **1a** and **1c** respectively. The oxazole ring plane and the connected Cp ring plane presented an interplanar angle of 15° and 17° for oxazole **1c** and **1a** respectively, where the oxazole ring tilts towards the un-substituted Cp ring. In both structures, the sulfonamido nitrogen atom was not conjugated with the oxazole.

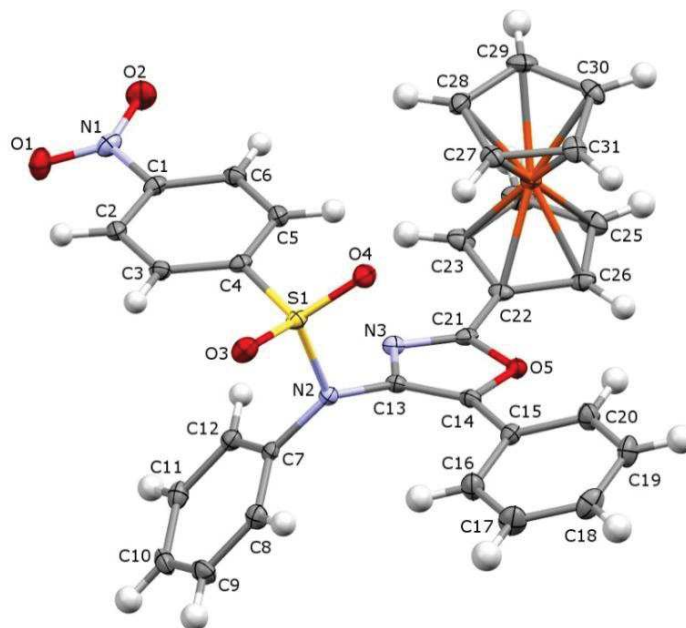


Figure 29: Crystallographic structures of oxazoles **1a**. Displacement ellipsoids – 50% probability.
(Data collection and structure resolution by Dr. Mateusz B. Pitak)

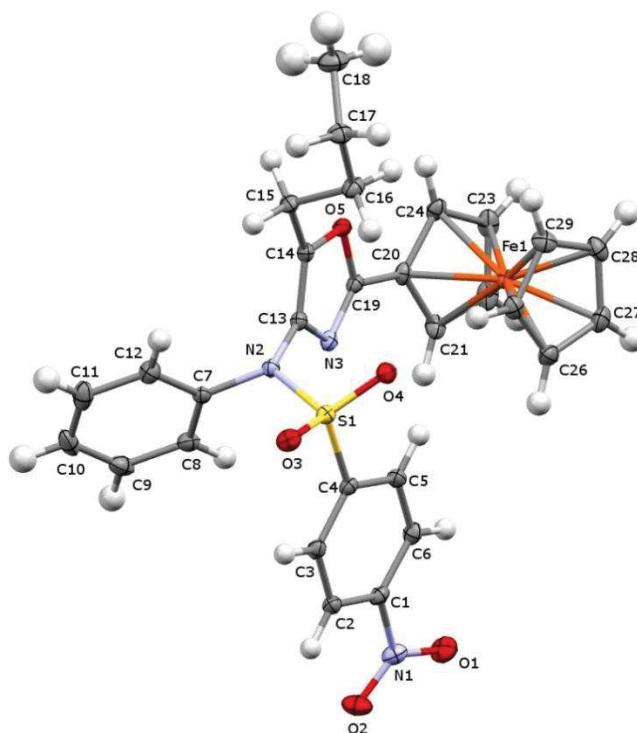


Figure 30: Crystallographic structures of oxazoles **1c**. Displacement ellipsoids – 50% probability.
(Data collection and structure resolution by Dr. Mateusz B. Pitak)

Hydrogen-bonding interactions exist between two *para*-nitrophenyl units, occurring between the oxygen of the first molecule (O1) and the *meta* hydrogen of the other molecule (C6-H) with a distance $d_{\text{CH}\cdots\text{O}}$ of 3.468 Å and 3.340 Å for oxazole **1a** and **1c** respectively (Figure 31).

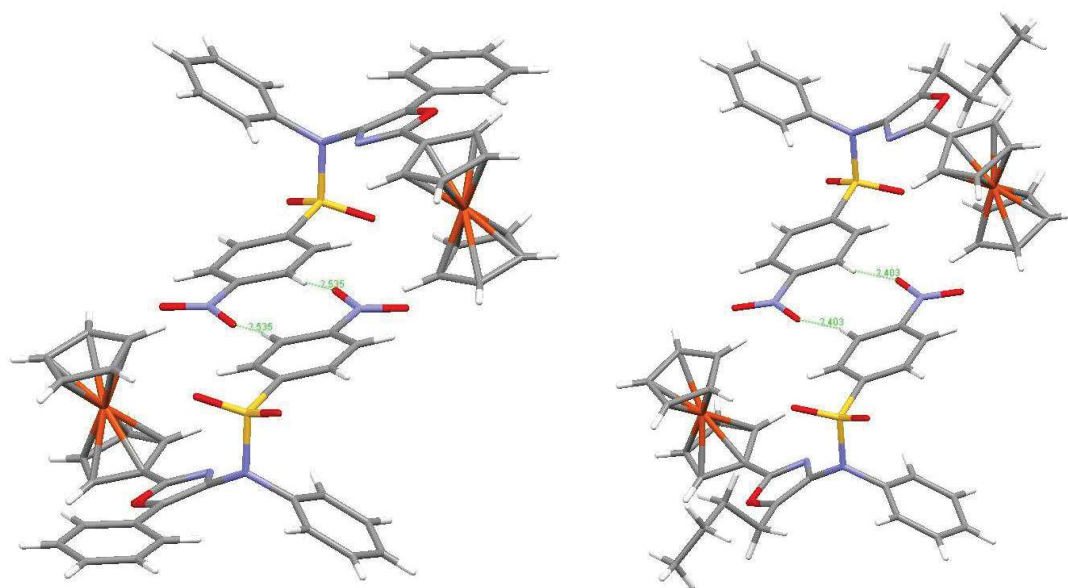


Figure 31: Intermolecular hydrogen bonding between 2 nitrophenyl moieties in **1a** ($d_{\text{H}\cdots\text{O}} = 2.53$ Å) and **1c** ($d_{\text{H}\cdots\text{O}} = 2.40$ Å). (Determined with the software Mercury 2.4. Data collection and structure resolution by Dr. Mateusz B. Pitak)

After the successful synthesis of this series of mono-oxazole ferrocenes, it was decided to investigate whether 1,1'-bisoxazole ferrocene could be made using this gold mediated procedure (Figure 32).

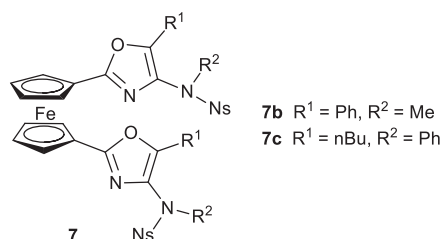
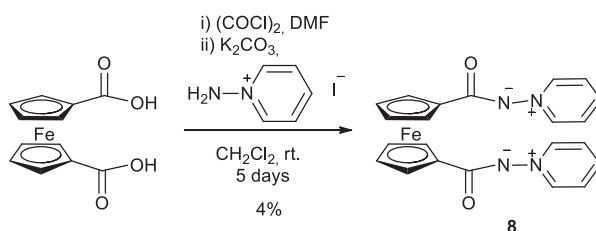


Figure 32: 1,1'-Bisoxazole ferrocene **7**

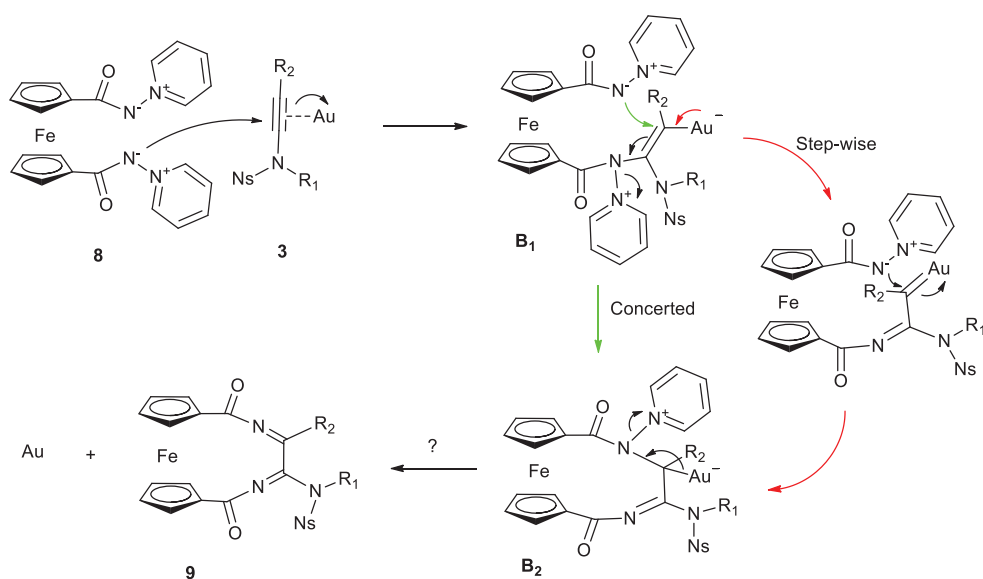
Following the described procedure, bis-ylide **8** was prepared from 1,1'-biscarboxylic acid ferrocene in an isolated yield of 4% (Scheme 23).



Scheme 23: Synthesis of 1,1'-bis-ylide ferrocene **8**

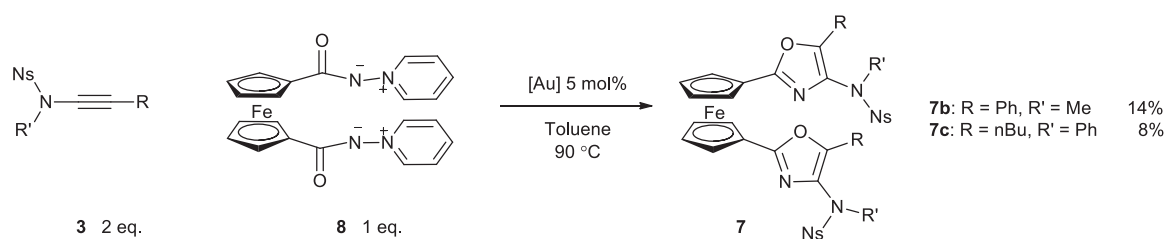
This compound was extremely polar and mostly remained on the silica phase during column chromatography, along with the unreacted deprotonated aminopyridinium, rendering the purification process rather difficult.

Compared to the case of mono-ylide **2**, the gold-catalysed cycloaddition of ynamide **3** onto bis-ylide **8** was a more challenging goal. The presence of two ylide moieties within the same molecule may generate a competitive reaction pathway. As shown in Scheme 24, the first nucleophilic attack of one aminide (giving **B₁**) would be followed by a second attack from the other aminide to form the macrocyclophane **B₂** (instead of the O-attack as described in section 2.1.3). Such a pathway may lead to compound **9**.



Scheme 24: Possible competitive reaction pathway with 1,1'-bis-aminide oxazole **8**

However analysis of the products revealed that the desired 1,1'-bis-oxazole ferrocene **7** could be formed during the reaction (Scheme 25). Bis-ylide **8** gave exclusively oxazoles **7b** and **7c** in 14% and 8% yields respectively, leaving most of the bis-ylide **8** unreacted.



Scheme 25: Gold-mediated formation of 1,1'-bisoxazole ferrocene **7**

2.2.2. Electrochemistry

Ferrocenyl oxazoles **1a-c** and ylide **2** (Figure 33) were analysed by cyclic voltammetry (Figure 34 and Figure 35 respectively) and each gave a reversible one-electron redox process (0.3 mM in dry dichloromethane, supporting electrolyte: tetrabutylammonium hexafluorophosphate 0.1 M, decamethylferrocene (dmfc) as internal reference reference).⁸¹

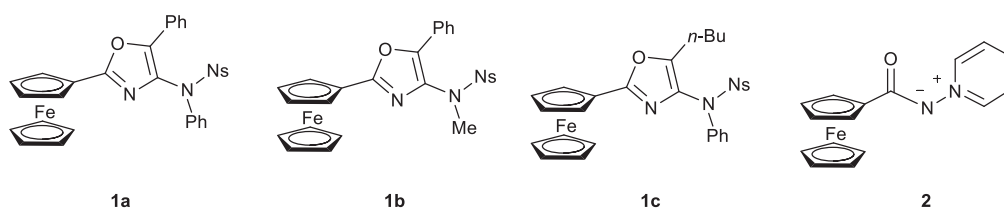


Figure 33: Compounds studied by electrochemistry

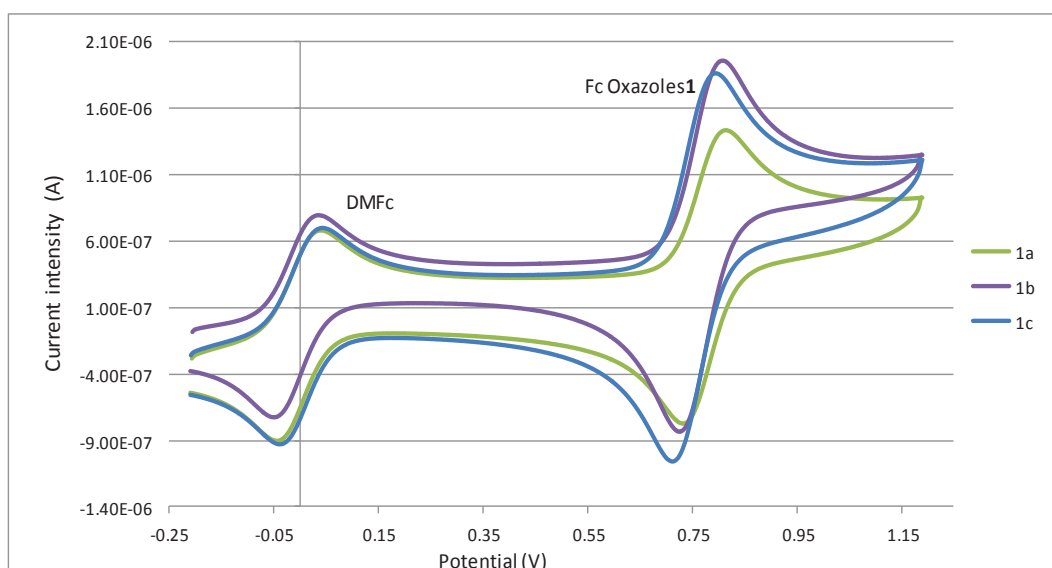


Figure 34: Cyclic voltammogram for 1a, 1b and 1c, potentials vs dmfc at 0.1 V.s⁻¹

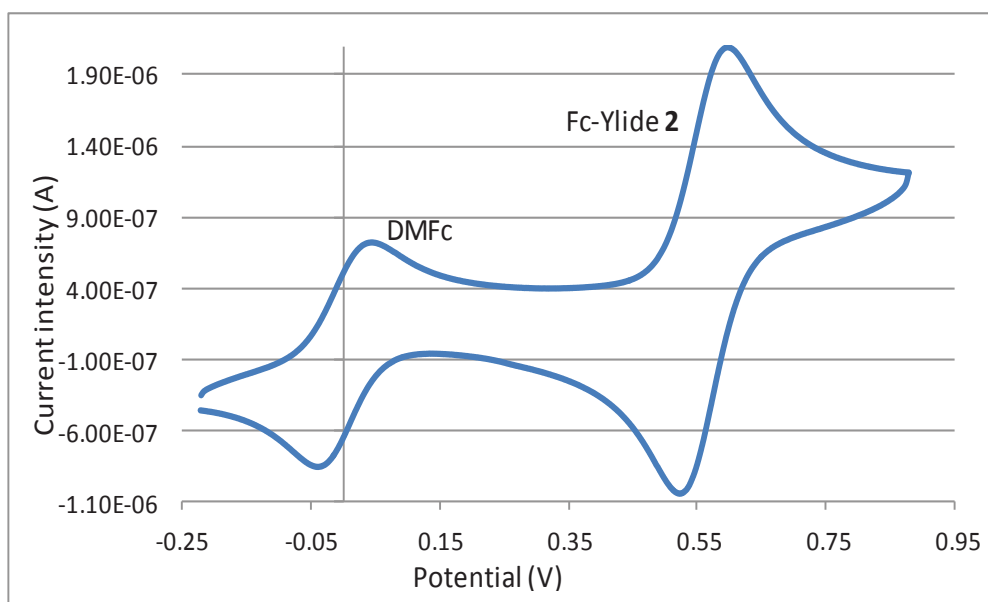


Figure 35: Cyclic voltammogram for 2. Potentials vs dmfc at 0.1 V.s⁻¹

The reversibility of these redox processes can be assessed by considering the Randles-Sevcik equation, which expresses the linear dependence between the peak currents and the square root of the scan rate for a reversible redox process as:

$$I_p = 2.69 \times 10^{-5} n^{3/2} A D^{1/2} C \nu^{1/2}$$

I_p = peak current (A)

n = number of electrons transferred per molecule

A = electrode surface area (cm^2)

D = diffusion coefficient of solution species ($\text{cm}^2 \cdot \text{s}^{-1}$)

C = bulk concentration ($\text{mol} \cdot \text{cm}^{-3}$)

ν = scan rate ($\text{V} \cdot \text{s}^{-1}$)

By plotting the anodic peak current against the square root of the scan rate, with scan rates ranging from 0.1 to 1.1 $\text{V} \cdot \text{s}^{-1}$, it can be concluded that oxazoles **1a-c** and ylide **2** display a fully reversible behaviour under these conditions (Figure 36).

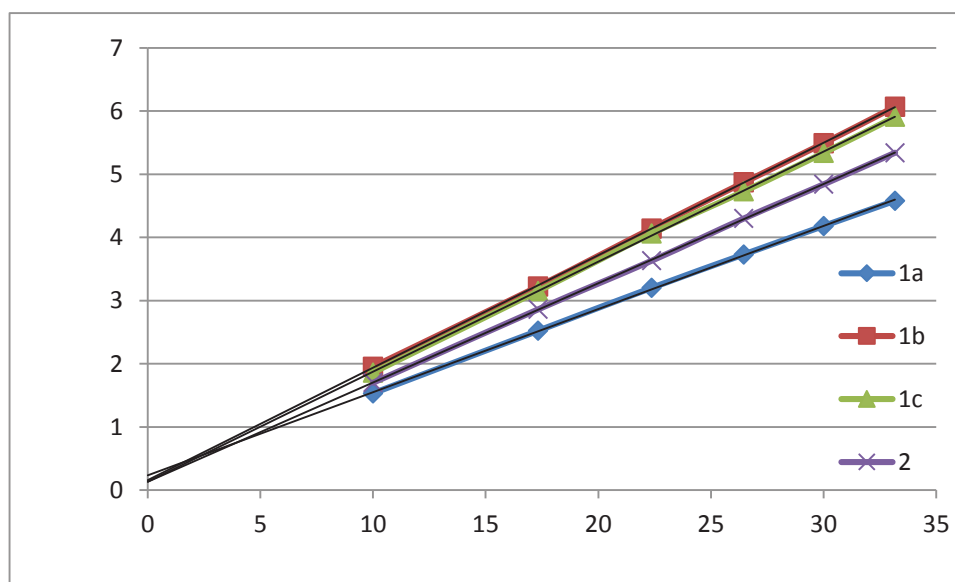


Figure 36: Linear dependence of anodic peak current on the square root of the scan rate for compounds **1a-c** and **2**.

As expected, given the electron deficiency of the oxazole moiety, compounds **1a-c** exhibited higher potential values than ferrocene (*ca.* 770 mV against 532 mV respectively, Table 5, Entry 1-3 and 5). Among the different ferrocenyl oxazoles characterised, only a slight variation in the $E_{1/2}$ values was observed, with 5-butyl oxazole **1c** exhibiting the lowest value ($E_{1/2} = 752$ mV, Table 5, Entry 3) compared to 5-phenyl oxazole **1a** ($E_{1/2} = 779$ mV, Table 5, Entry 1), suggesting a stronger electron donation through the oxazole ring by the butyl chain. By comparing **1a** and **1b**, it appears that the *N*-sulfonamido substituent has a very limited effect on the ferrocene moiety, as they oxidise at similar potentials ($E_{1/2} = 779$ mV and 775 mV respectively, Table 5, Entry 1 and 2). Tárraga and co-workers showed that 2-ferrocenyl-5-phenyloxazole oxidises at a higher potential than ferrocene by 128 mV in dichloromethane.⁷⁷ Comparatively, oxazole **1a** oxidises at 247 mV more than ferrocene. It is then possible to attribute this difference (+119 mV) to the *N*-nosyl at the 4-position of the ring.

Entry	Compound	E_{pc}	E_{pa}	$E_{1/2}$	ΔE_p
1	1a	739	818	779	79
2	1b	736	814	775	78
3	1c	713	794	752	81
4	2	507	581	559	74
5	Ferrocene	502	562	532	60

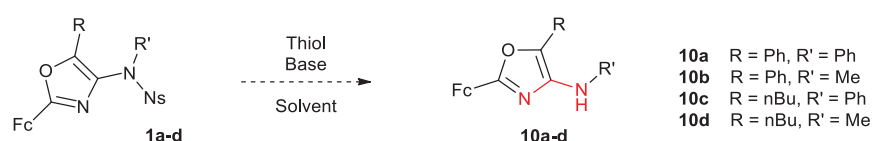
Table 5: Potential values (mV) from cyclic voltammetry, vs dmfc at 0.1 V.s⁻¹

Interestingly ylide **2** has an $E_{1/2}$ value 27 mV higher than ferrocene (559 mV against 532 mV respectively, Table 5, Entry 4). This may suggest that the ylide moiety can nearly compensate for the electron-withdrawing effect of the carbonyl group. Such a compensation could arise from an electro-donation by the negatively charged nitrogen. A one electron process would be characterised by a difference between the anodic and cathodic peak potentials, ΔE_p , of 59 mV.⁸² At 100 mV.s⁻¹, ΔE_p ranges from 74 mV for ylide **2** to 81 mV for oxazole **1c**. However in these conditions, these values are typical for ferrocene species. The low polarity of the solvent

(dichloromethane) implies an uncompensated resistance in the solution, increasing with the scan rate; which results in a larger ΔE_p .⁸³

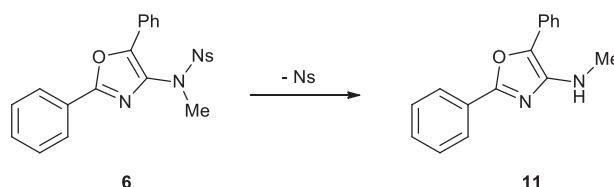
2.2.3. Deprotection of 4-*N*-Nosylamine oxazole

As mentioned in section 2.1.2, the aim was to prepare oxazoles **10a-d** by deprotection of the nosyl-protected oxazoles **1a-d** (Scheme 26). To date, the preparation of oxazoles bearing a secondary amine at the 4-position has not been reported in the literature.



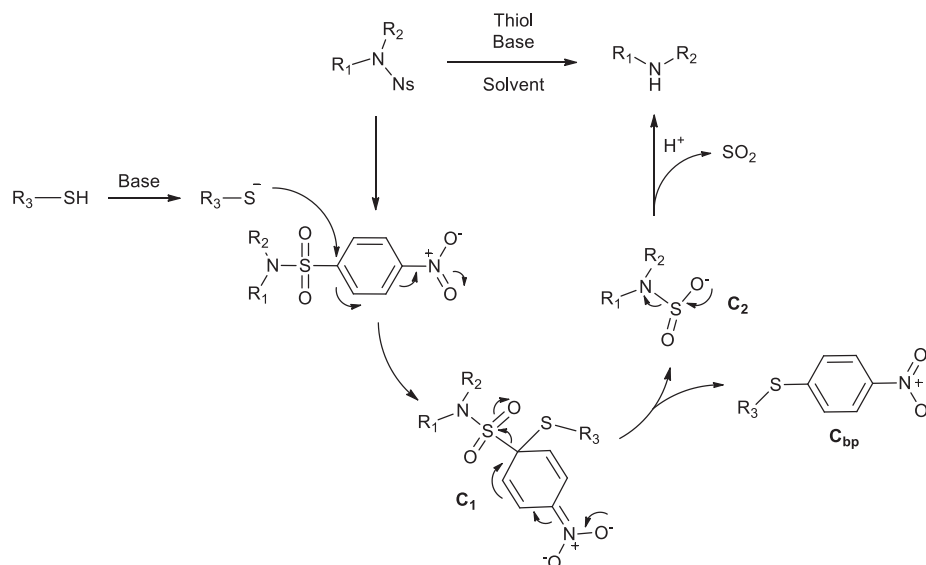
Scheme 26: Nosyl deprotection of oxazole **1a-d**

As described in section 1.2.1, oxazole **6** was prepared as a less expensive though similar model to oxazoles **1** and **7** for preliminary studies on the nosyl deprotection (Scheme 27).



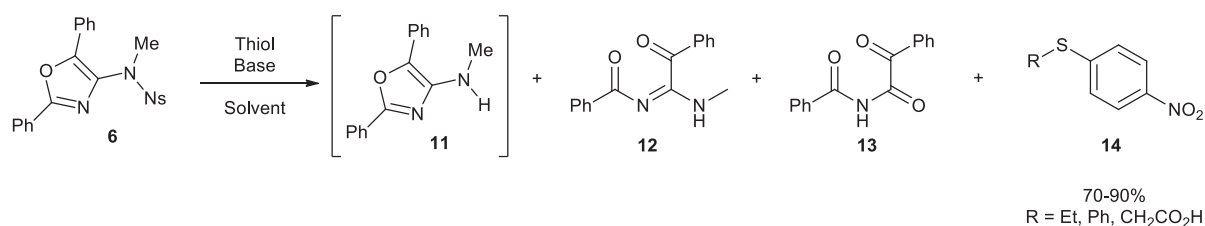
Scheme 27: 2-Phenyl-4-*N*-sulfonamide oxazole **6** to amine **11**

Sulfonamide **6** was subjected to deprotection conditions to access 4-*N*-amino oxazole **11**. Nucleophiles such as mercaptoacetic acid, thiophenol, thioethanol were tested, along with DBU (diazabicyclo[2.2.2]octane), triethylamine, potassium carbonate or sodium methanolate as base. The anticipated general mechanism for the deprotection of para-nitrobenzene sulfonamide is shown in Scheme 28. After deprotonation of the thiol, the nucleophilic thiolate attacks the ipso position of the benzene ring to form intermediate **C1**. Rearomatization of the ring releases intermediate of interest **C2** and by-product **C_{bp}**. Sulfur dioxide is then extruded from **C2** and the deprotected amine is produced upon protonation.



Scheme 28: Anticipated mechanism for nosyl deprotection

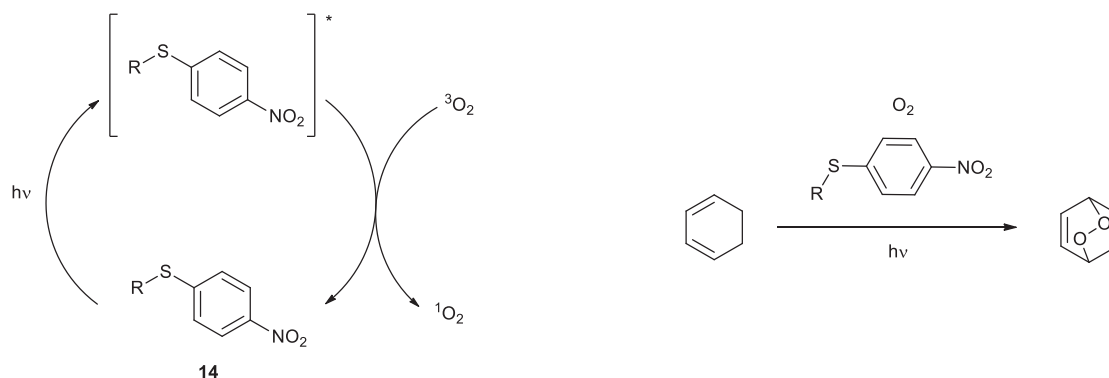
However it appeared that in our case, a side reaction took place regardless of the solvent (DMF or MeCN), or the nature and stoichiometry of the nucleophile (EtSH, PhSH or HSCH₂CO₂H) and the base (DBU), yielding oxidised compound **12** along with its hydrolysed derivative **13**. In a few instances the desired amine **11** was detected (HRMS: calculated for C₁₆H₁₄N₂O: 250.1106, found 250.1107), but this result could not be reproduced and the purification failed to deliver the amine as a pure compound. Nevertheless, the sulfide by-product **14** was isolated from the reaction mixture, indicating that the deprotection reaction did occur (Scheme 29).



Scheme 29: Deprotection products

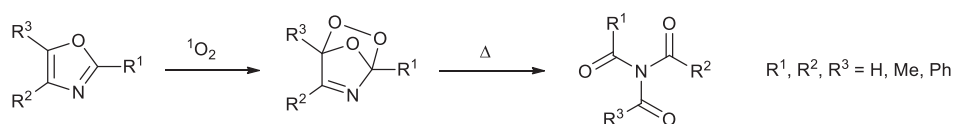
Interestingly, sulfides **14** (R = Et, Ph) have been reported to undergo self-induced photo-oxidation (to sulfoxides) when subjected to oxygen and light ($\lambda_{\text{max}} = 340 \text{ nm}$).⁸⁴ The mechanism involves photosensitiser-like behaviour of the sulfide which, upon irradiation, converts triplet oxygen into reactive singlet oxygen. When the authors trapped the formed singlet oxygen with a diene (1,3-cyclohexadiene), no sulfoxide was detected but only the endoperoxide product

from the Diels-Alder reaction between singlet oxygen and 1,3-cyclohexadiene (Scheme 30). This suggests that singlet oxygen reacts faster with a diene-type substrate than with sulfide **14**.



Scheme 30: 4-Nitrophenyl phenyl sulfide **14** as photosensitiser (R = Et, Ph)

Furthermore when substituted by hydrogen(s), methyl(s) and/or phenyl(s), the oxazole ring has been reported to be a suitable diene for the cycloaddition of singlet oxygen in acetonitrile.⁸⁵ The resulting endoperoxide, which was isolated, thermally collapsed to triacylamine (Scheme 31).⁸⁶



Scheme 31: Reaction of oxazoles with singlet oxygen and their thermal decomposition to triacylamine

To a certain extent oxazole **11** may behave in a similar fashion and form an endoperoxide intermediate, rearranging in a different way as to provide compound **12**. The structure of the latter was confirmed by X-ray crystallography (Figure 37).

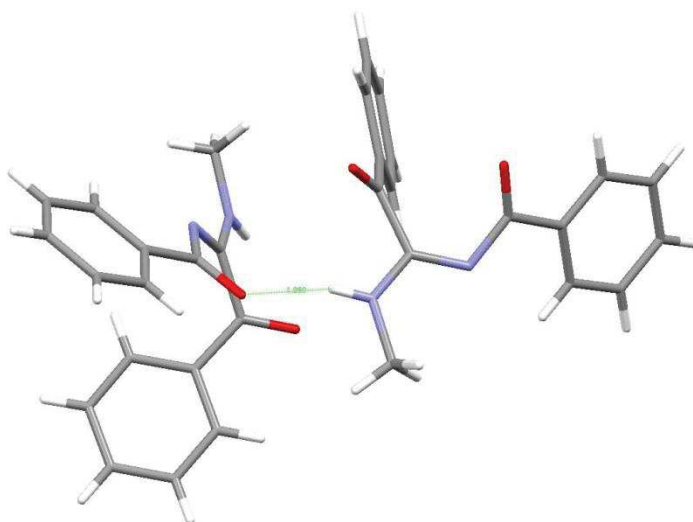
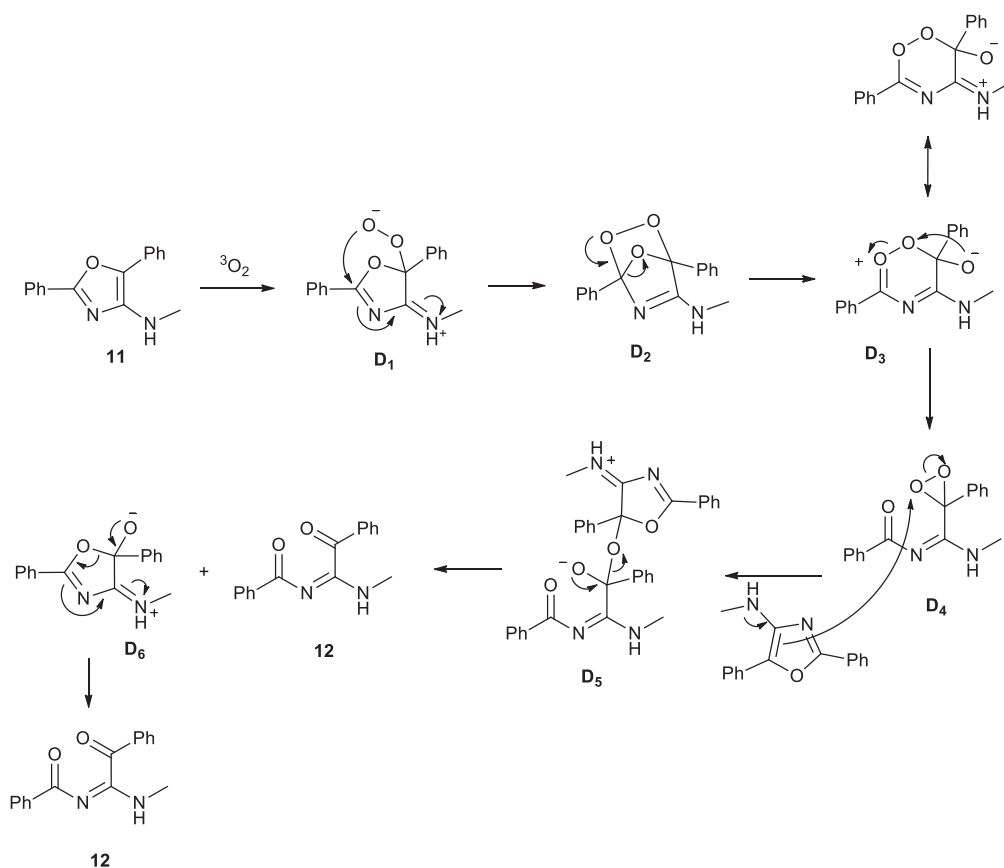


Figure 37: Crystallographic structure of compound **12**, presenting an inter-molecular H-bond between *NH* and O ($d_{NH-O} = 2.798 \text{ \AA}$). (Data collection and structure resolution by Dr. Mateusz B. Pitak)

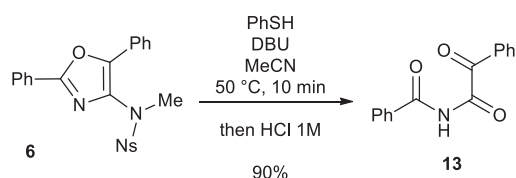
To test the hypothesis of the singlet oxygen / sulfide **14** / light-driven transformation of amine **11** into oxidised compound **12**, the deprotection was carried out under the same conditions described previously, with the exception of using de-oxygenated dry acetonitrile (dried over 3 Å molecular sieves overnight then through bubbling argon for 10 minutes) and isolating the reaction mixture from light by wrapping with aluminium foil (from the reaction flask to the end of the column). Unfortunately this did not stop the oxidation process from taking place and both oxidised compounds **12** and **13** were observed. The collected fraction became light-blue in colour when exposed to sunlight. A mechanism is therefore proposed for the oxidation of **11** to **12** (Scheme 32).



Scheme 32: Proposed mechanism for the oxidation of oxazole amine **11** by triplet oxygen

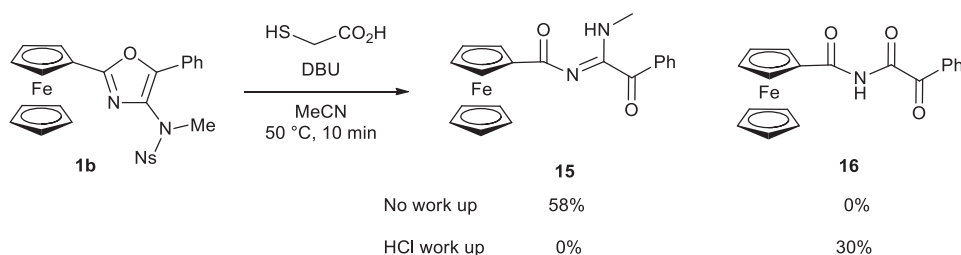
The enamine type reactivity of oxazole **11** allows for a nucleophilic attack on triplet oxygen to give intermediate **D1** which cyclises by Michael addition forming endoperoxide oxazole **D2**. Opening of the five-membered ring to the stabilised six-membered ring **D3** further rearranges to give dioxirane **D4**. The electrophilic character of the dioxirane allows a new molecule of amine **11** to attack, forming intermediate **D5**. Fragmentation of the latter gives oxidised compound **12** and **D6** which opens to form a second molecule of **11**.

Additionally, when the deprotection of sulfonamide **6** was followed by an acidic work-up (HCl 1 M), only compound **13** was obtained in a high yield of 90% (Scheme 33).



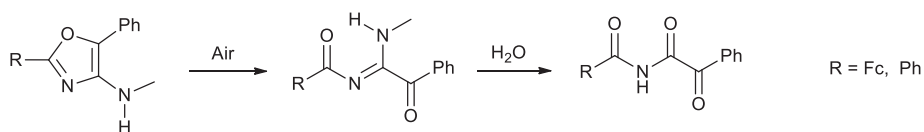
Scheme 33: Oxidative ring opening followed by acidic hydrolysis of oxazole sulfonamide **6**

The ferrocene version was next attempted as it was in hand. Once again, when 2-ferrocenyloxazole **1b** was subjected to the standard deprotection conditions followed by silica gel column chromatography, no desired amine was detected and only compound **15** was isolated (Scheme 34). Likewise, if an acidic work up was conducted with HCl 1M, then only compound **16** was isolated.



Scheme 34: Deprotection conditions applied to ferrocene oxazole **1b**

Hence the most likely explanation for this outcome is that the desired secondary amine is made but it then undergoes spontaneous oxidation when in contact with ³O₂ from the air and slowly hydrolyses with moisture (Scheme 35).



Scheme 35: Spontaneous oxidation and hydrolysis of 4-*N*-amino substituted oxazole

Given that protected compound **1** is air stable (as well as in HCl 1 M), it may be reasonable to suggest that the nosyl moiety prevents the heterocycle from a spontaneous air-oxidation, potentially attributable to its substantial electron-withdrawing effect.

2.3. Conclusion and future work

Novel mono-oxazole ferrocene **1** and 1,1'-bis-oxazole ferrocene **7** were successfully prepared via gold catalysis. Cyclic voltammetry studies of mono-oxazole **1** showed the reversible one electron redox process expected for a ferrocene species. They also emphasised the strong electron-withdrawing character of the oxazole ring, increasing the potential at which the ferrocene unit is oxidised (*ca.* +240 mV vs ferrocene). Almost half of this increase could be attributed to the presence of *N*-sulfonamido (*N*-Nosyl) at the 4-position of the oxazole (+119 mV for 2-ferrocenyl-4-*N*-(*N*-phenyl)sulfonamide-5-phenyl oxazole **1a** vs 2-ferrocenyl-5-phenyl oxazole). Finally, deprotection of the nosyl group led to the desired secondary amines **10** and **11**, which most likely underwent spontaneous oxidative ring opening with triplet oxygen to give compounds **15** and **12**, easily hydrolysed to compound **16** and **13** respectively. This difficulty with the synthesis precluded the study of 4-*N*-amino oxazole systems as new H-bonding receptors.

In order to stabilise the oxazole ring and avoid spontaneous oxidation, future work on gold-mediated preparation of 4-NH-substituted oxazole could move towards the replacement of the *N*-alkyl/aryl group with a more electron withdrawing group, such as amide or 3,5-(CF₃)-phenyl (Figure 38). This would potentially reduce the electron density available in the structure, hence improving its resistance towards oxidation.

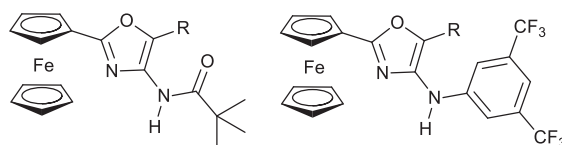


Figure 38: Potentially more stable modified 4-*N*-amino oxazoles as H-bonding receptors

2.4. References

-
- ⁵⁶ a) D. Davyt, G. Serra, *Mar. Drugs*, **2010**, *8*, 2755-2780; b) Z. Jin, *Nat. Prod. Rep.*, **2011**, *28*, 1143-1191.
- ⁵⁷ V. S. C. Yeh, *Tetrahedron*, **2004**, *60*, 11995-12042.
- ⁵⁸ X. Li, X-T. Yu, H-J. Chi, Y. Dong, G-Y. Xiao, P. Lei, D-Y. Zhang, Z. Cui, *Spectrochim. Acta, Part A*, **2013**, *116*, 473-477.
- ⁵⁹ P. Comba, N. Dovalil, G. Haberhauer, G. R. Hanson, Y. Kato, T. Taura, *J. Biol. Inorg. Chem.*, **2010**, *15*, 1129-1135.
- ⁶⁰ A. Pintér, G. Haberhauer, *Eur. J. Org. Chem.*, **2008**, 2375-2387.
- ⁶¹ A.O. Eseola, M. Zhang, J.-F. Xiang, W. Zuo, Y. Li, J.A.O. Woods, W.-H. Sun, *Inorg. Chim. Acta*, **2010**, 1970-1978.
- ⁶² a) J. Mazuela, P. Tolstoy, O. Pamies, P. G. Andersson, M. Dieguez, *Org. Biomol. Chem.*, **2011**, *9*, 941-946; b) M. Poyatos, A. Maisse-François, S. Bellemin-Laponnaz, L. H. Gade, *Organometallics*, **2006**, *25*, 2634-2641; c) A. O. Eseola, W. Li, O. G. Adeyemi, N. O. Obi-Egbedi, J. A. O. Woods, *Polyhedron*, **2010**, *29*, 1891-1901.
- ⁶³ a) D. S. Pilch, C. M. Barbieri, S. G. Rzuczek, E. J. LaVoie, J. E. Rice, *Biochimie*, **2008**, *90*, 1233-1249; b) K. Jantos, R. Rodriguez, S. Ladame, P. S. Shirude, S. Balasubramanian, *J. Am. Chem. Soc.*, **2006**, *128*, 13662-13663.
- ⁶⁴ J. D. Carr, L. Lambert, D. E. Hibbs, M. B. Hursthouse, K. M. A. Malik, J. H. R. Tucker, *Chem. Commun.*, **1997**, *17*, 1649-1650.
- ⁶⁵ P. W. Davies, A. Cremonesi, L. Dumitrescu, *Angew. Chem. Int. Ed.*, **2011**, *123*, 9093-9097.
- ⁶⁶ H. V. Nguyen, A. Sallustrau, J. Balzarini, M. R. Bedford, J. C. Eden, N. Georgousi, N. J. Hodges, J. Kedge, Y. Mehellou, C. Tselepis, J. H. R. Tucker, *J. Med. Chem.*, **2014**, *57*, 5817-5822.
- ⁶⁷ A. V. Gulevich, A. S. Dudnik, N. Chernyak, V. Gevorgyan, *Chem. Rev.*, **2013**, *113*, 3084-3213.
- ⁶⁸ a) D. A. Black, B. A. Arndtsen, *Tetrahedron*, **2005**, *61*, 11317-11321; b) H. v. Wachenfeldt, P. Röse, F. Paulsen, N. Loganathan, D. Strand, *Chem. Eur. J.*, **2013**, *19*, 7982-7988; c) A. Y. Shaw, Z Xu, C. Hulme, *Tetrahedron Lett.*, **2012**, *53*, 1998-2000; d) N. Elders, E. Ruijter, F. J. J. de Kanter, M. B. Groen, R. V. A. Orru, *Chem. Eur. J.*, **2008**, *14*, 4961-4973.
- ⁶⁹ a) C. Wan, L. Gao, Q. Wang, J. Zhang, Z. Wang, *Org. Lett.*, **2010**, *12*, 3902-3905; b) H. Jiang, H. Huang, H. Cao, C. Qi, *Org. Lett.*, **2010**, *12*, 5561-5563.
- ⁷⁰ A. Saito, A. Taniguchi, Y. Kambara, Y. Hanzawa, *Org. Lett.*, **2013**, *15*, 2672-2675.

- ⁷¹ Y-M. Pan, F-J. Zheng, H-X. Lin, Z-P. Zhan, *J. Org. Chem.*, **2009**, *74*, 3148-3151.
- ⁷² A. J. Phillips, Y. Uto, P. Wipf, M. J. Reno, D. R. Williams, *Org. Lett.*, **2000**, *2*, 1165-1168.
- ⁷³ a) X. Zhang, W. T. Teo, P. W. H. Chan, *J. Organomet. Chem.*, **2011**, *696*, 331-337; b) M. D. Milton, Y. Inada, Y. Nishibayashi, S. Uemura, *Chem. Commun.*, **2004**, 2712-2713; c) M. P. Kumar, R-S. Liu, *J. Org. Chem.*, **2006**, *71*, 4951-4955.
- ⁷⁴ a) A. S. K. Hashmi, J. P. Weyrauch, W. Frey, J. W. Bats, *Org. Lett.*, **2004**, *6*, 4391-4394; b) A. Saito, K. Iimura, Y. Hanzawa, *Tetrahedron Lett.*, **2010**, *51*, 1471-1474; c) A. Arcadi, S. Cacchi, L. Cascia, G. Fabrizi, F. Marinelli, *Org. Lett.*, **2001**, *3*, 2501-2504.
- ⁷⁵ a) K. J. Doyle, C. J. Moody, *Tetrahedron*, **1994**, *50*, 3761-3772; b) M. C. Bagley, R. T. Buck, S. L. Hind, C. J. Moody, A. M. Z. Slawin, *Synlett*, **1996**, 825-826; c) M. C. Bagley, R. T. Buck, S. L. Hind, C. J. Moody, *J. Chem. Soc., Perkin Trans. 1*, **1998**, 591-601; d) M. Austeri, D. Rix, W. Zeghida, J. Lacour, *Org. Lett.*, **2011**, *13*, 1394-1397; e) J. R. Davies, P. D. Kane, C. J. Moody, *Tetrahedron*, **2004**, *60*, 3967-3977.
- ⁷⁶ a) W. He, C. Li, L. Zhang, *J. Am. Chem. Soc.*, **2011**, *133*, 8482-8485; b) X. Li, L. Huang, H. Chen, W. Wu, H. Huang, H. Jiang, *Chem. Sci.*, **2012**, *3*, 3463-3468.
- ⁷⁷ A. Tárraga, P. Molina, D. Curiel, J. L. López, M. Desamparados Velasco, *Tetrahedron*, **1999**, *55*, 14701-14718.
- ⁷⁸ P. W. Davies, A. Cremonesi, N. Martin, *Chem. Commun.*, **2011**, *47*, 379-381.
- ⁷⁹ T. Hamada, X. Ye, S. S. Stahl, *J. Am. Chem. Soc.*, **2008**, *130*, 833-835.
- ⁸⁰ T. Kan, T. Fukuyama, *Chem. Commun.*, **2004**, 353-359.
- ⁸¹ I. Noviandri, K. N. Brown, D. S. Fleming, P. T. Gulyas, P. A. Lay, A. F. Masters, L. Phillips, *J. Phys. Chem. B*, **1999**, *103*, 6713-6722.
- ⁸² C. M. A. Brett, A. M. Oliviera, *Voltametric Sensors In Electroanalysis*, Oxford University Press: **1998**.
- ⁸³ R. S. Nicholson, *Anal. Chem.*, **1965**, *37*, 667-671.
- ⁸⁴ a) D. J. Pasto, F. Cottard, S. Horgan, *J. Org. Chem.*, **1993**, *58*, 4110-4112; b) D. J. Pasto, F. Cottard, L. Jumelle, *J. Am. Chem. Soc.*, **1994**, *116*, 8978-8984.
- ⁸⁵ K. Gollnick, S. Koegler, *Tetrahedron Lett.*, **1988**, *29*, 1003-1006.
- ⁸⁶ K. Gollnick, S. Koegler, *Tetrahedron Lett.*, **1988**, *29*, 1007-1010.

3. Ferrocenyl-(thio)ureas as organocatalysts

3.1. Introduction

3.1.1. Ferrocene-containing organocatalysts

Ferrocene has been used widely in supramolecular structures for sensing purposes. Another characteristic of ferrocene is its well-defined bulkiness, which allows for the development of effective chiral environments. This is of particular interest in the field of asymmetric catalysis, where the chiral information must be optimally transferred from the catalyst reaction site to the forming product. Although a great number of ferrocene-containing ligands have been designed for metal-catalysed transformations, there are relatively few examples in the field of organocatalysis. Early research by Fu and co-workers explored the nucleophilicity of N-heterocycle catalysts with planar chiral ferrocene structures.⁸⁷ Among them the remarkable Fc-DMAP (Figure 39) showed high performances in a wide array of asymmetric transformations.⁸⁸

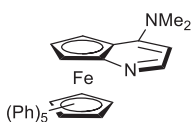


Figure 39: Fc-DMAP catalysts

More recently, Cozzi and co-workers reported efficient enamine catalysis using a ferrocenyl pyrrolidine,⁸⁹ in which the steric bulk of ferrocene was used to lock the conformation of the enantio-determining step, after the formation of the enamine (Figure 40).⁹⁰

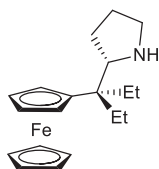


Figure 40: Ferrocenyl pyrrolidine for enamine catalysis

The addition of aldehydes to nitroalkenes was achieved in good yields and up to 95% ee. A similar example was published very recently, this time with a structure containing an amide bond linking a chiral α -methylferrocene to an *L*-proline unit (Figure 41).⁹¹

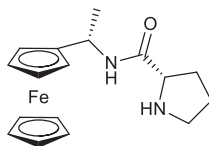


Figure 41: Ferrocene-proline organocatalyst

Finally, Chen and co-workers published promising results regarding their work on ferrocene-based phosphine-squaramide organocatalysts (Figure 42).⁹² This catalyst exhibited both central and planar chirality and was used in the intramolecular Morita-Baylis-Hillman reaction of 7-aryl-7-oxo-5-heptenals, forming a variety of 2-aryl-2-cyclohexenols in up to 96% ee.

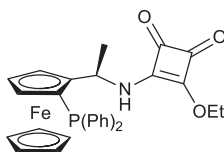


Figure 42: Ferrocene-based phosphine-squaramide organocatalyst

3.1.2. Project - Design

Taking advantage of the work done previously in the Tucker group on ferrocenyl (thio)urea,⁹³ it was decided to investigate the ferrocene scaffold in organocatalysed asymmetric transformations. Figure 43 summarises the different ferrocenyl (thio)ureas that have been prepared and tested.

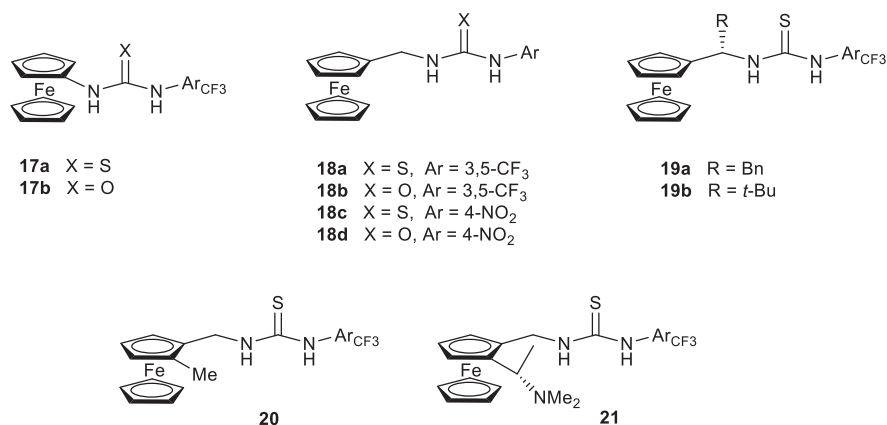


Figure 43: Overview of the different (thio)urea to be synthesised and tested

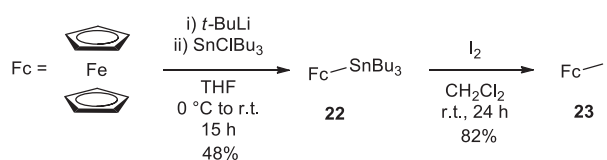
Compounds **17a-b** have the (thio)urea unit directly connected to the electron-rich ferrocene unit whereas compounds **18a-d** contain a methylene linker between the two units. Thioureas **19a,b** integrate a stereogenic centre at the methylene linker, while compound **20** features planar chirality on the ferrocene. Thiourea **21** exhibits a tertiary amine that is expected to have a nucleophilic character, similar to Takemoto's bi-functional catalyst.²⁸ These catalysts have been tested in: 1) the Henry reaction of nitromethane and benzaldehyde, 2) the Morita-Baylis-Hillman reaction between nitromethane and cyclohexenone, 3) the enamine co-catalysed aldol reaction of acetone and nitro-styrene, and 4) the double Michael addition to prepare tetra-substituted cyclopentane. A more detailed background of these reactions is presented in section 1.5.

3.2. Results and discussion

3.2.1. Synthesis

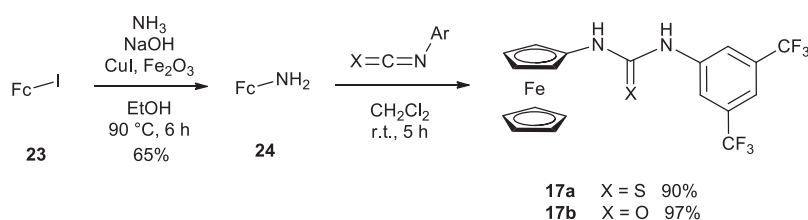
3.2.1.1. Preparation of achiral ferrocenyl thiourea

Ferrocene was deprotonated using *tert*-butyllithium at 0 °C and the lithiated ferrocene was trapped with tributyltin chloride in THF overnight to form stannylferrocene species **22**, before being converted to the 1-iodoferrocene **23** by stirring it with iodide in dichloromethane for one day (Scheme 36).⁹⁴ This two-step procedure has the advantage of relying on ferrocene tin species that are more easily purified by column chromatography than their iodo equivalents.



Scheme 36: Two-step procedure for the preparation of iodoferrocene **23** from ferrocene

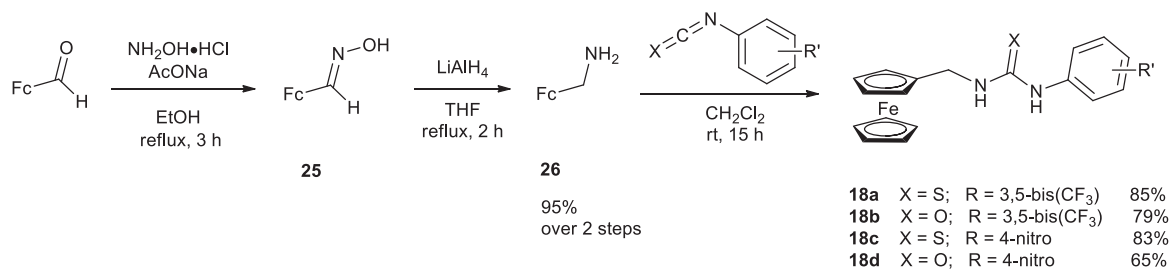
Subsequent copper (I) / iron (III) catalysis in the presence of ammonia and sodium hydroxide in ethanol at 90 °C gave aminoferrocene **24** in good yield.⁹⁵ The addition of 3,5-bis(trifluoromethyl)phenyl iso(thio)cyanate in dichloromethane offered the desired ferrocenyl(thio)urea **17a-b** in excellent yields (Scheme 37).



Scheme 37: Preparation of achiral (thio)ureas **17a-b** from iodoferrocene **23**

3.2.1.2. Preparation of achiral ferrocene-methylene thiourea

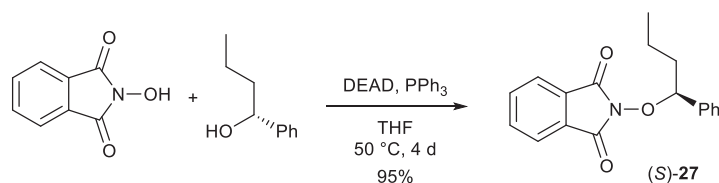
Ferrocenecarboxaldehyde was converted to the corresponding aldoxime **25** with hydroxylamine hydrochloride under basic conditions,⁹⁶ followed by a reduction with lithium aluminium hydride to yield 95% of ferrocenemethylamine **26** over two steps.⁹⁷ The latter was reacted with the appropriate iso(thio)cyanate to offer the achiral catalysts **18a-d** in good yields (Scheme38).



Scheme 38: Preparation of achiral (thio)ureas **18a-d** from ferrocene carboxaldehyde

3.2.1.3. Preparation of central chiral thiourea

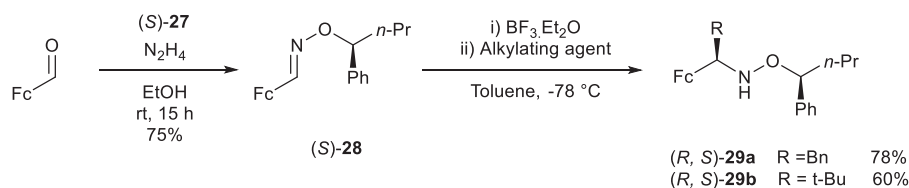
To access enantiopure catalysts, a chiral auxiliary derived from (*R*)-1-phenyl-1-butanol was used. Preparation of the chiral auxiliary was achieved by a Mitsunobu reaction between hydroxyphthalimide and (*R*)-1-phenyl-1-butanol to offer (*S*)-alkoxyphthalimide **27** (Scheme 39).⁹⁸



Scheme 39: Preparation of chiral auxiliary **27**

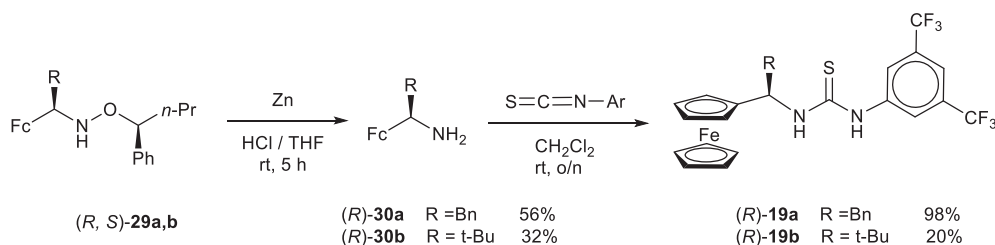
Ferrocenecarboxaldehyde was reacted with chiral auxiliary (*S*)-**27** in the presence of hydrazine, giving the ether aldoxime (*S*)-**28** in 71% yield over 2 steps (Scheme 40).⁹⁹ Diastereoselective alkylation of (*S*)-**28**, via activation by boron trifluoride diethyl etherate and addition of the

appropriate alkylating agent (RMgCl or RLi), gave the desired enantiopure hydroxylamine ether (*R, S*)-**29a,b** with the expected order of yields regarding to the bulkiness of the R groups, ranging from 60% to 89% for R = *t*-Bu and Me respectively. The organo-magnesium alkylating agent BnMgCl was reactive enough to generate (*R, S*)-**29a**, while the lithium analogue (*t*-BuLi) was required to install the bulkier *t*-Bu group onto the oxime carbon, giving (*R, S*)-**29b**.



Scheme 40: Installation of centrale chirality via hydroxylamine ethers (*R, S*)-**29a,b**

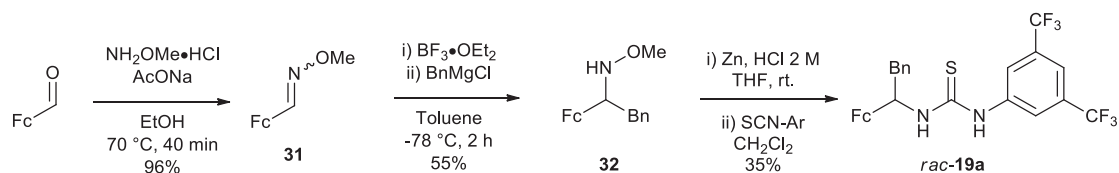
Cleavage of the N-O bond was achieved by reacting (*R, S*)-**29** with zinc powder under acidic conditions (Scheme 41). The different amines (*R*)-**30a,b** were produced in low to moderate yield, and were treated with (trifluoromethyl)phenyl isothiocyanate to form the corresponding central chirality-containing thioureas (*R*)-**19a,b**.



Scheme 41: Reductive cleavage of hydroxylamines (*R, S*)-**29a,b** and coupling to isothiocyanate giving chiral thioureas (*R*)-**19a,b**

The (*S*) enantiomer of **19b** was prepared in similar yields following the same procedure starting with (*R*)-**27**. The preparation of racemic thiourea **19a** was undertaken using a similar symmetric strategy, starting from ferrocene carboxaldehyde (Scheme 42). It was subjected to methoxyamine hydrogen chloride in the presence of sodium acetate in hot ethanol to yield oxime **31** almost quantitatively. Subsequent activation by boron trifluoride diethyl etherate at -78 °C and alkylation by BnMgCl led to hydroxylamine ether **32a** in moderate yields. Further

reduction using zinc powder in an acidic medium and sonication produced the corresponding amine **79**, which was directly coupled with (3,5-bis(CF₃)phenyl)isothiocyanate to give *rac*-**19a**.



Scheme 42: Preparation of racemic thiourea **19a**

Chiral HPLC analysis of **19a** and **19b** (see Appendix) showed an enantiomeric excess of 96% for (*R*)-**19a** (AD column, 5% IPA in hexane, 1 mL·min⁻¹, R_t = 18.4 min) and 96% for (*R*)- and (*S*)-**19b** (OD column, 10% IPA in hexane, 1 mL·min⁻¹, R_t = 5.1 min and 4.5 min respectively).

3.2.1.4. Preparation of planar chiral thiourea

The synthesis of enantiopure catalyst (*R_p*)-**20** relies on the diastereoselective ortho-lithiation of dioxane **33** (Figure 44) developed by Kagan's group.¹⁰⁰

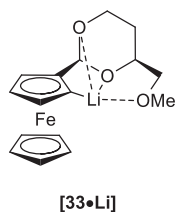
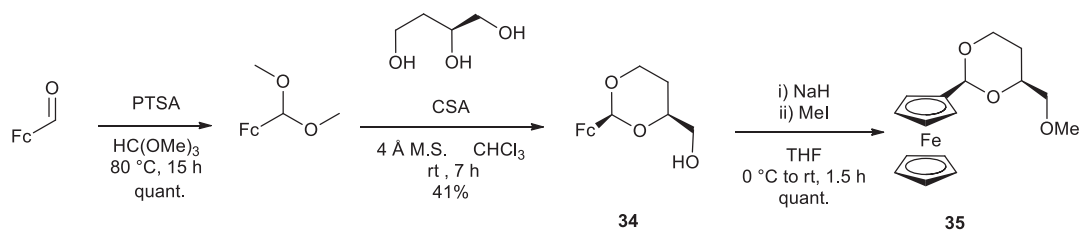


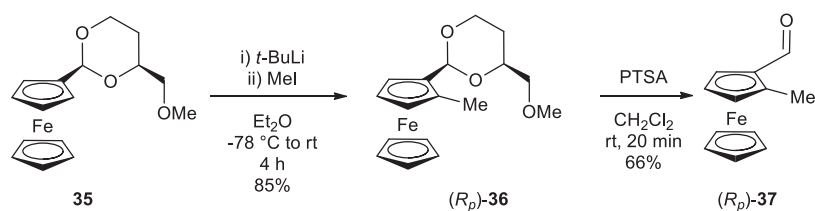
Figure 44: Diastereoselectively ortho-lithiated key intermediate **33**

Ferrocenecarboxaldehyde was first transformed into the corresponding dimethoxyacetal before being trans-acylated to dioxane **34** with (*S*)-1,2,4-butanetriol. The two possible diastereoisomers were present and were carefully separated by column chromatography. Pure compound **34** was then subjected to sodium hydride and methyl iodide, giving the ether **35** with 40% yield over 3 steps (Scheme 43).



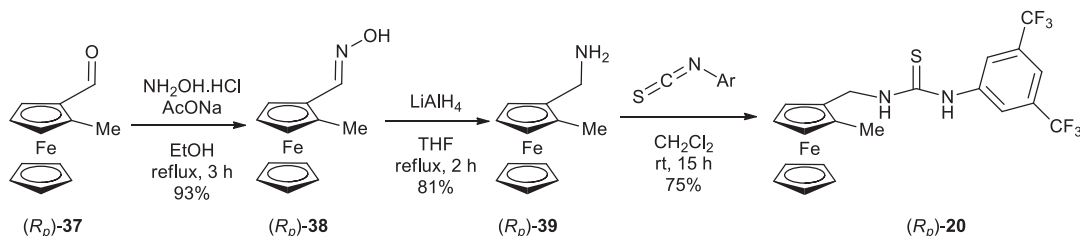
Scheme 43: Preparation of enantio-pure dioxane **35**

Subsequent deprotonation of **35** by *tert*-butyllithium at $-78\text{ }^{\circ}\text{C}$ was *ortho* directed by the chiral dioxane moiety, and the resulting *ortho*-lithiated species were quenched with methyl iodide (Scheme 44). Planar chiral ferrocene **36** was then obtained in 85% yield and only one diastereoisomer was detected by ^1H NMR. Deprotection of the aldehyde under acid conditions gave compound (*R_p*)-**37** in good yield (66%).



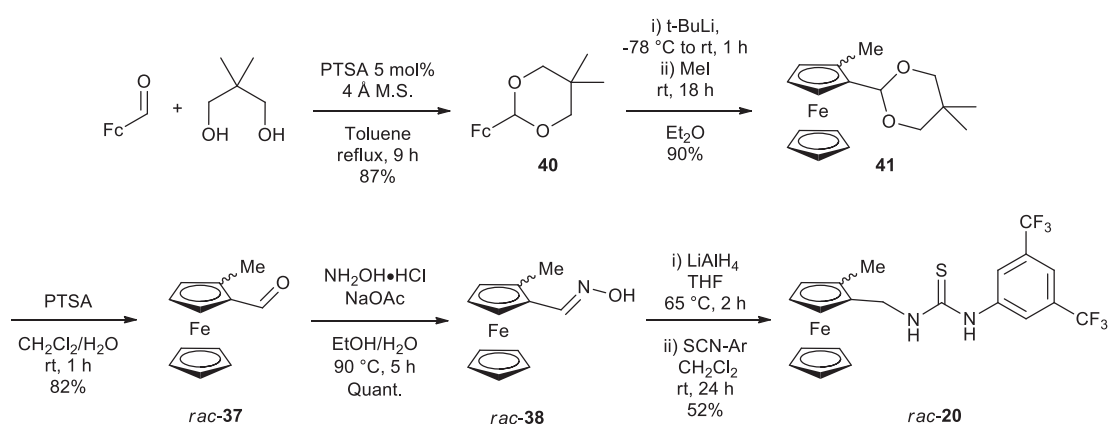
Scheme 44: Installation of planar chirality and deprotection of the dioxane to give aldehyde (*R_p*)-**37**

Further reaction with hydroxylamine hydrochloride gave the aldoxime (*R_p*)-**38** in excellent yield (Scheme 45). Reduction to the corresponding amine (*R_p*)-**39** with lithium aluminium hydride in refluxing THF and addition to 3,5-bis(trifluoromethyl)phenyl isothiocyanate gave the planar chiral containing thiourea (*R_p*)-**20** with a moderate yield of 60% over two steps.



Scheme 45: Preparation of thiourea (*R_p*)-**20** from aldehyde **37**

The preparation of racemic **20** was achieved via a similar route, with the difference that the dioxolane protecting group was not chiral, nor did it exhibit the stabilising methoxy group for the lithiation step (Scheme 46). Ferrocenecarboxaldehyde was first condensed with 2,2-dimethylpropan-1,3-diol by acid catalysis in toluene to generate dioxolane **40** in good yield. Subsequent lithiation by *t*-BuLi and quenching with methyl iodide gave the di-substituted ferrocene **41**. It is interesting to note that compound **41** was obtained in a similar yield to the asymmetric version (compound **36**), so the absence of the methoxy group was not detrimental to the stabilisation of the ortho-lithiated species prior to quenching. After the efficient deprotection of dioxolane **41** by PTSA in the presence of water, the resulting aldehyde *rac*-**37** was treated with hydroxylamine hydrogen chloride to quantitatively yield oxime *rac*-**38**. Finally, the reduction of *rac*-**38** was achieved with LiAlH₄ in refluxing THF, and the crude amine was then coupled to (3,5-bis(CF₃)phenyl)isothiocyanate to give *rac*-**20**.



Scheme 46: Preparation of racemic thiourea *rac*-**20**

The enantiomeric purity of thiourea (*R_p*)-**20** could not be accurately determined as the optimal HPLC conditions with the available chiral columns did not succeed in giving a full peak separation of the enantiomers of *rac*-**20** (see Appendix). However some separation was observed and the enantiomeric excess was estimated to be above 75%.

3.2.1.5. Preparation of bi-functional thiourea

The synthesis of the bi-functional thiourea **21** proceeded via diastereoselective *ortho*-lithiation of enantiopure 1-ferrocenyl-1-(*N,N*-dimethyl)amine ethyl **42** (Figure 45).¹⁰¹

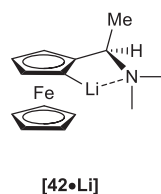
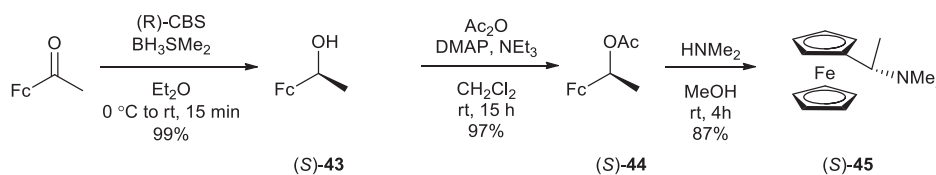


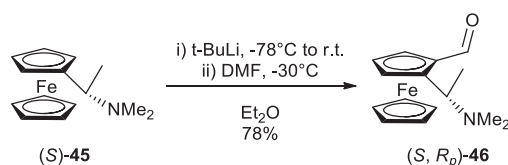
Figure 45: Diastereoselectively *ortho*-lithiated key intermediate **42**

The synthesis of bi-functional catalyst **21** started with the enantioselective reduction of acetylferrocene by borane di-methyl sulfide in the presence of CBS catalyst, offering the enantiopure alcohol **43**.¹⁰² Acylation of the latter followed by substitution with dimethylamine gave the chiral tertiary amine **45** in 84% yield over 3 steps (Scheme 47).



Scheme 47: Preparation of chiral intermediate (*S*)-**45**

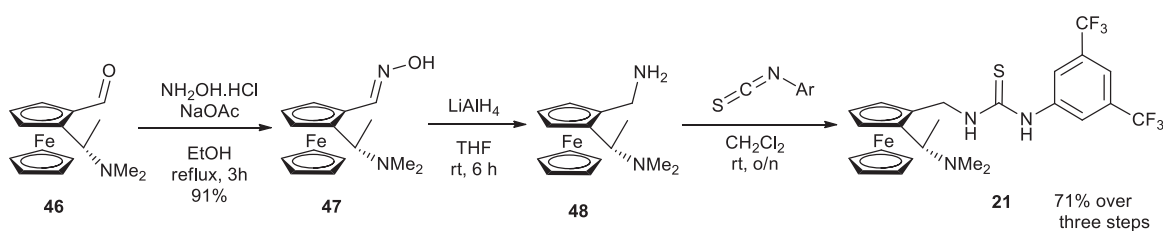
In order to functionalise the *ortho* position of the Cp ring, compound (*S*)-**45** was diastereoselectively deprotonated by *tert*-butyllithium at -78°C (Scheme 48), and the resulting *ortho*-lithiated ferrocene was quenched with dimethylformamide to afford the single diastereoisomer (*S, R_p*)-**46** in 78% yield.



Scheme 48: Diastereoselective formylation of (*S*)-**45** to planar chiral ferrocene (*S, R_p*)-**46**

As for previous catalysts, the obtained aldehyde (*S, R_p*)-**46** was then converted to the aldoxime (*S, R_p*)-**47** and quantitatively reduced to the amine (*S, S_p*)-**48** by reaction with LiAlH_4 in

refluxing THF. Finally, treatment with 3,5-bis(trifluoromethyl)phenyl isothiocyanate gave the enantiopure bi-functional catalyst (*S, S_p*)-**21** in 79% yield (Scheme 49).



Scheme 49: Preparation of bi-functional ferrocene (*S, S_p*)-**21** from aldehyde (*S, R_p*)-**46**

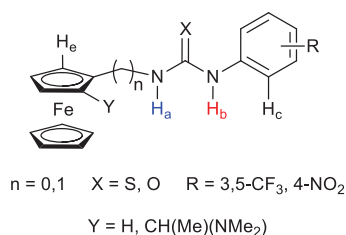
The enantiopurity of (*S, S_p*)-**21** was checked by chiral HPLC (OD column, 15% IPA in hexane, 1 mL.min⁻¹, monitored at 230 nm), with an enantiomeric excess of 99% for the (*S, S_p*) version (see Appendix). The other enantiomer (*R, R_p*)-**21** was also prepared, following the same procedure, and also showed an enantiomeric excess of 96%.

3.2.2. NMR studies

3.2.2.1. Achiral and bi-functional Fc-(thio)urea

For all compounds **17a-b** and **18a-d**, the presence of sulfur over oxygen increased the downfield shift of the (thio)urea protons, which is indicative of a higher acidity. Proton H_b was mostly influenced by the identity of the atom X with a difference of 0.8 ppm ($\delta = 9.4$ ppm with X = S, and $\delta = 8.6$ ppm with X = O) and to a much lesser extent by the nature of the *N*-substitution at the other end of the (thio)urea (Table 6, Entry 2 and 4). Proton H_a was almost equally affected by the nature of X ($\Delta\delta \approx 1.4$ ppm) than by the number of carbons ($n = 0, 1$) between its nitrogen and the ferrocene ($\Delta\delta \approx 1.4$ ppm). It was surprising that H_a was being unshielded by that magnitude when connected directly to the electron rich ferrocene ($n = 0$). By comparing **18a-b** (Table 6, Entry 3 and 4) and **18c-d** (Table 6, Entry 5 and 6), it appears

that the substitution of the phenyl ring (3,5-bis(CF₃) or 4-NO₂ respectively) does not have a significant influence on the NH protons.



Entry	Compound	n	X	δH_a	δH_b	δH_c
1	17a	0	S	9.04	9.37	8.34
2	17b	0	O	7.68	8.53	8.18
3	18a	1	S	7.73	9.43	8.31
4	18b	1	O	6.21	8.61	8.16
5	18c	1	S	7.66	9.43	7.95
6	18d	1	O	6.18	8.64	7.73
7	21	1	S	9.14	9.14	8.12

Table 6: Chemical shift of selected protons in achiral and bi-functional (thio)ureas (¹H NMR, \approx 50 mM in acetone d₆, ppm)

¹H NMR spectra of compound **21** showed both of the NH protons resonating at the same chemical shift (*c.a.* 9 ppm in acetone d₆). Hydrogen H_a is connected to a non-electron-withdrawing moiety (-CH₂Fc) and yet resonates +1.4 ppm more downfield than its analogue **18a**. This could indicate a possible H-bonding interaction between H_a and the tertiary amine, adding an electron-withdrawing effect to proton H_a and increasing its chemical shift (Figure 46).¹⁰³

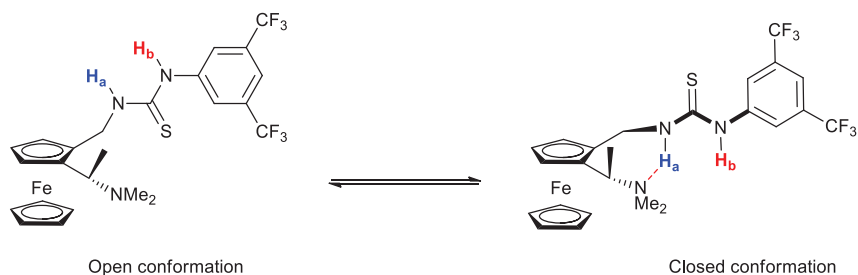


Figure 46: Proposed equilibrium between an unbound open conformation and the intramolecularly H-bond closed conformation of thiourea **21**

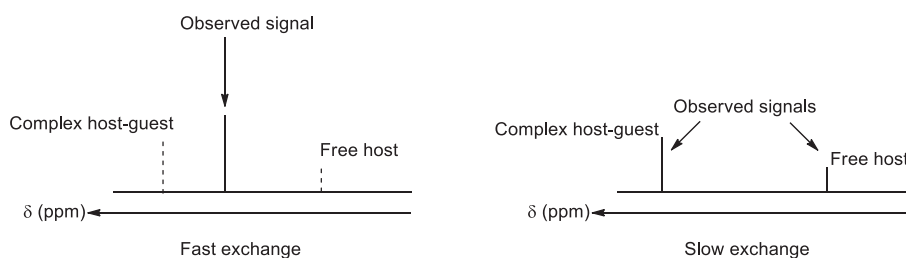


Figure 47: Observed ^1H NMR signal of proton under the influence of a fast exchange (left) and slow exchange (right)

The concentration of the (thio)urea receptors was set at 5 mM, and the carboxylate guests were added from a stock solution prepared at *c.a.* 0.2 M in CD_3CN . The stoichiometry of the receptor-guest had been previously established by the Tucker group as 1:1 on similar receptors using Job plots.¹⁰⁵

➤ **H-bonding with guest acetate**

Acetate **49** was added to receptors **17b**, **18a-b** and (*S*, *S*_p)-**21** in CD_3CN . The obtained titration curves showed that full complexation was reached after one equivalent of carboxylate **49** for the mono-functional receptors **17b** and **18a-b**, indicating strong binding under these conditions (Figure 48). The maximal variation in chemical shift for H_a (full lines) and H_b (dashed lines) are 4.4 ppm and 5 ppm respectively for receptor **17b** (red lines), 4 ppm and 4.7 ppm respectively for **18b** (green lines), and 4.7 ppm and 5.2 ppm respectively for **18a** (orange lines).

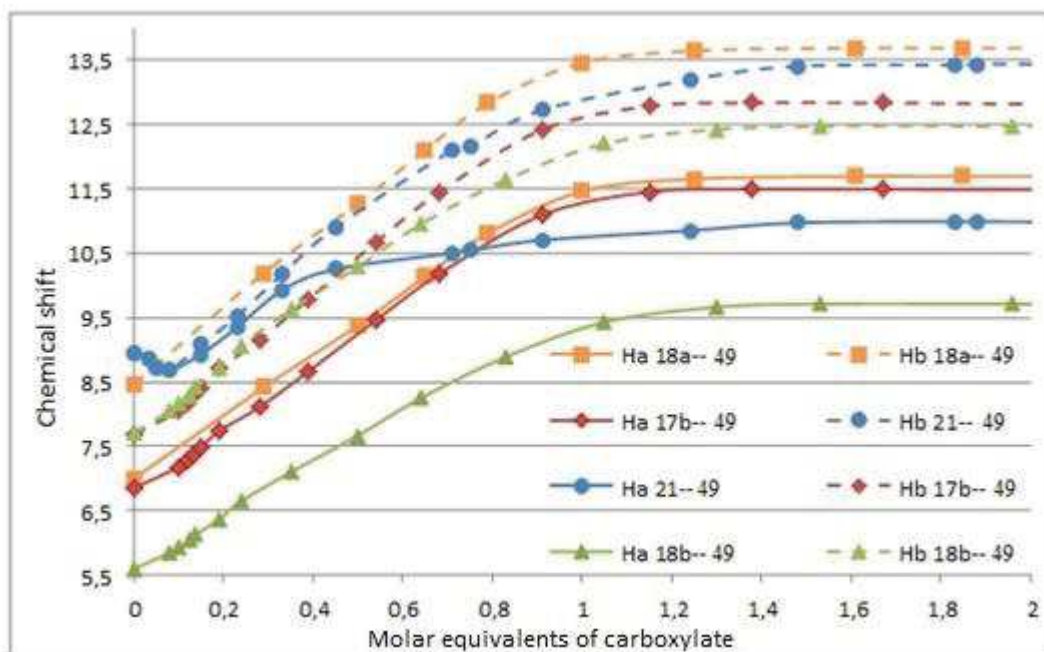
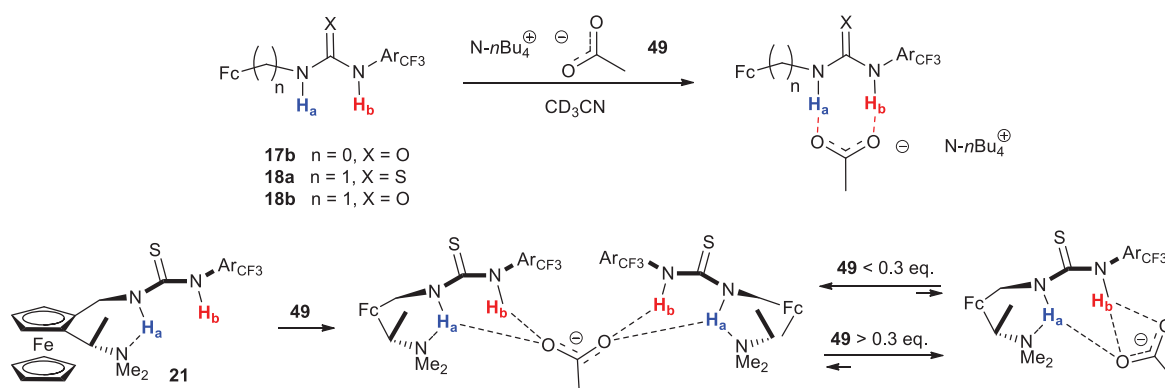


Figure 48: Chemical shift of protons H_a and H_b of **17b**, **18a-b** and (S, S_p) -**21** (5 mM in CD_3CN) upon addition of carboxylate **49**

The chemical shift of protons H_a and H_b of receptor (S, S_p) -**21** (blue lines) varied by 2 and 4.5 ppm respectively. The obtained curves showed different behaviours upon addition of guest. For both H_a and H_b , at first an unexpected decrease in chemical shift (-0.3 ppm) was observed until 0.15 equivalent of guest was added. It then quickly increased (+1 ppm), following the same curve, until 0.3 equivalents of guest was reached. This suggests that H_a and H_b still had the same electronic environment during this part of the titration; hence the intramolecular H-bond may have been preserved. Beyond 0.3 equivalent of guest added, the signal of H_a and H_b splits. While the signal of H_b continued to go up field (+3 ppm at full complexation), the signal of H_a started to form a plateau (+1 ppm at full complexation). This phenomenon was dependant on the concentration of guest, indicating the existence of an equilibrium between two assemblies. The first one consisting of a 2:1 complex (host:guest) at low guest concentrations, and the second one of a 1:1 complex as more guest was present. The proposed mode of binding is depicted in (Scheme 51).



Scheme 51: Proposed mode of binding between receptors **17b**, **18a-b** and (*S*, *S_p*)-**21** upon addition of acetate **49**

As the binding was too strong under these conditions,¹⁰⁶ the binding constant with the mono-functional receptors could not be determined by ¹H NMR, nor could be the binding constant with (*S*, *S_p*)-**21**, due to its peculiar behaviour.

➤ **H-bonding study with guest (*S*)-2-phenylbutyrate**

The H-bonding study with guest (*S*)-2-phenylbutyrate **50** was undertaken with receptors **18a** and (*S*, *S_p*)-**21**. The chemical shift variation of protons H_a (full lines) and H_b (dashed lines) upon addition of carboxylate is shown in Figure 49.

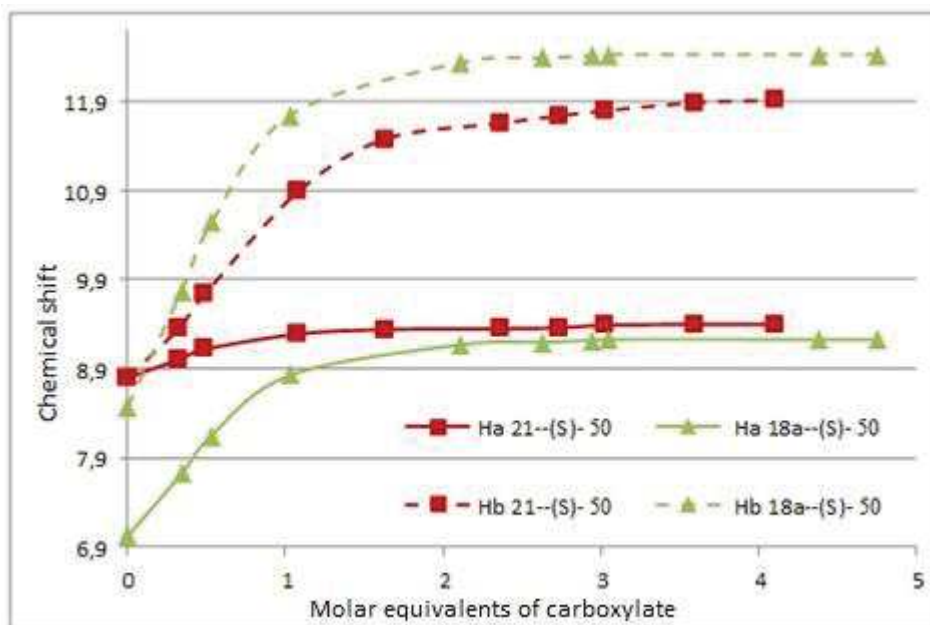
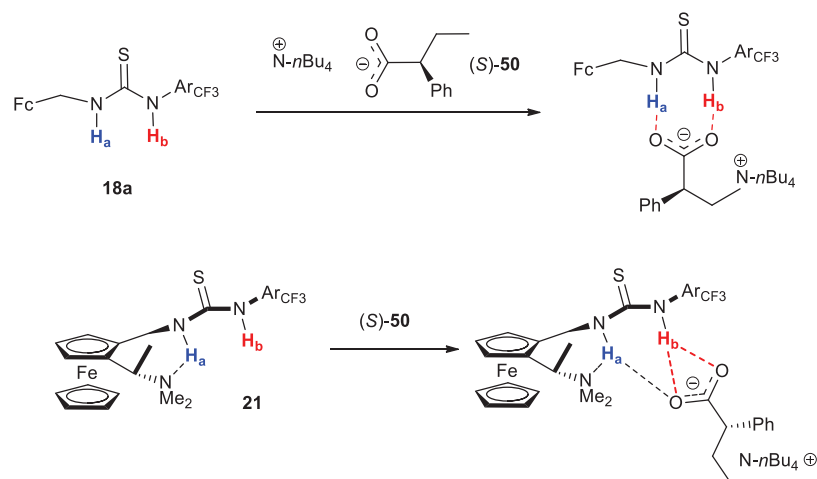


Figure 49: Chemical shift of protons H_a and H_b of **18a** and **21** (5 mM in CD₃CN) upon addition of carboxylate **50**. The peak of proton H_a of (*S*, *S*_p)-**21** was very broad

As with the guest acetate, **18a** (green lines) was fully complexed after one equivalent of added carboxylate, with again a strong binding observed, and a variation in chemical shift of 2.2 ppm and 4.5 ppm for H_a and H_b respectively. Bi-functional receptor (*S*, *S*_p)-**21** (red lines) showed a different behaviour than with acetate, as the signal of protons H_a and H_b split into two distinct signals directly after the first addition of carboxylate. The chemical shift of H_a varied very little upon addition of guest **50** (+0.6 ppm), suggesting a continuous H-binding with NMe₂ (intramolecular) and / or CO₂⁻ (intermolecular). The proposed mode of binding is thought to be a 1:1 complex as for the other receptors (Scheme 52).



Scheme 52: Proposed mode of binding between receptors **18a** and (*S*, *S_p*)-**21** upon addition of carboxylate **50**

The binding constant between (*S*, *S_p*)-**21** and **50** could be determined by following the signal of H_b as $K_{Hb\ 21-75} = 1.2 \times 10^3 \pm 0.1\ M^{-1}$ at room temperature using the program WinEqNMR.¹⁰⁷

➤ H-bonding study with guest mandelate

Further H-bonding studies were carried out with thiourea **18a** and bi-functional thiourea (*S*, *S_p*)-**21** with each of the enantiomers of mandelate **51**. The chemical shift variation of protons H_a and H_b upon addition of carboxylate is shown in Figure 50.

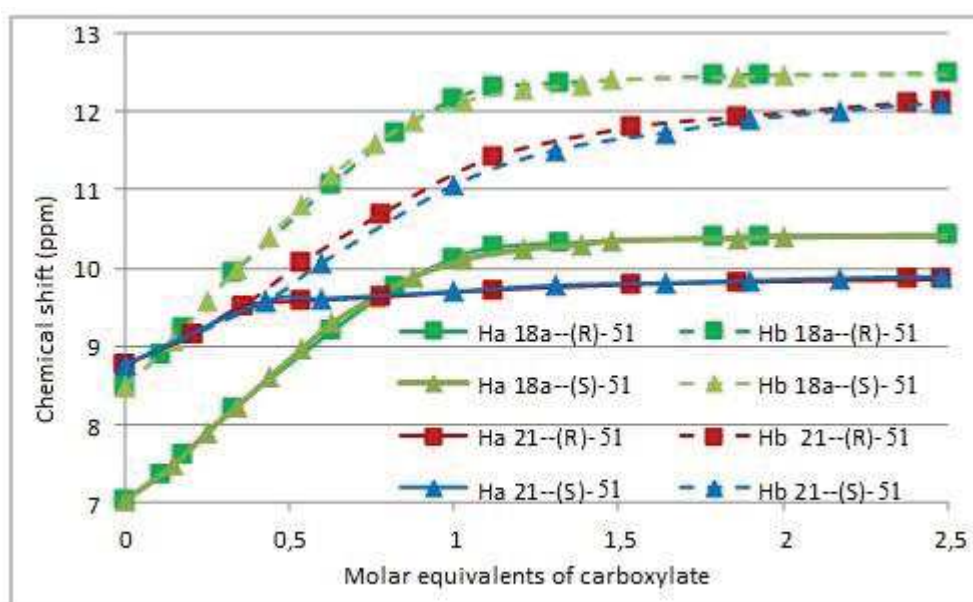
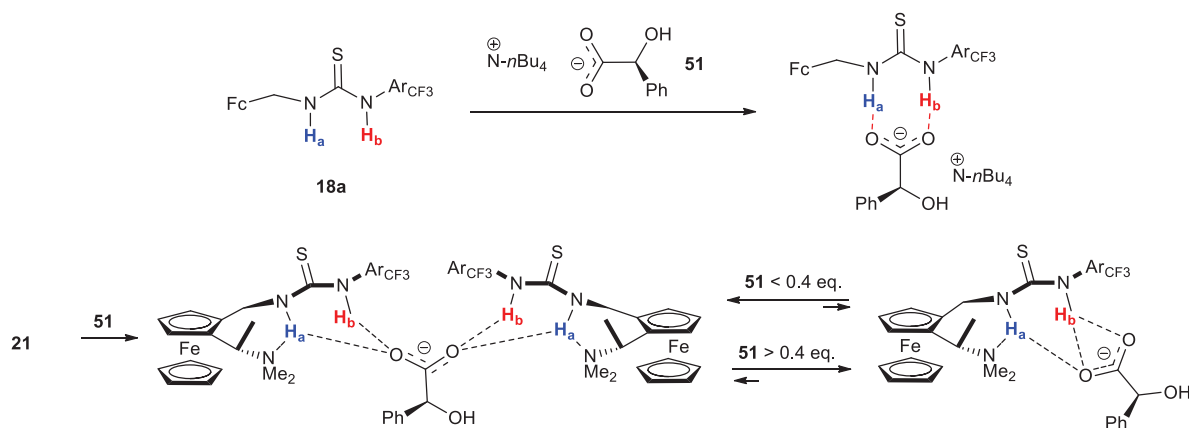


Figure 50: Chemical shift of protons H_a and H_b of **18a** and (*S*, *S_p*)-**21** (5 mM in CD_3CN) upon addition of carboxylate (*R*)- and (*S*)-**51**

Mono-functional receptor **18a** was fully bound after the addition of one equivalent of guest **51**, with a variation in chemical shift of 3.4 and 4 ppm for H_a and H_b respectively. As in the case of the receptor (*S*, *S*_p)-**21** and acetate guest **49**, a similar type of curve was obtained with (*S*, *S*_p)-**21** and butyrate guest **51** (both enantiomers). Protons H_a and H_b had the same variation of chemical shift until 0.4 equivalent of guest was reached, then their signal split into two signals. The associated binding constant could be determined with the signal of H_b as $K_{\text{Hb } 21-76} = 1.5 \times 10^3 \pm 0.1 \text{ M}^{-1}$ at room temperature using the program WinEqNMR.¹⁰⁷ The proposed mode of binding for **18a** and (*S*, *S*_p)-**21** to carboxylate **51** (both enantiomers) is depicted in Scheme 53.



Scheme 53: Proposed mode of binding of receptors **18a** and (*S*, *S*_p)-**21** upon addition of (*R*)- and (*S*)-mandelate **51**

3.2.3. Application of Fc-(thio)urea in organocatalysis

A summary of the different (thio)urea catalysts prepared is depicted in Figure 51.

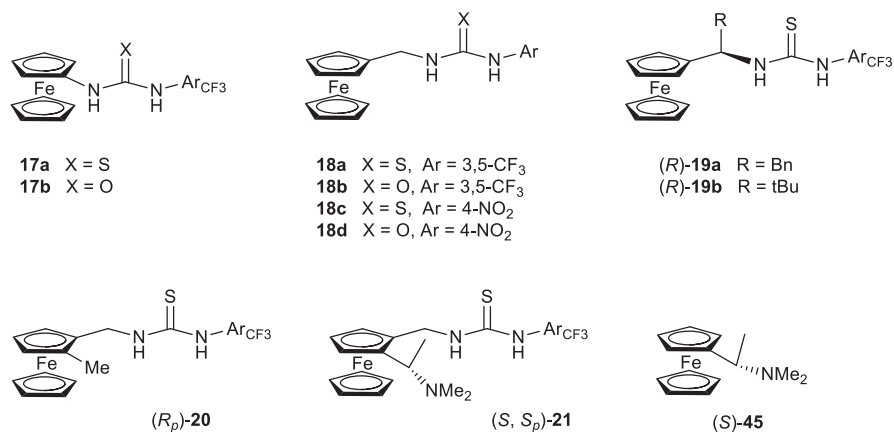
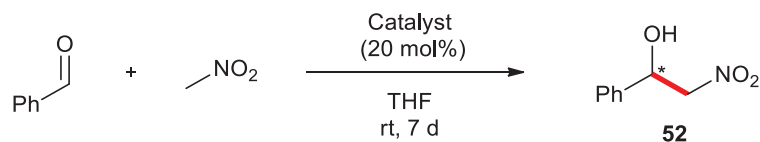


Figure 51: Ferrocenyl (thio)urea prepared to be tested as organocatalysts

These were examined in standard organocatalysed reactions (the Henry and the MBH reactions with every catalysts) and in more complex reactions (enamine co-catalysis and double Michael cycloaddition with catalyst **21** exclusively) in order to investigate their performance in different reactions.

3.2.3.1. The Henry reaction

The Henry reaction was carried out on benzaldehyde and nitromethane in THF with 20 mol% of HBD catalyst and DABCO (in the case of bi-functional catalyst (*S, S_p*)-**21** DABCO was omitted) at room temperature for seven days (Scheme 54).



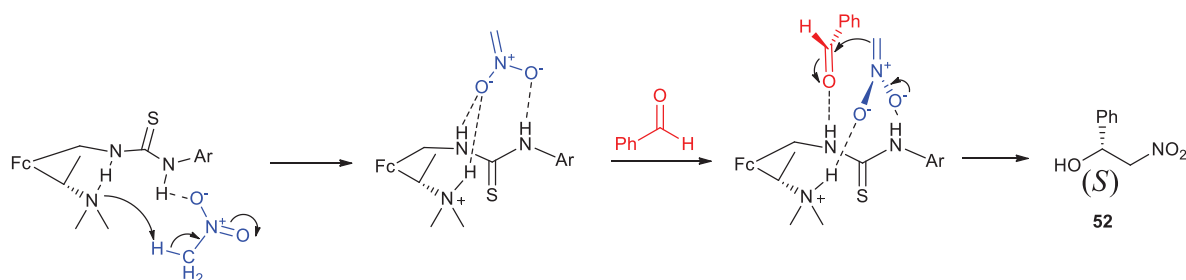
Scheme 54: Organocatalysed Henry reaction between benzaldehyde and nitromethane

Entry	Catalyst	Yield 52	Ee (%)
1	DABCO	84	-
2	18a + DABCO	55	-
3	19a + DABCO	96	0
4	19b + DABCO	78	0
5	20 + DABCO	92	0
6	21	63	10
7	18a + 21	82	0
8	18a	0	-
9	45	81	0
10	18a + 45	66	0
11	20 + 45	22	0

Table 7: Henry reaction between nitromethane and benzaldehyde. Each catalyst was loaded at 20 mol%. Ee determined by chiral HPLC: OD column, 20% IPA in hexane, 1 mL/min, monitored at 220 nm. Rt = 9.8 min and 12.0 min

As a base alone can catalyse the Henry reaction, a control reaction was first realised with DABCO as the sole catalyst (Table 7, Entry 1). This indicated the level of background reaction between the nitronate and the aldehyde without HBD assistance. When DABCO was used in combination with achiral thiourea **18a**, the reaction was less efficient (Table 7, Entries 1 vs 2). Such an outcome might be explained by invoking a strong affinity between the thiourea and one of the reaction intermediates, which may prevent the ammonium from transferring its proton to the product, hence slowing down the normal course of the reaction. Central chiral containing thiourea **19a** and planar chiral containing thiourea **20** effectively promoted the Henry reaction although no enantioselectivity was observed (Table 7, Entries 3 and 5). Thiourea **19b** did not enhance nor decreased the activity of DABCO as a similar yield was obtained (Table 7, Entry 4), and again no enantiomeric excess was observed. Tertiary amine **45** showed similar activity to DABCO (Table 7, Entries 9 and 10), indicating a sufficient basicity

for the deprotonation of nitromethane. Comparatively, bi-functional catalyst (*S, S_p*)-**21** was able to perform the reaction however in lower yield (Table 7, Entry 6), probably due to the unavailability of its basic amine (assumedly already engaged in intramolecular H-bonding).¹⁰³ Nevertheless, a small preference for the (*S*) enantiomer was observed, indicating some level of organisation. A model providing the (*S*) product is shown in Scheme 55. It relies on the steric hindrance of the methyl to orient the approaching aldehyde.

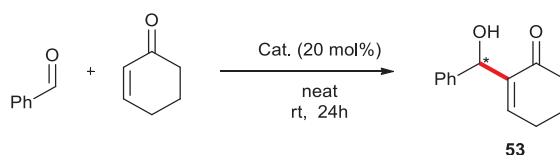


Scheme 55: Proposed mechanism for the Henry reaction catalysed by (*S, S_p*)-**21** giving (*S*)-**52**

However only 10% ee was obtained, which suggest that the background reaction between the nitronate and the aldehyde (without HBD assistance) may happen at a similar rate, so the product is not exclusively produced via catalyst assistance. The combination of **18a** and (*S, S_p*)-**21** was more productive than **18a** and DABCO or (*S, S_p*)-**21** alone or **18a** and tertiary amine (*S*)-**45**, probably due to the higher amount of HBD (Table 7, Entry 7 vs 2, 6 and 10). However it resulted in a complete loss of enantioselectivity compared to (*S, S_p*)-**21** used alone suggesting an unorganised structure during the C-C bond formation. In the absence of substantial ee further studies were undertaken in reactions where the background reactivity is less competitive.

3.2.3.2. The MBH reaction

The Morita-Baylis-Hillman reaction was tested with benzaldehyde and cyclohexenone in presence of 20 mol% of HBD catalyst and DABCO (except in the case of bi-functional catalyst **21**) without solvent. The reaction was carried out for 24 h at room temperature (Scheme 56).



Scheme 56: Organocatalysed MBH reaction between benzaldehyde and cyclohexenone

Entry	Catalyst	Yield 53 (7d)	Ee (%)
1	DABCO	0	-
2	18a	0	-
3	18a + DABCO	49 (79)	-
4	18b + DABCO	37 (56)	-
5	18c + DABCO	48 (72)	-
6	18d + DABCO	34 (58)	-
7	19a + DABCO	16	0
8	19b + DABCO	20	0
9	20 + DABCO	35	0
10	17a + DABCO	11	-
11	17b + DABCO	18	-
12	21	0	-
13	21 + DABCO	0	-
14	18a + 21	0	-
15	18a + 45	<5	-

Table 8: MBH reaction between cyclohexenone and benzaldehyde. Ee determined by chiral HPLC:

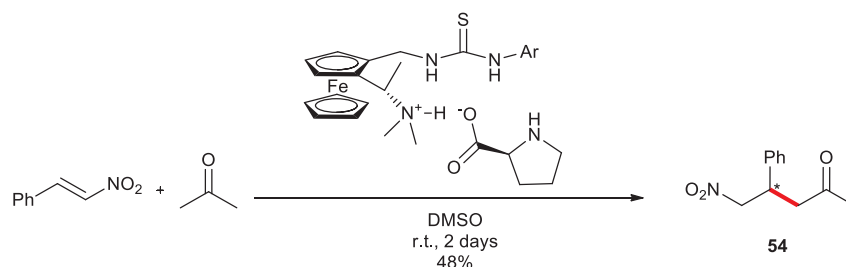
OD column, 10% IPA in hexane, 1mL/min, monitored at 220 nm. Rt = 11.1 min and 12.3 min

Control reactions with DABCO or HBD **18a** alone showed no conversion of the starting material (Table 8, Entries 1 and 2), only their combination promoted the transformation (Table 8, Entry 3), indicating the absence of background reactivity. In contrast with thioureas **18a** and **18c**, lower catalytic activities were observed with urea **18b** and **18d** (Table 8, Entries 3 vs 4 and 5 vs 6), while the substitution of the aromatic ring (3,5-CF₃ or 4-NO₂) did not have such a

significant effect (Table 8, Entries 3 vs 5 and 4 vs 6). Introducing elements of chirality with catalysts **19a,b** and **20** led to less efficient transformations and no enantiomeric excess, with no obvious correlation between the yield and the steric hindrance brought by the chiral elements (Table 8, Entries 7-9). The lack of enantioselectivity may be attributed to their remote location relative to the reaction site. Superior catalytic activity of catalyst **18a** was observed over catalysts **17a-b** (Table 8, Entries 2, 10 and 11), when the HBD moiety is connected to the ferrocene by one carbon linker instead of none. Whether used alone or in combination with DABCO, bi-functional thiourea **21** was inactive in this reaction (Table 8, Entries 12 and 13), suggesting the inability of its HBD unit to provide sufficient level of complexation and activation of the substrate. These observations may support the hypothesis of an intramolecular H-bond between the thiourea and the tertiary amine, rendering the thiourea less available for intermolecular H-bonding. Furthermore, when **18a** and **21** or **18a** and **45** were used, no conversion was observed (Table 8, Entries 14 and 15). This suggests the non-nucleophilicity of the tertiary amine, probably due to steric reasons.

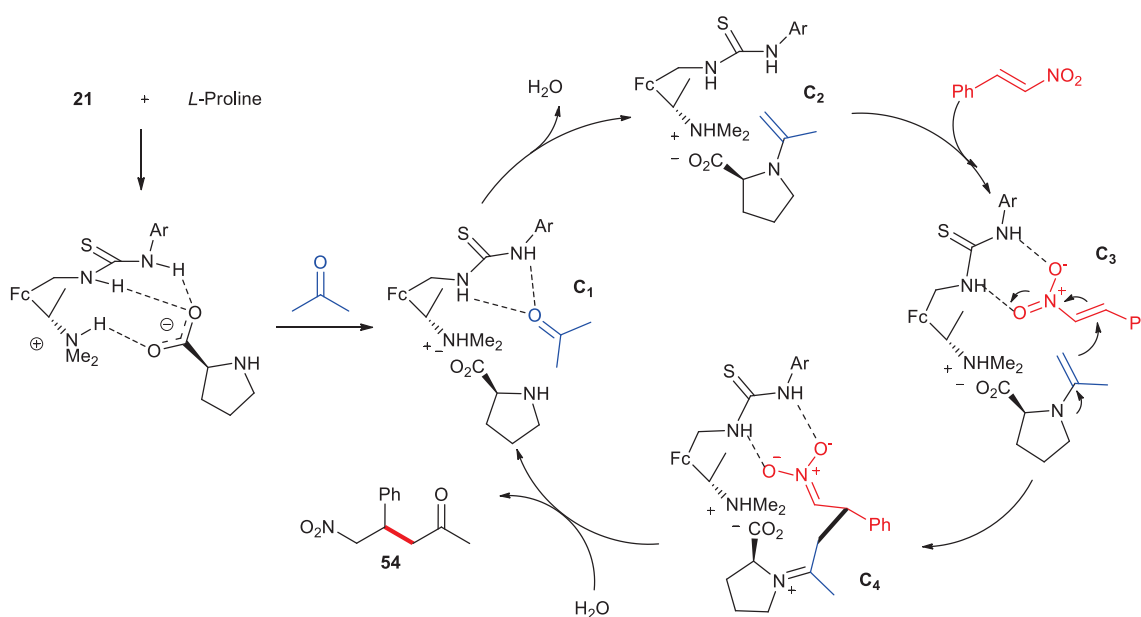
3.2.3.3. HBD / Enamine catalysis

Bi-functional catalyst **21** and *L*-proline were combined in DMSO, allowing for the two to self-assemble via acid/base proton exchange, prior to adding acetone and *trans*- β -nitrostyrene in the reaction mixture (Scheme 57).



Scheme 57: Ionic proline-thiourea catalyst for the addition of acetone to *trans*- β -nitrostyrene

After 2 days at room temperature, product **54** was obtained in 48% yield. Comparatively, when *L*-proline was used as the sole catalyst, only a trace amount of the product was detected.

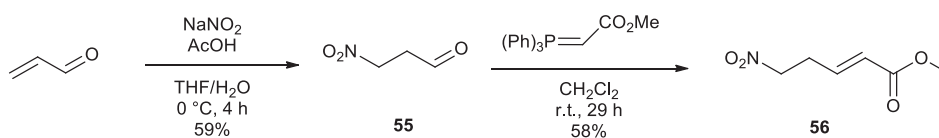


Scheme 58: Proposed mechanism for the addition of acetone to *trans*- β -nitrostyrene

The proposed mode of action (Scheme 58) requires the ionic assembly of *L*-proline and catalyst **21** as starting point, followed by condensation of acetone and *L*-proline to form enamine **C2**. As *trans*- β -nitrostyrene approaches, the nitro functionality would engage in H-bonding with the thiourea part of the assembly and would be presented to the enamine moiety, ideally in a stereocontrolled manner. Subsequent attack of the α -carbon of the enamine onto the α,β -unsaturated nitro and hydrolysis would then deliver the desired γ -nitro ketone **54**. Unfortunately, it was not possible to determine the enantiomeric excess with the chiral HPLC columns available.

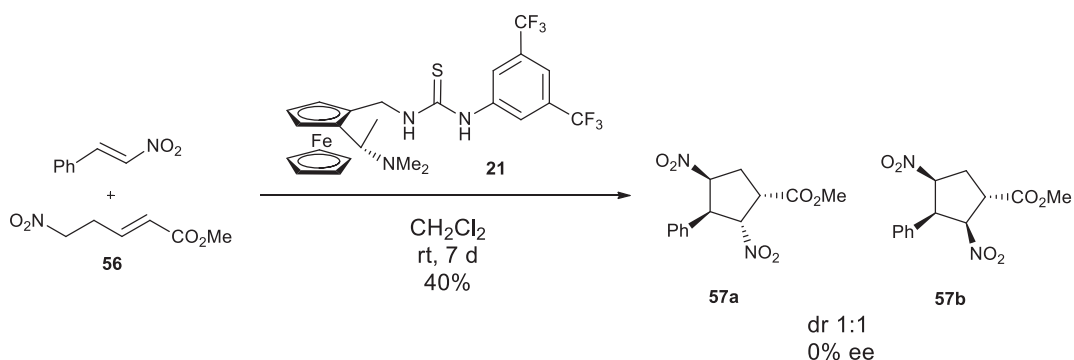
3.2.3.4. Formation of tetrasubstituted cyclopentane

The formation of a tetrasubstituted cyclopentane from *trans*- β -nitrostyrene and methyl-5-nitropent-2-enoate catalysed by bi-functional catalyst was investigated. Preparation of methyl-5-nitropent-2-enoate **56** required nitration of acrolein to **55** followed by a Wittig reaction with methyl-2-(triphenylphosphanylidene)acetate (Scheme 59).



Scheme 59: Preparation of substrate **56**

The catalysis reaction was carried out in dichloromethane at room temperature for 7 days at a concentration of 0.2 M (relative to **56**) and with 10 mol% of catalyst **21** (Scheme 60).



Scheme 60: Cycloaddition of *trans*- β -nitrostyrene and **56** catalysed by **21**

The isolation of the products was difficult by silica gel column chromatography; a single fraction containing two new products (**57a** and **57b**) along with unreacted substrate **56** was obtained. It is worthwhile to note that the reaction intermediate produced after the first C-C bond formation was not observed, similarly to the analogous tetrasubstituted cyclohexane formation reported by Cobb and co-workers.⁴⁷ Taken in a minimal amount of dichloromethane, a precipitate appeared upon addition of diethyl ether and was obtained as a white powder in a 9:1 ratio of diastereoisomers, as determined by HPLC (Figure 52).

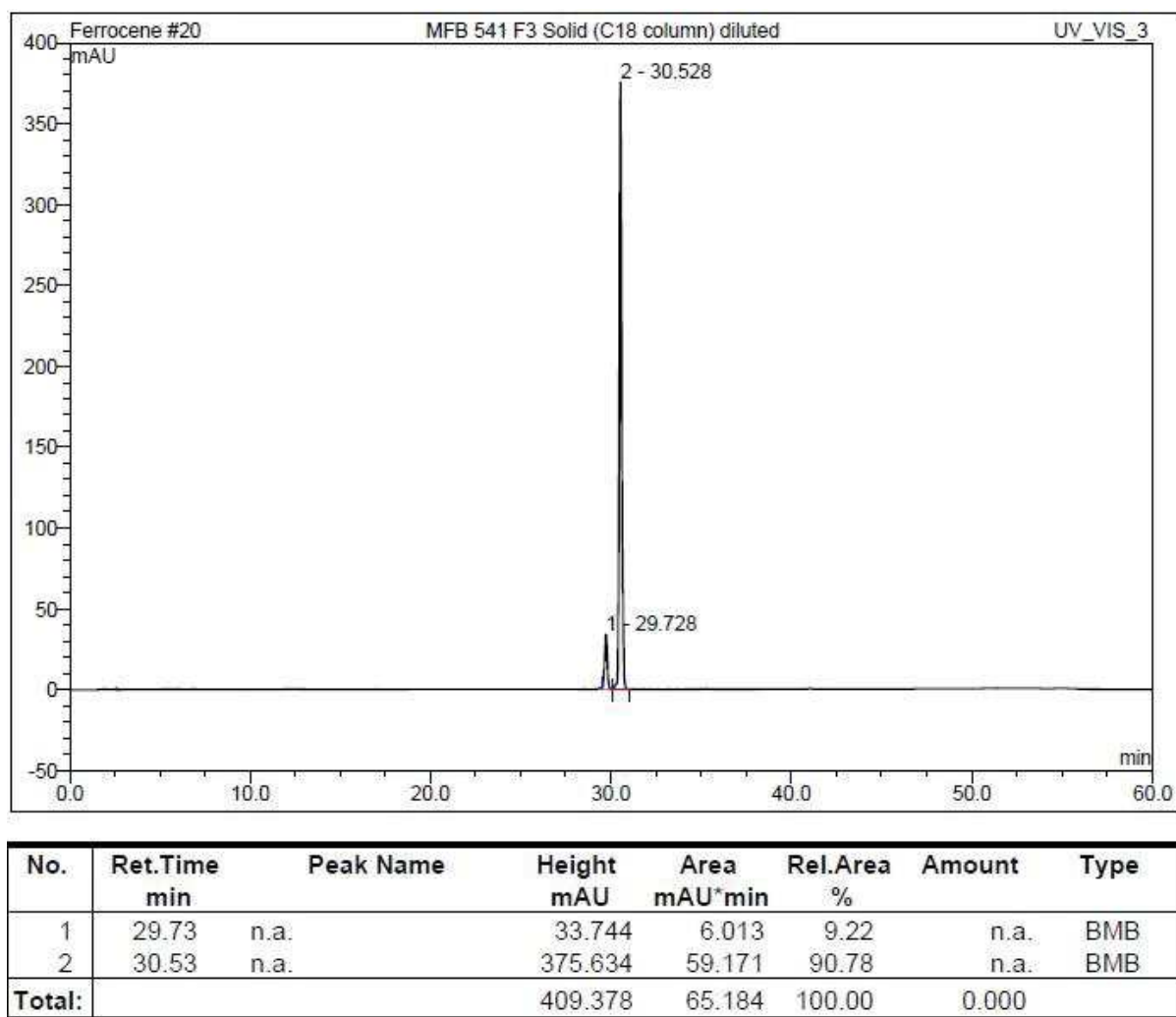


Figure 52: Analytical HPLC of the precipitated diastereoisomer **57a**. C18 column, MeCN/H₂O: 0/1 to 1/0, 1 mL.min⁻¹, monitored at 254 nm

NOE studies of the precipitate and the filtrate (containing **57a** and **57b**) resulted in the assignment of the relative stereochemistry of **57a** and **57b** (Figure 53).

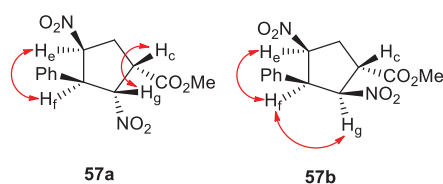
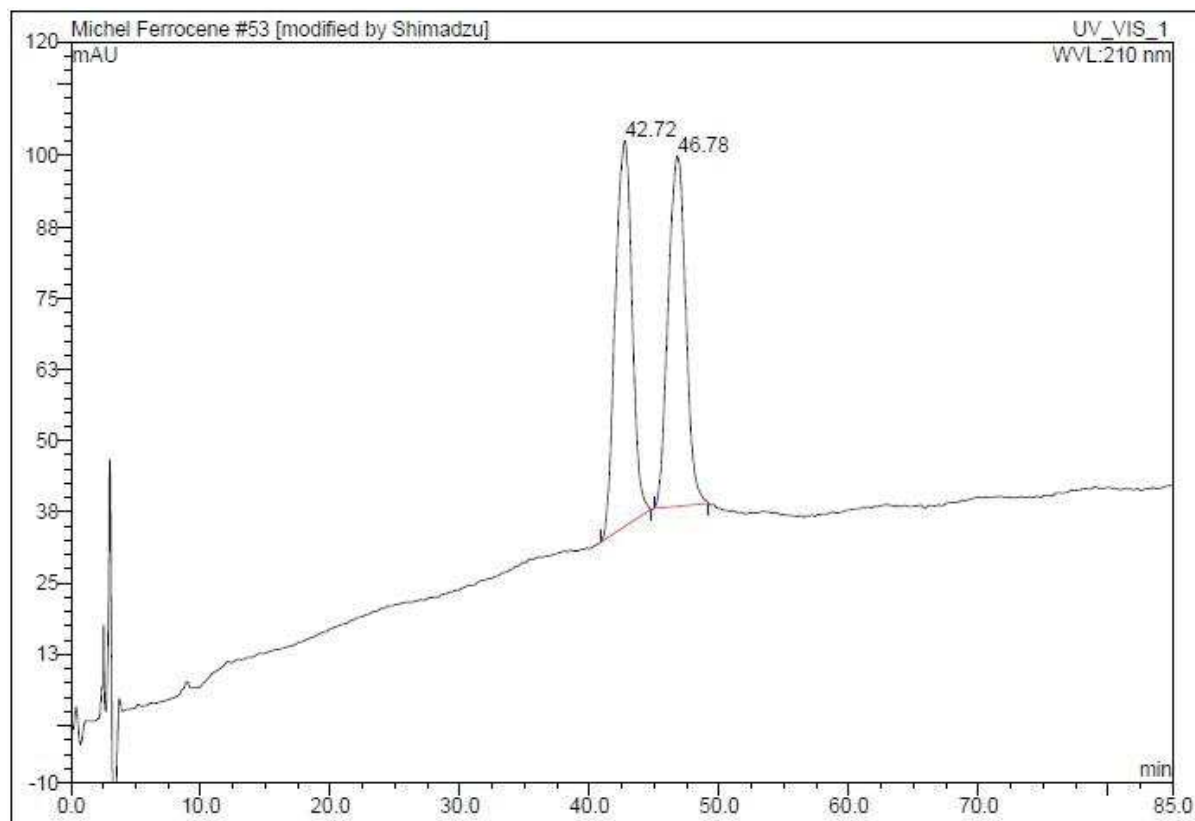


Figure 53: The two diastereoisomers of **57** at C₃

Product **57a** was assigned as the major diastereoisomer in the precipitate, and **57b** as the other diastereoisomer. For both diastereoisomers, protons H_e and H_f exhibited a strong correlation suggesting their *cis* configuration. While diastereoisomer **57b** showed one other strong

relationship between protons H_f and H_g, diastereoisomer **57a** exhibited a strong NoE effect between protons H_c and H_g, and a weak one between H_f and H_g. The precipitated material was purified by HPLC and pure **57a** was collected to be analysed by chiral HPLC, which revealed a racemic mixture of enantiomers (R_t = 43 and 47 min, Figure 54).

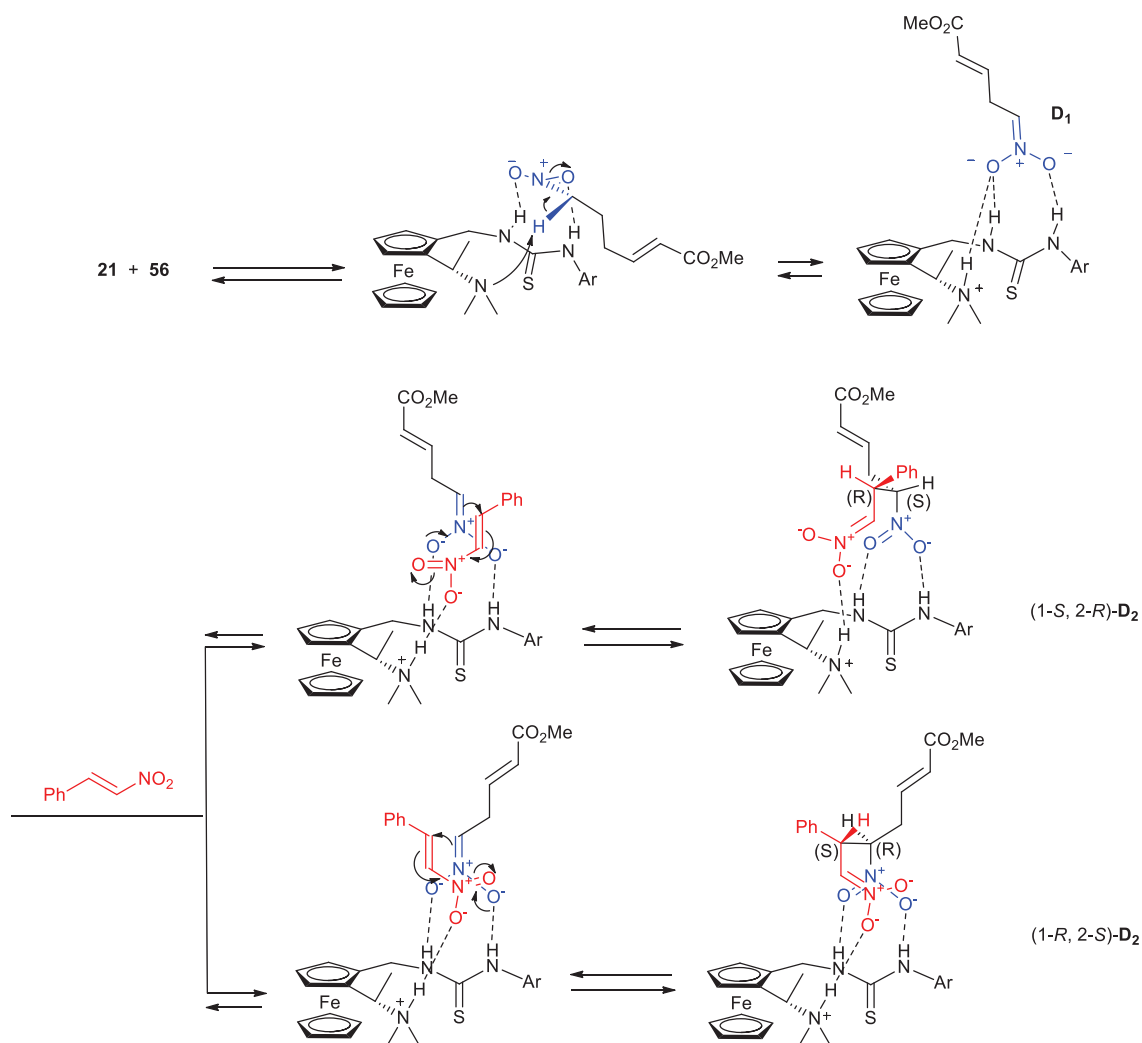


No.	Ret.Time min	Peak Name	Height mAU	Area mAU*min	Rel.Area %	Amount n.a.	Type
1	42.72	n.a.	67.709	101.939	51.27	n.a.	BMB*
2	46.78	n.a.	61.498	96.869	48.73	n.a.	BMB*
Total:			129.207	198.808	100.00	0.000	

Figure 54: Chiral HPLC of **57a**. Amylose 2 column, MeCN/H₂O: 30/70, 1 mL.min⁻¹, monitored at 210 nm

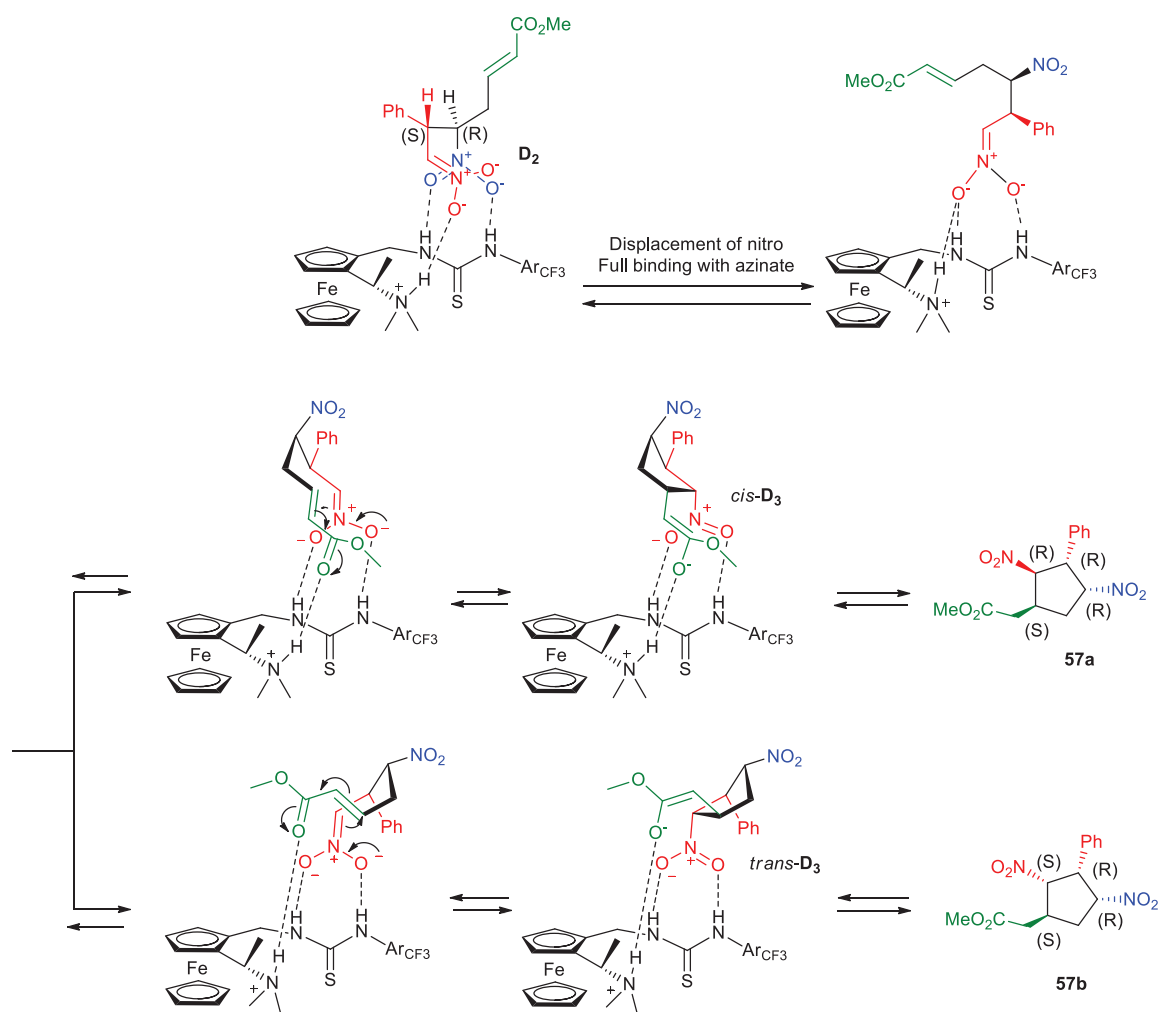
In order to rationalise the stereo-outcome of the catalysis, a mechanism is proposed in Scheme 61. After deprotonation of nitro compound **56**, the resulting methylenazinate **D**₁ (blue in Scheme 61) is stabilised by the thiourea unit while nitro-styrene (red in Scheme 61) binds to the newly formed ammonium cation in a manner that minimises the steric interactions. This favoured conformation leads diastereoselectively to the first nucleophilic attack giving

enantiomers (1-*S*, 2-*R*)-**D**₂ and (1-*R*, 2-*S*)-**D**₂, and setting the *cis* relationship between H_e and H_f in the future product.



Scheme 61: Proposed mechanism for the Michael addition of **56** onto *trans*- β -nitrostyrene forming intermediates azinate **D**₂

Upon displacement of the nitro group (blue in Scheme 62), the new azinate group in **D**₂ (red in Scheme 62) can be stabilised by three H-bonds, allowing for the free rotation of the rest of the molecule in order to bring the carbonyl of the enone ester (green in Scheme 62) towards the activating ammonium, initiating the nucleophilic cyclisation.



Scheme 62: Proposed mechanism for the cyclo-addition of (R, S) - D_2 forming cyclopentane (R, R, R, S) - $57a$ and (R, R, S, S) - $57b$. The same proposed mechanism is assumed for the transformation of the other enantiomer of D_2 (not depicted)

As there was no trace of protonated D_2 in the reaction mixture, the cyclisation seems to be a relatively fast process. Both cis and $trans$ conformations, relative to the azinate and enone ester prior to cyclisation, were favoured. Proton transfer from the ammonium to the produced enolates cis - and $trans$ - D_3 led to products $57a$ and $57b$. It was noteworthy the reaction did not take place when 3,3-dimethylprop-2-enal was used instead of $trans$ - β -nitrostyrene.

3.2.4. Boron-containing Fc thiourea

From the analysis of the Henry and MBH reactions, it appeared that the stereogenic elements in catalysts **19a-c** (Me, Bn and *t*-Bu) and **20** (Me) had no control over the enantioselectivity, presumably due to their distance from the reactive centre. In order to improve this, a new catalyst design was required. As a new strategy it was decided to act on the flexibility of the thiourea moiety by locking it in a well-defined position, coplanar with the connected Cp ring, utilizing the work of Smith²¹ and Mattson²² on boron activated ureas (Figure 55).

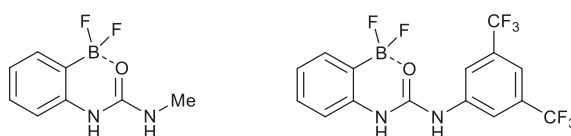


Figure 55: Boronate-urea HBD by Smith (left) and Matson (right)

Boronate-urea ferrocenes **58-61** and **62** (Figure 56) were to be synthesised, hoping that this new structure would bring more enantioselectivity in the test reactions.

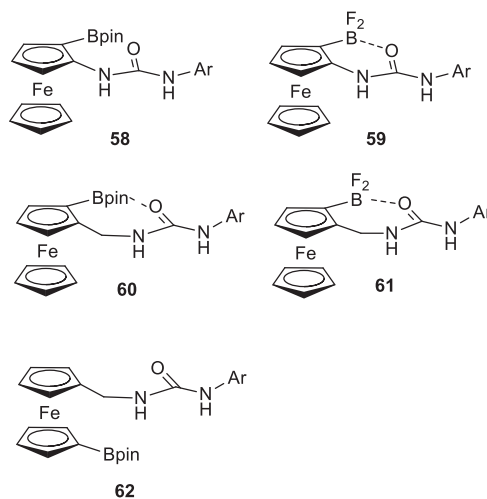


Figure 56: Structure of the different boronate-urea to be prepared

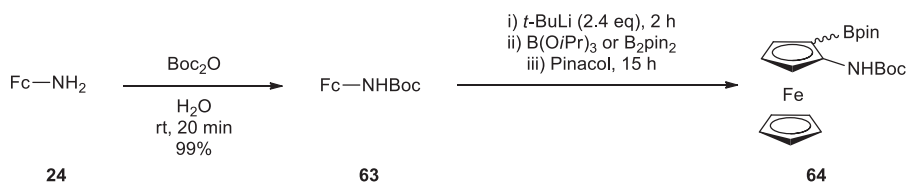
This design relies on the O-B interaction between the urea and the boronate, with the preparation of difluoroboronate species to greatly enhance this interaction compared with the pinacolboronate ester analogue. Along with the asymmetric preparations of these catalysts,

shorter racemic preparations were undertaken to assess their catalytic activity. Difficulties encountered during the synthesis prevented the completion of this study.

3.2.4.1. Preparation of 1-urea-2-boronate ferrocene

➤ Racemic synthesis

The racemic synthesis of catalysts **58** and **59** was based on the ortho-lithiation of *N*-Boc-ferroceneamine **63** (Scheme 63).¹⁰⁸ Compound **63** was quantitatively prepared from ferroceneamine **24** and Boc₂O in water.¹⁰⁹ The results of the lithiation of **63** with *t*-BuLi and quenching with boron pinacol to form **64** are summarised in Table 9.



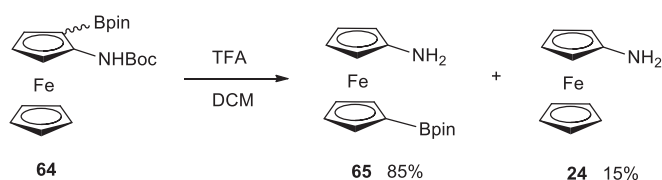
Scheme 63: Preparation of disubstituted ferrocene **64**

Entry	Solvent	i) T (°C)	Boron	ii) T (°C)	Product
1	THF	-78 to -20	B(O <i>i</i> Pr) ₃	-20 to rt	18%
2	THF	-78 to -20	B ₂ pin ₂	-20 to rt	SM
3	THF	-78	B(O <i>i</i> Pr) ₃	-78 to rt	SM
4	THF/Et ₂ O	-78 to -20	B(O <i>i</i> Pr) ₃	-20 to rt	Complex mixture
5	THF/Et ₂ O	-78 to -20	B ₂ pin ₂	-20 to rt	Complex mixture

Table 9: Study of the ortho-lithiation of **63** leading to di-substituted ferrocene **64**

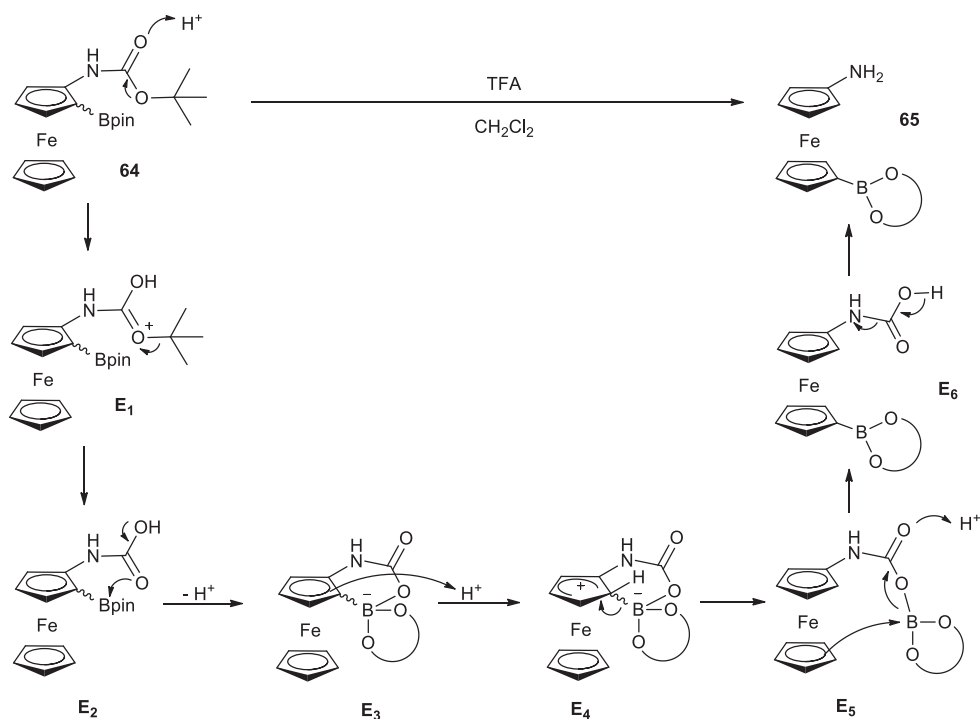
Product **64** was obtained in 18% yield when the lithiation was conducted in THF at -20 °C for 2 h and boron triisopropoxide was the electrophile (Table 9, Entry 1). The use of bis(pinacolato) diboron as electrophile was unsuccessful (Table 9, Entry 2) and deprotonation of ferrocene **63** at -78 °C did not occur (Table 9, Entry 3). When the solvent system was THF/Et₂O, a complex mixture of di- (**64**) and 1,1'-substituted ferrocene was obtained (Table 9, Entry 4 and 5). ¹³C NMR of **64** (and of other boronate ferrocene) did not show the carbon connected to the boron, due to the magnetic interaction with the boron nuclei provoking the fast relaxation of the

carbon.^{54b} ^{11}B NMR ($\delta = 15.1$ ppm, broad signal, ref: $\text{B}(\text{O}i\text{-Pr})_3$ in CDCl_3) indicated the trigonal nature of the boronate; hence an absence of interaction between the boron and the oxygen of the carbamate.¹¹⁰ Subsequent deprotection of Boc-protected amine **64** with TFA led unexpectedly to 1,1'-substituted ferrocene **65** and amine **24** (Scheme 64).



Scheme 64: TFA deprotection of Boc-protected amine **64**. NMR yield estimation

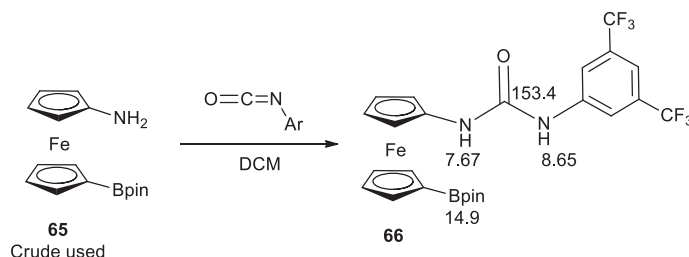
An important change in colour just after the addition of TFA, from orange to dark green then orange again after 10 minutes, happened during the reaction. An attempt to explain this surprising outcome is depicted in Scheme 65.



Scheme 65: Suggested mechanism for the transformation of **64** to **65**

The proposed mechanism involves the expected first steps of a TFA *N*-Boc deprotection, leading to carbamic acid **E2** by loss of *t*-butyl cation. Subsequent nucleophilic attack of the

oxygen onto the boron may give spiro-boronate **E**₃. Protonation of the Cp ring can form intermediate **E**₄, which rearomatises to compound **E**₅ by cleavage of the C-B bond. The unsubstituted Cp ring, being more electron rich and at better distance than the substituted Cp ring, can then react in a Friedel-Crafts fashion on the electron-poor boron to produce the 1,1'-bis-substituted ferrocene **E**₆. Decarboxylation of **E**₆ generates product **65**.

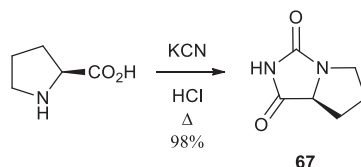


Scheme 66: Formation of bis substituted ferrocene **56**. Relevant NMR chemical shifts (ppm) of ¹H, ¹³C and ¹¹B are indicated

Subjecting amine **65** to 3,5-bis(trifluoromethyl)phenyl-isocyanate in dichloromethane afforded urea **66** in 63% yield (Scheme 66) from the protected amine **63**. Analysis of **66** (¹H, ¹³C and ¹¹B NMR) showed no evidence of interaction between the urea and the pinacol boron ester.^{21a} The chemical shift of the NH protons and C=O carbon were similar to those of the non-borated analogue ferrocene thiourea **17b** ($\delta = 7.68$ and 8.53 ppm for H_a and H_b respectively, and 153.5 ppm for the carbonyl). The boron NMR of **66** confirmed the trigonal geometry of the boron atom ($\delta = 15.1$ ppm, ref: B(O*i*-Pr)₃ in CDCl₃).

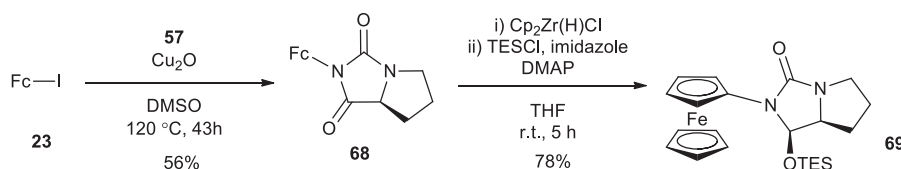
➤ Asymmetric synthesis

Until very recently, no chiral auxiliary for aminoferrocene had been reported. Metallinos and co-workers developed in 2012 the first example of chiral directing group for *N*-substituted ferrocene.¹¹¹ Following their procedure, the straightforward preparation of *L*-proline hydantoin **67** was carried out by heating *L*-proline and potassium cyanide in 6 N HCl (Scheme 67).



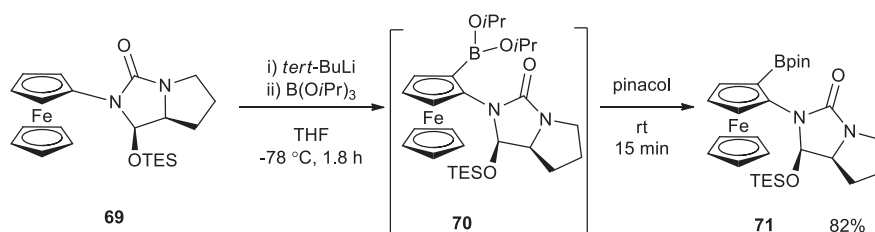
Scheme 67: Preparation of *L*-proline hydantoin **67**

The copper catalysed reaction of **67** with iodoferrocene **23** afforded compound **68** in 56% yield (Scheme 68). Relying on the selective reduction of amide before urea type carbonyls, compound **68** was subjected to Schwartz's reagent ($\text{Cp}_2\text{Zr}(\text{H})\text{Cl}$), followed by treatment with triethylsilylchloride. The chiral environment provided by the hydantoin moiety afforded only one diastereoisomer of the key compound **69**.



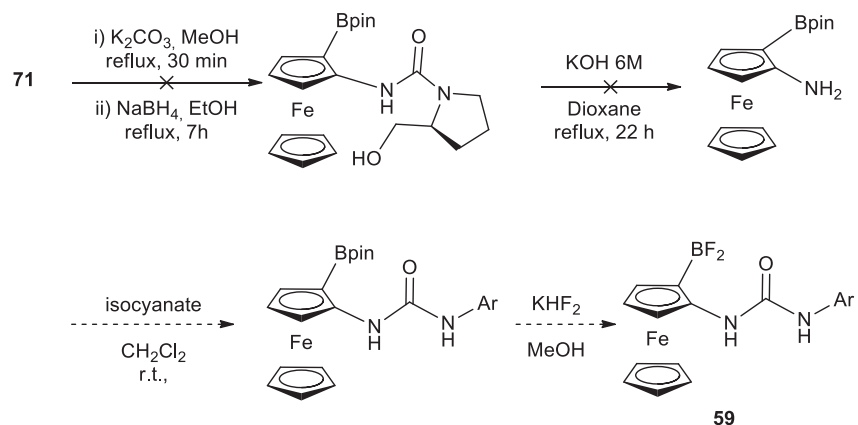
Scheme 68: Preparation of key intermediate **69**

Diastereoselective ortho-lithiation of **69** with *t*-BuLi at $-78\text{ }^\circ\text{C}$ and quenching with boron triisopropoxide led to boronic isopropyl ester **70**, which was directly esterified with pinacol to compound **71** in high yield (Scheme 69).



Scheme 69: Diastereoselective ortho-lithiation of **69** leading to di-substituted ferrocene **71**

Unfortunately, the synthesis towards the preparation of urea **59** stopped at that point as the required deprotection conditions were not efficient in the case of compound **71** (Scheme 70). Starting material was mostly recovered along with some degradation product.

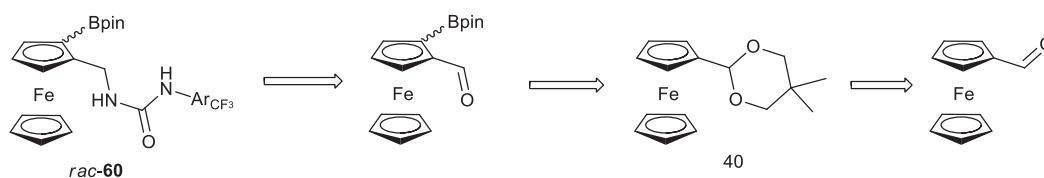


Scheme 70: Unsuccessful cleavage of the chiral auxiliary in the preparation of urea **59**

3.2.4.2. Preparation of 1-methyleneurea-2-boronate ferrocene

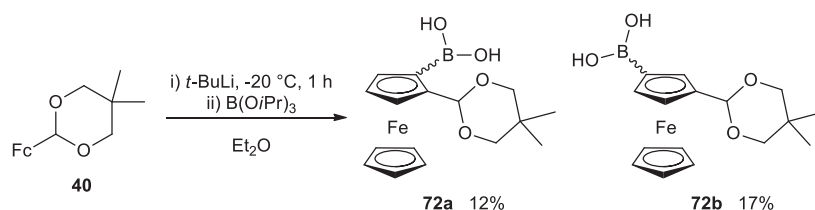
➤ Racemic preparation

The preparation of di-substituted boronate-urea ferrocene **60** was attempted via the lithiation of ferrocenyl dioxolane **40** (Scheme 71).



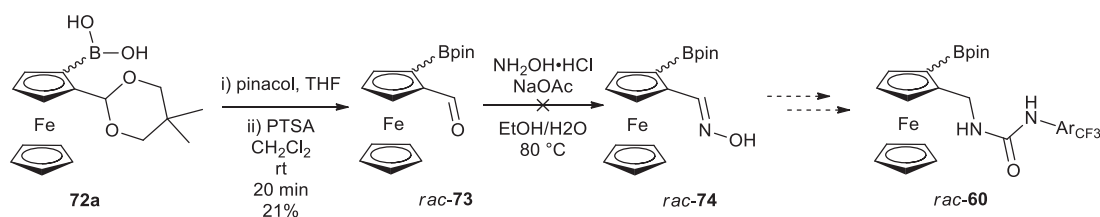
Scheme 71: Retro-synthesis of boronate-urea **60**

Lithiation of dioxolane **40** by *t*-BuLi in Et_2O and quenching with $B(Oi-Pr)_3$ resulted in a poor yield of *ortho*- and *meta*-lithiated species leading to compounds **72a** and **72b** respectively (Scheme 72).



Scheme 72: Lithiation of dioxolane **40**

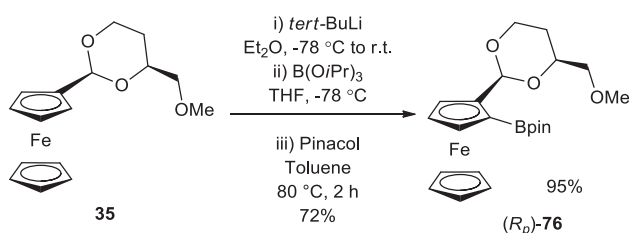
Reactions in THF or at lower temperature failed to improve this yield. Addition of pinacol to **72a** in THF gave the desired boron pinacol ester analogue, which was deprotected with PTSA to yield aldehyde *rac*-**73** (Scheme 73). Subjection to hydroxylamine hydrogen chloride in hot ethanol/water mix and in the presence of sodium acetate did not offer the expected ferrocene oxime *rac*-**74**.



Scheme 73: Unsuccessful synthesis towards di-substituted boronate-urea ferrocene *rac*-**60**

➤ Asymmetric synthesis

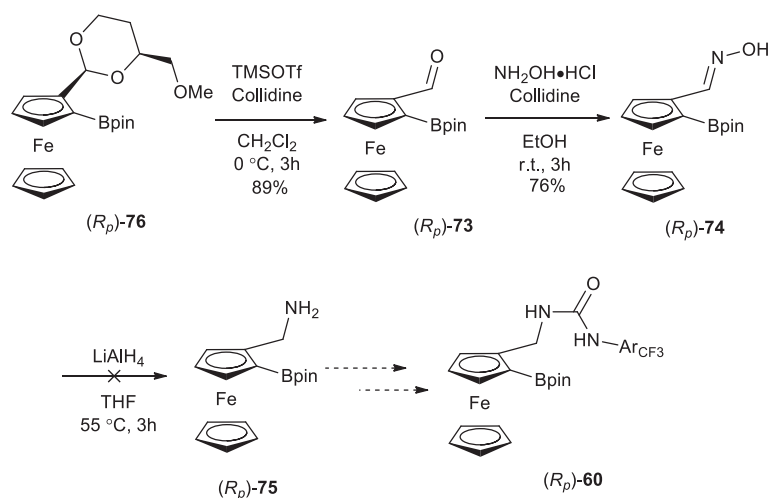
As for compound **20** the planar chirality was introduced via compound **35**, quenching the resulting ortho-lithiated ferrocene with tri-isopropoxide boron, thus obtaining the non-racemic boronic acid which was almost quantitatively converted to boronic pinacol ester **76** by reacting it with pinacol in hot toluene for 2 h (Scheme 74).



Scheme 74: Ortho-lithiation of dioxolane **35** to form (*R_p*)-**76**

The chiral auxiliary was removed using trimethylsilyltriflate and 2,4,6-collidine followed by aqueous quenching to offer the aldehyde (*R_p*)-**73** in 89% yield (Scheme 75).¹¹² Another deprotection method was attempted with PTSA but the yields were generally lower with some degradation occurring. The aldehyde was then transformed into aldoxime (*R_p*)-**74** in 76% yield

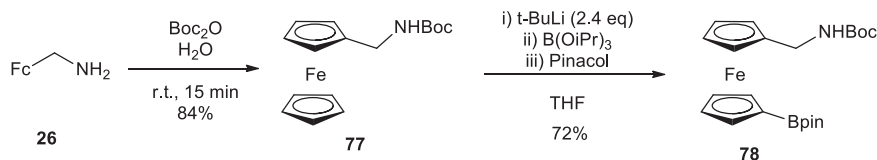
by a modified procedure using 2,4,6-collidine instead of potassium carbonate and keeping the reaction at room temperature. The reduction of aldoxime (R_p)-74 to primary amine (R_p)-75 was tried unsuccessfully with lithium aluminium hydride. Different temperature, concentration, stoichiometry and reaction time were investigated but none of them produced the desired amine, although the starting aldoxime was fully consumed and more polar product(s) appeared (TLC).



Scheme 75: Unsuccessful synthesis towards di-substituted boronate-urea ferrocene (R_p)-60

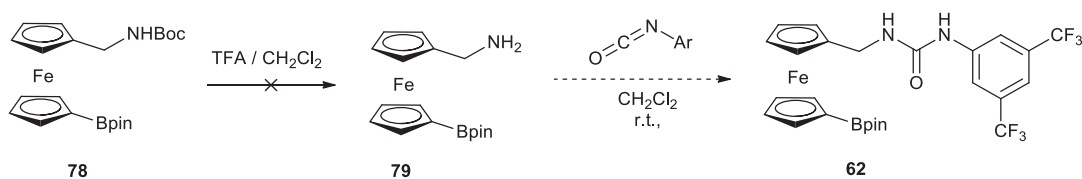
3.2.4.3. Synthesis of 1-methyleneurea-1'-boronate ferrocene

The preparation of 1,1'-heterobis-substituted ferrocene **78** relied on the selective 1'-lithiation of *NH*-Boc protected ferrocene **77** (Scheme 76).¹¹³ The latter was easily prepared from amine **26** and Boc_2O in water.¹¹⁴ Subsequent 1'-lithiation by *t*-BuLi and quenching by triisopropoxide boron gave the resulting boronic acid which was directly esterified by pinacol to offer compound **78** in good yield.



Scheme 76: Preparation of 1,1'-heterobis-substituted ferrocene **78** from amine **26**

Unfortunately, in the presence of TFA compound **78** did not yield the desired amine **79** but only the starting material (Scheme 77).



Scheme 77: Unsuccessful attempt to prepare 1,1'-bis-substituted boronate-urea ferrocene **62**

3.3. Conclusions and future work

New ferrocene (thio)ureas have been synthesised, with a number of structural differences including 1) no linker between Fc and the (thio)urea (**17a,b**) or with a methylene linker (**18a-d**), 2) with central chirality on the methylene linker (**19a,b**) or with planar chirality on the ferrocene (**20**), and 3) both chiralities within bi-functional structure **21**. The latter is suspected of developing an intramolecular H-bond between NH of the thiourea and the tertiary amine forming a seven-membered ring. A study of the H-bonding complexation properties between (thio)urea receptors (**17b**, **18a,b** and **21**) and tetrabutylammonium carboxylates (**49**, **50**, **51**) in acetonitrile was carried out by ^1H NMR spectroscopy. Simple achiral receptors **17b** and **18a,b** exhibited full complexation after the addition of one equivalent of guest, indicative of a large binding constant ($K > 10^3 \text{ M}^{-1}$). Bi-functional receptor **21** had slightly lower levels of H-bonding to carboxylates ($K \approx 10^3 \text{ M}^{-1}$), and showed further signs of an intramolecular H-bonding interaction. The binding curves between host **21** and mandelate guests (*R*)- and (*S*)-**76** were identical, indicative of no enantioselectivity. Studies regarding the organocatalytic

properties of ferrocene (thio)ureas **17-21**, in the Henry and the Morita-Baylis-Hillman reactions, showed varying degrees of success in these transformations. The transfer of chirality from the catalyst to the product was mostly inefficient, with only catalyst **21** showing any sign of enantioselectivity in the Henry reaction. The proline-catalysed addition of acetone onto nitrostyrene, co-catalysed by thiourea **21**, was achieved with a moderate yield. The formation of tetrasubstituted cyclopentane via double Michael addition was undertaken with thiourea **21** in a moderate yield but with no enantioselectivity. Finally, the synthesis towards the preparation of planar chiral ferrocene boronate-ureas was presented. Future work would involve the completion of the ferrocene boronate-ureas synthesis, to ultimately assess whether this design would allow for an increased activity and more importantly, an increased enantioselectivity. Further design could lead to more constrained structures, in which the catalytic site is closer to the chiral elements (Figure 57 and Scheme 78).

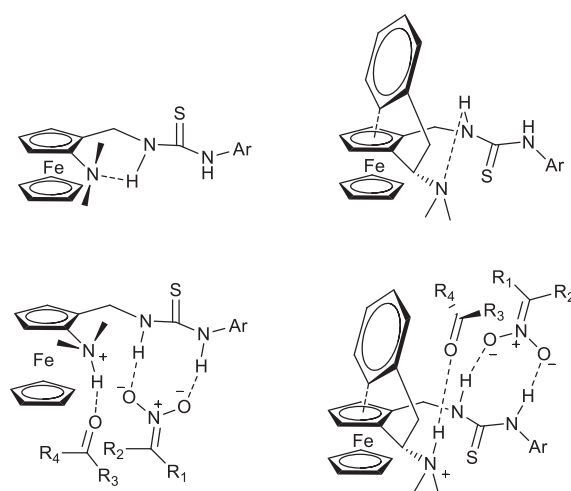
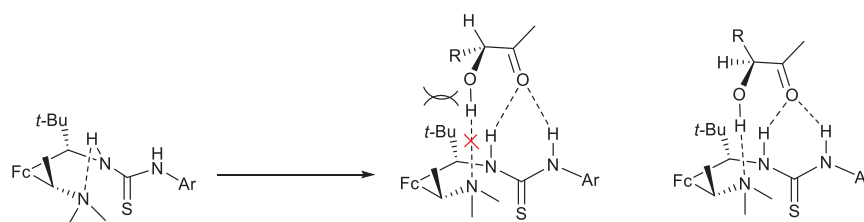


Figure 57: Modification of bi-functional catalyst with higher enantio-control



Scheme 78: Modification of bis-functional receptor for enantio-recognition of α -hydroxy-ketone

3.4. References

-
- ⁸⁷ a) J. C. Ruble, G. C. Fu, *J. Org. Chem.*, **1996**, *61*, 7230-7231; b) G. C. Fu, *Acc. Chem. Res.* **2000**, *33*, 412-420.
- ⁸⁸ a) G. C. Fu, *Acc. Chem. Res.*, **2004**, *37*, 542-547; b) S. L. Wiskur, G. C. Fu, *J. Am. Chem. Soc.*, **2005**, *127*, 6176-6177; c) E. C. Lee, B. L. Hodous, E. Bergin, C. Shih, G. C. Fu, *J. Am. Chem. Soc.*, **2005**, *127*, 11586-11587; d) S. Yunmi Lee, J. M. Murphy, A. Ukai, G. C. Fu, *J. Am. Chem. Soc.*, **2012**, *134*, 15149-15153.
- ⁸⁹ D. Petruzzello, M. Stenta, A. Mazzanti, P. G. Cozzi, *Chem. Eur. J.*, **2013**, *19*, 7696-7700.
- ⁹⁰ M. Braun, *Angew. Chem. Int. Ed.*, **2012**, *51*, 2550-2562; b) U. Groselj, D. Seebach, D. M. Badine, W. B. Schweizer, A. K. Beck, I. Krossing, P. Klose, Y. Hayashi, T. Uchimaru, *Helv. Chim. Acta*, **2009**, *92*, 1225-1259.
- ⁹¹ A. Patti, S. Pedotti, *Eur. J. Org. Chem.*, **2014**, 624-630.
- ⁹² X. Zhang, P. Ma, D. Zhang, Y. Lei, S. Zhang, R. Jiang, W. Chen, *Org. Biomol. Chem.*, **2014**, *12*, 2423-2426.
- ⁹³ A. Mulas, Y. Willener, J. Carr-Smith, K. M. Joly, L. Male, C. J. Moody, S. L. Horswell, H. V. Nguyen, J. H. R. Tucker, *Dalton Trans.*, **2015**, *44*, 7268; Y. Willener, K. M. Joly, C. J. Moody, J. H. R. Tucker, *J. Org. Chem.*, **2008**, *73*, 1225-1233
- ⁹⁴ D. Guillaneux, H. B. Kagan, *J. Org. Chem.*, **1995**, *60*, 2502-2505.
- ⁹⁵ A. Leonidova, T. Joshi, D. Nipkow, A. Frei, J-E. Penner, S. Konatschnig, M. Patra, G. Gasser, *Organometallics*, **2013**, *32*, 2037-2040.
- ⁹⁶ S. Huikai, W. Qingmin, H. Runqiu, L. Heng, L. Yonghong, *Organomet. Chem.*, **2002**, *655*, 182-185.
- ⁹⁷ P. D. Beer, D. K. Smith, *J. Chem. Soc. Dalton Trans.*, **1998**, 417-423.
- ⁹⁸ C. J. Moody, A. P. Lightfoot, P. T. Gallagher, *J. Org. Chem.*, **1997**, *62*, 746-748.
- ⁹⁹ P. Laurent, H. Miyaji, S. R. Collinson, I. Prokes, C. J. Moody, J. H. R. Tucker, A. M. Z. Slawin, *Org. Lett.*, **2002**, *4*, 4037-4040.
- ¹⁰⁰ O. Riant, O. Samuel, T. Flessner, S. Taudien, H. B. Kagan, *J. Org. Chem.* **1997**, *62*, 6733-6745.
- ¹⁰¹ a) D. Marquarding, H. Klusacek, G. Gokel, P. Hoffmann, I. Ugi, *J. Am. Chem. Soc.*, **1970**, *92*, 5389-5394; b) D. Marquarding, H. Klusacek, G. Gokel, P. Hoffmann, I. Ugi, *Angew. Chem. Int. Ed. Engl.*, **1970**, *9*, 371-372.

- ¹⁰² a) A. Hirao, S. Itsuno, S. Nakahama, N. Yamazaki, *J. Chem. Soc. Chem. Commun.*, **1981**, 7, 315-317; b) E. J. Corey, R. K. Bakshi, S. Shibata, *J. Am. Chem. Soc.*, **1987**, *109*, 5551-5553; c) E. J. Corey, R. K. Bakshi, S. Shibata, C. P. Chen, V. K. Singh, *J. Am. Chem. Soc.*, **1987**, *109*, 7925-7926.
- ¹⁰³ Z. Zhang, K. M. Lippert, H. Hausmann, M. Kotke, P. R. Schreiner, *J. Org. Chem.*, **2011**, *76*, 9764-9776.
- ¹⁰⁴ Carboxylate salt **77** was obtained from Sigma-Aldrich, and carboxylate salts **75** and **76** were prepared in the Tucker group by Dr. A. Mulas.
- ¹⁰⁵ Y. S. I. Willener, “*Organometallic Receptors and Sensors for Chiral Carboxylates and Other Anions*”, University of Birmingham, Birmingham, **2009**.
- ¹⁰⁶ K. Hirose, *J. Inclusion Phenom.* **2001**, *39*, 193-209.
- ¹⁰⁷ M. J. Hynes, *J. Chem. Soc., Dalton Trans.*, **1993**, 311-312.
- ¹⁰⁸ a) J. M. Muchowski, M. C. Venuti, *J. Org. Chem.* **1980**, *45*, 4798-4801; b) P. Stanetty, H. Koller, M. Mihovilovic, *J. Org. Chem.*, **1992**, *57*, 6833-6837.
- ¹⁰⁹ S. V. Chankeshwara, A. K. Chakraborti, *Org. Lett.*, **2006**, *15*, 3259-3262.
- ¹¹⁰ a) M. Scheibitz, M. Bolte, J. W. Bats, H-W. Lerner, I. Nowik, R. H. Herber, A. Krapp, M. Lein, M. C. Holthausen, M. Wagner, *Chem. Eur. J.*, **2005**, *11*, 584-603; b) E. R. Reddy, R. Trivedi, L. Giribabu, B. Sridhar, K. Pranay kumar, M. Srinivasa Rao, A. V. S. Sarma, *Eur. J. Inorg. Chem.*, **2013**, 5311-5319; c) S. Hermanek, *Chem. Rev.*, **1992**, *92*, 325-362.
- ¹¹¹ C. Metallinos, J. John, J. Zaifman, K. Embersona, *Adv. Synth. Catal.*, **2012**, *354*, 602-606.
- ¹¹² H. Fujioka, T. Okitsu, Y. Sawama, N. Murata, R. Li, Y. Kita, *J. Am. Chem. Soc.*, **2006**, *128*, 5930-5938.
- ¹¹³ J. M. Chong, L. S. Hegedus, *Organometallics*, **2004**, *23*, 1010-1014.
- ¹¹⁴ S. V. Chankeshwara, A. K. Chakraborti, *Org. Lett.*, **2006**, *8*, 3259-3262.

4. Experimental section

4.1. General

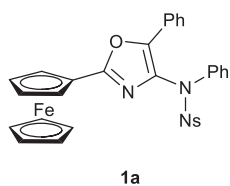
Commercially available reagents and solvents were used without further purification, except toluene, Et₂O, THF, MeCN and CH₂Cl₂, which were dried in Pure Solv™ Solvent Purification Systems. Flash chromatography was carried out using silica 60, with the eluent specified. ¹H NMR spectra were recorded at 300 MHz on a Bruker AVIII300 NMR spectrometer, ¹³C NMR spectra at 100 MHz on a Bruker AVIII400 NMR spectrometer, at room temperature. Chemical shifts (δ) are in ppm and coupling constants (J) are in Hz. Analytical HPLC was performed using a reversed phase C18 column with a water/MeCN method (0-40 mins 0% MeCN – 100% MeCN) with a flow rate of 1.0 mL/min and monitoring at 220 and 254 nm. The enantiomeric excess of the receptors was calculated from the area of the peaks obtained in the chiral HPLC, performed with an AD, OD (eluent IPA in hexane) or Amylose 2 column (eluent MeCN/water) with a flow rate of 1 mL/min and monitoring at 210, 220 and 254 nm. MS were recorded with a Waters/Micromass spectrometer using the ES+ method unless otherwise stated. IR spectrum were recorded on Perkin-Elmer Spectrum 100 (FTIR spectrometer).

4.2. Synthesis

4.2.1. Ferrocene Oxazoles

4.2.1.1. Synthesis of Fc-oxazoles

General procedure for the formation of oxazoles 1a-d and 6: To a solution of the appropriate ynamide **3** (1 eq, 0,1 M) and *N*-pyridinium ylide in toluene at 90 °C was added dichloro(2-pyridinecarboxylato)gold (5 mol%). After the time indicated, the mixture was filtered through a pad of silica to collect the crude oxazole (EtOAc) and the unreacted ylide (EtOAc:MeOH 4:1). The crude oxazole was purified by silica gel column chromatography (Hexane:EtOAc 9:1) to yield an orange solid.

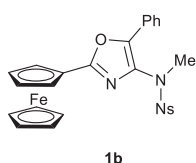


2-Ferrocenyl-4-N-(N-phenyl)nosylamide-5-phenyloxazole 1a: Using

ynamide **3a** (70 mg, 0.18 mmol), ylide **2** (145 mg, 0.47 mmol) and gold

catalyst (3.6 mg, 0.009 mmol). Reacted for 48 hours. Orange crystals (51

mg, yield 46%). $^1\text{H-NMR}$ (300 MHz, CDCl_3) δ = 8.34-8.28 (m, 2 H), 8.03-7.99 (m, 4 H), 7.53-7.47 (m, 4 H), 7.41-7.24 (m, 4 H), 4.90 (t, J = 1,9 Hz, 2 H), 4.39 (t, J = 1,9 Hz, 2 H), 4.20 (s, 5 H); $^{13}\text{C-NMR}$ (101 MHz, CDCl_3) δ = 161.0, 150.3, 145.5, 144.0, 139.3, 133.2, 130.5, 129.3, 128.9 (2C), 128.1, 127.1, 126.9, 125.1, 123.5, 70.9, 70.3, 70.0, 67.8; IR (neat) ν (cm^{-1}) = 3099, 3065, 3038, 2924, 2859, 1595, 1524, 1366, 1346, 1169; mp = 203-205 °C (decomposition); m/z = 605.1 [M^+] (100%), 606.1 [$\text{M}+\text{H}^+$] (67%), 628.1 [$\text{M}+\text{Na}^+$] (78%); HR-MS: calc. for $\text{C}_{31}\text{H}_{24}\text{N}_3\text{O}_5\text{SFe}$: 606.0786, found 606.0785 .

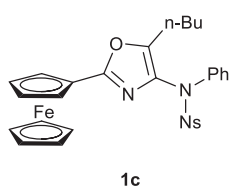


2-Ferrocenyl-4-N-(N-methyl)nosylamide-5-phenyloxazole 1b: Using

ynamide **3b** (57 mg, 0.18 mmol), ylide **2** (110 mg, 0.36 mmol) and gold

catalyst (3.6 mg, 0.009 mmol). Reacted for 6 days. Orange crystals (36 mg,

yield 37%). $^1\text{H-NMR}$ (300 MHz, CDCl_3) δ = 8.41 (m, 2 H), 8.14 (m, 2 H), 7.98 (d, J = 7.3 Hz, 2 H), 7.50 (t, J = 7.5 Hz, 2 H), 7.39 (m, 1 H), 4.84 (s, 2 H), 4.46 (s, 2 H), 4.19 (s, 5 H), 3.22 (s, 3 H); $^{13}\text{C-NMR}$ (101 MHz, CDCl_3) δ = 161.1, 150.4, 144.8, 143.6, 133.6, 130.1, 128.9 (2C), 127.0, 125.1, 123.9, 70.8, 70.3, 69.9, 67.7, 37.7; IR (neat) ν (cm^{-1}) = 3692, 3667, 3117, 2990, 2971, 2903, 1742, 1597, 1525, 1365, 1066; mp = 202-204 °C (decomposition); m/z = 566.3 [$\text{M}+\text{Na}^+$] (100%); HR-MS: calc. for $\text{C}_{26}\text{H}_{21}\text{N}_3\text{O}_5\text{NaSFe}$: 566.0436, found 566.0449.

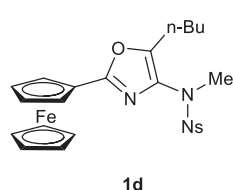


2-Ferrocenyl-4-N-(N-phenyl)nosylamide-5-butyloxazole 1c: Using

ynamide **3c** (100 mg, 0.28 mmol), ylide **2** (128 mg, 0.42 mmol) and gold

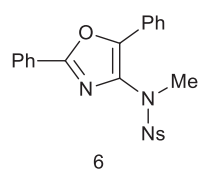
catalyst (5.5 mg, 0.014 mmol). Reacted for 6 days. Orange crystals (54 mg,

yield 51%). $^1\text{H-NMR}$ (300 MHz, CDCl_3) δ = 8.36-8.31 (m, 2 H), 7.99-7.93 (m, 2 H), 7.43-7.39 (m, 2 H), 7.35-7.28 (m, 3 H), 4.79 (t, J = 1,9 Hz, 2 H), 4.39 (t, J = 1,9 Hz, 2 H), 4.14 (s, 5 H), 2.79 (t, J = 7.5 Hz, 2 H), 1.65 (dt, J = 15.2 Hz, 7.5 Hz, 2 H), 1.33 (qd, J = 14.5, 5.3 Hz, 2 H), 0.91 (t, J = 7.3 Hz, 3 H); $^{13}\text{C-NMR}$ (101 MHz, CDCl_3) δ = 160.3, 150.2, 149.3, 144.4, 139.9, 130.2, 129.2, 128.0, 127.5, 123.5, 70.9, 70.3, 69.7, 67.4, 29.5, 22.4, 13.7; IR (neat) ν (cm^{-1}) = 3270, 3105, 2961, 1606, 1526, 1346, 1162; mp = 167-169 °C; m/z = 585.2 [M^+] (50%), 586.2 [$\text{M}+\text{H}^+$] (100%), 608.2 [$\text{M}+\text{Na}^+$] (87%); HR-MS: calc. for $\text{C}_{29}\text{H}_{28}\text{N}_3\text{O}_5\text{SFe}$: 586.1071, found 586.1099.



2-Ferrocenyl-4-N-(N-methyl)nosylamide-5-butyloxazole 1d: Using ynamide **3d** (53 mg, 0.18 mmol), ylide **2** (82 mg, 0.27 mmol) and gold catalyst (3.6 mg, 0.009 mmol). Reacted for 24 hours. Orange crystals (54 mg, yield 10%).

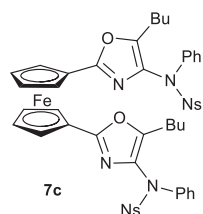
$^1\text{H-NMR}$ (300 MHz, CDCl_3) δ = 8.37 (d, J = 7.3 Hz, 2 H), 7.99 (d, J = 7.3 Hz, 2 H), 4.90 (s, 2 H), 4.52 (s, 2 H), 4.28 (s, 5 H), 3.12 (s, 3 H), 2.80 (t, J = 7.0 Hz, 2 H), 1.71 (m, 2 H), 1.42 (m, 2 H), 0.98 (t, J = 7.2 Hz, 3 H); m/z = 524.1 [$\text{M}+\text{H}^+$] (100%); HR-MS: calc. for $\text{C}_{29}\text{H}_{28}\text{N}_3\text{O}_5\text{SFe}$: 523.0864, found 523.0859.



2-Phenyl-4-N-(N-methyl)nosylamide-5-phenyloxazole 6: Using ynamide **3b** (200 mg, 0.63 mmol), *N*-benzoylpyridinium ylide (188 mg, 0.95 mmol) and gold catalyst (12 mg, 0.03 mmol). Reacted for 24 hours. White solid (218 mg, yield 80%).

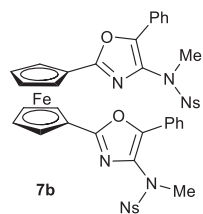
$^1\text{H-NMR}$ (300 MHz, CDCl_3) δ = 8.43-8.37 (m, 2 H), 8.18-8.13 (m, 2 H), 8.06-8.01 (m, 2 H), 7.97-7.90 (m, 2 H), 7.56-7.38 (m, 6 H), 3.23 (s, 3 H); $^{13}\text{C-NMR}$ (101 MHz, CDCl_3) δ = 157.9, 150.4, 145.9, 143.3, 131.0, 129.3, 129.0, 126.7, 126.2, 125.4, 123.9, 37.8; IR (neat) ν (cm^{-1}) = 3088, 3058, 2937, 1527, 1449, 1351, 1302, 1160; mp = 164-166 °C; m/z =

458.1 [M+Na⁺] (100%), 436.1 [M+H⁺] (56%); HR-MS: calc. for C₂₂H₁₈N₃O₅S: 436.0967, found 436.0978.



1,1'-Bis(4-*N*-(*N*-phenyl)nosylamide-5-butylloxazole)ferrocene 7c: Using ynamide **3c** (69 mg, 0.2 mmol), ylide **13** (43 mg, 0.1 mmol) and gold catalyst (3.9 mg, 0.01 mmol). Reacted for 2 hours. Orange crystals (8 mg, yield 8%).

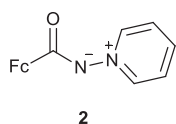
¹H-NMR (300 MHz, CDCl₃) δ = 8.30 (d, *J* = 9 Hz, 2 H), 7.95 (d, *J* = 9 Hz, 2 H), 7.43-7.38 (m, 2 H), 7.33-7.27 (m, 2 H), 4.79 (t, *J* = 1.8 Hz, 2 H), 4.30 (t, *J* = 1.8 Hz, 2 H), 2.71 (t, *J* = 7.5 Hz, 2 H), 1.67-1.56 (m, 2 H), 1.37-1.28 (m, 2 H), 0.90 (t, *J* = 7.3 Hz, 3 H); mp = 97-99 °C; *m/z* = 1007.5 [M+Na⁺] (100%).



1,1'-Bis(4-*N*-(*N*-methyl)nosylamide-5-phenylloxazole)ferrocene 7b:

Using ynamide **3d** (121 mg, 0.38 mmol), ylide **13** (65 mg, 0.15 mmol) and gold catalyst (7.4 mg, 0.019 mmol). Reacted for 24 hours. Orange crystals (10 mg, yield 11%). ¹H-NMR (300 MHz, CDCl₃) δ = 8.35 (d, *J* = 8.4 Hz, 2 H), 8.08 (d, *J* = 8.4 Hz, 2 H), 7.85 (d, *J* = 7.2 Hz, 2 H), 7.42-7.32 (m, 3 H), 4.82 (s, 2 H), 4.44 (s, 2 H), 3.10 (s, 3 H); ¹³C NMR (101 MHz, CDCl₃) δ = 150.9, 141.8, 131.7, 129.2, 128.6, 124.6, 122.0, 82.6, 76.8, 69.9, 39.7; IR (neat) ν (cm⁻¹) = 3106, 2924, 2854, 1683, 1593, 1524, 1346, 1159, 844, 737; mp = 124-126 °C.

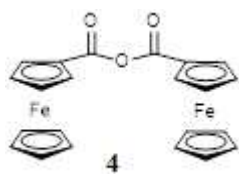
4.2.1.2. Synthesis of ylides



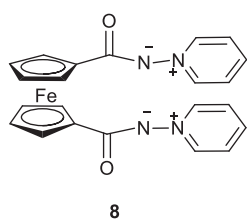
Ferrocenyl *N*-pyridinium amidine 2: Oxalyl chloride (111 μL, 1.3 mmol) and DMF (2 drops) were added to ferrocenecarboxylic acid (150 mg, 0.652 mmol)

in dry dichloromethane (10 mL) and stirred for 6 hours under Ar. The mixture was then evaporated to dryness by means of vacuum (50 mbar) for 1 hour. To the dark red solid, still

under Ar, were added aminopyridinium iodide (159 mg, 0.717 mmol), potassium carbonate (197 mg, 1.43 mmol) and dry dichloromethane (10 mL). After being stirred for 5 days at room temperature, the mixture was passed through a pad of silica gel, eluted with EtOAc followed by EtOAc:MeOH (4:1) to collect **2**. The ylide was further purified by silica gel column chromatography (EtOAc:MeOH 9:1) to afford ylide **2** as an orange solid (259 mg, yield 65%). ^1H NMR (CDCl_3 , 300 MHz) δ = 8.80 (dd, J = 6.9, 1.2 Hz, 2 H), 7.88 (tt, J = 7.2, 1.2 Hz, 1 H), 7.64 (dd, J = 7.7, 6.8 Hz, 2 H), 4.77 (t, J = 1.9 Hz, 2 H), 4.29 (t, J = 1.9 Hz, 2 H), 4.242 (s, 5 H); ^{13}C NMR (CDCl_3 , 100 MHz) δ = 174.2, 143.3, 136.3, 125.8, 80.1, 69.5, 69.3, 69.0; IR (neat) ν (cm^{-1}) = 3341, 3027, 2923, 1613, 1550, 1460, 1367, 1301; m/z = 329.1 [$\text{M}+\text{Na}^+$] (100%), 307.2 [$\text{M}+\text{H}^+$] (13%); HR-MS: calc. for $\text{C}_{16}\text{H}_{14}\text{N}_2\text{ONaFe}$: 329.0339, found: 329.0353; mp = 155 -157 °C (decomposition).



Ferrocenecarboxylic anhydride 4: ^1H NMR (CDCl_3 , 300 MHz) δ = 4.90 (s, 4 H), 4.56 (s, 4 H), 4.37 (s, 10 H); m/z = 465 [$\text{M}+\text{Na}^+$] (100%). Data in agreement with that previously reported.¹¹⁵

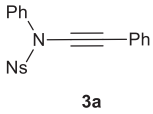


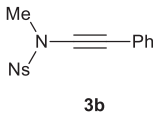
Bis ferrocenyl N-pyridinium aminide 8: Obtained from 1,1'-bisferrocene carboxylic acid (1.13 g, 4.1 mmol) reacted first with oxalyl chloride (2 mL, 24.6 mmol), DMF (0.3 mL, 0.02mmol) in dry CH_2Cl_2 (30 mL), then with aminopyridinium iodide (2.00 g, 9 mmol), potassium carbonate (2.83 g, 20.1 mmol) in dry CH_2Cl_2 (20 mL) as an orange solid (65 mg, yield 4%). ^1H -NMR (300 MHz, CDCl_3) δ = 8.97 (d, J = 6.0 Hz, 2 H), 7.85 (t, J = 7.5 Hz, 1 H), 7.56 (t, J = 6.9 Hz, 2 H), 4.95 (t, J = 1.8 Hz, 2 H), 4.35 (t, J = 1.8 Hz, 2 H); ^{13}C NMR (CDCl_3 , 100 MHz) δ = 173.6, 144.7, 136.5, 125.8, 80.9, 72.0, 70.6, 70.5; IR (neat) ν (cm^{-1}) = 3395, 3105, 3064, 3064, 3042, 1642, 1541, 1491, 1325, 1193, 1038, 766; m/z = 449.0 [$\text{M}+\text{Na}^+$] (48%), 427.1

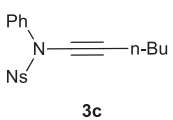
[M+H⁺] (100%); HR-MS: calc. for C₂₂H₁₉N₄O₂Fe: 427.0857, found 427.0870; mp = 173-175 °C (decomposition).

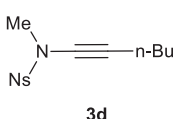
4.2.1.3. Synthesis of ynamides

General procedure for the formation of ynamides 3: Following the method of Stahl, copper (II) chloride (27 mg, 0.2 mmol), the appropriate sulfonamide (5 mmol) and potassium carbonate (212 mg, 2 mmol) were added to a flame-dried 250 mL three-necked round-bottomed flask. The flask was purged with oxygen for 15 minutes and toluene (5 mL) followed by dry pyridine (1.6 mL, 2 mmol) were added. A balloon filled with oxygen was connected to the flask and the stirred mixture was heated at 70 °C. After 15 minutes, a solution of the appropriate alkyne (1 mmol) in toluene (5 mL) was added by syringe pump over a period of 4 hours. The mixture was allowed to stir at 70 °C for another 4 hours and was then cooled to room temperature. After filtration over a pad of silica, the reaction mixture was dry loaded on silica and purified by silica gel column chromatography (Hexane:EtOAc 9:1) to yield the desired ynamide as a white solid.


4-Nitro-*N*-phenyl-*N*-(phenylethynyl)benzenesulfonamide 3a: 298 mg, yield 79%. ¹H-NMR (300 MHz, CDCl₃) δ = 8.40-8.32 (m, 2 H), 7.96-7.88 (m, 2 H), 7.42-7.35 (m, 5 H), 7.35-7.28 (m, 5 H); ¹³C-NMR (101 MHz, CDCl₃) δ = 141.2, 138.3, 131.8, 129.6, 129.0, 128.7, 128.6, 126.3, 124.3, 121.9, 81.8, 71.3; *m/z* = 401.1 [M+Na⁺] (100%). Data in agreement with that previously reported.⁷⁹

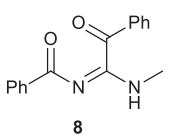

4-Nitro-*N*-methyl-*N*-(phenylethynyl)benzenesulfonamide 3b: 290 mg, yield 92%. ¹H-NMR (300 MHz, CDCl₃) δ = 8.48-8.40 (m, 2 H), 8.18-8.11 (m, 2 H), 7.40-7.28 (m, 5 H), 3.23 (s, 3 H); ¹³C-NMR (101 MHz, CDCl₃) δ = 150.8, 141.6, 131.6, 129.0, 128.4, 124.5, 121.9, 82.5, 69.8, 39.6. Data in agreement with that previously reported.¹¹⁵

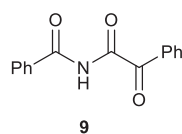

4-Nitro-*N*-phenyl-*N*-(butylethynyl)benzenesulfonamide 3c: 288 mg, yield 80%. ¹H-NMR (300 MHz, CDCl₃) δ = 8.35 (m, 2 H), 7.85 (m, 2 H), 7.39-7.33 (m, 3 H), 7.29-7.22 (m, 2 H), 2.32 (t, *J* = 7.0 Hz, 2 H), 1.51 (m, 2 H), 1.41 (m, 2 H), 0.92 (t, *J* = 7.2 Hz, 3 H); *m/z* = 399.2 [M+K⁺]. Data in agreement with that previously reported.¹¹⁵


4-Nitro-*N*-methyl-*N*-(butylethynyl)benzenesulfonamide 3d: 238 mg, yield 80%. ¹H-NMR (300 MHz, CDCl₃) δ = 8.44-8.38 (m, 2 H), 8.11-8.05 (m, 2 H), 3.08 (s, 3 H), 2.24 (t, *J* = 6.9 Hz, 2 H), 1.51-1.40 (m, 2 H), 1.40-1.29 (m, 2 H), 0.90 (t, *J* = 7.2 Hz, 3 H); *m/z* = 319.3 [M+Na⁺] (100%). Data in agreement with that previously reported.¹¹⁵

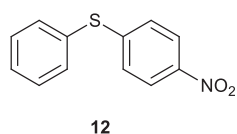
4.2.1.4. Deprotection of nosyl

To a solution of the appropriate protected amine (0.5 mmol) in acetonitrile (8 ml) at 50° C was added mercaptoacetic acid (1 mmol) followed by DBU (2.5 mmol). After full conversion of starting material (TLC monitoring), either HCl (1M) was added followed by silica gel column chromatography to give the hydroxy derivative **12**, or the reaction mixture was directly chromatographed to yield compound **13**. Compound **14** was eluted first.

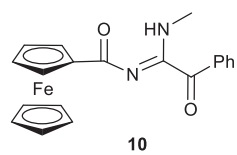

(*E*)-*N*-(1-(methylamino)-2-oxo-2-phenylethylidene)benzamide 12: ¹H-NMR (300 MHz, CDCl₃) δ = 8.15 (d, *J* = 7.4 Hz, 2 H), 8.07 (d, *J* = 8.5 Hz, 2 H), 7.67 (t, *J* = 7.5 Hz, 1 H), 7.54-7.49 (m, 1 H), 7.41-7.35 (m, 4 H), 6.01 (br s, 1 H), 3.03 (s, 3 H); ¹³C-NMR (101 MHz, CDCl₃) δ = 133.8 (C, Ph *ipsos*), 132.5 (C, Ph *ipsos*), 130.0 (CH, Ph), 129.2 (CH, Ph), 128.9 (CH, Ph), 128.8 (CH, Ph), 128.3 (CH, Ph), 29.3 (CH₃); IR (neat) ν (cm⁻¹) = 3352, 3204, 3064, 2924, 1662, 1336; *m/z* (TOF-EI) = 267.1 [M+H⁺] (100%), 289.1 [M+Na⁺] (53%).



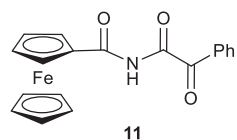
***N*-(2-oxo-2-phenylacetyl)benzamide 13:** $^1\text{H-NMR}$ (300 MHz, CDCl_3): $\delta = 9.81$ (s, 1 H), 8.14 (d, $J = 8$ Hz, 2 H), 7.92 (d, $J = 8.5$ Hz, 2 H), 7.70-7.61 (m, 2 H), 7.58-7.49 (m, 4 H); IR (neat) ν (cm^{-1}) = 3400-2800 (bs), 3061, 1648, 1595, 1536, 1375, 1227; m/z (TOF-EI) = 276.1 [$\text{M}+\text{Na}^+$] (100%); mp = 135-137 °C. Data in agreement with that previously reported.¹¹⁶



(4-nitrophenyl)(phenyl)sulfane 14: $^1\text{H-NMR}$ (300 MHz, CDCl_3) $\delta = 8.06$ (d, $J = 9.0$ Hz, 2 H), 7.57-7.52 (m, 2 H), 7.49-7.44 (m, 3 H), 7.17 (d, $J = 9.0$ Hz, 2 H); $m/z = 231.0$ [M^+]. Data in agreement with that previously reported.¹¹⁷



(*E*)-*N*-(1-(methylamino)-2-oxo-2-phenylethylidene)ferroceneamide 15: $^1\text{H-NMR}$ (300 MHz, CDCl_3) $\delta = 8.07$ (d, $J = 7.8$ Hz, 2 H), 7.67 (t, $J = 7.8$ Hz, 1 H), 7.55 (t, $J = 7.8$ Hz, 2 H), 5.71 (br s, 1 H), 4.42 (s, 2 H), 4.39 (s, 1 H), 4.20 (s, 5 H), 3.00 (s, 3 H); $^{13}\text{C-NMR}$ (101 MHz, CDCl_3) $\delta = 133.9$ (C, Ph *ipso*s), 129.2 (CH, Ph), 128.9 (CH, Ph), 128.8 (CH, Ph), 71.6 (CH, Cp ring), 70.4 (CH, Cp ring), 70.1 (CH, unsubstituted Cp ring), 29.3 (CH_3); m/z (TOF-EI) = 375 [$\text{M}+\text{H}^+$] (100%), 397 [$\text{M}+\text{Na}^+$] (90%).

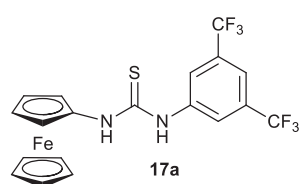


***N*-(2-oxo-2-phenylacetyl)ferroceneamide 16:** $^1\text{H-NMR}$ (300 MHz, CDCl_3) $\delta = 9.05$ (br s, 1 H), 8.08 (d, $J = 6.7$ Hz, 2 H), 7.66 (t, $J = 7.2$ Hz, 1 H), 7.54 (t, $J = 7.2$ Hz, 2 H), 4.86 (s, 2 H), 4.62 (s, 2 H), 4.37 (s, 5 H); $^{13}\text{C-NMR}$ (101 MHz, CDCl_3) $\delta = 207.3$ (CO), 173.9 (CO), 134.7 (CH, Ph), 130.1 (CH, Ph), 129.1 (CH, Ph), 73.1 (CH, Cp ring), 70.7 (CH, Cp ring), 69.4 (CH, Cp ring); $m/z = 384.0$ [$\text{M}+\text{Na}^+$]; m/z (TOF-ES-) = 359.9 [$\text{M}-\text{H}^+$].

4.2.2. Ferrocene (thio)ureas

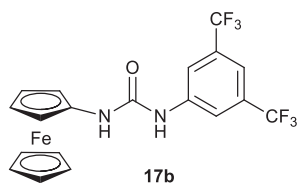
4.2.2.1. General procedure for preparation of (thio)urea

The appropriate amine (1 eq) was dissolved in dry CH₂Cl₂ (0.1 M) and the appropriate iso(thio)cyanate (1.1 eq) was added at room temperature. The mixture was stirred until completion (TLC monitoring), and the solvent removed under reduced pressure. The residue was purified by silica gel column chromatography (Hexane:EtOAc 9:1) to yield the desired compound. Chiral HPLC traces and conditions are in the appendix.

***N*-Ferrocenyl-*N'*-(3,5-bis(trifluoromethyl)phenyl)thiourea 17a:**

Using amine **24** (50 mg, 0.25 mmol) and 3,5-bis(trifluoromethyl)phenyl isothiocyanate (49 μ L, 0.27 mmol).

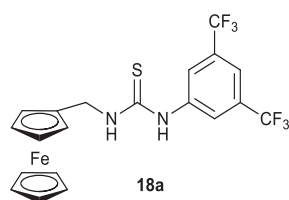
Obtained as an yellow-orange powder (107 mg, yield 90%). ¹H NMR (Acetone d₆, 300 MHz) δ = 9.37 (br s, 0.7 H), 9.04 (s, 0.7 H), 8.34 (s, 2 H), 7.75 (s, 1 H), 4.63 (s, 2 H), 4.31 (s, 5 H), 4.17 (s, 2 H); ¹³C NMR (Acetone d₆, 300 MHz) δ = 180.7 (C, CS), 142.8 (C, Ph *ipsos*), 131.8 (C, q, J = 33.2 Hz, Ph *meta*), 124.8 (CH, Ph *ortho*), 124.4 (C, q, J = 272.1 Hz, CF₃), 118.2 (CH, Ph *para*), 94.6 (C, Cp ring), 70.2 (CH, unsubstituted Cp ring), 66.7 (CH, Cp ring), 65.7 (CH, Cp ring); IR (neat): ν (cm⁻¹) = 3233, 3093, 1698, 1535, 1378, 1274, 1170, 1126, 885, 700, 681; m/z = 494.8 [M+Na⁺] (100%); HR-MS: calc for C₁₉H₁₄N₂F₆SFeNa: 495.0029, found 495.0035; mp = 57-59 °C.

***N*-Ferrocenyl-*N'*-(3,5-bis(trifluoromethyl)phenyl)urea 17b:**

Using amine **24** (50 mg, 0.25 mmol) and 3,5-bis(trifluoromethyl)phenyl isocyanate (47 μ L, 0.27 mmol). Obtained as an orange powder (166

mg, yield 97%). ¹H NMR (Acetone d₆, 300 MHz) δ = 8.58 (s, 0.7 H), 8.18 (s, 2 H), 7.66 (s, 2 H), 4.63 (s, 2 H), 4.31 (s, 5 H), 4.17 (s, 2 H).

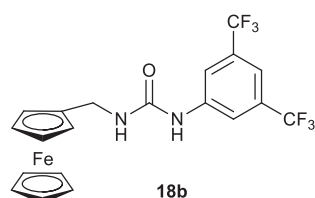
0.7 H), 7.57 (s, 1 H), 4.64 (s, 2 H), 4.18 (s, 5 H), 4.02 (s, 2 H); ^{13}C NMR (Acetone d_6 , 300 MHz) δ = 153.5 (C, CO), 143.2 (C, Ph *ipso*s), 132.5 (C, q, J = 32.8 Hz, CF_3), 124.6 (C, q, J = 271.7 Hz, Ph *meta*), 118.9 (CH, Ph *ortho*), 115.3 (CH, Ph *para*), 97.4 (C, Cp ring), 70.0 (CH, unsubstituted Cp), 65.1 (CH, Cp ring), 62.1 (CH, Cp ring); IR (neat): ν (cm^{-1}) = 3291, 3099, 1647, 1569, 1384, 1274, 1173, 1120, 883, 701, 680; m/z (TOF – ES+) = 478.9 [$\text{M}+\text{Na}^+$] (100%), 455.9 [M^+] (80%); HR-MS: calc. for $\text{C}_{19}\text{H}_{14}\text{N}_2\text{F}_6\text{OFe}$: 456.0360, found 456.0349; mp = 178-180 °C (decomposition).



***N*-(methylferrocene)-*N'*-(3,5-bis(trifluoromethyl)phenyl)thiourea**

18a: Using amine **26** (200 mg, 0.9 mmol) and 3,5-bis(trifluoromethyl)phenyl isothiocyanate (202 μL , 1.1 mmol).

Obtained as a yellow powder (384 mg, yield 86%). ^1H NMR (Acetone d_6 , 300 MHz) δ = 9.43 (s, 1H), 8.31 (s, 2H), 7.75 (s, 1H), 7.73 (s, 1H), 4.59 (d, J = 5.0 Hz, 2H), 4.33 (d, J = 1.8 Hz, 2H), 4.21 (s, 5H), 4.15 (t, J = 1.8 Hz, 2H); ^{13}C NMR (Acetone d_6 , 100 MHz): δ = 181.6 (C, CS), 143.0 (C, Ph *ipso*s), 131.6 (C, q, J = 33.0 Hz, Ph *meta*), 124.4 (C, q, J = 272.1 Hz, CF_3), 123.4 (CH, Ph *ortho*), 117.4 (CH, Ph *para*), 85.3 (C, Cp ring), 69.4 (CH, unsubstituted Cp ring), 69.3 (CH, Cp ring), 68.8 (CH, Cp ring), 44.5 (CH_2); IR (neat) ν (cm^{-1}) = 3247, 3083, 3048, 2920, 1556, 1536, 1463, 1380, 1276, 1172, 1122, 948, 884, 678; mp = 127-129 °C; m/z = 486.0 [M^+] (100%); HR-MS: calc. for $\text{C}_{20}\text{H}_{16}\text{N}_2\text{SF}_6\text{Fe}$: 486.0228, found 486.0284.

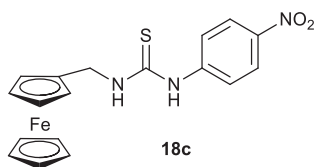


***N*-(methylferrocene)-*N'*-(3,5-bis(trifluoromethyl)phenyl)urea**

18b: Using amine **26** (129 mg, 0.60 mmol) and 3,5-bis(trifluoromethyl)phenyl isocyanate (114 μL , 0.66 mmol).

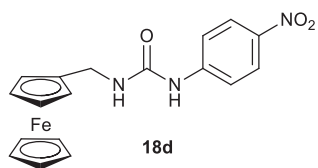
Obtained as a yellow powder (223 mg, yield 79%). ^1H NMR (Acetone d_6 , 300 MHz) δ = 8.61 (s, 1 H), 8.16 (s, 2 H), 7.53 (s, 1 H), 6.21 (t, J = 5.1 Hz, 1 H), 4.24 (t, J = 1.8 Hz, 2 H), 4.19 (s,

5 H), 4.17 (d, $J = 5.2$ Hz, 2 H), 4.11 (t, $J = 1.8$ Hz, 2 H); ^{13}C NMR (Acetone d_6 , 100 MHz) $\delta = 155.4$ (C, CO), 143.7 (C, Ph *ipso*s), 132.4 (C, q, $J = 33.0$ Hz, Ph *meta*), 124.6 (C, q, $J = 272.2$ Hz, CF_3), 118.5 (CH, Ph *ortho*), 114.8 (CH, Ph *para*), 87.3 (C, Cp ring), 69.3 (CH, unsubstituted Cp ring), 68.9 (CH, Cp ring), 68.6 (CH, Cp ring), 39.7 (CH_2); IR (neat) ν (cm^{-1}) = 3327, 3088, 2911, 1640, 1552, 1472, 1384, 1273, 1169, 1118, 1106, 881, 815, 676, 647; mp = 201-203 °C; $m/z = 470.0$ [M^+] (100%); HR-MS: calcd for $\text{C}_{20}\text{H}_{16}\text{N}_2\text{O}_6\text{Fe}$: 470.0516, found 470.0515.



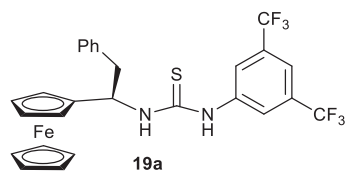
***N*-(methylferrocene)-*N'*-(4-nitrophenyl)thiourea 18c:** Using amine **26** (251 mg, 1.1 mmol) and 4-nitrophenyl isothiocyanate (231 mg, 1.3 mmol). Obtained as a brown solid (383 mg, yield 83%). ^1H NMR

(Acetone d_6 , 300 MHz) $\delta = 9.43$ (s, 1 H), 8.20 (d, $J = 9.3$ Hz, 2 H), 7.95 (d, $J = 9.3$ Hz, 2 H), 7.66 (t, $J = 5.1$ Hz, 1 H), 4.58 (d, $J = 5.2$ Hz, 2 H), 4.32 (t, $J = 1.8$ Hz, 2 H), 4.20 (s, 5 H), 4.15 (t, $J = 1.8$ Hz, 2 H); IR (neat) ν (cm^{-1}) = 3373, 3328, 3162, 3075, 2994, 1593, 1525, 1500, 1321, 1299, 1242, 1163, 1106, 1034, 821, 740, 644. Data in agreement with that previously reported.¹¹⁸



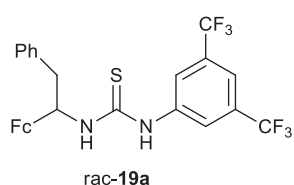
***N*-(methylferrocene)-*N'*-(4-nitrophenyl)urea 18d:** Using amine **26** (224 mg, 1.0 mmol) and 4-nitrophenyl isocyanate (188 mg, 1.1 mmol). Obtained as a yellow-brown powder (258 mg, yield 65%).

^1H NMR (Acetone d_6 , 300 MHz) $\delta = 8.64$ (s, 1 H), 8.15 (d, $J = 8.3$ Hz, 2 H), 7.73 (d, $J = 8.3$ Hz, 2 H), 6.18 (t, $J = 5.1$ Hz, 1 H), 4.23 (t, $J = 1.7$ Hz, 2 H), 4.19 (s, 5 H), 4.17 (d, $J = 5.2$ Hz, 2 H), 4.11 (t, $J = 1.7$ Hz, 2 H); IR (neat) ν (cm^{-1}) = 3377, 3239, 2993, 1641, 1510, 1340, 1223, 1104, 1040, 829, 829, 676. Data in agreement with that previously reported.¹¹⁸



(R)-N-(3,5-bis(trifluoromethyl)phenyl)-N'-(1-ferrocene-2-phenylethyl)thiourea 19a: Using the general procedure for the formation of thiourea with amine **30a** (80 mg, 0.26 mmol) and

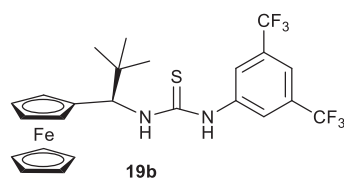
3,5-bis(trifluoromethyl)phenyl isothiocyanate (51 μ L, 0.3 mmol). Obtained as a yellow powder (149 mg, yield 98%). $^1\text{H-NMR}$ (300 MHz, CDCl_3) δ = 9.53 (1 H, s), 8.40 (2 H, s), 7.82 (1 H, d, J = 8.7 Hz), 7.80 (1 H, s), 7.36 – 7.25 (5 H, m), 5.94 (1 H, s), 4.36 (1 H, s), 4.28 (5 H, s), 4.23 (1H, dd, J = 3.5, 2.2 Hz), 4.20 (2 H, dd, J = 2.4, 1 Hz), 3.29 (2 H, d, J = 6.8 Hz); $^{13}\text{C-NMR}$ (101 MHz, CDCl_3) δ = 181.0 (C, CS), 142.7 (C, Ph *ipsos*), 139.0 (C, Bn *ypsos*), 131.9 (C, q, J = 33.1 Hz, Ph *meta*), 130.4 (CH, Bn *meta*), 128.8 (CH, Bn *ortho*), 127.0 (CH, Bn *para*), 124.3 (C, q, J = 272.1 Hz, CF_3), 123.5 (CH, Ph *ortho*), 117.5 (CH, Ph *para*), 90.5 (C, Cp ring), 69.4 (CH, unsubstituted Cp ring), 68.5 (CH, Cp ring), 68.1 (2 CH, Cp ring), 66.9 (CH, Cp ring), 55.3 (CH_2), 42.7 (CH, CpCH); IR (neat) ν (cm^{-1}) = 3249, 3211, 3030, 2971, 2939, 1538, 1469, 1382, 1274, 1171, 1127, 897, 825, 682; m/z = 599.0 [$\text{M}+\text{Na}^+$] (45%), 576.1 [M^+] (100%); HR-MS calc. for $\text{C}_{27}\text{H}_{22}\text{N}_2\text{F}_6\text{SFe}$: 576.0757, found 576.0754; mp = 55-57 $^\circ\text{C}$.



N-(3,5-bis(trifluoromethyl)phenyl)-N'-(1-ferrocenyl-2-phenylethyl)thiourea 19a: To methoxyamine **32** (151 mg, 0.45 mmol) dissolved in THF (2 mL) was added 2 M HCl (10 mL)

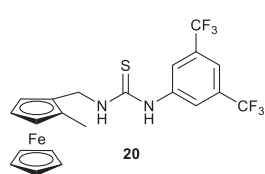
followed by zinc powder (883 mg, 13.5 mmol). The mixture was stirred at room temperature for 30 minutes, then water (5 mL) and Et_2O (10 mL) were added and the phases were separated. The aqueous phase was basified with sodium hydroxide to pH \approx 12 and extracted with Et_2O (6 \times 10 mL). The organic phases were gathered and dried over sodium sulfate, filtered and concentrated under reduced pressure. The residue was passed through a short column of silica (EtOAc then $\text{EtOAc}:\text{MeOH}:\text{NEt}_3$ 90:5:5) to give the racemic amine **30a** (64 mg, yield 46%) which was directly treated with 3,5-bis(trifluoromethyl)phenyl isothiocyanate (36 μ L, 0.2

mmol) in CH₂Cl₂ (1.3 mL) at room temperature for 16 hours. Evaporation of the solvent and purification by silica gel column chromatography yielded the racemic thiourea 19a (87 mg, 72%). ¹H-NMR (300 MHz, CDCl₃) δ = 9.42 (s, 1 H), 8.30 (s, 1 H), 7.72 (s, 1 H), 7.29-7.14 (m, 5 H), 5.84 (s, 1 H), 4.28 (s, 1 H), 4.20 (s, 5 H), 4.15 (s, 1 H), 4.11 (s, 2 H), 3.20 (d, *J* = 6.8 Hz, 2 H).



(*R*)-*N*-(3,5-bis(trifluoromethyl)phenyl)-*N'*-(1-ferrocene-2-*tert*-butyl)thiourea 19b: Using the general procedure for the formation of thiourea with amine **30b** (43 mg, 0.16 mmol) and

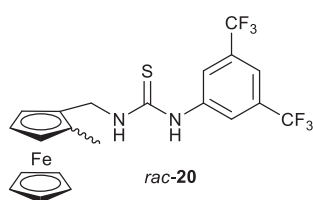
3,5-bis(trifluoromethyl)phenyl isothiocyanate (32 μL, 0.19 mmol). Obtained as a yellow powder (81 mg, yield 97%). ¹H-NMR (300 MHz, Acetone d₆) δ = 9.54 (1 H, s), 8.48 (2 H, s), 8.04 (1 H, d, *J* = 10.0 Hz), 7.71 (1 H, s), 5.40 (1 H, d, *J* = 10.1 Hz), 4.29 (1 H, dt, *J* = 2.4 Hz, 1.3 Hz), 4.24 (5 H, s), 4.19 – 4.15 (2 H, m), 4.15 – 4.12 (1 H, dd, *J* = 2.4, 1 Hz), 0.88 (9 H, s); ¹³C-NMR (101 MHz, Acetone d₆) δ = 182.1 (C, CS), 143.4 (C, Ph *ipso*s), 132.0 (C, q, *J* = 33.2 Hz, Ph *meta*), 124.5 (C, q, *J* = 272.0 Hz, CF₃), 123.4 (CH, q, *J* = 3.8 Hz, Ph *para*), 117.4 (CH, dq, *J* = 7.6, 3.8 Hz, Ph *ortho*), 89.6 (C, Cp ring), 71.1 (CH, Cp ring), 69.6 (CH, unsubstituted Cp ring), 68.4 (CH, Cp ring), 67.4 (CH, Cp ring), 66.3 (CH, Cp ring), 62.1 (CH, CpCH), 37.6 (C, *t*-Bu), 27.2 (CH₃); IR (neat) ν (cm⁻¹) = 3253, 3204, 3060, 2965, 1741, 1542, 1467, 1379, 1272, 1175, 1134, 1106, 954, 891, 817; *m/z* = 542.1 [M]⁺ (28%); HR-MS: calc. for C₂₄H₂₄N₂F₆SFe: 542.0914, found 542.0911; mp = 176-178 °C.



(*R_p*)-1-Thiourea-2-methyl ferrocene 20: (*R_p*)-1-carboxaldoxime-2-methylferrocene **37** (164 mg, 0.67 mmol) was dissolved in dry THF (20 mL) and LiAlH₄ (256 mg, 6.7 mmol) was added portion-wise. The

mixture was stirred at 80 °C for 2 hours and quenched at room temperature with NH₄Cl_(sat).

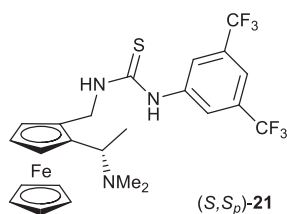
Amine **39** was extracted with Et₂O, dried over sodium sulfate, filtered and evaporated under reduced pressure. It was then dissolved in CH₂Cl₂ (5 mL) and 3,5-(trifluoromethyl)phenyl isothiocyanate (96 μL, 0.52 mmol) was added. The solution was stirred for 15 hours and the solvent was then removed under reduced pressure. The residue was purified by silica gel column chromatography (Hexane:EtOAc 9:1) to give the title compound as a brown powder (165 mg, yield 49%). ¹H NMR (CDCl₃, 300 MHz) δ = 9.43 (s, 1 H), 8.43 (s, 2 H), 7.78 (s, 1 H), 7.69 (s, 1 H), 4.78 (d, *J* = 14.0 Hz, 1 H), 4.66 (d, *J* = 14.0 Hz, 1 H), 4.33 (app s, 2 H), 4.20 (s, 5 H), 4.10 (app s, 1 H), 2.12 (s, 3 H); ¹³C NMR (CDCl₃, 100 MHz) δ = 181.4 (C, CS), 143.0 (C, Ph *ipso*s), 131.9 (C, q, *J* = 33.0 Hz, Ph *meta*), 124.2 (C, q, *J* = 272.9 Hz, CF₃), 123.2 (CH, Ph *ortho*), 117.4 (CH, Ph *para*), 84.2 (C, Cp ring), 83.5 (C, Cp ring), 70.6 (CH, Cp ring), 70.0 (CH, unsubstituted Cp ring), 69.1 (CH, Cp ring), 66.7 (CH, Cp ring), 43.4 (CH₂), 13.3 (CH₃); IR (neat) ν (cm⁻¹) = 3253, 3071, 2918, 1639, 1551, 1384, 1277, 1126, 887, 700, 681; *m/z* = 523.0 [M+Na⁺] (69%), 500.0 [M⁺] (100%); HR-MS: calc. for C₂₁H₂₄N₂F₆SFe: 500.0444, found 500.0445; mp = 149-151 °C.



Rac-1-Thiourea-2-methyl ferrocene 20: ¹H NMR (Acetone d₆,

300 MHz) δ = 9.33 (s, 1 H), 8.34 (s, 2 H), 7.70 (s, 1 H), 7.60 (t, *J* = 4.9 Hz, 1 H), 4.69 (dd, *J* = 14.4, 5.1 Hz, 1 H), 4.57 (dd, *J* = 14.4, 4.7

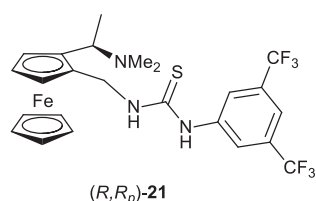
Hz, 1 H), 4.24 (dd, *J* = 2.3, 1.5 Hz, 1 H), 4.14-4.12 (m, 1 H), 4.12 (s, 5 H), 4.01 (t, *J* = 2.4 Hz, 1 H), 2.03 (s, 3 H).



(S,S_p)-1-[N-(N'-(3,5-(trifluoromethyl)phenyl)thiourea)]

methylene-2-(α-N-dimethylamine)ethylferrocene 21: To a solution of (S)-(R_p)-1-aminomethyl-2-(α-N-dimethylamine)ethylferrocene **48** (171 mg, 0.60 mmol) in dry CH₂Cl₂ (10 mL) was added drop-wise

3,5-(trifluoromethyl)phenylisothiocyanate (115 μL , 0.63 mmol). The mixture was stirred at room temperature for 16 hours. The crude mixture was then dry loaded on silica and purified by silica gel column chromatography (EtOAc:Hexane:NEt₃ 45:50:5) to yield a yellow powder (266 mg, yield 79%). ¹H-NMR (300 MHz, Acetone d₆) δ = 9.14 (br s, 2 H), 8.12 (s, 2 H), 7.67 (s, 1 H), 4.97 (d, J = 12.7 Hz, 1 H), 4.43 (d, J = 14.2 Hz, 1 H), 4.36 (dd, J = 2.2, 1.5 Hz, 1 H), 4.21 (dd, J = 2.3, 1.4 Hz, 1 H), 4.14 (s, 5 H), 4.10 (t, J = 2.4 Hz, 1 H), 4.05 (q, J = 7.2 Hz, 1 H), 1.97 (s, 6 H), 1.29 (s, 3 H), 1.27 (s, 3 H); ¹³C-NMR (101 MHz, Acetone d₆) δ (ppm) = 181.2 (C, CS), 143.0 (C, Ph *ipso*s), 132.1 (C, q, J = 33.0 Hz, Ph *meta*), 124.4 (C, q, J = 272.2 Hz, CF₃), 123.7 (CH, Ph *para*), 117.5 (CH, Ph *ortho*), 91.0 (C, Cp ring), 83.8 (C, Cp ring), 71.1 (CH, Cp ring), 70.2 (CH, unsubstituted Cp ring), 68.2 (CH, Cp ring), 66.5 (CH, Cp ring), 57.6 (CH, CpCHCH₃), 44.7 (CH₂), 39.1 (CH₃, NCH₃), 7.6 (CH₃, CpCHCH₃); IR (neat): ν (cm⁻¹) = 3096, 2977, 2941, 2867, 2830, 2786, 1529, 1375, 1274, 1126; m/z = 579.9 [M+Na⁺] (25%), 557.9 [M+H⁺] (100%), 512.9 [M⁺-NMe₂] (95%); HR-MS: calc. for C₂₄H₂₆N₃F₆SFe: 558.1101, found 558.1093; mp = 72-74°C.

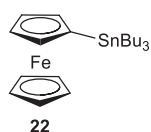


(*R,R_p*)-1-[N-(N'-(3,5-(trifluoromethyl)phenyl)thiourea)]

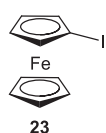
methylene-2-(α -N-dimethylamine)ethylferrocene 21: ¹H-NMR

(300 MHz, Acetone d₆) δ = 9.15 (br s, 2 H), 8.12 (s, 2 H), 7.67 (s, 1 H), 4.97 (d, J = 12.7 Hz, 1 H), 4.42 (dd, J = 13.4, 7.2 Hz, 1 H), 4.36 (dd, J = 2.3, 1.4 Hz, 1 H), 4.21 (dd, J = 2.3, 1.3 Hz, 1 H), 4.13 (s, 5 H), 4.10 (t, J = 2.4 Hz, 1 H), 4.05 (q, J = 7.2 Hz, 1 H), 1.97 (s, 6 H), 1.29 (s, 3 H), 1.27 (s, 3 H).

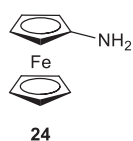
4.2.2.2. Precursors for achiral ferrocene (thio)ureas



(Tri-*n*-butylstannyl)ferrocene 22: to ferrocene (8.0 g, 43 mmol) in THF (40 mL) at 0 °C was added *t*-BuLi (38.0 mL, 64 mmol) over a period of 20 minutes. After 30 minutes, tetrabutyltin chloride (17.4 mL, 64 mmol) was added to the mixture and allowed to warm up to room temperature for 2 hours. A solution of sodium hydroxide (30 mL, 1M) was then added carefully, followed by Et₂O (40 mL). The organic phase was separated, washed with water (3×40 mL), dried over sodium sulfate and filtered. The solvents were removed by evaporation under reduced pressure and the residue was purified by silica gel flash chromatography (Hexane) to yield the title compound (10 g, yield 49%). ¹H NMR (300 MHz, CDCl₃) δ = 4.36 (t, *J* = 1.7 Hz, 2 H), 4.13 (s, 5 H), 4.04 (t, *J* = 1.7 Hz, 2 H), 1.66-1.54 (m, 6 H), 1.44-1.32 (m, 6 H), 1.07-1.01 (m, 6 H), 0.94 (t, *J* = 7.3 Hz, 9 H); ¹³C NMR (101 MHz, CDCl₃) δ = 74.6, 70.2, 68.6, 67.9, 29.2, 27.4, 13.7, 10.2. Data in agreement with that previously reported.¹¹⁹

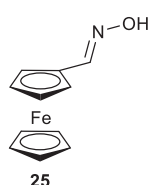


Iodoferrocene 23: Diiodide (5.9 g, 23.2 mmol) and tributylstannylferrocene **22** were stirred for 24 hours in CH₂Cl₂ (100 mL) at room temperature. The reaction mixture was then washed with sodium meta-bisulfite (4×40 mL), the organic phase was dried over sodium sulfate and the solvent was removed under reduced pressure. The residue was purified by silica gel column chromatography (Hexane) to give compound **23** (5.4 g, yield 82%). ¹H NMR (300 MHz, CDCl₃) δ = 4.43 (s, 2 H), 4.21 (s, 5 H), 4.17 (s, 2 H); ¹³C NMR (101 MHz, CDCl₃) δ = 74.6 (CH, Cp ring), 71.2 (CH, unsubstituted Cp ring), 68.9 (CH, Cp ring). Data in agreement with that previously reported.¹¹⁹



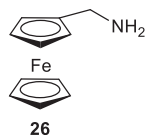
Ferrocene amine 24: iodoferrocene **23** (400 mg, 1.28 mmol), copper(I) iodide (25 mg, 0.13 mmol), iron(III) oxide (20 mg, 0.13 mmol) and sodium hydroxide

(120 mg, 2.94 mmol) were mixed in EtOH (12 mL). Aqueous ammonia (6 mL, 13.5 M) was added and the solution was heated in a pressure-proof vessel at 90 °C for 8 h. After cooling down to room temperature, Et₂O (150 mL) were added. The organic phase was washed with NaOH 1M (3x80 mL), dried over sodium sulfate, filtered and evaporated under reduced pressure. The residue was purified by silica gel column chromatography (Hexane:EtOAc 9:1 then 1:1) to yield compound **24** as an orange solid (166 mg, 65%). ¹H NMR (300 MHz, CDCl₃) δ = 4.11 (s, 5 H), 4.01 (s, 2 H), 3.86 (s, 2 H), 2.57 (s, 2 H); *m/z* = 224.1 [M+Na⁺]. Data in agreement with that previously reported.¹²⁰



1-Ferrocenyl methenoxime 25: Hydroxylamine hydrogen chloride (323 mg, 4.7 mmol) in water (2.5 mL) and sodium acetate (573 mg, 7.0 mmol) were added to a solution of ferrocene carboxaldehyde (498 mg, 2.3 mmol) in ethanol (10 mL).

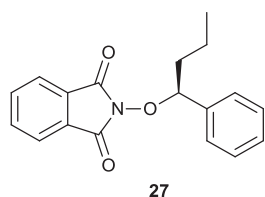
After 3 hours at reflux, the reaction mixture was allowed to cool down and was concentrated under reduced pressure. Chloroform was poured onto the residue and the mixture was stirred for 20 minutes, filtered and dried over sodium sulfate. The solvent was removed under reduced pressure to yield oxime **25** (635 mg, quantitative). ¹H NMR (300 MHz, CDCl₃) δ = 7.98 (s, 1 H), 4.54 (t, *J* = 1.9 Hz, 2 H), 4.36 (t, *J* = 1.9 Hz, 2 H), 4.22 (s, 5 H); *m/z* (TOF-ES⁻) = 228.0 [M-H⁺] (100%). Data in agreement with that previously reported.¹²¹



1-Ferrocenyl methanamine 26: A solution of oxime **25** (635 mg, 2.3 mmol) and lithium aluminium hydride (436 mg, 11.5 mmol) in THF (15 mL) was put at reflux for 2 hours. After cooling down to room temperature, sodium hydroxide 1 M was added dropwise until all the inorganics precipitated leaving a clear yellow solution, followed by Et₂O. The organic phase was separated and the precipitate washed with Et₂O (3x20 mL), dried over sodium sulfate, filtered and evaporated under reduced pressure. The residue was purified by

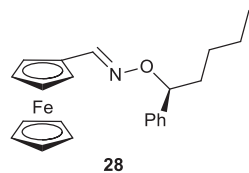
silica gel chromatography (EtOAc:Hexane:MeOH 1:1:0 to 9:0:1 with 5% NEt_3) to yield the desired product (470 mg, yield 95%). ^1H NMR (300 MHz, CDCl_3) δ = 4.33 (s, 2 H), 4.23 (s, 2 H), 4.16 (s, 5 H), 3.77 (s, 2 H), 2.13 (br s, 2 H); ^{13}C NMR (101 MHz, CDCl_3) δ = 86.5, 68.4, 67.8, 48.2. Data in agreement with that previously reported.¹²²

4.2.2.3. Precursors central chiral ferrocene (thio)ureas



(S)-N-(1-phenylbutoxy)phthalimide 27: (*R*)-1-phenylbutan-1-ol (1.215 g, 8 mmol), hydroxyphthalimide (1.320 g, 8 mmol) and triphenylphosphine (2.121 g, 8 mmol) were dissolved in dry THF (43

mL) and cooled to 0 °C. Diethyl azodicarboxylate (1.4 mL, 8.9 mmol) was added and the solution was stirred at 0 °C for 20 minutes and at 50 °C for another four days. The reaction mixture was then concentrated under reduced pressure and the residue was purified by silica gel column chromatography (Hexane:EtOAc 9:1) to give the title compound as a white solid (2.3 g, yield 95%). ^1H NMR (CDCl_3 , 300 MHz) δ = 7.74-7.63 (m, 4 H), 7.48-7.43 (m, 2 H), 7.36-7.28 (m, 3 H), 5.33 (t, J = 7.1 Hz, 1 H), 2.17 (dddd, J = 13.5, 9.9, 6.8, 5.7 Hz, 1 H), 1.89 (dddd, J = 13.5, 9.8, 7.3, 5.9 Hz, 1 H), 1.55 – 1.27 (m, 2 H), 0.97 (t, J = 7.4 Hz, 3 H); m/z = 318.1 [$\text{M}+\text{Na}^+$] (100%). Data in agreement with that previously reported.⁹⁸

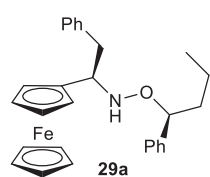


(E)-(S)-(+)-O-(1-phenylbutyl)ferrocene-1-carboxaloxime 28:

Compound **27** was dissolved in EtOH at 50 °C and the solution was left to cool down until precipitation started to occur, hydrazine hydrate (0.21 mL, 4.3 mmol) was added as followed by ferrocene carboxaldehyde (840 mg, 3.9 mmol). The mixture was stirred for 15 h at room temperature. The solvent was then evaporated under reduced pressure and the residue was taken with CH_2Cl_2 and filtered. The filtrate was concentrated under reduced pressure and purified by silica gel column chromatography

(Hexane:EtOAc 95:5) to give the title compound as a red solid (1.207 g, yield 85%). ^1H NMR (CDCl₃, 300 MHz) δ = 7.89 (s, 1 H), 7.27-7.18 (m, 5 H), 5.03 (t, J = 6.7, 1 H), 4.40 (d, J = 15.6, 2 H), 4.21 (s, 2 H), 4.00 (s, 5 H), 1.89 (m, 1 H), 1.68 (m, 1 H), 1.32 (m, 2 H), 0.87 (t, J = 7.3, 3 H); ^{13}C NMR (CDCl₃, 100 MHz) δ = 149.0 (CH), 143.0 (C), 128.3 (CH), 127.4 (CH), 126.9 (CH), 84.8 (CH), 76.8 (C), 70.2 (CH), 70.0 (CH), 69.5 (CH), 68.3 (CH), 67.4 (CH), 38.4 (C), 19.0 (C), 14.2 (CH₃); m/z (TOF-EI) = 384.1 (M+Na⁺, 100%). Data in agreement with that previously reported.⁹⁸

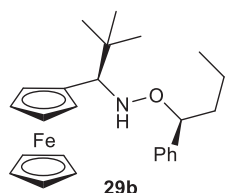
General procedure for alkylation of (E)-(S)-(+)-O-(1-phenylbutyl)ferrocene-1-carboxaloxime: The oxime (1 eq) was dissolved in dry toluene (0.36 M), cooled to -78 °C and BF₃.OEt₂ (3 eq) was added. After 15 minutes the alkylating agent (excess) was added dropwise and the mixture was stirred for 3 h. Saturated ammonium chloride was then added dropwise to quench the solution which was extracted with EtOAc (until no coloration). The organic phase was dried over sodium sulfate, filtered and evaporated under reduced pressure. The residue was purified by silica gel column chromatography (Hexane:EtOAc 9:1).



***N*-(1*R*)-(1'*S*)-1-Ferrocenyl-2-phenyl-*N*-(1-phenylbutoxy)-1-ethylamine**

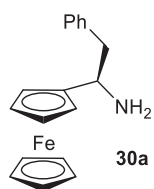
29a: Obtained from the oxime (215 mg, 0.6 mmol), BF₃.OEt₂ (0.22 mL, 1.8 mmol) and BnMgCl (2 mL, 1.9 mmol) as an orange solid (211 mg, yield 78%). ^1H NMR (CDCl₃, 300 MHz) δ = 7.55-7.20 (m, 10 H), 5.90 (s, 1 H), 4.72 (dd, J = 7.8, 5.9 Hz, 1 H), 4.20-4.14 (m, 3 H), 4.09 (s, 5 H), 4.01-3.94 (m, 2 H), 3.44 (dd, J = 13.1, 6.0 Hz, 1 H), 2.99 (dd, J = 13.1, 7.3 Hz, 1 H), 2.04-1.90 (m, 1 H), 1.77-1.57 (m, 2 H), 1.54-1.42 (m, 1 H), 1.09 (t, J = 7.2 Hz, 3 H); ^{13}C NMR (101 MHz, CDCl₃) δ = 143.4 (C, Ar), 139.3 (C, Ar), 129.8 (CH, Ar), 128.5 (CH, Ar), 128.1 (CH, Ar), 127.5 (CH, Ar), 126.7 (CH, Ar), 126.0 (CH, Ar), 88.7 (C, Cp ring), 85.2 (CH, OCH), 68.4 (CH, unsubstituted Cp ring), 67.6 (CH, Cp ring),

67.0 (CH, Cp ring), 66.4 (CH, Cp ring), 61.7 (CH, CpCH), 40.9 (CH₂, CpCHCH₂), 38.8 (CH₂, OCHCH₂), 19.4 (CH₂, OCHCH₂CH₂), 14.3 (CH₃); IR (neat) ν (cm⁻¹) = 3248, 3086, 3026, 2952, 2930, 2882, 2863, 1600, 1494, 1454, 1408, 1106, 821, 769, 750, 698. Data in agreement with that previously reported.¹²³



***N*-(1*R*)-(1'*S*)-1-Ferrocenyl-1-*t*-butyl-*N*-(1-phenylbutoxy)-1-ethylamine**

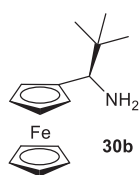
29b: Obtained from the oxime (394 mg, 1.1 mmol), BF₃.OEt₂ (0.41 mL, 3.3 mmol) and *t*-BuLi (1.9 mL, 3.3 mmol) as an orange yellow solid (274 mg, yield 60%). ¹H NMR (CDCl₃, 300 MHz) δ = 7.47-7.36 (m, 4 H), 7.34-7.27 (m, 1 H), 6.03 (s, 1 H), 4.68 (t, *J* = 7.1 Hz, 1 H), 4.15-3.90 (m, 8 H), 3.74 (s, 1 H), 3.29 (s, 1 H), 1.95-1.80 (m, 1 H), 1.68-1.55 (m, 1 H), 1.53-1.39 (m, 1H), 1.34-1.21 (m, 1 H), 0.93 (t, *J* = 7.4 Hz, 3 H), 0.86 (s, 9 H); ¹³C NMR (101 MHz, CDCl₃) δ = 143.2 (C, P h *ypsos*), 128.6 (CH, Ph), 127.7 (CH, Ph,), 127.3 (CH, Ph), 89.8 (C, Cp ring), 84.7 (CH, CHO), 70.5 (CH, Cp ring), 68.5 (H, unsubstituted Cp ring), 68.1 (CH, Cp ring), 67.3 (CH, CpCH), 66.2 (CH, Cp ring), 66.1 (CH, Cp ring), 38.5 (CH₂, CH₃CH₂CH), 34.7 (C, *t*-Bu), 27.7 (CH₃, *t*-Bu), 19.5 (CH₂, CH₃CH), 14.3 (CH₃, CH₂CH); IR (neat) ν (cm⁻¹) = 3210, 3086, 3025, 2954, 2869, 1454, 1427, 1361, 1105, 973, 823, 695. Data in agreement with that previously reported.¹²³



(*R*)-1-Ferrocenyl-2-phenyl-1-ethylamine 30a: *N*-(1*R*)-(1'*S*)-1-ferrocenyl-2-

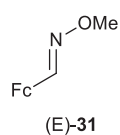
phenyl-*N*-(1-phenylbutoxy)-1-ethylamine **29a** (218 mg, 0.5 mmol) was added to acetic acid (10 mL), water (10 mL) and THF (3 mL). Zinc powder (1.25 g, 19 mmol) was added and the reaction mixture was heated at 40 °C for 21 h. After cooling down to room temperature, Et₂O (20 mL) was added and the solution was filtered and extracted with Et₂O. The aqueous phase was back extracted with CH₂Cl₂. The organic phases were washed with sodium hydroxide 1 M (pH=12), dried over sodium sulfate, filtered and evaporated under

reduced pressure. The crude amine was purified by silica gel column chromatography (EtOAc:MeOH:NEt₃ 1:0:0 then 90:5:5) to yield an orange solid (83 mg, yield 56%). ¹H NMR (300 MHz, CDCl₃) δ = 7.30-7.05 (m, 5 H), 4.16-4.13 (m, 1 H), 4.07 (s, 5 H), 4.06-4.02 (m, 2 H), 4.00-3.98 (m, 1 H), 3.80 (dd, *J* = 8.9, 4.6 Hz, 1 H), 2.89 (dd, *J* = 13.2, 4.5 Hz, 1 H), 2.60 (dd, *J* = 13.2, 8.9 Hz, 1 H), 1.86 (s, 2 H); ¹³C NMR (101 MHz, CDCl₃) δ = 139.3 (C, Ph *ypsos*), 129.5 (CH, Ph *ortho*), 128.5 (CH, Ph *meta*), 126.4 (CH, Ph *para*), 94.5 (C, Cp ring), 68.4 (CH, unsubstituted Cp ring), 67.6 (CH, Cp ring), 67.5 (CH, Cp ring), 52.4 (CH, CpCH), 46.2 (CH₂); IR (neat) ν (cm⁻¹) = 3357, 3282, 3102, 2963, 2866, 1595, 1479, 1386, 1360, 1234, 1104, 917, 811; *m/z* = 305.1 [M]⁺ (10%), 288.1 [M-NH₂]⁺ (100%); HR-MS: calc. for C₁₈H₁₉NFe: 305.0867, found 305.0869; mp = 51-53 °C. Data in agreement with that previously reported.¹²³

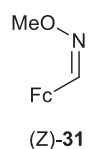


(R)-2,2-Dimethyl-1-ferrocenylpropan-1-amine 30b: A stirred mixture of hydroxylamine (255 mg, 0.6 mmol), THF (10 mL), HCl 1 M (50 mL) and zinc powder (3.18 g, 48 mmol) was heated at 80 °C for 16 h. After cooling to room

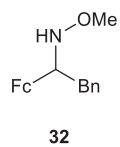
temperature, the solution was extracted with dichloromethane, and the organic phase was washed with NaOH_(aq) (pH=12), dried over sodium sulfate, filtered and evaporated under reduced pressure. The crude amine was purified by silica gel column chromatography (Hexane:EtOAc:NEt₃ 75:15:5) to yield a yellow solid (53 mg, yield 32%). ¹H-NMR (300 MHz, CDCl₃) δ = 4.21 (1H, dd, *J* = 3.5, 1.7 Hz), 4.15 (5H, s), 4.12 – 4.08 (3H, m), 3.37 (1H, s), 1.68 (2H, s), 0.81 (9H, s); ¹³C-NMR (101 MHz, CDCl₃) δ = 92.7, 69.7, 68.3, 67.0, 66.7, 66.0, 60.1, 34.7; IR (neat) ν (cm⁻¹) = 3357, 3282, 3102, 2963, 2866, 2825, 1595, 1479, 1386, 1360, 1234, 1104, 917, 811; *m/z* = 271.2 [M]⁺ (47%), 255.1 [M⁺-NH₂] (100%), 214.1 [M⁺-tBu] (38%); HR-MS: calc. for C₁₅H₂₁NFe: 271.1023, found 271.1024. Data in agreement with that previously reported.¹²³



(E)-O-(methoxy)ferrocene carboxaldoximine 31: *O*-methoxyamine hydrogen chloride (390 mg, 4.7 mmol) and sodium acetate (573 mg, 7.0 mmol) were added to a solution of ferrocene carboxaldehyde (498 mg, 2.3 mmol) in ethanol (10 mL). After 40 minutes at reflux, the reaction mixture was allowed to cool down and was concentrated under reduced pressure. The residue was dissolved in chloroform, filtered and dried over sodium sulfate. The solvent was removed under reduced pressure and the residue was purified by silica gel column chromatography (EtOAc:Hexane 1:9) to yield oxime **78** (ratio *E:Z* = 3:1) (545 mg, yield 96%). ¹H-NMR (300 MHz, CDCl₃) δ = 7.89 (s, 1 H), 4.53 (s, 2 H), 4.35 (s, 2 H), 4.22 (s, 5 H), 3.88 (s, 3 H); *m/z* = 244.1 [M+H⁺] (100%), 266.1 [M+Na⁺] (83%).

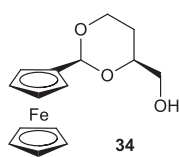


(Z)-O-(methoxy)ferrocene carboxaldoximine 31: ¹H-NMR (300 MHz, CDCl₃) δ = 7.13 (s, 1 H), 4.73 (s, 2 H), 4.35 (s, 2 H), 4.19 (s, 5 H), 3.96 (s, 3 H); *m/z* = 244.1 [M+H⁺] (100%), 266.1 [M+Na⁺] (83%).



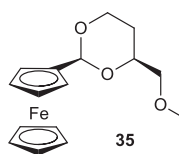
1-Ferrocenyl-2-phenyl-*N*-(methoxy)-1-ethylamine 32: Oxime **31** (200 mg, 0.82 mmol) was dissolved in toluene (5 mL), cooled to -78 °C and BF₃·OEt₂ (310 μL, 2.47 mmol) was added. After 15 minutes, BnMgCl (2.47 mL, 2.47 mmol) was added drop-wise and the mixture was stirred for 2 hours. Saturated ammonium chloride (4 mL) was then added drop-wise to quench the solution which was extracted with CH₂Cl₂. The organic phase was dried over sodium sulfate, filtered and evaporated under reduced pressure. The residue was purified by silica gel column chromatography (Hexane:EtOAc 9:1) to yield the title compound (151 mg, yield 55%). ¹H-NMR (300 MHz, CDCl₃) δ = 7.33-7.22 (m, 3 H), 7.20-7.16 (m, 2 H), 5.91 (br s, 1 H), 4.24-4.22 (m, 1 H), 4.16 (s, 5 H), 4.15-4.13 (m, 1 H), 4.11-4.09 (m, 1 H), 3.92 (dd, *J* = 7.7, 6.2 Hz, 1 H), 3.46 (s, 3 H), 3.08 (qd, *J* = 13.5, 6.9 Hz, 2 H).

4.2.2.4. Precursors for planar chiral ferrocene (thio)urea



(2*S*,4*S*)-4-(hydroxymethyl)-2-ferrocenyl-1,3-dioxolane 34: Ferrocene carboxaldehyde (4 g, 18.6 mmol) was dissolved in HC(OMe)₃ (40 mL) and PTSA (177 mg, 0.9 mmol) was added. After stirring for 23 hours at 80 °C,

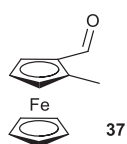
cooling to room temperature, potassium carbonate (200 mg, 1.4 mmol) was added and the mixture was filtered through Celite (CH₂Cl₂). The solvents were removed under reduced pressure and the residue was dried under high vacuum for 8 hours. The crude acetal (4.8 g) was then dissolved in CHCl₃ (7 mL) and injected to a mixture of (*S*)-1,2,4-butanetriol (1.95 g, 18.4 mmol), Camphorsulfonic acid (213 mg, 0.9 mmol), and activated 4 Å molecular sieves (10 g) in CHCl₃ (23 mL). The reaction mixture was stirred at room temperature for 19 hours and potassium carbonate (200 mg, 1.4 mmol) was added. After filtration over Celite (CH₂Cl₂), the solvents were removed under reduced pressure and the residue was purified by silica gel column chromatography (Hexane:EtOAc 3:2) to yield orange yellow crystals (2.39 g, yield 43%). ¹H NMR (CDCl₃, 300 MHz) δ = 5.39 (s, 1 H), 4.35 (d, *J* = 3.9 Hz, 2 H), 4.27- 4.12 (m, 9 H), 3.97- 3.85 (m, 2 H), 3.71- 3.55 (m, 2 H), 2.23 (t, *J* = 5.7 Hz, 1 H), 1.83 (ddd, *J* = 24.4, 12.6, 5.1 Hz, 1 H), 1.39 (ddd, *J* = 13.2, 4.0, 2.5 Hz, 1 H); ¹³C NMR (CDCl₃, 100 MHz) δ = 100.3 (CH, CpCH), 85.9 (C, Cp ring), 77.3 (CH, OCHCH₂OCH₃), 69.0 (CH, unsubstituted Cp ring), 68.2 (CH, Cp ring), 66.8 (CH, Cp ring), 66.6 (CH, Cp ring), 66.6 (CH₂, CH₂CH₂O), 65.8 (CH₂, CH₂OH), 27.0 (CH₂, OCH₂CH₂CHO). Data in agreement with that previously reported.¹⁰⁰



(2*S*,4*S*)-4-(methoxymethyl)-2-ferrocenyl-1,3-dioxolane 35: (2*S*,4*S*)-4-(hydroxymethyl)-2-ferrocenyl-1,3-dioxolane **34** (1.59 g, 5.3 mmol) in dry THF (12 mL) was added to a solution of NaH (190 mg, 7.9 mmol) in dry THF

(3 mL), followed by MeI (0.48 mL, 7.9 mmol). The mixture was stirred at room temperature

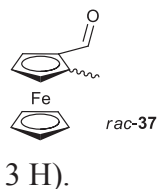
for 40 min and MeOH (1 mL) was slowly injected. Evaporation of the solvents under reduced pressure and purification by silica gel column chromatography (Hexane:EtOAc 7:3) yielded a dark orange oil (1.58 g, 95%). ^1H NMR (CDCl_3 , 300 MHz) δ = 5.37 (s, 1H), 4.35 (ddd, J = 4.8, 3.1, 1.8 Hz, 2H), 4.23 (ddd, J = 11.4, 5.1, 1.6 Hz, 1H), 4.18 (s, 5H), 4.12 (t, J = 1.8 Hz, 2H), 3.99 (dddd, J = 11.4, 6.3, 4.5, 2.5 Hz, 1H), 3.90 (ddd, J = 12.3, 11.4, 2.7 Hz, 1H), 3.53 (dd, J = 10.3, 6.1 Hz, 1H), 3.42 (s, 3H), 3.40 (dd, J = 10.3, 4.5 Hz, 1H), 1.77 (qd, J = 12.4, 5.1 Hz, 1H), 1.48 (dtd, J = 13.2, 2.5, 1.4 Hz, 1H); ^{13}C NMR (CDCl_3 , 100 MHz) δ = 100.0 (CH, CpCH), 86.0 (C, Cp ring), 76.0 (CH, $\text{OCHCH}_2\text{OCH}_3$), 75.6 (CH_2 , $\text{CH}_2\text{CH}_2\text{O}$), 68.9 (CH, unsubstituted Cp ring), 67.9 (CH, Cp ring), 66.7 (CH, Cp ring), 66.7 (CH_2 , CH_2OCH_3), 59.4 (CH_3), 28.0 (CH_2 , $\text{OCH}_2\text{CH}_2\text{CHO}$). Data in agreement with that previously reported.¹⁰⁰



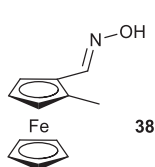
(*R_p*)-1-Carboxaldehyde-2-methylferrocene 37: (*2S,4S*)-4-(methoxymethyl)-2-ferrocenyl-1,3-dioxalane **35** (239 mg, 0.75 mmol) was dissolved in dry Et_2O (5

mL) and cooled to $-78\text{ }^\circ\text{C}$. A solution of *t*-BuLi (0.49 mL, 0.83 mmol) was added drop-wise and the solution was stirred 10 minutes at this temperature before removal of the cooling bath. After 1 hour, MeI (0.2 mL, 3 mmol) was injected at $-10\text{ }^\circ\text{C}$ and the mixture was slowly allowed to warm up to room temperature and stirred for 19 hours. After quenching with MeOH the solvents were removed under reduced pressure. The crude alkylated ferrocene **36** was reacted with PTSA (200 mg, 1 mmol) in CH_2Cl_2 (7 mL) and water (3 mL) for 20 min. The solution was then extracted with CH_2Cl_2 , dried over sodium sulfate, filtered and evaporated under reduced pressure. Purification by silica gel column chromatography (Hexane:EtOAc 9:1) yielded compound **37** as an orange solid (135 mg, yield 66%). ^1H NMR (CDCl_3 , 300 MHz) δ = 10.10 (s, 1 H), 4.69 (dd, J = 2.7, 1.5 Hz, 1 H), 4.49 (m, 1H), 4.46 (t, J = 2.6 Hz, 1 H), 4.20 (s, 5 H), 2.25 (s, 3 H); ^{13}C NMR (CDCl_3 , 100 MHz) δ = 194.0 (CH, CHO), 87.2 (C, CpCH₃),

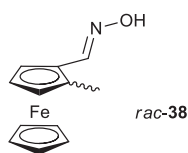
75.2 (CH, Cp ring), 71.2 (CH, Cp ring), 70.3 (CH, unsubstituted Cp ring), 69.6 (CH, Cp ring), 13.7 (CH₃). Data in agreement with that previously reported.¹⁰⁰



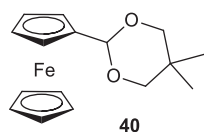
Rac-1-Carboxaldehyde-2-methylferrocene 37: ¹H NMR (CDCl₃, 300 MHz) δ = 10.09 (s, 1 H), 4.68 (s, 1 H), 4.48 (s, 1 H), 4.45 (s, 1 H), 4.19 (s, 5 H), 2.24 (s, 3 H).



(Rp)-1-Carboxaldoxime-2-methylferrocene 38: Hydroxylamine hydrogen chloride (82 mg, 1.2 mmol) in water (1.5 mL) was added to a solution of (*R_p*)-1-carboxaldehyde-2-methylferrocene **37** (135 mg, 0.6 mmol) and NaOAc (145 mg, 1.8 mmol) in EtOH (8 mL). The mixture was stirred at 80 °C for 5 hours, after which it was concentrated under reduced pressure. The residue was taken in CHCl₃ and filtered, yielding **38** an orange oil which was pure enough to be used without purification (134 mg, 93%). ¹H NMR (CDCl₃, 300 MHz) δ = 8.06 (s, 1 H), 4.49 (dd, *J* = 2.4, 1.5 Hz, 1 H), 4.22 (m, 1 H), 4.18 (t, *J* = 2.5 Hz, 1 H), 4.11 (s, 5 H), 2.10 (s, 3 H).



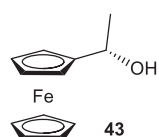
Rac-1-Carboxaldoxime-2-methylferrocene 38: ¹H NMR (CDCl₃, 300 MHz) δ = 8.11 (s, 1 H), 4.52 (dd, *J* = 2.3, 1.4 Hz, 1 H), 4.28 (t, *J* = 1.4 Hz, 1 H), 4.24 (t, *J* = 2.5 Hz, 1 H), 4.14 (s, 5 H), 2.10 (s, 3 H). Data in agreement with that previously reported.¹²³



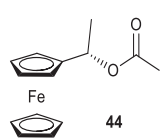
2-Ferrocenyl-4,4-dimethyl-1,3-dioxolane 40: Ferrocene carboxaldehyde (600 mg, 2.8 mmol) was dissolved in toluene (10 mL) and 2,2-dimethylpropanediol (732 mg, 7 mmol) and PTSA (27 mg, 0.1 mmol) were

added. After refluxing for 9 hours, the solution was cooled down to room temperature and evaporated under reduced pressure. The residue was purified by silica gel column chromatography (Hexane:EtOAc 4:1) to yield orange yellow crystals (724 mg, yield 86%). ^1H NMR (300 MHz, CDCl_3) δ = 5.25 (s, 1 H), 4.33 (t, J = 1.9 Hz, 2 H), 4.20 (s, 5 H), 4.14 (t, J = 1.9 Hz, 2 H), 3.71 (d, J = 11.2 Hz, 2 H), 3.58 (d, J = 10.8 Hz, 2 H), 1.26 (s, 3 H), 0.77 (s, 3 H); ^{13}C NMR (101 MHz, CDCl_3) δ = 100.6 (CH, CpCH), 86.4 (C, Cp ring), 77.7 (2 CH_2), 69.2 (CH, unsubstituted Cp ring), 68.3 (CH, Cp ring), 66.8 (CH, Cp ring), 30.3 (C, CH_3C), 23.2 (CH_3), 22.1 (CH_3); IR (neat) ν (cm^{-1}) = 3103, 2947, 2861, 2810, 1491, 1384, 1099, 1013, 807.

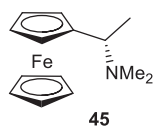
4.2.2.5. Precursors for the bi-functional ferrocene-thiourea



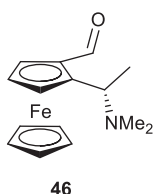
(S)-1-Hydroxy-1-ferrocenylethane 43: In dry THF (10 mL) at 0 °C was added (*R*)-CBS (364 mg, 1.32 mmol) and 20% of the total BH_3SMe_2 (0.44 mL, 0.88 mmol). After 5 minutes, acetylferrocene (1 g, 4.38 mmol) in dry THF (10 mL) and the rest of BH_3SMe_2 (1.75 mL, 3.5 mmol) were added simultaneously to the reaction mixture, which was left at room temperature for 15 minutes. MeOH was added until no bubbling occurred, the resulting solution was poured in $\text{NH}_4\text{Cl}_{(\text{sat})}$ and extracted with Et_2O . The etheral phase was washed with water and brine, dried over sodium sulfate, filtered and evaporated under reduced pressure. The residue was purified by silica gel column chromatography (Hexane:EtOAc 7:3) to yield the title compound as a yellow powder (998 mg, yield 99%). ^1H NMR (CDCl_3 , 300 MHz) δ = 4.59-4.51 (m, 1 H), 4.24-4.14 (m, 9 H), 1.89 (d, J = 4.7 Hz, 1 H), 1.44 (d, J = 6.4 Hz, 3 H); ^{13}C NMR (CDCl_3 , 100 MHz) δ = 95.4 (C, Cp ring), 68.8 (CH, unsubstituted Cp ring), 68.4 (CH, Cp ring), 66.7 (CH, Cp ring), 66.6 (CH, Cp ring), 65.7 (CH, CpCH), 23.8 (CH_3). Data in agreement with that previously reported.¹⁰¹



(S)-1-Acetoxy-1-ferrocenylethane 44: A solution of (*S*)-1-hydroxy-1-ferrocenylethane **43** (786 mg, 3.43 mmol), acetic anhydride (0.69 mL, 7.35 mmol), triethylamine (1.02 mL, 7.35 mmol) and DMAP (26 mg, 0.2 mmol) in dry CH₂Cl₂ (15 mL) was stirred at room temperature for 16 hours. The resulting mixture was washed with NaHCO₃ (3x20 mL), dried over sodium sulfate, filtered and evaporated under reduced pressure to yield the title compound as an orange solid (902 mg, yield 97%). ¹H NMR (CDCl₃, 300 MHz) δ = 5.83 (q, *J* = 6.5 Hz, 1 H), 4.28-4.27 (m, 1 H), 4.23-4.21 (m, 1 H), 4.18-4.15 (m, 2 H), 4.14 (s, 5 H), 2.03 (s, 3 H), 1.56 (d, *J* = 6.4 Hz, 3 H); ¹³C NMR (CDCl₃, 100 MHz) δ = 170.6 (C, CO), 88.1 (C, Cp ring), 69.2 (CH, Cp ring), 68.9 (CH, unsubstituted Cp ring), 68.5 (2 CH, Cp ring), 68.1 (CH, Cp ring), 66.1 (CH, CpCH), 21.5 (CH₃, acetyl), 21.1 (CH₃, CpCHCH). Data in agreement with that previously reported.¹⁰¹

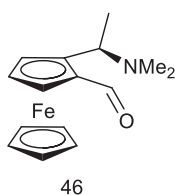


(S)-1-N-Dimethylamine-1-ferrocenylethane 45: (*S*)-1-acetoxy-1-ferrocenylethane **44** (2.75 g, 10.1 mmol) and dimethylamine (10 mL, 40% in H₂O) in MeOH (40 mL) were stirred for 24 hours at room temperature. Water (30 mL) was then added (a yellow precipitate appeared) and the solution was extracted with CH₂Cl₂. The organic phase was washed twice with water, dried over Na₂SO₄, filtered and evaporated under reduced pressure. The residue was purified by silica gel column chromatography (Hexane:EtOAc 2:3 then EtOAc:MeOH 9:1) to yield the title compound as an orange oil (2.47 mg, yield 95%). ¹H NMR (CDCl₃, 300 MHz) δ = 4.15- 4.06 (m, 9 H), 3.58 (q, *J* = 6.9 Hz, 1 H), 2.06 (s, 6 H), 1.43 (d, *J* = 6.9 Hz, 3 H); ¹³C NMR (CDCl₃, 100 MHz) δ = 86.9 (C, Cp ring), 69.4 (CH, Cp ring), 68.6 (CH, unsubstituted Cp ring), 67.4 (CH, Cp ring), 67.3 (CH, Cp ring), 66.9 (CH, Cp ring), 58.7 (CH, CpCHCH₃), 40.6 (CH₃, NCH), 16.1 (CH₃, CpCHCH); IR (neat) ν (cm⁻¹) = 3093, 2971, 2934, 2818, 2776, 1641, 1454, 1366, 1105, 1038, 1000, 814. Data in agreement with that previously reported.¹⁰¹



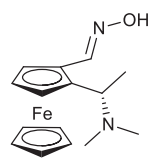
(*S,R_p*)-1-Carboxaldehyde- 2-((α -*N*-dimethylamine)ethyl)ferrocene 46: (*S*-

(α -*N*-dimethylamine)ethylferrocene **45** (502 mg, 1.95 mmol) was dissolved in dry Et₂O (8 mL) and cooled to -78 °C. *t*-BuLi (1.8 mL, 2.15 mmol) was added drop-wise and the mixture was stirred for 10 minutes. The cooling bath was then removed and the solution allowed warming up to room temperature. An orange precipitate formed as the temperature rose. After 1 hour, DMF was added drop-wise and the precipitate disappeared within seconds. Quenching with MeOH (4 mL) after 45 minutes yielded a red solution that was dry loaded on silica. Purification by silica gel column chromatography (Et₂O:NEt₃ 95:5) gave the aldehyde as a red-orange oil (494 mg, yield 88%). ¹H NMR (CDCl₃, 300 MHz) δ = 10.11 (s, 1 H), 4.80 (dd, J = 2.7, 1.5 Hz, 1 H), 4.58 (t, J = 2.7 Hz, 1 H), 4.55 (dd, J = 2.7, 1.5 Hz, 1 H), 4.22 (s, 5 H), 4.15 (q, J = 6.9 Hz, 1 H), 2.08 (s, 6 H), 1.48 (d, J = 6.9 Hz, 3 H); ¹³C NMR (CDCl₃, 100 MHz) δ = 193.4 (C, CHO), 91.6 (C, Cp ring), 72.6 (CH, Cp ring), 71.4 (CH, Cp ring), 70.5 (CH, unsubstituted Cp ring), 69.6 (CH, Cp ring), 55.7 (CH, CpCHCH₃), 40.5 (CH₃, NCH), 14.8 (CH₃, CpCHCH); m/z = 308.1 [M+Na⁺] (35%), 286.1 [M+H⁺] (84%), 241.0 [M⁺-NMe₂] (100%); HR-MS: calc. for C₁₅H₂₀NOFe: 286.0894, found 286.0897.



(*R,S_r*)-1-Carboxaldehyde- 2-((α -*N*-dimethylamine)ethyl)ferrocene 46: ¹H

NMR (CDCl₃, 300 MHz) δ = 10.10 (s, 1 H), 4.79 (dd, J = 2.6, 1.4 Hz, 1 H), 4.57 (t, J = 2.6 Hz, 1 H), 4.53 (dd, J = 2.6, 1.4 Hz, 1 H), 4.21 (s, 5 H), 4.12 (q, J = 6.8 Hz, 1 H), 2.08 (s, 6 H), 1.46 (d, J = 6.9 Hz, 3 H).



47

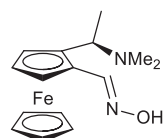
(*S,R_p*)-1-Carboxaldoxime-2-(α -*N*-dimethylamine)ethylferrocene 47: (*S, R_p*)-

1-carboxaldehyde-2-(α -*N*-dimethylamine)ethylferrocene **46** (83 mg, 0.29 mmol)

was dissolved in absolute ethanol (4 mL), and hydroxylamine hydrochloride (40

mg, 0.58 mmol) in water (0.75 mL) was then added, followed by sodium acetate

(71 mg, 0.87 mmol). The mixture was refluxed for 3 hours. After cooling down to room temperature, ethanol was removed under reduced pressure and the residue was stirred with chloroform (3 mL) for 5 min. The organic phase was separated, dried over sodium sulfate and filtered. Purification by silica gel column chromatography (EtOAc:MeOH:NEt₃ 94:3:3) gave the titled compound as an orange solid (80 mg, yield 91%). ¹H NMR (CDCl₃, 300 MHz) δ = 8.00 (s, 1 H), 4.69 (q, J = 7.0 Hz, 1 H), 4.45 (app t, J = 2.0 Hz, 1 H), 4.33-4.29 (m, 2 H), 4.16 (s, 5 H), 2.11 (s, 6 H), 1.63 (d, J = 7.0 Hz, 3 H); ¹³C NMR (CDCl₃, 100 MHz) δ = 148.7 (CH, aldoxime), 85.7 (C, Cp ring), 76.6 (C, Cp ring), 70.0 (CH, unsubstituted Cp ring), 69.5 (CH, Cp ring), 68.4 (CH, Cp ring), 68.3 (CH, Cp ring), 55.3 (CH, CpCHCH₃), 39.9 (2 CH₃, NCH₃), 17.1 (CH₃, CpCHCH₃); IR (neat) ν (cm⁻¹) = 3080, 2954, 2869, 2558 (br), 1637, 1445, 1376, 1240, 1199, 964, 819; m/z (TOF-AP+) = 301.1 [M+H⁺] (5%), 283.1 [M⁺-OH] (58%), 256.0 [M⁺-NMe₂] (88%), 239.0 [M⁺-NMe₂-OH] (100%); HR-MS: calc. for C₁₅H₂₁N₂OFe: 301.1003, found 301.0997; mp = 141-143 °C.



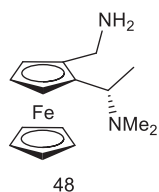
47

(*R,S_r*)-1-Carboxaldoxime-2-(α -*N*-dimethylamine)ethylferrocene 47: ¹H

NMR (CDCl₃, 300 MHz) δ = 8.00 (s, 1 H), 4.70 (q, J = 6.9 Hz, 1 H), 4.45 (dd,

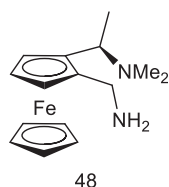
J = 2.3, 1.6 Hz, 1 H), 4.33-4.30 (m, 2 H), 4.16 (s, 5 H),), 2.11 (s, 6 H), 1.63 (d,

J = 7.0 Hz, 3 H).



(*S,S_p*)-1-(α -*N*-dimethylamine)ethyl-2-methylamineferrocene 48: to a solution of (*S*, *R_p*)-1-(α -*N*-dimethylamine)ethyl-2-methyloximeferrocene **47** (372 mg, 1.24 mmol) in THF (40 mL) was added LiAlH₄ (470 mg, 12.4 mmol).

The mixture was heated at 80 °C for 2 hours. After cooling down with an ice bath, ice was carefully dropped in the reaction mixture, followed by water. The compound was extracted with diethyl ether to quantitatively yield the title compound as an orange oil (353 mg, yield 99%). ¹H NMR (CDCl₃, 300 MHz) δ = 4.10-4.05 (m, 2 H), 4.02-3.96 (m, 6 H), 3.88 (q, J = 6.7 Hz, 1 H), 3.65 (d, J = 13.8 Hz, 1 H), 3.36 (d, J = 13.7 Hz, 1 H), 2.12 (br s, 2 H), 2.08 (s, 6 H), 1.22 (d, J = 6.7 Hz, 3 H); ¹³C NMR (CDCl₃, 100 MHz) δ = 89.7, 89.5, 69.0, 68.6, 67.3, 65.3, 56.9, 41.1, 39.5, 8.2; IR (neat) ν (cm⁻¹) = 3091, 2970, 2932, 2857, 2819, 2776, 1639, 1569, 1451, 1365, 1104, 1071, 999, 933, 808, 748; m/z (TOF-AP+) = 287.1 [M+H⁺] (100%); HR-MS: calc. for C₁₅H₂₃N₂Fe: 287.1211, found 287.1206.

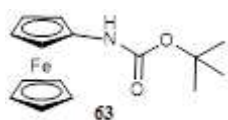


(*R,R_p*)-1-(α -*N*-dimethylamine)ethyl-2-methylamineferrocene 42: ¹H NMR (CDCl₃, 300 MHz) δ = 4.09-4.05 (m, 2 H), 3.98 (s, 5 H), 3.99-3.96 (m, 1 H), 3.87 (q, J = 6.7 Hz, 1 H), 3.64 (d, J = 13.8 Hz, 1 H), 3.35 (d, J = 13.8 Hz, 1 H),

2.33 (br s, 2 H), 2.07 (s, 6 H), 1.21 (d, J = 6.7 Hz, 3 H).

4.2.2.6. Ferrocene Boronate-Urea

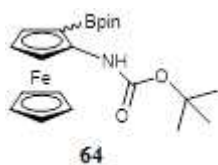
➤ Racemic synthesis of 1-urea-2-boronate ferrocene



***N*-Ferrocenyl-*O*-*tert*-butylcarbamate 63:** ferrocene amine **24** (175 mg, 0.87 mmol) and water (1 mL) were introduced in a vial and di-(*tert*-

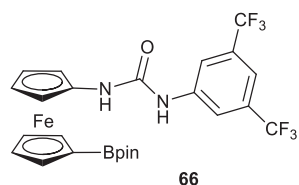
butyl)carbamate anhydride (208 mg, 0.96 mmol) was added. The heterogeneous mixture was

vigorously shaken for 20 minutes and extracted with EtOAc. The organic phase was dried over sodium sulfate, filtered and evaporated under reduced pressure to offer the title compound as an orange solid (260 mg, yield 99%). ^1H NMR (300 MHz, CDCl_3) δ = 5.68 (s, 1 H), 4.43 (s, 2 H), 4.16 (s, 5 H), 3.98 (t, J = 1.9 Hz, 2 H), 1.50 (s, 9 H); ^{13}C NMR (101 MHz, CDCl_3) δ = 97.0 (C, Cp ring), 69.2 (CH, unsubstituted Cp ring), 64.4 (CH, Cp ring), 61.0 (CH, Cp ring), 28.5 (CH_3); IR (neat) ν (cm^{-1}) = 3319, 3081, 2976, 2931, 1810, 1693, 1547, 1366, 1250, 1156, 1070, 814, 667; m/z = 301.1 [M^+] (90%), 245.0 [$\text{M}-t\text{Bu}+\text{H}^+$] (100%), 201.0 [$\text{FcNH}+\text{H}^+$] (20%); HR-MS: calc. for $\text{C}_{15}\text{H}_{19}\text{FeNO}_2$: 301.0765, found 301.0769; mp = 179-181 °C.



1-(N-Boc)-2-boronpinacol ferrocene 64: *N*-ferrocenyl-*O*-*tert*-butylcarbamate **63** (50 mg, 0.17 mmol) was dissolved in dry THF (1 mL) and cooled to -78 °C. *t*-BuLi (0.23 mL, 0.4 mmol) was then added drop-

wise and the mixture was warm up to -20 °C for 2.5 hours, after which $\text{B}(\text{O}i\text{-Pr})_3$ (48 μL , 0.21 mmol) was injected and left at this temperature for 10 minutes. The cooling bath was removed and the mixture stirred for 1.3 hours. Pinacol (29 mg, 0.25 mmol) was added and the reaction stirred for 18 hours at room temperature. The mixture was then diluted with Et_2O (3 mL) and water (1 mL) was added. Extraction with Et_2O followed by drying over sodium sulfate, filtration and evaporation under reduced pressure left a residue that was purified by silica gel column chromatography (Hexane:EtOAc 9:1) to give the title compound as orange dot-like crystals (13 mg, yield 18%). ^1H NMR (300 MHz, CDCl_3) δ = 6.13 (s, 1 H), 4.40 (s, 5 H), 4.36 (s, 1 H), 3.97 (t, J = 1.9 Hz, 2 H), 1.48 (s, 9 H), 1.36 (s, 12 H); ^{13}C NMR (101 MHz, CDCl_3) δ = 83.5 (C, CpN), 74.9 (CH, NCCH), 73.3 (CH, CHCHCH), 65.6 (CH, unsubstituted Cp ring), 63.7 (CH, BCCH), 28.8 (CH_3 , *t*-Bu), 25.0 (CH_3 , pinacol); ^{11}B NMR (128 MHz, CDCl_3) δ = 15.1; m/z = 427.2 [M^+] (17%), 345.1 [boronic acid $^+$] (100%) ; HR-MS: calc. for $\text{C}_{21}\text{H}_{30}^{11}\text{BFeNO}_4$: 427.1617, found 427.1619.



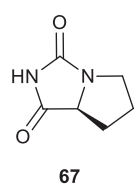
1-*N*-((*N'*-3,5-bis(trifluoromethyl)phenyl)urea-1'-

pinacolatoboron)ferrocene 66: The protected amine **64** (13 mg,

0.03 mmol) was dissolved in CH₂Cl₂ (2 mL) at 0 °C and

trifluoroacetic acid (0.5 mL, 6.5 mmol) was added. The cooling bath removed and the solution was stirred for 10 minutes. Saturated sodium hydrogenocarbonate (5 mL) was added and the mixture was extracted with EtOAc. The organic phase was dried over sodium sulfate, filtered and evaporated under reduced pressure. The residue was taken in dry CH₂Cl₂ (0.5 mL) and 3,5-bis(trifluoromethyl)phenyl isocyanate (5 μL, 0.03 mmol) was added. After 3.5 h stirring at room temperature, the solvent was removed under reduced pressure and the crude oil was purified by silica gel column chromatography (Hexane:EtOAc 4:1) to yield a yellow orange solid (11 mg, yield 63%). ¹H NMR (300 MHz, Acetone d₆) δ = 8.65 (s, 0.5 H), 8.20 (s, 2 H), 7.67 (s, 0.5 H), 7.58 (s, 1 H), 4.58 (t, *J* = 1.9 Hz, 2 H), 4.39 (t, *J* = 1.7 Hz, 2 H), 4.32 (t, *J* = 1.7 Hz, 2 H), 3.96 (t, *J* = 1.9 Hz, 2 H), 1.31 (s, 12 H); ¹³C NMR (101 MHz, Acetone d₆) δ = 153.4 (C, CO), 143.2 (C, Ph *ipso*s), 132.5 (C, q, *J* = 33.0 Hz, Ph *meta*), 124.6 (C, q, *J* = 272.4 Hz, CF₃), 118.9 (CH, Ph *ortho*), 115.3 (CH, Ph *para*), 97.4 (C, CpN), 83.9 (C, CpB), 75.5 (CH, Cp ring), 74.2 (CH, Cp ring), 65.7 (CH, Cp ring), 62.6 (CH, Cp ring), 25.4 (CH₃); ¹¹B NMR (MHz, Acetone) δ = 14.9; IR (neat) ν (cm⁻¹) = 3334, 3102, 2981, 2931, 1666, 1564, 1471, 1383, 1276, 1175, 1125, 735; *m/z* = 582.1 [M]⁺ (100%); HR-MS: calc. for C₂₅H₂₅¹¹BF₆FeN₂O₃: 582.1240, found 582.1246.

➤ Asymmetric synthesis of 1-urea-2-boronate ferrocene

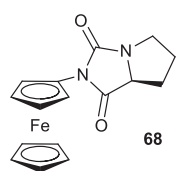


(*S*)-Tetrahydro-1H-pyrrolo[1,2-*c*]imidazole-1,3(2H)-dione 67: *L*-Proline (4.0

g, 34 mmol) and potassium isocyanate (3.7 g, 45 mmol) was stirred for 45 minutes

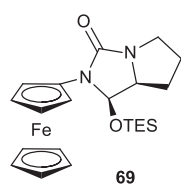
in water (20 mL) at 70 °C, then HCl 6 N (20 mL) was added to the mixture which

was heated up to reflux for 30 minutes. After allowing cooling down to room temperature, the solution was further cooled down with an ice-bath, upon which crystals started to appear. The solid liquid mixture was put at 5 °C for 16 hours and then filtered to give the title compound as white crystals (4.7 g, yield 98%). ¹H NMR (300 MHz, CDCl₃) δ = 8.93 (s, 1 H), 4.12 (t, *J* = 8.2 Hz, 1 H), 3.67 (dt, *J* = 10.6, 7.6 Hz, 1 H), 3.27 – 3.02 (m, 1 H), 2.28-2.16 (m, 1 H), 2.15-1.98 (m, 2 H), 1.83-1.69 (m, 1 H); ¹³C NMR (101 MHz, CDCl₃) δ = 174.8, 160.7, 64.8, 45.3, 27.5, 27.2. Data in agreement with that previously reported.¹¹¹



(-)-2-Ferrocenyl-7a*S*-tetrahydropyrrolo[1,2-*c*]imidazole-1,3-dione 68: A

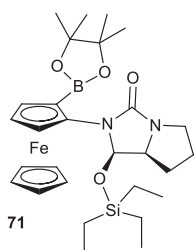
solution of iodoferrocene (2.18 g, 6.98 mmol), hydantoinone **67** (1.46 g, 10.48 mmol) and copper(I) oxide (800 mg, 5.59 mmol) in DMSO (7 mL) was stirred at 120 °C for 44 hours. After cooling down to room temperature, the mixture was extracted with Et₂O until not coloured. The organic phase was washed twice with water, brine, and was dried over sodium sulfate, filtered and evaporated under reduced pressure. The residue was purified by silica gel column chromatography (Hexane:EtOAc 4:1 then 7:3) to yield an orange solid (1.28 g, 56%). ¹H NMR (300 MHz, CDCl₃) δ = 4.95 (s, 1 H), 4.92 (s, 1 H), 4.20 (s, 5 H), 4.14 -4.08 (m, 3 H), 3.80 -3.71 (m, 1 H), 3.35 -3.27 (m, 1 H), 2.35 -2.25 (m, 1 H), 2.17 -2.02 (m, 2 H), 1.80 -1.67 (m, 1 H); ¹³C NMR (101 MHz, CDCl₃) δ = 172.3, 159.3, 89.1, 69.6, 65.4, 62.7, 62.8, 62.6, 46.0, 28.0, 26.9. Data in agreement with that previously reported.¹¹¹



(+)-2-Ferrocenyl-1*R*-triethylsilyloxy-7a*S*-hexahydropyrrolo[1,2-*c*]imidazol-

3-one 69: Amide **68** (1.13 g, 3.5 mmol) and Cp₂Zr(H)Cl (1.17 g, 4.5 mmol) were stirred in dry THF (10 mL) until the solution became clear. Triethylchlorosilane (0.76 mL, 4.5 mmol), imidazole (545 mg, 8.0 mmol) and DMAP (38 mg, 0.3 mmol) were then added to the solution and stirred at room temperature for 6 h. Et₂O (15 mL)

and water (5 mL) were then added. The organic phase was washed with saturated copper sulfate 10% (2x15 mL), sodium hydrogenocarbonate and water. After filtration over Celite (EtOAc), the organic phase was dried over sodium sulfate, filtered and evaporated under reduced pressure. The residue was purified by silica gel column chromatography (Hexane:EtOAc 4:1) to yield an orange solid (1.19 g, yield 78%). ^1H NMR (300 MHz, CDCl_3) δ = 5.42 (d, J = 5.9 Hz, 1 H), 4.80 (s, 1 H), 4.30 (s, 1 H), 4.18 (s, 5 H), 4.04 (s, 1 H), 3.95 -3.89 (m, 2 H), 3.64 - 3.56 (m, 1 H), 3.13 -3.06 (m, 1 H), 1.95 -1.85 (m, 3 H), 1.75 -1.67 (m, 1 H), 0.88 (t, J = 7.9 Hz, 9 H), 0.58 -0.50 (m, 6 H); ^{13}C NMR (101 MHz, CDCl_3) δ = 159.2, 96.7, 82.7, 69.2, 65.2, 63.7, 62.0, 61.7, 61.6, 45.8, 26.5, 25.3, 6.9, 5.1. Data in agreement with that previously reported.¹¹¹



(+)-(2S_P-((1R,7aS)-3-Oxo-1-((triethylsilyl)oxy)tetrahydro-1H-pyrrolo[1,2-c]imidazol-2(3H)-yl)ferrocenyl)boronic pinacol ester 71: Hydantoinine **69**

(711 mg, 1.6 mmol) was dissolved in dry THF (20 mL) at -78 °C and *t*-BuLi (2.1 mL, 3.6 mmol) was added drop-wise. After 45 minutes, boron tri-

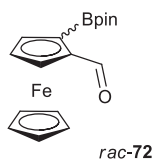
isopropoxide (0.9 mL, 4.1 mmol) was injected and the mixture was stirred for another hour. Pinacol (955 mg, 8.1 mmol) was then added, the cooling bath removed. The solution stirred for 15 min and wet Et₂O (20 mL) was added. After evaporation of the solvents under reduced pressure, the residue was purified by silica gel column chromatography (Hexane:EtOAc 7:3) to offer the title compound as an orange solid (759 mg, yield 82%). ^1H NMR (300 MHz, CDCl_3) δ = 5.40 (d, J = 6.4 Hz, 1 H), 4.30 (dd, J = 2.6, 1.3 Hz, 1 H), 4.25 -4.23 (m, 6 H), 4.14 (t, J = 2.5 Hz, 1 H), 3.91 (q, J = 6.8 Hz, 1 H), 3.59 (dt, J = 10.6, 6.8 Hz, 1 H), 3.06 (ddd, J = 10.6, 7.3, 5.3 Hz, 1 H), 2.02 -1.78 (m, 3 H), 1.75 -1.62 (m, 1 H), 1.28 (s, 6 H), 1.27 (s, 6 H), 0.87 (t, J = 7.9 Hz, 9 H), 0.50 (ddd, J = 11.6, 7.9, 2.9 Hz, 6 H); ^{13}C NMR (101 MHz, CDCl_3) δ = 159.8, 98.5, 84.6, 82.8, 71.3, 69.8, 67.3, 67.0, 62.0, 46.4, 26.5, 25.6, 25.2, 24.9, 6.9, 5.0; IR (neat) ν

(cm^{-1}) = 3094, 2955, 2877, 1712, 1461, 1377, 1311, 1138, 1117, 1107, 728; m/z = 566.2 $[\text{M}]^+$ (55%), 512.2 $[\text{M}-\text{CH}_2\text{CH}_2\text{CH}_2\text{CH}]^+$ rearrangement (100%); HR-MS: calc. for $\text{C}_{28}\text{H}_{43}\text{BFeN}_2\text{O}_4\text{Si}$: 566.2435, found 566.2430; mp = 98-100 °C.

➤ **Racemic synthesis of 1-methyleneurea-2-boronate ferrocene**

2-(2-boronic acid)ferrocenyl-4,4-dimethyl-1,3-dioxolane 72a: Dioxolane **40** (300 mg, 1.0 mmol) was dissolved in dry Et₂O (8 mL) and the solution was cooled down to -20 °C before *t*-BuLi (0.70 mL, 1.2 mmol) was added drop-wise. After 1 hour, boron tri-isopropyl (0.35 mL, 1.5 mmol) was added and the solution was stirred at -20 °C for 3.5 hours. Water (8 mL) was then added and the mixture was extracted with Et₂O. The organic phase was washed with brine, dried over sodium sulfate, filtered and evaporated under reduced pressure. The residue was purified by silica gel column chromatography (Hexane:EtOAc 9:1). Order of elution was the recovered starting dioxolane **40**, then the ortho-substituted product **72a** (41 mg, 12%). ¹H NMR (300 MHz, CDCl₃) δ = 5.69 (s, 1 H), 4.68 (dd, J = 2.3, 1.4 Hz, 1 H), 4.41 (dd, J = 2.4, 1.4 Hz, 1 H), 4.37 (t, J = 2.4 Hz, 1 H), 4.16 (s, 5 H), 3.84-3.72 (m, 4 H), 1.33 (s, 3 H), 0.81 (s, 3 H); ¹¹B NMR (128 MHz, CDCl₃) δ = 11.3.

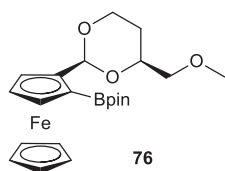
2-(3-boronic acid)ferrocenyl-4,4-dimethyl-1,3-dioxolane 72b: *meta*-substituted product **72b** (60 mg, 17%) came at later elution. ¹H NMR (300 MHz, CDCl₃) δ = 5.45 (s, 1 H), 4.66 (app s, 1 H), 4.59 (app s, 1 H), 4.40 (app s, 1 H), 4.27 (s, 5 H), 3.74 (dt, J = 11.1, 2.5 Hz, 2 H), 3.63 (dd, J = 11.2, 5.8 Hz, 2 H), 1.29 (s, 3 H), 0.77 (s, 3 H); ¹¹B NMR (128 MHz, CDCl₃) δ = 11.4.



1-Carboxaldehyde-2-pinacolatoboronylferrocene 73: Boronic acid **72a** (41 mg, 0.16 mmol) was dissolved in THF (2 mL) and pinacol (19 mg, 0.16 mmol)

was added. After one hour, the solvent was removed under reduced pressure and the residue was treated with PTSA (38 mg, 0.2 mmol) in CH₂Cl₂ (5 mL) at room temperature for 20 minutes. Water (5 mL) was added and the solution was extracted with CH₂Cl₂, dried over sodium sulfate, filtered and evaporated under reduced pressure. Purification by silica gel column chromatography (Hexane:EtOAc 9:1) yielded compound **72** as an orange solid (11 mg, yield 21%). ¹H NMR (300 MHz, CDCl₃) δ = 10.41 (s, 1 H), 5.10 (dd, *J* = 2.3, 1.5 Hz, 1 H), 4.79 (dd, *J* = 2.6, 1.5 Hz, 1 H), 4.78 (td, *J* = 2.6, 0.8 Hz, 1 H), 4.25 (s, 5 H), 1.37 (s, 6 H), 1.36 (s, 6 H).

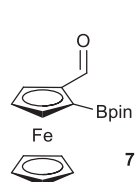
➤ **Asymmetric synthesis of 1-methaneurea-2-boronate ferrocene**



(2*S*,4*S*,*S*_{Fe})-4-(Methoxymethyl)-2-[α-pinacolboronoferrocenyl]-1,3-dioxolane 76: (2*S*,4*S*)-4-(methoxymethyl)-2-ferrocenyl-1,3-dioxalane **35** (386 mg, 1.22 mmol) was dissolved in dry Et₂O (6 mL) and cooled to -78

°C. A solution of *t*-BuLi (0.71 mL, 1.34 mmol) was added drop-wise and the solution was stirred 10 minutes at this temperature before removal of the cooling bath. After 1 hour, the temperature was set at -78 °C and B(*Oi*-Pr)₃ (0.42 mL, 1.83 mmol) was injected and the mixture was left at this temperature for 2 hours. Water (3 mL) was then added and the solution allowed warming up to room temperature. The phases were separated and the aqueous phase was saturated in sodium chloride. After extraction with EtOAc, the organic phases were gathered, dried over sodium sulfate, filtered and evaporated under reduced pressure. The residue was reacted with pinacol (164 mg, 1.39 mmol) in toluene (10 mL) at 90 °C for 1 hour. Evaporation of the solvent and purification by silica gel column chromatography (Hexane:EtOAc 7:3)

yielded the title compound as an orange yellow solid (384 mg, yield 72%). ^1H NMR (300 MHz, CDCl_3) δ = 5.71 (s, 1 H), 4.63 (s, 1 H), 4.33 (d, J = 7.7 Hz, 2 H), 4.28 (dd, J = 12.1, 5.2 Hz, 1 H), 4.13 (s, 5 H), 3.99 (t, J = 10.7 Hz, 1 H), 3.45 (dd, J = 10.4, 5.8 Hz, 1 H), 3.35-3.29 (m, 4 H), 1.77 (ddd, J = 17.1, 12.4, 5.2 Hz, 1 H), 1.50 (d, J = 13.2 Hz, 1 H), 1.34 (s, 6 H), 1.33 (s, 6 H); ^{13}C NMR (101 MHz, CDCl_3) δ = 100.6 (CH, CpCH), 91.3 (C, CpCHO), 83.0 (C, CpB), 76.2 (CH, $\text{OCHCH}_2\text{OCH}_3$), 75.7 (CH_2 , CH_2OCH_3), 74.5 (CH, Cp ring), 71.4 (CH, Cp ring), 70.2 (CH, Cp ring), 69.5 (CH, unsubstituted Cp ring), 67.1 (CH_2 , OCHCH_2), 59.4 (CH_3 , OCH_3), 28.6 (CH_2 , $\text{OCH}_2\text{CHCHCH}_2\text{OCH}_3$), 25.3 (CH_3 , pinacol), 24.9 (CH_3 , pinacol); IR (neat) ν (cm^{-1}) = 3092, 2976, 2951, 2915, 2874, 2805, 1667, 1462, 1320, 1139, 1001, 822, 750; m/z = 466.1 [$\text{M}(^{11}\text{B})+\text{Na}^+$] (45%), 465.1 [$\text{M}(^{10}\text{B})+\text{Na}^+$] (86%), 442.1 [$(^{11}\text{B})\text{M}^+$] (100%), 441.1 [$\text{M}(^{10}\text{B})$] $^+$ (48%); HR-MS: calc. for $\text{C}_{22}\text{H}_{31}^{11}\text{BFeO}_5$: 442.1614, found 442.1623; mp = 89-91 °C.

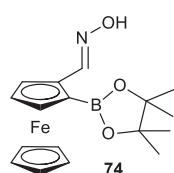


(*R_p*)-1-Carboxaldehyde-2-pinacolatoboronylferrocene 73: (*2S,4S,S_{Fe}*)-4-

(Methoxymethyl)-2-[α -pinacolboronoferrocenyl]-1,3-dioxolane **76** (117 mg,

73 0.26 mmol) was dissolved in CH_2Cl_2 (3 mL) and put at 0 °C. 2,4,6-collidine (141 μL , 0.78 mmol) was added, followed by TMSOTf (70 μL , 0.53 mmol). After completion (TLC monitoring, typically 3 h) the reaction mixture was quenched with water (2.5 mL) and the ice-bath removed. The solution was stirred 10 more minutes and then extracted with CH_2Cl_2 . The organic phases were dried over sodium sulfate, filtered and evaporated under reduced pressure. The residue was purified by silica gel column chromatography (EtOAc:Hexane 1:4) to yield the title compound as orange-red crystals (79 mg, yield 89%). ^1H NMR (300 MHz, CDCl_3) δ = 10.43 (s, 1 H), 5.11 (dd, J = 2.3, 1.5 Hz, 1 H), 4.80 (dd, J = 2.6, 1.5 Hz, 1 H), 4.79 (td, J = 2.6, 0.8 Hz, 1 H), 4.25 (s, 5 H), 1.37 (s, 6 H), 1.36 (s, 6 H); ^{13}C NMR (101 MHz, CDCl_3) δ = 196.8, 84.4, 83.7, 79.7, 77.4, 76.2, 71.4, 70.3, 25.1; ^{11}B NMR (128 MHz, CDCl_3) δ = 14.5; IR

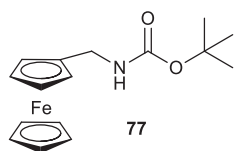
(neat) ν (cm^{-1}) = 3098, 2976, 2922, 2852, 1663, 1462, 1319, 1141; m/z = 363.1 [$\text{M}(^{11}\text{B})+\text{Na}^+$] (100%), 340.1 [$\text{M}(^{11}\text{B})^+$] (6%), 339.1 [$\text{M}(^{10}\text{B})^+$] (18%); HR-MS: calc. for $\text{C}_{17}\text{H}_{21}^{10}\text{BFeO}_3$: 339.0969, found 339.0964; mp = 118-120 °C.



(*R_p*)-1-Carboxaldoxime-2-pinacolatoboronylferrocene 74: (*R_p*)-1-

carboxaldehyde-2-pinacolatoboronylferrocene **73** (759 mg, 2.23 mmol) was dissolved in EtOH (10 mL) at 0 °C and 2,4,6-collidine (1.21 mL, 6.69 mmol) was added, followed by hydroxylamine hydrochloride (310 mg, 4.46 mmol). The mixture was stirred for 10 minutes at 0 °C and then concentrated under reduced pressure. The residue was purified by neutralised silica gel column chromatography (Hexane:EtOAc:NEt₃ 87:8:5) to yield an orange solid (500 mg, yield 63%). ¹H NMR (300 MHz, CDCl₃) δ = 8.47 (s, 1H), 4.94 (s, 1 H), 4.60 (d, J = 2.4 Hz, 1 H), 4.56 (t, J = 2.2 Hz, 1 H), 4.20 (s, 5 H), 1.35 (s, 12 H); ¹³C NMR (101 MHz, CDCl₃) δ = 151.5, 83.5, 81.5, 76.2, 73.7, 69.9, 69.2, 25.1 25.0; IR (neat) ν (cm^{-1}) = 3400-3180, 3096, 2977, 1622, 1458, 1313, 1139, 995, 950, 854, 812, 695; m/z = 355.1 [M^+] (100%), 338.3 [$\text{M}-\text{OH}^+$] (65%), 273.0 [boronic acid]⁺ (77%); HR-MS: calc. for $\text{C}_{17}\text{H}_{22}^{11}\text{BFeNO}_3$: 355.1042, found 355.1049; mp = 57-59 °C.

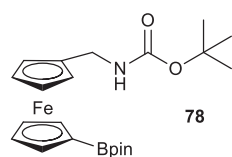
➤ **Synthesis of 1-methyleneurea-1'-boronate ferrocene**



***N*-Methylferrocene-*O*-*tert*-butylcarbamate 77:** aminomethylferrocene

26 (509 mg, 2.36 mmol) and water (2.4 mL) were introduced in a vial and di-(*tert*-butyl)carbamate anhydride (568 mg, 2.60 mmol) was added. The heterogeneous mixture was vigorously shaken for 20 minutes and extracted with EtOAc. The organic phase was dried over sodium sulfate, filtered and evaporated under reduced pressure. The residue was purified by silica gel column chromatography (Hexane:EtOAc 9:1) to offer

the title compound as an orange solid (598 mg, yield 80%). ^1H NMR (300 MHz, CDCl_3) δ = 4.75 (s, 1 H), 4.16 (s, 2H), 4.15 (s, 5 H), 4.11 (s, 2 H), 4.00 (d, J = 5.5 Hz, 2 H), 1.45 (s, 9 H); ^{13}C NMR (101 MHz, CDCl_3) δ = 155.7 (C, carbamate), 85.8 (C, *t*-Bu), 79.3 (C, Cp ring), 68.6 (CH, unsubstituted Cp ring), 68.1 (2 C, Cp ring), 39.9 (CH_2), 28.5 (CH_3); IR (neat) ν (cm^{-1}) = 3323, 3096, 2973, 2924, 1701, 1683, 1523, 1363, 1274, 1247, 1156, 815; m/z = 338.1 [$\text{M}+\text{Na}^+$] (86%), 315.1 [M^+] (100%), 259.0 [$\text{M}-t\text{Bu}+\text{H}^+$] (16%), 199.0 [$\text{M}^+-\text{NH}\text{Boc}$]; mp = 178-180 °C.



1-(*O*-*tert*-butylcarbamate)methyl-1'-(pinacol)boronylferrocene 78: *N*-

methylferrocene-*O*-*tert*-butylcarbamate **77** (150 mg, 0.48 mmol) was

dissolved in THF (1.2 mL) and cooled to -78 °C. *t*-BuLi (0.67 mL, 1.14

mmol) was then added drop-wise, stirred for 15 minutes. The mixture was warm up to -15 °C for 2.5 hours, and cooled again to -78 °C and boron tri-isopropoxide (48 μL , 0.21 mmol) in dry THF (0.4 mL) was injected. The cooling bath was removed and the mixture stirred for 1.5 hour. Pinacol (100 mg, 0.80 mmol) was added and the reaction stirred for 1 hour at room temperature. The mixture was then diluted with Et_2O (3 mL) and water (1 mL) was added. After extraction with Et_2O , the organic phase was washed twice with brine, dried over sodium sulfate, filtered and evaporated under reduced pressure. The residue was purified by silica gel column chromatography (Hexane: EtOAc 9:1) to give the title compound as orange oil (144 mg, yield 72%). ^1H NMR (300 MHz, CDCl_3) δ = 6.13 (s, 1 H), 4.41 (t, J = 1.8 Hz, 2 H), 4.31 (t, J = 1.8 Hz, 2 H), 4.17 (t, J = 1.8 Hz, 2 H), 4.07 (t, J = 1.8 Hz, 2 H), 4.00 (d, J = 6.1 Hz, 2 H), 1.42 (s, 9 H), 1.34 (s, 12 H); ^{13}C NMR (101 MHz, CDCl_3) δ = 155.9 (C, CO), 86.3 (C, *t*-Bu), 83.5 (C, CpB), 79.4 (C, Cp CH_2), 74.4 (CH, Cp ring), 72.5 (CH, Cp ring), 68.4 (CH, Cp ring), 68.1 (CH, Cp ring), 39.9 (CH_2), 28.7 (CH_3 , *t*-Bu), 25.1 (CH_3 , pinacol); m/z = 441.2 [M^+] (100%), 385.1 [$\text{M}-t\text{Bu}+\text{H}^+$] (11%), 325.1 [$\text{M}^+-\text{NH}\text{Boc}$] (52%); HR-MS: calc. for $\text{C}_{22}\text{H}_{32}^{11}\text{BNO}_4\text{Fe}$: 441.1774, found 441.1779.

4.3. Electrochemistry

Electrochemical studies were performed on a BAS 100W electrochemical analyser, with BAS 100W software. All measurements were carried out at 298 K in dry CH_2Cl_2 , in which tetrabutylammomium hexafluorophosphate (TBAPF_6) was dissolved as a supporting electrolyte (0.1 M). A conventional 3-electrode system was employed. The working electrode (WE) was a platinum disc electrode (diameter: 1.6 mm). Silver/silver chloride ($\text{Ag}|\text{AgCl}$) was used as an external reference electrode and a platinum wire was used as auxiliary electrode. Decamethylferrocene, dmfc (in a concentration comparable to the concentration of the analyte) was used as an internal reference. The concentration of the studied compounds was set at 0.3 mM. All cyclic voltammograms were carried out at a scan rate of $100 \text{ mV}\cdot\text{s}^{-1}$ unless otherwise stated. The cells and the volumetric flasks used were cleaned using a 1:1 solution of ammonia and hydrogen peroxide, rinsed 10 times using MilliQ® water, purified with a Millipore Elix-Gradient A10 system ($18 \text{ M}\Omega \text{ cm}$, $\text{toc} \leq 5 \text{ ppb}$, Millipore, France), and dried in the oven overnight. Prior to use, the platinum electrode was polished by hand using an eight pattern on aqueous slurries of $0.05 \mu\text{m}$ alumina powder pads and then thoroughly rinsed in deionised water followed by MeOH and drying in a directed stream of nitrogen. To check the electrochemical reversibility, voltammetric cycles were performed at different scan rates (0.1 to $1.1 \text{ V}\cdot\text{s}^{-1}$) between -250 and 900 mV (vs. $\text{Ag}|\text{AgCl}$) with plots of anodic peak current versus the square root of the scan rate, giving a straight line.

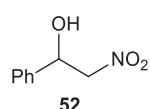
4.4. ^1H -NMR binding studies

Measurements were performed at 300 MHz on a Bruker AVIII300 NMR spectrometer at 294 K. Each ferrocenyl receptor was dissolved in deuterated acetonitrile (5 mM) and introduced in an NMR tube. The carboxylate guests were prepared as a 0.2 M stock solution (in deuterated

acetonitrile) to avoid dilution effect. Spectrum were recorded after each addition of the guest into the NMR tube and the urea signal was used to produce the different binding plots. When possible, the binding constant K was determined using the program WinEqNMR.¹⁰⁶

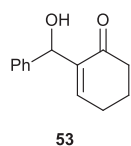
4.5. Procedures for Organocatalysis

4.5.1. General procedure for the Henry Reaction



1-Phenyl-2-nitroethan-1-ol 52: Nitromethane (540 μ L, 10 mmol), benzaldehyde (102 μ L, 1 mmol), DABCO (22 mg, 0.2 mmol) and the appropriate catalyst (0.2 mmol) in dry THF (1 mL) were stirred at room temperature for the time indicated. The mixture was directly purified by silica gel column chromatography (Hexane:EtOAc 9:1) to yield compound **52**. ^1H NMR (300 MHz, CDCl_3) δ = 7.43-7.33 (m, 5 H), 5.40 (dd, J = 9.4, 3.4 Hz, 1 H), 4.56 (dd, J = 13.2, 9.5 Hz, 1 H), 4.46 (dd, J = 13.2, 3.3 Hz, 1H), 3.24 (d, J = 3.8 Hz, 1 H); m/z (TOF-ES) = 166.2 [M-H^+]. Data in agreement with that previously reported.¹²⁴

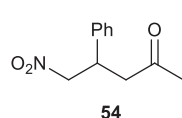
4.5.2. General procedure for the Morita-Baylis-Hillman



2-(hydroxy(phenyl)methyl)cyclohex-2-enone 53: 2-cyclohexenone (150 μ L, 1.55 mmol), benzaldehyde (79 μ L, 0.77 mmol), DABCO (21.6 mg, 0.155 mmol) and the appropriate catalyst (0.155 mmol) were stirred at room temperature for 24 hours. Work-up: addition of saturated ammonium chloride (1 mL) and extraction with EtOAc (2x3 mL). The organic phase was dried over sodium sulfate, filtered and evaporated under reduced pressure. Purification by silica gel column chromatography (Hexane:EtOAc 9:1) yielded compound **53** as a colourless oil. ^1H NMR (300 MHz, CDCl_3) δ = 7.36-7.20 (m, 5 H), 6.75 (t, J = 4.0 Hz, 1 H), 5.53 (s, 1 H), 3.57 (br s, 1 H), 2.44-2.34 (m, 4 H), 1.97 (dt, J = 12.5,

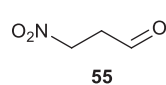
6.1 Hz, 2 H); m/z (TOF-ES-) = 201.2 [M-H⁺]. Data in agreement with that previously reported.¹²⁵

4.5.3. General procedure for the HBD/Enamine catalysis



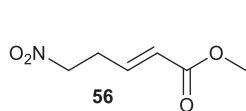
5-Nitro-4-phenylpentan-2-one 54: to a solution of catalyst **21** (11.1 mg, 0.02 mmol) in DMSO (1 mL) was added L-proline (2.3 mg, 0.02 mmol). Acetone (50 μ L, 0.7 mmol) and *trans*- β -nitrostyrene (14.9 mg, 0.1 mmol) were then introduced in the reaction mixture. The reaction was stirred for 2 days at room temperature. Addition of brine and extraction with CH₂Cl₂ gave the crude product which was purified by silica gel column chromatography (Hexane:EtOAc 9:1) to yield compound **54** (10 mg, 48%). ¹H NMR (300 MHz, CDCl₃) δ = 7.36-7.20 (m, 5 H), 4.70 (dd, J = 12.3, 6.9 Hz, 1 H), 4.60 (dd, J = 12.3, 7.7 Hz, 1 H), 4.01 (p, J = 7.1 Hz, 1 H), 2.92 (d, J = 7.0 Hz, 1 H), 2.12 (s, 3 H); ¹³C NMR (101 MHz, CDCl₃) δ = 205.5, 138.9, 129.2, 128.1, 127.5, 79.6, 46.3, 39.2, 30.6. Data in agreement with that previously reported.¹²⁶

4.5.4. General procedure for the formation of tetrasubstituted cyclopentane



3-Nitropropanaldehyde 55: freshly distilled acroleine (0.66 mL, 10.0 mmol) was added to a mixture of sodium nitrite (863 mg, 12.5 mmol) in THF (4 mL) and water (2.5 mL) at 0 °C. Acetic acid (0.63 mL, 11 mmol) was added drop-wise over a period of 40 minutes and the reaction mixture was stirred at 0 °C for 3 hours. EtOAc (5 mL) was then added, followed by saturated sodium carbonate (5 mL). After extraction with EtOAc, the organic phase was washed 3 times with brine, dried over sodium sulfate, filtered, evaporated under reduced pressure and further dried under high vacuum. A yellow oil was obtained (607 mg, yield 59%). ¹H NMR (300 MHz, CDCl₃) δ = 9.79 (s, 1 H), 4.67 (t, J = 6.0 Hz, 2 H), 3.17

(t, $J = 6.0$ Hz, 2 H); ^{13}C NMR (101 MHz, CDCl_3) $\delta = 196.8$ (CH, CHO), 67.7 (CH_2 , CH_2CHO), 39.6 (CH_2 , CH_2NO_2). Data in agreement with that previously reported.¹²⁷

**Methyl-(*E*)-5-nitropent-2-enoate****56:**

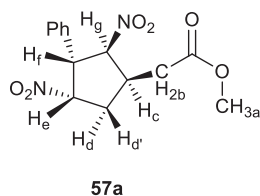
methyl-2-

(triphenylphosphanylidene)acetate (1.304 g, 3.9 mmol) and 3-

nitropropanaldehyde (607 mg, 5.9 mmol) were stirred in dry CH_2Cl_2 (15 mL) at room temperature for 29 hours. Saturated ammonium chloride (10 mL) and water (30 mL) were then added and the mixture was extracted with CH_2Cl_2 . The organic phase was dried over sodium sulfate, filtered and evaporated under reduced pressure. The residue was purified by silica gel column chromatography (Hexane:EtOAc 6:4) to yield the title compound as a colourless oil (361 mg, yield 58%). ^1H NMR (300 MHz, CDCl_3) $\delta = 6.77$ (dt, $J = 15.7, 6.9$ Hz, 1 H), 5.84 (ddd, $J = 15.4, 5.5, 4.0$ Hz, 1 H), 4.45 (t, $J = 6.8$ Hz, 2 H), 3.62 (s, 3 H), 2.80 (qd, $J = 6.8, 1.5$ Hz, 2 H); ^{13}C NMR (101 MHz, CDCl_3) $\delta = 165.9$ (C, COO), 141.7 (CH, CHCOO), 124.1 (CH, CHCH₂), 73.2 (CH_2 , CH_2NO_2), 51.5 (CH_3 , OCH₃), 29.2 (CH_2 , $\text{CH}_2\text{CH}_2\text{NO}_2$). Data in agreement with that previously reported.¹²⁷

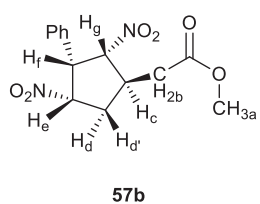
Catalysis: methyl-(*E*)-5-nitropent-2-enoate **56** (253 mg, 1.59 mmol) and β -trans-nitrostyrene (261 mg, 1.75 mmol) were mixed in dry CH_2Cl_2 (7.9 mL) at room temperature. Catalyst **21** (88 mg, 0.16 mmol) was then added and the solution was stirred for 7 days. Water (5 mL) was then added and the mixture was extracted with CH_2Cl_2 . The organic phase was dried over sodium sulfate, filtered and evaporated under reduced pressure. The residue was purified by silica gel column chromatography (Hexane:EtOAc 9:1 then 8:2) to yield a fraction containing 2 products along with some remaining starting methyl-(*E*)-5-nitropent-2-enoate. This fraction was evaporated under reduced pressure and the resulting oil was taken in a minimum amount of CH_2Cl_2 and Et_2O until, upon slow mixing, a thin white precipitate appears. The solid was

filtered and washed with a small amount of cold Et₂O to obtain an off-white powder (19 mg, yield 4%):



Methyl 2-(2,4-dinitro-3-phenylcyclopentyl)acetate 57a: ¹H NMR (300 MHz, CDCl₃) δ = 7.43-7.31 (m, 3 H, Ar), 7.25-7.17 (m, 2 H, Ar), 5.18 (dd, *J* = 7.7, 4.5 Hz, 1 H, H_g), 5.01 (dt, *J* = 9.7, 7.6 Hz, 1 H, H_e), 4.69 (dd, *J* = 7.8, 4.5 Hz, 1 H, H_f), 3.72 (s, 3 H, H_a), 3.19-3.10 (m, 1 H, H_c), 2.84-2.77 (m, 1 H, H_d), 2.57 (app dt, *J* = 12.7, 9.8 Hz, 1 H, H_d), 2.53 (d, *J* = 7.3 Hz, 2 H, H_b); ¹³C NMR (101 MHz, CDCl₃) δ = 171.2 (C, CO), 137.3 (C, Ph *ypsos*), 129.7 (CH, Ph), 128.8 (CH, Ph *para*), 127.3 (CH, Ph), 93.6 (CH, O₂NCHCHCH₂), 89.6 (CH, O₂NCHCH₂), 53.9 (CH, CHPh), 52.4 (CH₃), 38.6 (CH, CH₂CHCH₂), 35.7 (CH₂, cyclopentane), 33.7 (CH₂, CHCOOCH₃); *m/z* = 331.1 [M+Na⁺]; HR-MS: calc for C₁₄H₁₆N₂O₆Na: 331.0906, found 331.0910.

The filtrate still contained the sus-described product along with some starting methyl-(E)-5-nitropent-2-enoate and the other diastereoisomer:



Methyl 2-(2,4-dinitro-3-phenylcyclopentyl)acetate 57b: ¹H NMR (300 MHz, CDCl₃) δ = 7.43-7.31 (m, 3 H, Ar), 7.25-7.17 (m, 2 H, Ar), 5.71 (app q, *J* = 9.0 Hz, 1 H, H_e), 5.18 (dd, *J* = 3.6, 7.7 Hz, 1 H, H_g), 4.35 (dd, *J* = 10.4, 8.2 Hz, 1 H, H_f), 3.74 (s, 3 H, H_a), 3.32-3.25 (m, 1 H, H_c), 3.07 (dt, *J* = 13.4, 8.2 Hz, 1 H, H_d), 2.73 (d, *J* = 7.0 Hz, 2 H, H_b), 2.20 (dt, *J* = 13.4, 8.9 Hz, 1 H, H_d); ¹³C NMR (101 MHz, CDCl₃) δ = 171.0 (C, CO), 129.2 (CH, Ph), 128.7 (CH, Ph *para*), 127.5 (CH, Ph), 93.4 (CH, O₂NCHCHCH₂), 86.2 (CH, O₂NCHCH₂), 53.7 (CH, CHPh), 52.3 (CH₃), 38.4 (CH, CH₂CHCH₂), 37.6 (CH₂, CHCOOCH₃), 36.2 (CH₂, cyclopentane); *m/z* (TOF-AP⁺) = 309.1 [M+H⁺]; HR-MS: calc for C₁₄H₁₇N₂O₆: 309.1087, found 309.1082.

4.6. References

-
- ¹¹⁵ W. Qingmin, H. Runqiu, *J. Organomet. Chem.*, **2001**, 637, 94-98.
- ¹¹⁶ X. Wu, Q. Gao, S. Liu, A. Wu, *Org. Lett.*, **2014**, 16, 2888-2891.
- ¹¹⁷ I. M. Yonova, C. A. Osborne, N. S. Morrissette, E. R. Jarvo, *J. Org. Chem.*, **2014**, 79, 1947-1953.
- ¹¹⁸ H. Miyaji, S. R. Collinson, I. Prokes, J. H. R. Tucker, *Chem. Commun.*, **2003**, 64-65.
- ¹¹⁹ D. Guillaneux, H. B. Kagan, *J. Org. Chem.*, **1995**, 60, 2502-2505.
- ¹²⁰ A. Leonidova, T. Joshi, D. Nipkow, A. Frei, J-E. Penner, S. Konatschnig, M. Patra, G. Gasser, *Organometallics*, **2013**, 32, 2037-2040.
- ¹²¹ Y. Wang, A. Rapakousiou, C. Latouche, J-C. Daran, A. Singh, I. Ledoux-Rak, J. Ruiz, J-Y. Saillard, D. Astruc, *Chem. Commun.*, **2013**, 49, 5862-5864.
- ¹²² H. B. Kraatz, *J. Organomet. Chem.*, **1999**, 579, 222-226.
- ¹²³ A. Mulas, “*Ferrocene-based Chiral Monomers and Oligomers for Sensing Applications*”, University of Birmingham, **2013**.
- ¹²⁴ P. P. Bora, G. Bez, *Eur. J. Org. Chem.*, **2013**, 2922-2929.
- ¹²⁵ J. C. Gomes, M. T. Rodrigues Jr., A. Moyano, F. Coelho, *Eur. J. Org. Chem.*, **2012**, 6861-686.
- ¹²⁶ X-Y. Chen, G-J. Chen, J-L. Wang, Q. Wu, X-F. Lin, *Adv. Synth. Catal.*, **2013**, 355, 864-868.
- ¹²⁷ R. A. Bunce, J. T. Parker, *Synth. Comm.*, **1992**, 22, 377-380.

Appendix

- Crystal data and structure refinement (by Dr. Mateusz B. Pitak)

Fc-oxazole 1a:

Table 1. Crystal data and structure refinement details.

Identification code	2012ncs0119 (MFB 150 F2)	
Empirical formula	C ₃₁ H ₂₃ FeN ₃ O ₅ S	
Formula weight	605.43	
Temperature	100(2) K	
Wavelength	0.71075 Å	
Crystal system	Triclinic	
Space group	P-1	
Unit cell dimensions	$a = 7.4138(15)$ Å	$\alpha = 106.851(14)^\circ$
	$b = 11.173(2)$ Å	$\beta = 97.751(15)^\circ$
	$c = 16.823(3)$ Å	$\gamma = 101.490(14)^\circ$
Volume	1279.1(4) Å ³	
Z	2	
Density (calculated)	1.572 Mg / m ³	
Absorption coefficient	0.721 mm ⁻¹	
$F(000)$	624	
Crystal	Block; Red	
Crystal size	0.17 × 0.15 × 0.06 mm ³	
θ range for data collection	3.04 – 25.00°	
Index ranges	-8 ≤ h ≤ 8, -13 ≤ k ≤ 13, -20 ≤ l ≤ 16	
Reflections collected	13812	
Independent reflections	4457 [$R_{int} = 0.0242$]	
Completeness to $\theta = 25.00^\circ$	98.9 %	
Absorption correction	Semi-empirical from equivalents	
Max. and min. transmission	0.9580 and 0.8872	
Refinement method	Full-matrix least-squares on F^2	
Data / restraints / parameters	4457 / 0 / 370	
Goodness-of-fit on F^2	1.045	
Final R indices [$F^2 > 2\sigma(F^2)$]	$RI = 0.0267$, $wR2 = 0.0670$	
R indices (all data)	$RI = 0.0285$, $wR2 = 0.0680$	
Largest diff. peak and hole	0.333 and -0.304 e Å ⁻³	

Diffraction: AFC12 (Right): Kappa 3 circle with Rigaku Saturn724+ (2x2 bin mode) detector (profile data from ω -scans **Cell determination:** CrystalClear-SM Expert 2.0 r7 (Rigaku, 2011) **Data collection:** CrystalClear-SM Expert 2.0 r7 (Rigaku, 2011) **Data reduction and cell refinement:** CrystalClear-SM Expert 2.0 r7 (Rigaku, 2011) **Absorption**

correction: CrystalClear-SM Expert 2.0 r7 (Rigaku, 2011) **Structure solution:** SHELXS97 (Sheldrick, G.M. (2008). Acta Cryst. A64, 112-122.) **Structure refinement:** SHELXL97 (G Sheldrick, G.M. (2008). Acta Cryst. A64, 112-122.).

Table 2. Atomic coordinates [$\times 10^4$], equivalent isotropic displacement parameters [$\text{\AA}^2 \times 10^3$] and site occupancy factors. U_{eq} is defined as one third of the trace of the orthogonalized U^{ij} tensor.

Atom	<i>x</i>	<i>y</i>	<i>z</i>	U_{eq}	<i>S.o.f.</i>
C1	5033(2)	10882(2)	3443(1)	14(1)	1
C2	5059(2)	11398(2)	2790(1)	14(1)	1
C3	5764(2)	10793(2)	2097(1)	14(1)	1
C4	6411(2)	9707(2)	2088(1)	13(1)	1
C5	6330(2)	9188(2)	2746(1)	15(1)	1
C6	5634(2)	9786(2)	3439(1)	15(1)	1
C7	10585(2)	10933(2)	1801(1)	12(1)	1
C8	10625(2)	11802(2)	2586(1)	15(1)	1
C9	11454(2)	13103(2)	2760(1)	19(1)	1
C10	12240(2)	13528(2)	2155(1)	20(1)	1
C11	12176(2)	12648(2)	1368(1)	20(1)	1
C12	11341(2)	11346(2)	1187(1)	16(1)	1
C13	10623(2)	8884(2)	2093(1)	12(1)	1
C14	11440(2)	7908(2)	1803(1)	13(1)	1
C15	11941(2)	7249(2)	1010(1)	14(1)	1
C16	12162(3)	7844(2)	394(1)	20(1)	1
C17	12664(3)	7205(2)	-347(1)	24(1)	1
C18	12960(3)	5988(2)	-481(1)	22(1)	1
C19	12721(3)	5384(2)	122(1)	22(1)	1
C20	12211(2)	6009(2)	864(1)	19(1)	1
C21	11194(2)	8187(2)	3119(1)	13(1)	1
C22	11212(2)	7776(2)	3861(1)	14(1)	1
C23	10266(2)	8209(2)	4539(1)	18(1)	1
C24	10383(3)	7409(2)	5055(1)	21(1)	1
C25	11372(2)	6486(2)	4702(1)	20(1)	1
C26	11887(2)	6704(2)	3964(1)	16(1)	1
C27	7162(2)	5908(2)	2721(1)	16(1)	1
C28	6292(2)	6249(2)	3428(1)	19(1)	1
C29	6424(2)	5360(2)	3876(1)	21(1)	1
C30	7397(2)	4477(2)	3453(1)	18(1)	1
C31	7852(2)	4815(2)	2738(1)	17(1)	1
Fe1	9039(1)	6327(1)	3836(1)	12(1)	1
N1	4324(2)	11541(1)	4189(1)	17(1)	1
N2	9783(2)	9554(1)	1608(1)	12(1)	1
N3	10498(2)	9075(1)	2938(1)	13(1)	1
O1	4102(2)	12626(1)	4258(1)	24(1)	1
O2	4005(2)	10976(1)	4699(1)	26(1)	1
O3	7034(2)	9544(1)	584(1)	18(1)	1
O4	7056(2)	7643(1)	1082(1)	19(1)	1

O5	11831(2)	7448(1)	2469(1)	13(1)	1
S1	7467(1)	9007(1)	1240(1)	13(1)	1

Table 3. Bond lengths [Å] and angles [°].

C1–C2	1.381(2)
C1–C6	1.382(2)
C1–N1	1.481(2)
C2–C3	1.391(2)
C2–H2	0.9500
C3–C4	1.387(2)
C3–H3	0.9500
C4–C5	1.393(2)
C4–S1	1.7777(16)
C5–C6	1.385(2)
C5–H5	0.9500
C6–H6	0.9500
C7–C12	1.387(2)
C7–C8	1.387(2)
C7–N2	1.457(2)
C8–C9	1.388(2)
C8–H8	0.9500
C9–C10	1.389(2)
C9–H9	0.9500
C10–C11	1.389(3)
C10–H10	0.9500
C11–C12	1.388(2)
C11–H11	0.9500
C12–H12	0.9500
C13–C14	1.351(2)
C13–N3	1.393(2)
C13–N2	1.421(2)
C14–O5	1.3828(19)
C14–C15	1.461(2)
C15–C16	1.394(2)
C15–C20	1.395(2)
C16–C17	1.385(2)
C16–H16	0.9500
C17–C18	1.380(3)
C17–H17	0.9500
C18–C19	1.383(3)
C18–H18	0.9500
C19–C20	1.384(2)
C19–H19	0.9500
C20–H20	0.9500

C21–N3	1.297(2)
C21–O5	1.3668(19)
C21–C22	1.450(2)
C22–C26	1.432(2)
C22–C23	1.434(2)
C22–Fe1	2.0297(16)
C23–C24	1.420(3)
C23–Fe1	2.0374(17)
C23–H23	0.9500
C24–C25	1.420(3)
C24–Fe1	2.0465(18)
C24–H24	0.9500
C25–C26	1.419(2)
C25–Fe1	2.0474(18)
C25–H25	0.9500
C26–Fe1	2.0375(17)
C26–H26	0.9500
C27–C31	1.421(2)
C27–C28	1.421(2)
C27–Fe1	2.0500(17)
C27–H27	0.9500
C28–C29	1.420(3)
C28–Fe1	2.0360(18)
C28–H28	0.9500
C29–C30	1.419(3)
C29–Fe1	2.0428(17)
C29–H29	0.9500
C30–C31	1.423(2)
C30–Fe1	2.0456(17)
C30–H30	0.9500
C31–Fe1	2.0497(17)
C31–H31	0.9500
N1–O2	1.2233(19)
N1–O1	1.2304(19)
N2–S1	1.6672(14)
O3–S1	1.4292(12)
O4–S1	1.4302(12)
C2–C1–C6	123.66(15)
C2–C1–N1	118.15(15)
C6–C1–N1	118.19(14)
C1–C2–C3	118.04(16)
C1–C2–H2	121.0
C3–C2–H2	121.0
C4–C3–C2	119.24(15)
C4–C3–H3	120.4
C2–C3–H3	120.4

C3-C4-C5	121.64(15)
C3-C4-S1	119.11(12)
C5-C4-S1	119.19(13)
C6-C5-C4	119.44(16)
C6-C5-H5	120.3
C4-C5-H5	120.3
C1-C6-C5	117.94(15)
C1-C6-H6	121.0
C5-C6-H6	121.0
C12-C7-C8	121.04(15)
C12-C7-N2	118.31(14)
C8-C7-N2	120.63(14)
C7-C8-C9	119.19(15)
C7-C8-H8	120.4
C9-C8-H8	120.4
C8-C9-C10	120.33(16)
C8-C9-H9	119.8
C10-C9-H9	119.8
C9-C10-C11	119.89(16)
C9-C10-H10	120.1
C11-C10-H10	120.1
C12-C11-C10	120.19(16)
C12-C11-H11	119.9
C10-C11-H11	119.9
C7-C12-C11	119.34(16)
C7-C12-H12	120.3
C11-C12-H12	120.3
C14-C13-N3	110.92(14)
C14-C13-N2	126.69(14)
N3-C13-N2	122.01(14)
C13-C14-O5	106.25(14)
C13-C14-C15	137.52(15)
O5-C14-C15	116.22(14)
C16-C15-C20	119.24(15)
C16-C15-C14	120.89(15)
C20-C15-C14	119.87(15)
C17-C16-C15	119.76(17)
C17-C16-H16	120.1
C15-C16-H16	120.1
C18-C17-C16	120.66(17)
C18-C17-H17	119.7
C16-C17-H17	119.7
C17-C18-C19	119.95(16)
C17-C18-H18	120.0
C19-C18-H18	120.0
C18-C19-C20	119.98(17)
C18-C19-H19	120.0

C20–C19–H19	120.0
C19–C20–C15	120.39(16)
C19–C20–H20	119.8
C15–C20–H20	119.8
N3–C21–O5	114.13(14)
N3–C21–C22	129.83(15)
O5–C21–C22	115.66(14)
C26–C22–C23	108.07(15)
C26–C22–C21	125.08(15)
C23–C22–C21	125.96(16)
C26–C22–Fe1	69.68(9)
C23–C22–Fe1	69.65(9)
C21–C22–Fe1	117.93(11)
C24–C23–C22	107.31(16)
C24–C23–Fe1	69.99(10)
C22–C23–Fe1	69.07(9)
C24–C23–H23	126.3
C22–C23–H23	126.3
Fe1–C23–H23	126.2
C25–C24–C23	108.66(15)
C25–C24–Fe1	69.75(10)
C23–C24–Fe1	69.30(10)
C25–C24–H24	125.7
C23–C24–H24	125.7
Fe1–C24–H24	126.9
C26–C25–C24	108.28(16)
C26–C25–Fe1	69.30(10)
C24–C25–Fe1	69.67(10)
C26–C25–H25	125.9
C24–C25–H25	125.9
Fe1–C25–H25	126.7
C25–C26–C22	107.67(15)
C25–C26–Fe1	70.05(10)
C22–C26–Fe1	69.10(9)
C25–C26–H26	126.2
C22–C26–H26	126.2
Fe1–C26–H26	126.3
C31–C27–C28	107.83(15)
C31–C27–Fe1	69.71(10)
C28–C27–Fe1	69.12(10)
C31–C27–H27	126.1
C28–C27–H27	126.1
Fe1–C27–H27	126.7
C29–C28–C27	108.14(15)
C29–C28–Fe1	69.89(10)
C27–C28–Fe1	70.18(10)
C29–C28–H28	125.9

C27–C28–H28	125.9
Fe1–C28–H28	125.6
C30–C29–C28	108.03(15)
C30–C29–Fe1	69.79(10)
C28–C29–Fe1	69.37(10)
C30–C29–H29	126.0
C28–C29–H29	126.0
Fe1–C29–H29	126.4
C29–C30–C31	107.93(15)
C29–C30–Fe1	69.58(9)
C31–C30–Fe1	69.83(9)
C29–C30–H30	126.0
C31–C30–H30	126.0
Fe1–C30–H30	126.1
C27–C31–C30	108.06(15)
C27–C31–Fe1	69.73(9)
C30–C31–Fe1	69.52(9)
C27–C31–H31	126.0
C30–C31–H31	126.0
Fe1–C31–H31	126.4
C22–Fe1–C28	123.53(7)
C22–Fe1–C23	41.28(7)
C28–Fe1–C23	105.70(7)
C22–Fe1–C26	41.22(7)
C28–Fe1–C26	161.48(7)
C23–Fe1–C26	69.38(7)
C22–Fe1–C29	160.93(7)
C28–Fe1–C29	40.74(7)
C23–Fe1–C29	123.84(7)
C26–Fe1–C29	156.62(7)
C22–Fe1–C30	156.38(7)
C28–Fe1–C30	68.50(7)
C23–Fe1–C30	161.67(7)
C26–Fe1–C30	121.57(7)
C29–Fe1–C30	40.63(7)
C22–Fe1–C24	68.66(7)
C28–Fe1–C24	120.05(8)
C23–Fe1–C24	40.71(7)
C26–Fe1–C24	68.56(7)
C29–Fe1–C24	107.75(7)
C30–Fe1–C24	125.87(7)
C22–Fe1–C25	68.73(7)
C28–Fe1–C25	155.83(7)
C23–Fe1–C25	68.78(8)
C26–Fe1–C25	40.65(7)
C29–Fe1–C25	121.55(7)
C30–Fe1–C25	108.97(7)

C24–Fe1–C25	40.58(8)
C22–Fe1–C31	120.50(7)
C28–Fe1–C31	68.41(7)
C23–Fe1–C31	155.17(7)
C26–Fe1–C31	108.14(7)
C29–Fe1–C31	68.33(7)
C30–Fe1–C31	40.66(7)
C24–Fe1–C31	163.19(7)
C25–Fe1–C31	126.35(7)
C22–Fe1–C27	106.45(7)
C28–Fe1–C27	40.70(7)
C23–Fe1–C27	119.32(7)
C26–Fe1–C27	124.94(7)
C29–Fe1–C27	68.39(7)
C30–Fe1–C27	68.38(7)
C24–Fe1–C27	154.86(8)
C25–Fe1–C27	162.67(7)
C31–Fe1–C27	40.56(7)
O2–N1–O1	124.29(14)
O2–N1–C1	118.05(14)
O1–N1–C1	117.65(14)
C13–N2–C7	119.11(13)
C13–N2–S1	116.20(10)
C7–N2–S1	117.05(11)
C21–N3–C13	103.63(13)
C21–O5–C14	105.03(12)
O3–S1–O4	121.92(7)
O3–S1–N2	106.17(7)
O4–S1–N2	105.92(7)
O3–S1–C4	107.45(8)
O4–S1–C4	108.41(7)
N2–S1–C4	105.94(7)

Symmetry transformations used to generate equivalent atoms:

Table 4. Anisotropic displacement parameters [$\text{\AA}^2 \times 10^3$]. The anisotropic displacement factor exponent takes the form: $-2\pi^2[h^2 a^{*2} U^{11} + \dots + 2 h k a^* b^* U^{12}]$.

Atom	U^{11}	U^{22}	U^{33}	U^{23}	U^{13}	U^{12}
C1	11(1)	16(1)	12(1)	1(1)	3(1)	2(1)
C2	11(1)	13(1)	19(1)	6(1)	3(1)	3(1)
C3	13(1)	16(1)	15(1)	7(1)	4(1)	3(1)
C4	10(1)	14(1)	13(1)	3(1)	2(1)	1(1)
C5	14(1)	13(1)	20(1)	6(1)	4(1)	4(1)
C6	15(1)	17(1)	15(1)	8(1)	3(1)	3(1)
C7	10(1)	12(1)	16(1)	6(1)	2(1)	5(1)
C8	14(1)	17(1)	16(1)	6(1)	4(1)	6(1)
C9	19(1)	16(1)	19(1)	1(1)	1(1)	8(1)
C10	21(1)	12(1)	26(1)	8(1)	0(1)	4(1)
C11	22(1)	21(1)	22(1)	14(1)	5(1)	5(1)
C12	18(1)	18(1)	14(1)	6(1)	3(1)	6(1)
C13	11(1)	12(1)	13(1)	5(1)	3(1)	1(1)
C14	12(1)	14(1)	14(1)	8(1)	2(1)	1(1)
C15	12(1)	14(1)	14(1)	3(1)	2(1)	4(1)
C16	26(1)	20(1)	19(1)	8(1)	8(1)	10(1)
C17	32(1)	30(1)	18(1)	12(1)	10(1)	13(1)
C18	23(1)	28(1)	13(1)	0(1)	4(1)	10(1)
C19	26(1)	18(1)	21(1)	3(1)	5(1)	12(1)
C20	25(1)	18(1)	18(1)	8(1)	6(1)	9(1)
C21	10(1)	14(1)	14(1)	2(1)	4(1)	-1(1)
C22	11(1)	14(1)	14(1)	4(1)	1(1)	-2(1)
C23	20(1)	14(1)	14(1)	0(1)	3(1)	-2(1)
C24	26(1)	22(1)	9(1)	2(1)	2(1)	-4(1)
C25	20(1)	22(1)	16(1)	10(1)	-2(1)	-1(1)
C26	12(1)	21(1)	15(1)	7(1)	1(1)	2(1)
C27	14(1)	15(1)	15(1)	4(1)	-1(1)	1(1)
C28	13(1)	16(1)	26(1)	4(1)	5(1)	4(1)
C29	15(1)	21(1)	22(1)	6(1)	6(1)	-4(1)
C30	21(1)	13(1)	17(1)	5(1)	-1(1)	-1(1)
C31	19(1)	14(1)	13(1)	0(1)	-1(1)	2(1)
Fe1	13(1)	12(1)	11(1)	3(1)	3(1)	2(1)
N1	14(1)	21(1)	14(1)	3(1)	3(1)	5(1)
N2	11(1)	12(1)	13(1)	4(1)	2(1)	3(1)
N3	12(1)	13(1)	12(1)	4(1)	3(1)	2(1)
O1	31(1)	21(1)	22(1)	4(1)	9(1)	14(1)
O2	35(1)	32(1)	18(1)	11(1)	13(1)	12(1)
O3	17(1)	26(1)	12(1)	6(1)	3(1)	7(1)
O4	17(1)	14(1)	21(1)	1(1)	4(1)	2(1)
O5	14(1)	14(1)	13(1)	5(1)	5(1)	5(1)
S1	12(1)	14(1)	12(1)	2(1)	3(1)	4(1)

Table 5. Hydrogen coordinates [$\times 10^4$] and isotropic displacement parameters [$\text{\AA}^2 \times 10^3$].

Atom	<i>x</i>	<i>y</i>	<i>z</i>	<i>U</i> _{eq}	<i>S.o.f.</i>
H2	4609	12143	2813	17	1
H3	5801	11119	1636	17	1
H5	6749	8430	2720	18	1
H6	5572	9453	3897	18	1
H8	10093	11510	3000	18	1
H9	11483	13707	3295	22	1
H10	12819	14418	2279	24	1
H11	12706	12939	953	24	1
H12	11289	10744	648	20	1
H16	11969	8684	483	24	1
H17	12807	7610	-768	29	1
H18	13327	5565	-987	27	1
H19	12906	4541	27	26	1
H20	12044	5591	1276	23	1
H23	9672	8901	4627	22	1
H24	9883	7480	5553	26	1
H25	11642	5835	4923	24	1
H26	12559	6225	3603	19	1
H27	7264	6334	2310	19	1
H28	5720	6950	3576	22	1
H29	5945	5357	4372	25	1
H30	7691	3783	3618	22	1
H31	8503	4385	2342	20	1

Fc-oxazole 1c:**Table 1.** Crystal data and structure refinement details.

Identification code	2012ncs0117 (MFB 125 F2)	
Empirical formula	C ₂₉ H ₂₇ FeN ₃ O ₅ S	
Formula weight	585.45	
Temperature	100(2) K	
Wavelength	0.71075 Å	
Crystal system	Triclinic	
Space group	<i>P</i> -1	
Unit cell dimensions	<i>a</i> = 7.5361(2) Å	<i>α</i> = 101.502(7)°
	<i>b</i> = 11.3993(3) Å	<i>β</i> = 98.011(7)°
	<i>c</i> = 15.8905(11) Å	<i>γ</i> = 101.244(7)°
Volume	1289.24(10) Å ³	
<i>Z</i>	2	
Density (calculated)	1.508 Mg / m ³	
Absorption coefficient	0.713 mm ⁻¹	
<i>F</i> (000)	608	
Crystal	Block; Red	
Crystal size	0.15 × 0.15 × 0.09 mm ³	
<i>θ</i> range for data collection	3.31 – 27.48°	
Index ranges	-7 ≤ <i>h</i> ≤ 9, -14 ≤ <i>k</i> ≤ 14, -20 ≤ <i>l</i> ≤ 20	
Reflections collected	17297	
Independent reflections	5850 [<i>R</i> _{int} = 0.0345]	
Completeness to <i>θ</i> = 27.48°	98.9 %	
Absorption correction	Semi-empirical from equivalents	
Max. and min. transmission	0.9386 and 0.9006	
Refinement method	Full-matrix least-squares on <i>F</i> ²	
Data / restraints / parameters	5850 / 0 / 353	
Goodness-of-fit on <i>F</i> ²	1.088	
Final <i>R</i> indices [<i>F</i> ² > 2σ(<i>F</i> ²)]	<i>R</i> 1 = 0.0289, <i>wR</i> 2 = 0.0789	
<i>R</i> indices (all data)	<i>R</i> 1 = 0.0319, <i>wR</i> 2 = 0.0806	
Largest diff. peak and hole	0.377 and -0.349 e Å ⁻³	

Diffractometer: AFC12 (Right): Kappa 3 circle with Rigaku Saturn724+ (2x2 bin mode) detector (profile data from \w-scans **Cell determination:** CrystalClear-SM Expert 2.0 r7 (Rigaku, 2011) **Data collection:** CrystalClear-SM Expert 2.0 r7 (Rigaku, 2011) **Data reduction and cell refinement:** CrystalClear-SM Expert 2.0 r7 (Rigaku, 2011) **Absorption correction:** CrystalClear-SM Expert 2.0 r7 (Rigaku, 2011) **Structure solution:** SHELXS97 (Sheldrick, G.M. (2008). Acta Cryst. A64, 112-122.) **Structure refinement:** SHELXL97 (G Sheldrick, G.M. (2008). Acta Cryst. A64, 112-122.).

Table 2. Atomic coordinates [$\times 10^4$], equivalent isotropic displacement parameters [$\text{\AA}^2 \times 10^3$] and site occupancy factors. U_{eq} is defined as one third of the trace of the orthogonalized U^{ij} tensor.

Atom	x	y	z	U_{eq}	$S.o.f.$
C1	4826(2)	3727(1)	1471(1)	14(1)	1
C2	4715(2)	3138(1)	2152(1)	15(1)	1
C3	3930(2)	3634(1)	2838(1)	15(1)	1
C4	3285(2)	4690(1)	2822(1)	13(1)	1
C5	3431(2)	5278(1)	2135(1)	16(1)	1
C6	4211(2)	4789(1)	1447(1)	16(1)	1
C7	-890(2)	3531(1)	3193(1)	13(1)	1
C8	-873(2)	2682(1)	2437(1)	17(1)	1
C9	-1736(2)	1457(1)	2334(1)	23(1)	1
C10	-2611(2)	1089(1)	2979(1)	26(1)	1
C11	-2620(2)	1947(2)	3735(1)	24(1)	1
C12	-1751(2)	3170(1)	3846(1)	18(1)	1
C13	-873(2)	5537(1)	2811(1)	13(1)	1
C14	-1818(2)	6366(1)	3112(1)	13(1)	1
C15	-2352(2)	6824(1)	3956(1)	16(1)	1
C16	-1054(2)	8047(1)	4459(1)	19(1)	1
C17	-1626(2)	8599(1)	5308(1)	19(1)	1
C18	-3300(2)	9140(2)	5150(1)	30(1)	1
C19	-1417(2)	6419(1)	1789(1)	13(1)	1
C20	-1347(2)	7014(1)	1066(1)	15(1)	1
C21	-292(2)	6792(1)	392(1)	19(1)	1
C22	-347(2)	7721(1)	-84(1)	22(1)	1
C23	-1415(2)	8513(2)	286(1)	21(1)	1
C24	-2034(2)	8087(1)	999(1)	17(1)	1
C25	2471(2)	8662(1)	2368(1)	18(1)	1
C26	3449(2)	8518(1)	1666(1)	20(1)	1
C27	3356(2)	9500(1)	1245(1)	22(1)	1
C28	2298(2)	10248(1)	1682(1)	20(1)	1
C29	1759(2)	9731(1)	2378(1)	19(1)	1
Fe1	772(1)	8489(1)	1200(1)	12(1)	1
N1	5628(2)	3186(1)	734(1)	18(1)	1
N2	-44(2)	4818(1)	3308(1)	13(1)	1
N3	-655(2)	5549(1)	1955(1)	14(1)	1
O1	5994(2)	3802(1)	204(1)	26(1)	1
O2	5886(2)	2149(1)	691(1)	27(1)	1
O3	2599(1)	4688(1)	4371(1)	18(1)	1
O4	2632(1)	6592(1)	3826(1)	18(1)	1
O5	-2195(1)	6950(1)	2450(1)	14(1)	1
S1	2200(1)	5280(1)	3679(1)	13(1)	1

Table 3. Bond lengths [Å] and angles [°].

C1–C6	1.384(2)
C1–C2	1.385(2)
C1–N1	1.4734(17)
C2–C3	1.3871(19)
C2–H2	0.9500
C3–C4	1.3863(19)
C3–H3	0.9500
C4–C5	1.3957(19)
C4–S1	1.7710(14)
C5–C6	1.3835(19)
C5–H5	0.9500
C6–H6	0.9500
C7–C12	1.3854(19)
C7–C8	1.3872(19)
C7–N2	1.4453(17)
C8–C9	1.388(2)
C8–H8	0.9500
C9–C10	1.383(2)
C9–H9	0.9500
C10–C11	1.391(2)
C10–H10	0.9500
C11–C12	1.385(2)
C11–H11	0.9500
C12–H12	0.9500
C13–C14	1.3443(19)
C13–N3	1.3947(17)
C13–N2	1.4157(17)
C14–O5	1.3790(16)
C14–C15	1.4781(18)
C15–C16	1.531(2)
C15–H15A	0.9900
C15–H15B	0.9900
C16–C17	1.5273(19)
C16–H16A	0.9900
C16–H16B	0.9900
C17–C18	1.521(2)
C17–H17A	0.9900
C17–H17B	0.9900
C18–H18A	0.9800
C18–H18B	0.9800
C18–H18C	0.9800
C19–N3	1.2916(18)
C19–O5	1.3676(16)
C19–C20	1.4481(19)
C20–C21	1.4329(19)

C20–C24	1.435(2)
C20–Fe1	2.0339(14)
C21–C22	1.422(2)
C21–Fe1	2.0377(14)
C21–H21	0.9500
C22–C23	1.419(2)
C22–Fe1	2.0409(14)
C22–H22	0.9500
C23–C24	1.420(2)
C23–Fe1	2.0482(15)
C23–H23	0.9500
C24–Fe1	2.0396(14)
C24–H24	0.9500
C25–C26	1.420(2)
C25–C29	1.422(2)
C25–Fe1	2.0533(14)
C25–H25	0.9500
C26–C27	1.423(2)
C26–Fe1	2.0416(15)
C26–H26	0.9500
C27–C28	1.424(2)
C27–Fe1	2.0442(15)
C27–H27	0.9500
C28–C29	1.425(2)
C28–Fe1	2.0423(15)
C28–H28	0.9500
C29–Fe1	2.0509(14)
C29–H29	0.9500
N1–O1	1.2251(17)
N1–O2	1.2260(17)
N2–S1	1.6534(12)
O3–S1	1.4290(10)
O4–S1	1.4298(11)

C6–C1–C2	123.26(13)
C6–C1–N1	118.55(12)
C2–C1–N1	118.19(12)
C1–C2–C3	118.21(13)
C1–C2–H2	120.9
C3–C2–H2	120.9
C4–C3–C2	119.41(13)
C4–C3–H3	120.3
C2–C3–H3	120.3
C3–C4–C5	121.51(12)
C3–C4–S1	119.08(10)
C5–C4–S1	119.39(11)
C6–C5–C4	119.46(13)

C6-C5-H5	120.3
C4-C5-H5	120.3
C5-C6-C1	118.13(13)
C5-C6-H6	120.9
C1-C6-H6	120.9
C12-C7-C8	120.90(13)
C12-C7-N2	118.50(12)
C8-C7-N2	120.58(12)
C7-C8-C9	119.40(14)
C7-C8-H8	120.3
C9-C8-H8	120.3
C10-C9-C8	120.16(15)
C10-C9-H9	119.9
C8-C9-H9	119.9
C9-C10-C11	119.98(14)
C9-C10-H10	120.0
C11-C10-H10	120.0
C12-C11-C10	120.26(15)
C12-C11-H11	119.9
C10-C11-H11	119.9
C11-C12-C7	119.29(14)
C11-C12-H12	120.4
C7-C12-H12	120.4
C14-C13-N3	111.05(12)
C14-C13-N2	125.53(12)
N3-C13-N2	123.17(12)
C13-C14-O5	106.40(11)
C13-C14-C15	135.81(13)
O5-C14-C15	117.53(11)
C14-C15-C16	111.31(11)
C14-C15-H15A	109.4
C16-C15-H15A	109.4
C14-C15-H15B	109.4
C16-C15-H15B	109.4
H15A-C15-H15B	108.0
C17-C16-C15	113.17(12)
C17-C16-H16A	108.9
C15-C16-H16A	108.9
C17-C16-H16B	108.9
C15-C16-H16B	108.9
H16A-C16-H16B	107.8
C18-C17-C16	112.51(13)
C18-C17-H17A	109.1
C16-C17-H17A	109.1
C18-C17-H17B	109.1
C16-C17-H17B	109.1
H17A-C17-H17B	107.8

C17–C18–H18A	109.5
C17–C18–H18B	109.5
H18A–C18–H18B	109.5
C17–C18–H18C	109.5
H18A–C18–H18C	109.5
H18B–C18–H18C	109.5
N3–C19–O5	114.35(12)
N3–C19–C20	129.35(13)
O5–C19–C20	115.70(12)
C21–C20–C24	107.91(12)
C21–C20–C19	126.04(13)
C24–C20–C19	125.06(13)
C21–C20–Fe1	69.54(8)
C24–C20–Fe1	69.59(8)
C19–C20–Fe1	117.57(9)
C22–C21–C20	107.39(13)
C22–C21–Fe1	69.72(8)
C20–C21–Fe1	69.25(8)
C22–C21–H21	126.3
C20–C21–H21	126.3
Fe1–C21–H21	126.3
C23–C22–C21	108.76(13)
C23–C22–Fe1	69.98(8)
C21–C22–Fe1	69.48(8)
C23–C22–H22	125.6
C21–C22–H22	125.6
Fe1–C22–H22	126.5
C22–C23–C24	108.18(13)
C22–C23–Fe1	69.42(9)
C24–C23–Fe1	69.35(8)
C22–C23–H23	125.9
C24–C23–H23	125.9
Fe1–C23–H23	126.9
C23–C24–C20	107.76(13)
C23–C24–Fe1	70.00(8)
C20–C24–Fe1	69.16(8)
C23–C24–H24	126.1
C20–C24–H24	126.1
Fe1–C24–H24	126.3
C26–C25–C29	107.88(13)
C26–C25–Fe1	69.26(8)
C29–C25–Fe1	69.64(8)
C26–C25–H25	126.1
C29–C25–H25	126.1
Fe1–C25–H25	126.6
C25–C26–C27	108.26(13)
C25–C26–Fe1	70.15(8)

C27–C26–Fe1	69.71(9)
C25–C26–H26	125.9
C27–C26–H26	125.9
Fe1–C26–H26	125.8
C26–C27–C28	107.86(13)
C26–C27–Fe1	69.52(8)
C28–C27–Fe1	69.54(8)
C26–C27–H27	126.1
C28–C27–H27	126.1
Fe1–C27–H27	126.4
C27–C28–C29	107.88(13)
C27–C28–Fe1	69.68(8)
C29–C28–Fe1	69.96(8)
C27–C28–H28	126.1
C29–C28–H28	126.1
Fe1–C28–H28	125.9
C25–C29–C28	108.12(13)
C25–C29–Fe1	69.82(8)
C28–C29–Fe1	69.31(8)
C25–C29–H29	125.9
C28–C29–H29	125.9
Fe1–C29–H29	126.5
C20–Fe1–C21	41.21(6)
C20–Fe1–C24	41.26(6)
C21–Fe1–C24	69.32(6)
C20–Fe1–C22	68.74(6)
C21–Fe1–C22	40.80(6)
C24–Fe1–C22	68.59(6)
C20–Fe1–C26	123.44(6)
C21–Fe1–C26	105.73(6)
C24–Fe1–C26	161.41(6)
C22–Fe1–C26	120.08(7)
C20–Fe1–C28	156.96(6)
C21–Fe1–C28	161.03(6)
C24–Fe1–C28	121.74(6)
C22–Fe1–C28	125.09(6)
C26–Fe1–C28	68.59(6)
C20–Fe1–C27	160.47(6)
C21–Fe1–C27	123.30(6)
C24–Fe1–C27	156.78(6)
C22–Fe1–C27	107.15(6)
C26–Fe1–C27	40.77(6)
C28–Fe1–C27	40.78(6)
C20–Fe1–C23	68.80(6)
C21–Fe1–C23	68.82(6)
C24–Fe1–C23	40.66(6)
C22–Fe1–C23	40.60(6)

C26–Fe1–C23	155.89(6)
C28–Fe1–C23	108.54(6)
C27–Fe1–C23	121.32(6)
C20–Fe1–C29	121.11(6)
C21–Fe1–C29	155.77(6)
C24–Fe1–C29	108.44(6)
C22–Fe1–C29	162.63(7)
C26–Fe1–C29	68.31(6)
C28–Fe1–C29	40.74(6)
C27–Fe1–C29	68.43(6)
C23–Fe1–C29	126.13(6)
C20–Fe1–C25	106.83(6)
C21–Fe1–C25	119.74(6)
C24–Fe1–C25	125.13(6)
C22–Fe1–C25	155.17(7)
C26–Fe1–C25	40.59(6)
C28–Fe1–C25	68.49(6)
C27–Fe1–C25	68.43(6)
C23–Fe1–C25	162.60(6)
C29–Fe1–C25	40.55(6)
O1–N1–O2	124.22(12)
O1–N1–C1	117.98(12)
O2–N1–C1	117.80(12)
C13–N2–C7	120.03(11)
C13–N2–S1	117.26(9)
C7–N2–S1	118.01(9)
C19–N3–C13	103.33(11)
C19–O5–C14	104.80(10)
O3–S1–O4	121.10(6)
O3–S1–N2	106.56(6)
O4–S1–N2	106.41(6)
O3–S1–C4	107.34(6)
O4–S1–C4	107.97(6)
N2–S1–C4	106.65(6)

Symmetry transformations used to generate equivalent atoms:

Table 4. Anisotropic displacement parameters [$\text{\AA}^2 \times 10^3$]. The anisotropic displacement factor exponent takes the form: $-2\pi^2[h^2 a^{*2} U^{11} + \dots + 2 h k a^* b^* U^{12}]$.

Atom	U^{11}	U^{22}	U^{33}	U^{23}	U^{13}	U^{12}
C1	11(1)	18(1)	13(1)	1(1)	2(1)	2(1)
C2	13(1)	14(1)	18(1)	4(1)	3(1)	3(1)
C3	13(1)	17(1)	16(1)	7(1)	3(1)	3(1)
C4	10(1)	15(1)	13(1)	2(1)	2(1)	2(1)
C5	14(1)	15(1)	19(1)	6(1)	3(1)	4(1)
C6	15(1)	19(1)	15(1)	7(1)	3(1)	2(1)
C7	12(1)	13(1)	14(1)	4(1)	2(1)	4(1)
C8	15(1)	19(1)	18(1)	1(1)	2(1)	6(1)
C9	20(1)	17(1)	28(1)	-2(1)	-2(1)	7(1)
C10	21(1)	14(1)	37(1)	9(1)	-6(1)	0(1)
C11	21(1)	26(1)	27(1)	15(1)	0(1)	0(1)
C12	18(1)	22(1)	15(1)	6(1)	3(1)	4(1)
C13	13(1)	12(1)	12(1)	3(1)	2(1)	1(1)
C14	14(1)	13(1)	14(1)	4(1)	3(1)	2(1)
C15	18(1)	16(1)	15(1)	4(1)	7(1)	5(1)
C16	17(1)	21(1)	17(1)	0(1)	4(1)	2(1)
C17	21(1)	20(1)	16(1)	0(1)	4(1)	6(1)
C18	27(1)	32(1)	30(1)	-2(1)	6(1)	12(1)
C19	11(1)	14(1)	13(1)	1(1)	3(1)	0(1)
C20	13(1)	16(1)	13(1)	2(1)	0(1)	-1(1)
C21	22(1)	16(1)	13(1)	-2(1)	3(1)	-1(1)
C22	27(1)	24(1)	10(1)	3(1)	2(1)	-4(1)
C23	20(1)	23(1)	18(1)	9(1)	-3(1)	-1(1)
C24	12(1)	22(1)	18(1)	7(1)	0(1)	2(1)
C25	17(1)	17(1)	18(1)	4(1)	-2(1)	1(1)
C26	13(1)	19(1)	27(1)	3(1)	2(1)	3(1)
C27	16(1)	22(1)	24(1)	4(1)	5(1)	-3(1)
C28	23(1)	13(1)	21(1)	2(1)	-2(1)	0(1)
C29	22(1)	19(1)	13(1)	-2(1)	-1(1)	5(1)
Fe1	13(1)	13(1)	10(1)	2(1)	3(1)	1(1)
N1	15(1)	25(1)	14(1)	2(1)	2(1)	6(1)
N2	12(1)	12(1)	14(1)	3(1)	2(1)	2(1)
N3	14(1)	15(1)	13(1)	2(1)	3(1)	1(1)
O1	31(1)	33(1)	19(1)	10(1)	12(1)	10(1)
O2	33(1)	27(1)	23(1)	2(1)	8(1)	16(1)
O3	19(1)	25(1)	12(1)	5(1)	3(1)	7(1)
O4	16(1)	16(1)	20(1)	0(1)	2(1)	2(1)
O5	14(1)	15(1)	14(1)	5(1)	4(1)	5(1)
S1	12(1)	15(1)	12(1)	2(1)	2(1)	3(1)

Table 5. Hydrogen coordinates [$\times 10^4$] and isotropic displacement parameters [$\text{\AA}^2 \times 10^3$].

Atom	<i>x</i>	<i>y</i>	<i>z</i>	<i>U</i> _{eq}	<i>S.o.f.</i>
H2	5164	2415	2148	18	1
H3	3835	3254	3315	18	1
H5	2997	6007	2140	19	1
H6	4322	5173	972	19	1
H8	-277	2938	1993	21	1
H9	-1724	869	1820	28	1
H10	-3206	250	2906	31	1
H11	-3224	1693	4176	29	1
H12	-1745	3756	4364	22	1
H15A	-2323	6207	4313	19	1
H15B	-3626	6938	3848	19	1
H16A	205	7915	4596	23	1
H16B	-1017	8641	4081	23	1
H17A	-1906	7952	5634	23	1
H17B	-585	9252	5674	23	1
H18A	-3047	9761	4809	45	1
H18B	-3571	9524	5712	45	1
H18C	-4362	8485	4828	45	1
H21	331	6144	283	22	1
H22	235	7798	-570	26	1
H23	-1672	9208	90	25	1
H24	-2772	8448	1366	21	1
H25	2320	8138	2761	22	1
H26	4061	7876	1506	24	1
H27	3902	9634	758	26	1
H28	2004	10964	1535	25	1
H29	1047	10046	2780	23	1

Ylide 2:**Table 1.** Crystal data and structure refinement details.

Identification code	2012ncs0118 (MFB 127 Ylide)	
Empirical formula	C ₁₆ H ₁₆ FeN ₂ O ₂	
Formula weight	324.16	
Temperature	120(2) K	
Wavelength	0.71075 Å	
Crystal system	Monoclinic	
Space group	P21/c	
Unit cell dimensions	$a = 13.1358(3) \text{ \AA}$	$\alpha = 90^\circ$
	$b = 7.33560(10) \text{ \AA}$	$\beta = 103.668(7)^\circ$
	$c = 15.2031(10) \text{ \AA}$	$\gamma = 90^\circ$
Volume	1423.47(10) Å ³	
Z	4	
Density (calculated)	1.513 Mg / m ³	
Absorption coefficient	1.064 mm ⁻¹	
$F(000)$	672	
Crystal	Fragment; orange	
Crystal size	0.50 × 0.30 × 0.10 mm ³	
θ range for data collection	3.10 – 25.00°	
Index ranges	–15 ≤ h ≤ 15, –8 ≤ k ≤ 8, –18 ≤ l ≤ 17	
Reflections collected	6705	
Independent reflections	2463 [$R_{int} = 0.0160$]	
Completeness to $\theta = 25.00^\circ$	98.2 %	
Absorption correction	Semi-empirical from equivalents	
Max. and min. transmission	0.9010 and 0.6181	
Refinement method	Full-matrix least-squares on F^2	
Data / restraints / parameters	2463 / 3 / 196	
Goodness-of-fit on F^2	1.091	
Final R indices [$F^2 > 2\sigma(F^2)$]	$RI = 0.0223$, $wR2 = 0.0598$	
R indices (all data)	$RI = 0.0245$, $wR2 = 0.0610$	
Largest diff. peak and hole	0.245 and –0.257 e Å ⁻³	

Diffraction: Rigaku R-Axis Spider Diffractometer equipped with Rapid image plate detector (profile data from ω -scans) **Cell determination:** CrystalClear-SM Expert 2.0 r7 (Rigaku, 2011) **Data collection:** CrystalClear-SM Expert 2.0 r7 (Rigaku, 2011) **Data reduction and cell refinement:** CrystalClear-SM Expert 2.0 r7 (Rigaku, 2011) **Absorption correction:** CrystalClear-SM Expert 2.0 r7 (Rigaku, 2011) **Structure solution:** SHELXS97 (Sheldrick, G.M. (2008). Acta Cryst. A64, 112-122.) **Structure refinement:** SHELXL97 (G Sheldrick, G.M. (2008). Acta Cryst. A64, 112-122.).

Table 2. Atomic coordinates [$\times 10^4$], equivalent isotropic displacement parameters [$\text{\AA}^2 \times 10^3$] and site occupancy factors. U_{eq} is defined as one third of the trace of the orthogonalized U^{ij} tensor.

Atom	x	y	z	U_{eq}	$S.o.f.$
C1	1088(1)	4986(2)	-2805(1)	21(1)	1
C2	653(1)	6488(2)	-3296(1)	24(1)	1
C3	927(1)	8219(2)	-2963(1)	25(1)	1
C4	1628(1)	8405(2)	-2131(1)	25(1)	1
C5	2050(1)	6874(2)	-1657(1)	23(1)	1
C6	1973(1)	3268(2)	-805(1)	17(1)	1
C7	2509(1)	1643(2)	-327(1)	17(1)	1
C8	2179(1)	665(2)	368(1)	19(1)	1
C9	2923(1)	-735(2)	692(1)	22(1)	1
C10	3716(1)	-631(2)	192(1)	21(1)	1
C11	3462(1)	824(2)	-438(1)	19(1)	1
C12	3837(2)	4483(2)	1142(1)	28(1)	1
C13	3454(2)	3584(3)	1827(1)	29(1)	1
C14	4184(2)	2224(3)	2212(1)	28(1)	1
C15	5021(1)	2272(2)	1770(1)	26(1)	1
C16	4807(1)	3672(2)	1108(1)	26(1)	1
Fe1	3627(1)	1783(1)	851(1)	15(1)	1
N1	1778(1)	5203(2)	-2003(1)	18(1)	1
N2	2277(1)	3623(2)	-1563(1)	22(1)	1
O1	1305(1)	4122(2)	-494(1)	22(1)	1
O2	125(1)	2955(2)	727(1)	28(1)	1

Table 3. Bond lengths [\AA] and angles [$^\circ$].

C1-N1	1.346(2)
C1-C2	1.377(2)
C1-H1	0.9500
C2-C3	1.382(2)
C2-H2	0.9500
C3-C4	1.385(3)
C3-H3	0.9500
C4-C5	1.378(2)
C4-H4	0.9500
C5-N1	1.349(2)
C5-H5	0.9500
C6-O1	1.2578(19)
C6-N2	1.331(2)
C6-C7	1.485(2)
C7-C8	1.426(2)
C7-C11	1.435(2)

C7–Fe1	2.0324(16)
C8–C9	1.423(2)
C8–Fe1	2.0422(16)
C8–H8	0.9500
C9–C10	1.430(2)
C9–Fe1	2.0543(16)
C9–H9	0.9500
C10–C11	1.420(2)
C10–Fe1	2.0520(16)
C10–H10	0.9500
C11–Fe1	2.0447(16)
C11–H11	0.9500
C12–C16	1.418(3)
C12–C13	1.421(3)
C12–Fe1	2.0337(17)
C12–H12	0.9500
C13–C14	1.412(3)
C13–Fe1	2.0391(17)
C13–H13	0.9500
C14–C15	1.417(3)
C14–Fe1	2.0514(17)
C14–H14	0.9500
C15–C16	1.419(3)
C15–Fe1	2.0553(17)
C15–H15	0.9500
C16–Fe1	2.0464(17)
C16–H16	0.9500
N1–N2	1.4189(19)
O2–H1O	0.839(15)
O2–H2O	0.816(16)
N1–C1–C2	120.01(16)
N1–C1–H1	120.0
C2–C1–H1	120.0
C1–C2–C3	119.89(16)
C1–C2–H2	120.1
C3–C2–H2	120.1
C2–C3–C4	118.97(16)
C2–C3–H3	120.5
C4–C3–H3	120.5
C5–C4–C3	119.72(16)
C5–C4–H4	120.1
C3–C4–H4	120.1
N1–C5–C4	119.98(16)
N1–C5–H5	120.0
C4–C5–H5	120.0
O1–C6–N2	127.38(15)

O1-C6-C7	120.49(14)
N2-C6-C7	112.12(14)
C8-C7-C11	107.67(14)
C8-C7-C6	125.10(14)
C11-C7-C6	127.17(15)
C8-C7-Fe1	69.89(9)
C11-C7-Fe1	69.86(9)
C6-C7-Fe1	123.44(11)
C9-C8-C7	108.40(14)
C9-C8-Fe1	70.13(9)
C7-C8-Fe1	69.15(9)
C9-C8-H8	125.8
C7-C8-H8	125.8
Fe1-C8-H8	126.5
C8-C9-C10	107.70(14)
C8-C9-Fe1	69.21(9)
C10-C9-Fe1	69.54(9)
C8-C9-H9	126.2
C10-C9-H9	126.2
Fe1-C9-H9	126.7
C11-C10-C9	108.33(14)
C11-C10-Fe1	69.44(9)
C9-C10-Fe1	69.71(9)
C11-C10-H10	125.8
C9-C10-H10	125.8
Fe1-C10-H10	126.6
C10-C11-C7	107.90(14)
C10-C11-Fe1	69.99(9)
C7-C11-Fe1	68.94(9)
C10-C11-H11	126.0
C7-C11-H11	126.0
Fe1-C11-H11	126.6
C16-C12-C13	107.99(16)
C16-C12-Fe1	70.15(10)
C13-C12-Fe1	69.78(10)
C16-C12-H12	126.0
C13-C12-H12	126.0
Fe1-C12-H12	125.7
C14-C13-C12	107.97(16)
C14-C13-Fe1	70.28(10)
C12-C13-Fe1	69.37(10)
C14-C13-H13	126.0
C12-C13-H13	126.0
Fe1-C13-H13	125.9
C13-C14-C15	108.19(16)
C13-C14-Fe1	69.34(10)
C15-C14-Fe1	69.96(10)

C13–C14–H14	125.9
C15–C14–H14	125.9
Fe1–C14–H14	126.4
C14–C15–C16	107.99(16)
C14–C15–Fe1	69.66(10)
C16–C15–Fe1	69.42(10)
C14–C15–H15	126.0
C16–C15–H15	126.0
Fe1–C15–H15	126.5
C12–C16–C15	107.86(16)
C12–C16–Fe1	69.19(10)
C15–C16–Fe1	70.09(10)
C12–C16–H16	126.1
C15–C16–H16	126.1
Fe1–C16–H16	126.2
C7–Fe1–C12	105.90(7)
C7–Fe1–C13	119.49(7)
C12–Fe1–C13	40.85(8)
C7–Fe1–C8	40.96(6)
C12–Fe1–C8	122.45(7)
C13–Fe1–C8	105.51(7)
C7–Fe1–C11	41.20(6)
C12–Fe1–C11	121.45(7)
C13–Fe1–C11	156.27(7)
C8–Fe1–C11	68.80(6)
C7–Fe1–C16	124.04(7)
C12–Fe1–C16	40.66(8)
C13–Fe1–C16	68.41(8)
C8–Fe1–C16	160.00(7)
C11–Fe1–C16	108.65(7)
C7–Fe1–C10	68.81(6)
C12–Fe1–C10	157.86(7)
C13–Fe1–C10	160.67(8)
C8–Fe1–C10	68.49(6)
C11–Fe1–C10	40.56(7)
C16–Fe1–C10	123.34(7)
C7–Fe1–C14	155.23(7)
C12–Fe1–C14	68.25(7)
C13–Fe1–C14	40.39(8)
C8–Fe1–C14	120.39(7)
C11–Fe1–C14	162.34(7)
C16–Fe1–C14	68.11(7)
C10–Fe1–C14	125.51(7)
C7–Fe1–C9	68.86(7)
C12–Fe1–C9	159.30(7)
C13–Fe1–C9	122.93(7)
C8–Fe1–C9	40.66(6)

C11–Fe1–C9	68.62(7)
C16–Fe1–C9	158.54(7)
C10–Fe1–C9	40.75(7)
C14–Fe1–C9	107.65(7)
C7–Fe1–C15	161.84(7)
C12–Fe1–C15	68.22(7)
C13–Fe1–C15	68.08(8)
C8–Fe1–C15	156.76(7)
C11–Fe1–C15	125.97(7)
C16–Fe1–C15	40.49(7)
C10–Fe1–C15	109.78(7)
C14–Fe1–C15	40.38(8)
C9–Fe1–C15	122.71(7)
C1–N1–C5	121.42(15)
C1–N1–N2	117.91(14)
C5–N1–N2	120.49(13)
C6–N2–N1	111.61(13)
H1O–O2–H2O	106(2)

Symmetry transformations used to generate equivalent atoms:

Table 4. Anisotropic displacement parameters [$\text{\AA}^2 \times 10^3$]. The anisotropic displacement factor exponent takes the form: $-2\pi^2[h^2 a^{*2} U^{11} + \dots + 2 h k a^* b^* U^{12}]$.

Atom	U^{11}	U^{22}	U^{33}	U^{23}	U^{13}	U^{12}
C1	20(1)	26(1)	18(1)	-3(1)	6(1)	-2(1)
C2	21(1)	33(1)	17(1)	0(1)	2(1)	2(1)
C3	25(1)	28(1)	24(1)	6(1)	8(1)	4(1)
C4	29(1)	23(1)	26(1)	-2(1)	9(1)	-4(1)
C5	21(1)	29(1)	17(1)	-3(1)	3(1)	-4(1)
C6	12(1)	20(1)	16(1)	-4(1)	0(1)	-2(1)
C7	13(1)	19(1)	17(1)	-4(1)	2(1)	2(1)
C8	16(1)	17(1)	24(1)	-1(1)	6(1)	2(1)
C9	21(1)	14(1)	29(1)	1(1)	4(1)	1(1)
C10	17(1)	16(1)	28(1)	-7(1)	3(1)	4(1)
C11	16(1)	22(1)	19(1)	-8(1)	3(1)	1(1)
C12	40(1)	14(1)	25(1)	-5(1)	-4(1)	4(1)
C13	31(1)	30(1)	26(1)	-14(1)	7(1)	3(1)
C14	40(1)	28(1)	15(1)	-2(1)	2(1)	-2(1)
C15	24(1)	24(1)	26(1)	-4(1)	-5(1)	2(1)
C16	32(1)	24(1)	22(1)	-4(1)	4(1)	-8(1)
Fe1	17(1)	13(1)	15(1)	-1(1)	2(1)	4(1)

N1	16(1)	24(1)	15(1)	1(1)	6(1)	1(1)
N2	23(1)	24(1)	18(1)	4(1)	6(1)	8(1)
O1	19(1)	25(1)	24(1)	5(1)	9(1)	9(1)
O2	29(1)	28(1)	33(1)	12(1)	15(1)	12(1)

Table 5. Hydrogen coordinates [$\times 10^4$] and isotropic displacement parameters [$\text{\AA}^2 \times 10^3$].

Atom	<i>x</i>	<i>y</i>	<i>z</i>	<i>U</i> _{eq}	<i>S.o.f.</i>
H1	900	3795	-3033	25	1
H2	166	6336	-3862	29	1
H3	639	9264	-3300	30	1
H4	1818	9583	-1887	30	1
H5	2532	6995	-1086	27	1
H8	1566	907	578	23	1
H9	2898	-1585	1158	26	1
H10	4310	-1404	267	25	1
H11	3854	1191	-859	23	1
H12	3503	5456	772	34	1
H13	2819	3852	1996	35	1
H14	4125	1415	2686	34	1
H15	5619	1502	1895	32	1
H16	5237	4006	712	31	1
H1O	-384(15)	3680(30)	648(16)	42	1
H2O	481(16)	3290(30)	385(14)	42	1

Table 6. Hydrogen bonds [\AA and $^\circ$].

<i>D-H...A</i>	<i>d</i> (<i>D-H</i>)	<i>d</i> (<i>H...A</i>)	<i>d</i> (<i>D...A</i>)	\angle (<i>DHA</i>)
O2-H1O...O1 ⁱ	0.839(15)	1.998(17)	2.8171(16)	165(2)
O2-H2O...O1	0.816(16)	2.001(16)	2.8174(16)	178(2)

Symmetry transformations used to generate equivalent atoms:

(i) $-x, -y+1, -z$

Compound 8:

Table 1. Crystal data and structure refinement details.

Identification code	2012ncs0120 (MFB 190 F3)	
Empirical formula	C ₁₆ H ₁₄ N ₂ O ₂	
Formula weight	266.29	
Temperature	120(2) K	
Wavelength	0.71075 Å	
Crystal system	Monoclinic	
Space group	P21/n	
Unit cell dimensions	$a = 10.8895(2)$ Å	$\alpha = 90^\circ$
	$b = 7.7987(2)$ Å	$\beta = 103.124(7)^\circ$
	$c = 16.4558(11)$ Å	$\gamma = 90^\circ$
Volume	1360.99(10) Å ³	
Z	4	
Density (calculated)	1.300 Mg / m ³	
Absorption coefficient	0.087 mm ⁻¹	
$F(000)$	560	
Crystal	Prism; pale yellow	
Crystal size	0.70 × 0.60 × 0.40 mm ³	
θ range for data collection	3.24 – 27.48°	
Index ranges	-14 ≤ h ≤ 14, -10 ≤ k ≤ 10, -21 ≤ l ≤ 21	
Reflections collected	16991	
Independent reflections	3118 [$R_{int} = 0.0170$]	
Completeness to $\theta = 27.48^\circ$	99.8 %	
Absorption correction	Semi-empirical from equivalents	
Max. and min. transmission	0.9659 and 0.9414	
Refinement method	Full-matrix least-squares on F^2	
Data / restraints / parameters	3118 / 0 / 182	
Goodness-of-fit on F^2	1.053	
Final R indices [$F^2 > 2\sigma(F^2)$]	$RI = 0.0400$, $wR2 = 0.1064$	
R indices (all data)	$RI = 0.0424$, $wR2 = 0.1082$	
Largest diff. peak and hole	0.347 and -0.255 e Å ⁻³	

Diffraction: Rigaku R-Axis Spider Diffractometer equipped with Rapid image plate detector (profile data from ω -scans) **Cell determination:** CrystalClear-SM Expert 2.0 r7 (Rigaku, 2011) **Data collection:** CrystalClear-SM Expert 2.0 r7 (Rigaku, 2011) **Data reduction and cell refinement:** CrystalClear-SM Expert 2.0 r7 (Rigaku, 2011) **Absorption correction:** CrystalClear-SM Expert 2.0 r7 (Rigaku, 2011) **Structure solution:** SHELXS97 (Sheldrick, G.M. (2008). Acta Cryst. A64, 112-122.) **Structure refinement:** SHELXL97 (G Sheldrick, G.M. (2008). Acta Cryst. A64, 112-122.).

Table 2. Atomic coordinates [$\times 10^4$], equivalent isotropic displacement parameters [$\text{\AA}^2 \times 10^3$] and site occupancy factors. U_{eq} is defined as one third of the trace of the orthogonalized U^{ij} tensor.

Atom	x	y	z	U_{eq}	$S.o.f.$
C1	1862(1)	1397(2)	375(1)	27(1)	1
C2	2082(1)	535(2)	-315(1)	32(1)	1
C3	3120(1)	-540(2)	-224(1)	33(1)	1
C4	3927(1)	-771(2)	551(1)	32(1)	1
C5	3727(1)	111(2)	1244(1)	25(1)	1
C6	2693(1)	1207(2)	1155(1)	21(1)	1
C7	2418(1)	2169(2)	1872(1)	21(1)	1
C8	3479(1)	2382(1)	2656(1)	18(1)	1
C9	4042(1)	1884(2)	4152(1)	26(1)	1
C10	4733(1)	3942(1)	1978(1)	19(1)	1
C11	6029(1)	3951(1)	1812(1)	17(1)	1
C12	6219(1)	4822(1)	1108(1)	21(1)	1
C13	7404(1)	4835(2)	922(1)	24(1)	1
C14	8405(1)	3990(2)	1442(1)	25(1)	1
C15	8225(1)	3128(2)	2145(1)	24(1)	1
C16	7039(1)	3100(1)	2331(1)	20(1)	1
N1	3188(1)	1779(1)	3337(1)	21(1)	1
N2	4599(1)	3031(1)	2665(1)	20(1)	1
O1	1384(1)	2748(1)	1877(1)	31(1)	1
O2	3876(1)	4766(1)	1514(1)	25(1)	1

Table 3. Bond lengths [\AA] and angles [$^\circ$].

C1–C2	1.3865(18)
C1–C6	1.3995(15)
C1–H1	0.9500
C2–C3	1.388(2)
C2–H2	0.9500
C3–C4	1.388(2)
C3–H3	0.9500
C4–C5	1.3899(17)
C4–H4	0.9500
C5–C6	1.3940(16)
C5–H5	0.9500
C6–C7	1.4849(16)
C7–O1	1.2149(14)
C7–C8	1.5329(15)
C8–N2	1.3175(14)
C8–N1	1.3188(14)
C9–N1	1.4510(14)

C9-H9A	0.9800
C9-H9B	0.9800
C9-H9C	0.9800
C10-O2	1.2419(14)
C10-N2	1.3707(14)
C10-C11	1.4970(14)
C11-C12	1.3982(15)
C11-C16	1.3982(15)
C12-C13	1.3912(16)
C12-H12	0.9500
C13-C14	1.3893(17)
C13-H13	0.9500
C14-C15	1.3902(17)
C14-H14	0.9500
C15-C16	1.3934(15)
C15-H15	0.9500
C16-H16	0.9500
N1-H1A	0.8800

C2-C1-C6	120.23(12)
C2-C1-H1	119.9
C6-C1-H1	119.9
C1-C2-C3	119.51(12)
C1-C2-H2	120.2
C3-C2-H2	120.2
C2-C3-C4	120.51(12)
C2-C3-H3	119.7
C4-C3-H3	119.7
C3-C4-C5	120.33(12)
C3-C4-H4	119.8
C5-C4-H4	119.8
C4-C5-C6	119.38(11)
C4-C5-H5	120.3
C6-C5-H5	120.3
C5-C6-C1	119.98(11)
C5-C6-C7	122.01(10)
C1-C6-C7	118.00(10)
O1-C7-C6	123.24(10)
O1-C7-C8	118.40(10)
C6-C7-C8	118.31(9)
N2-C8-N1	121.84(10)
N2-C8-C7	124.74(10)
N1-C8-C7	113.36(9)
N1-C9-H9A	109.5
N1-C9-H9B	109.5
H9A-C9-H9B	109.5
N1-C9-H9C	109.5

H9A–C9–H9C	109.5
H9B–C9–H9C	109.5
O2–C10–N2	124.70(10)
O2–C10–C11	119.54(10)
N2–C10–C11	115.74(9)
C12–C11–C16	119.54(10)
C12–C11–C10	118.47(10)
C16–C11–C10	121.98(10)
C13–C12–C11	120.32(10)
C13–C12–H12	119.8
C11–C12–H12	119.8
C14–C13–C12	119.89(11)
C14–C13–H13	120.1
C12–C13–H13	120.1
C13–C14–C15	120.16(10)
C13–C14–H14	119.9
C15–C14–H14	119.9
C14–C15–C16	120.24(10)
C14–C15–H15	119.9
C16–C15–H15	119.9
C15–C16–C11	119.85(10)
C15–C16–H16	120.1
C11–C16–H16	120.1
C8–N1–C9	122.59(9)
C8–N1–H1A	118.7
C9–N1–H1A	118.7
C8–N2–C10	117.47(9)

Symmetry transformations used to generate equivalent atoms:

Table 4. Anisotropic displacement parameters [$\text{\AA}^2 \times 10^3$]. The anisotropic displacement factor exponent takes the form: $-2\pi^2[h^2 a^{*2} U^{11} + \dots + 2 h k a^* b^* U^{12}]$.

Atom	U^{11}	U^{22}	U^{33}	U^{23}	U^{13}	U^{12}
C1	27(1)	28(1)	23(1)	2(1)	0(1)	-1(1)
C2	40(1)	34(1)	20(1)	-2(1)	2(1)	-9(1)
C3	45(1)	29(1)	28(1)	-10(1)	16(1)	-10(1)
C4	34(1)	24(1)	38(1)	-6(1)	12(1)	1(1)
C5	25(1)	23(1)	25(1)	0(1)	4(1)	1(1)
C6	21(1)	21(1)	20(1)	1(1)	3(1)	-3(1)
C7	17(1)	23(1)	22(1)	1(1)	3(1)	0(1)
C8	16(1)	20(1)	20(1)	-2(1)	5(1)	2(1)

C9	23(1)	39(1)	18(1)	0(1)	5(1)	-2(1)
C10	17(1)	19(1)	20(1)	-3(1)	5(1)	0(1)
C11	16(1)	16(1)	20(1)	-2(1)	5(1)	0(1)
C12	22(1)	19(1)	22(1)	2(1)	6(1)	3(1)
C13	29(1)	22(1)	27(1)	3(1)	14(1)	-1(1)
C14	19(1)	24(1)	36(1)	0(1)	13(1)	-2(1)
C15	17(1)	23(1)	31(1)	2(1)	3(1)	1(1)
C16	19(1)	21(1)	21(1)	2(1)	4(1)	-1(1)
N1	16(1)	27(1)	20(1)	-1(1)	5(1)	-4(1)
N2	16(1)	24(1)	20(1)	-1(1)	6(1)	-2(1)
O1	18(1)	44(1)	31(1)	-3(1)	4(1)	6(1)
O2	19(1)	29(1)	28(1)	5(1)	7(1)	7(1)

Table 5. Hydrogen coordinates [$\times 10^4$] and isotropic displacement parameters [$\text{\AA}^2 \times 10^3$].

Atom	<i>x</i>	<i>y</i>	<i>z</i>	<i>U_{eq}</i>	<i>S.o.f.</i>
H1	1145	2118	319	32	1
H2	1527	681	-846	39	1
H3	3278	-1124	-697	39	1
H4	4621	-1536	609	38	1
H5	4288	-32	1773	30	1
H9A	4886	1512	4111	40	1
H9B	3737	1140	4544	40	1
H9C	4081	3071	4352	40	1
H12	5537	5408	755	25	1
H13	7527	5421	441	29	1
H14	9214	4002	1316	30	1
H15	8913	2557	2500	29	1
H16	6917	2503	2810	24	1
H1A	2447	1294	3295	25	1

➤ HPLC

Central chiral Thiourea 19a:

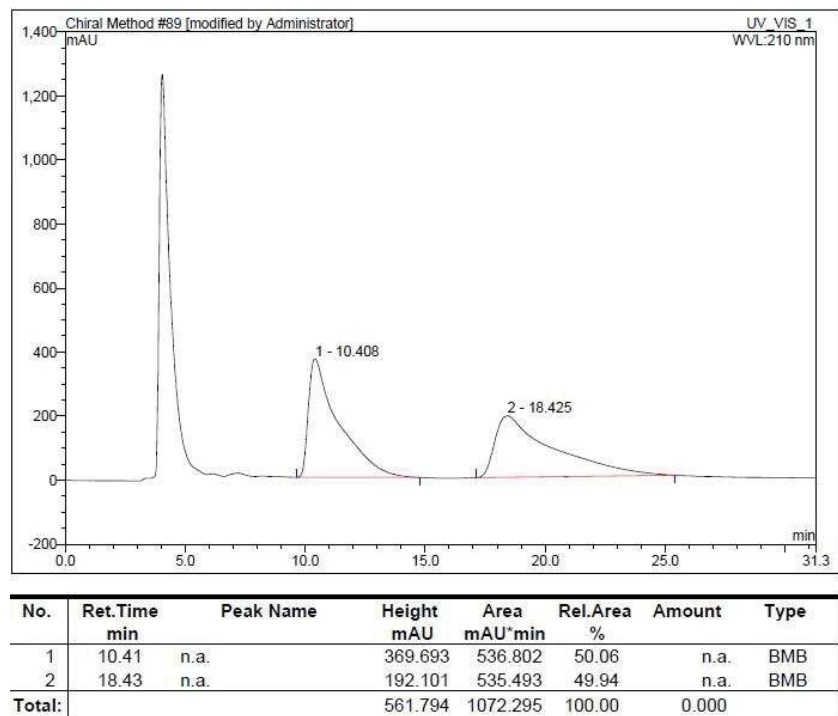


Figure 58 : Chiral HPLC of *rac*-19a. AD column, 5% IPA in hexane, 1 mL.min⁻¹, monitored at 210 nm

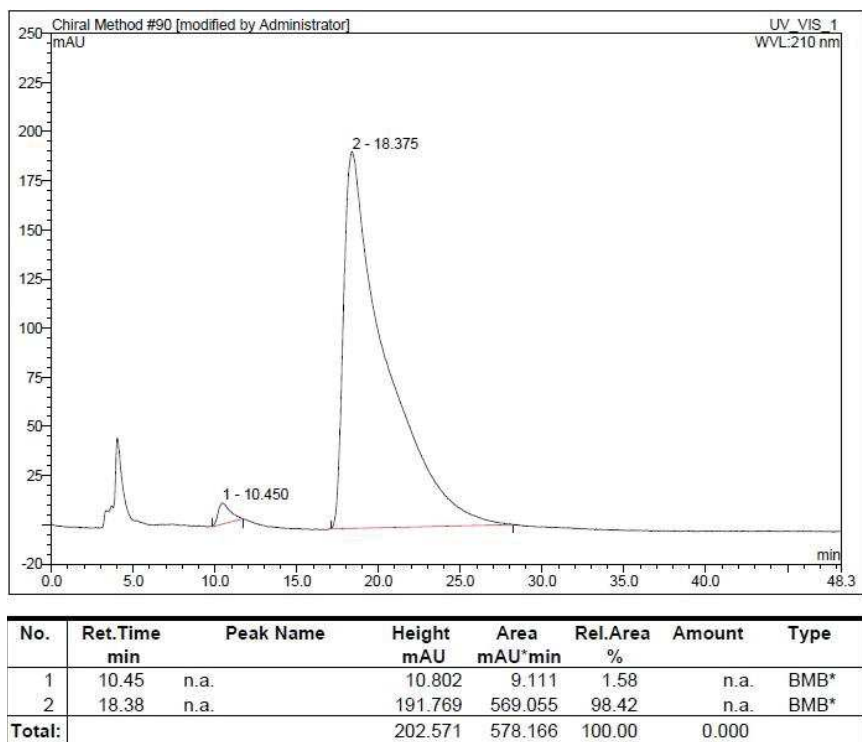


Figure 59: Chiral HPLC of (*S*)-19a. AD column, 5% IPA in hexane, 1 mL.min⁻¹, monitored at 210 nm

Central Chiral thiourea 19b:

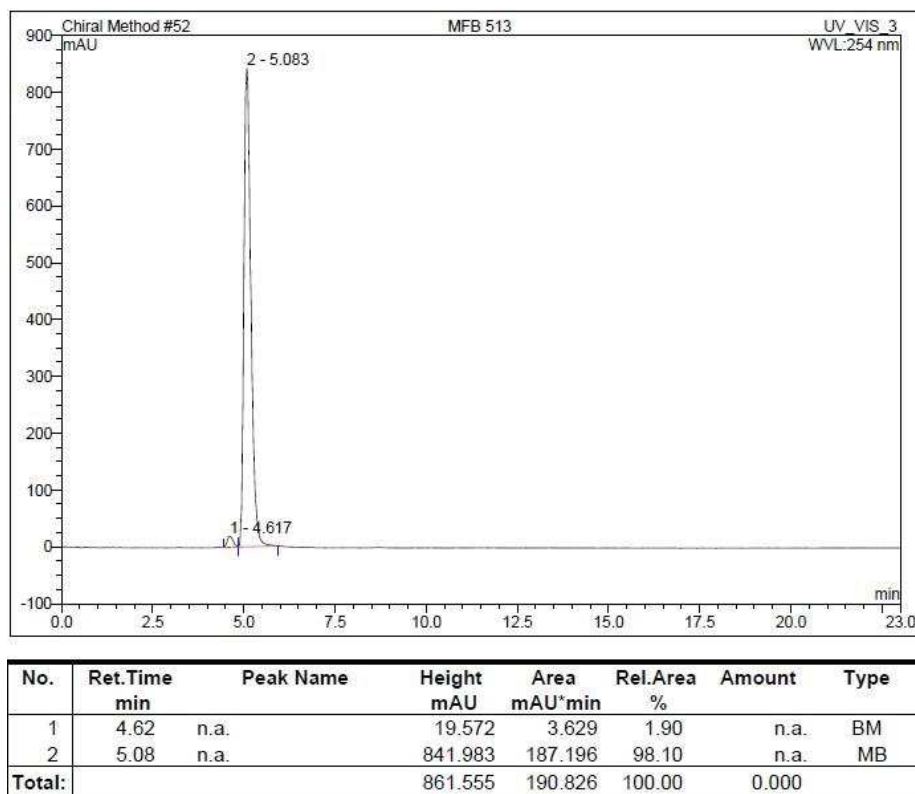


Figure 60: Chiral HPLC of (*R*)-**19b**. OD column, 10% IPA in hexane, 1 mL.min⁻¹, monitored at 254 nm

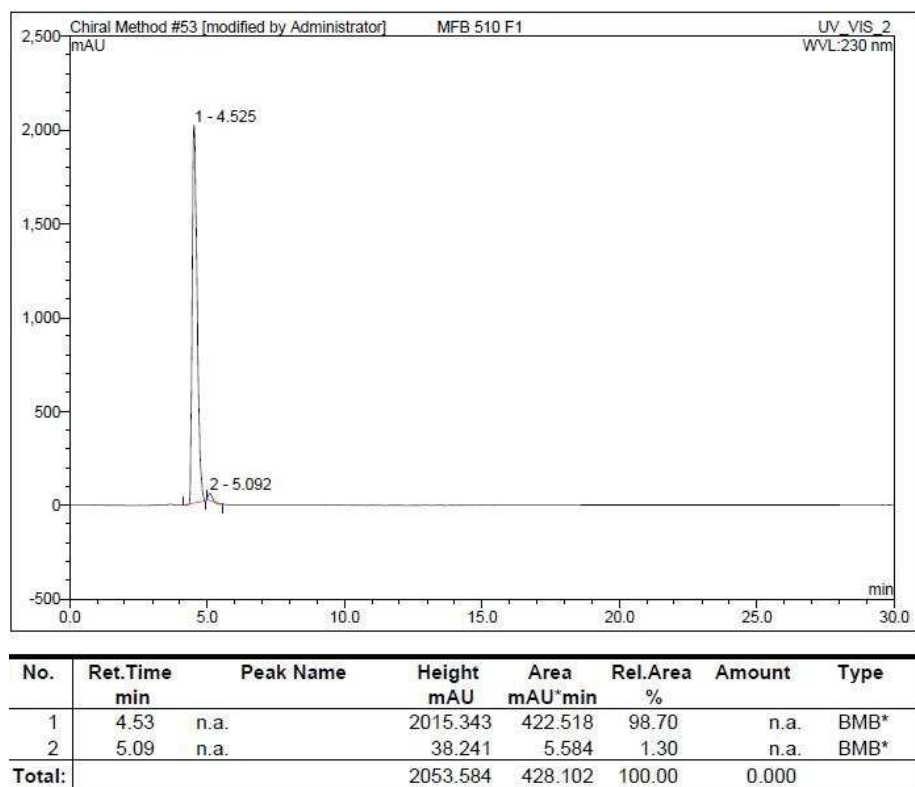


Figure 61: Chiral HPLC of (*S*)-**19b**. OD column, 10% IPA in hexane, 1 mL.min⁻¹, monitored at 230 nm

Planar chiral thiourea 20:

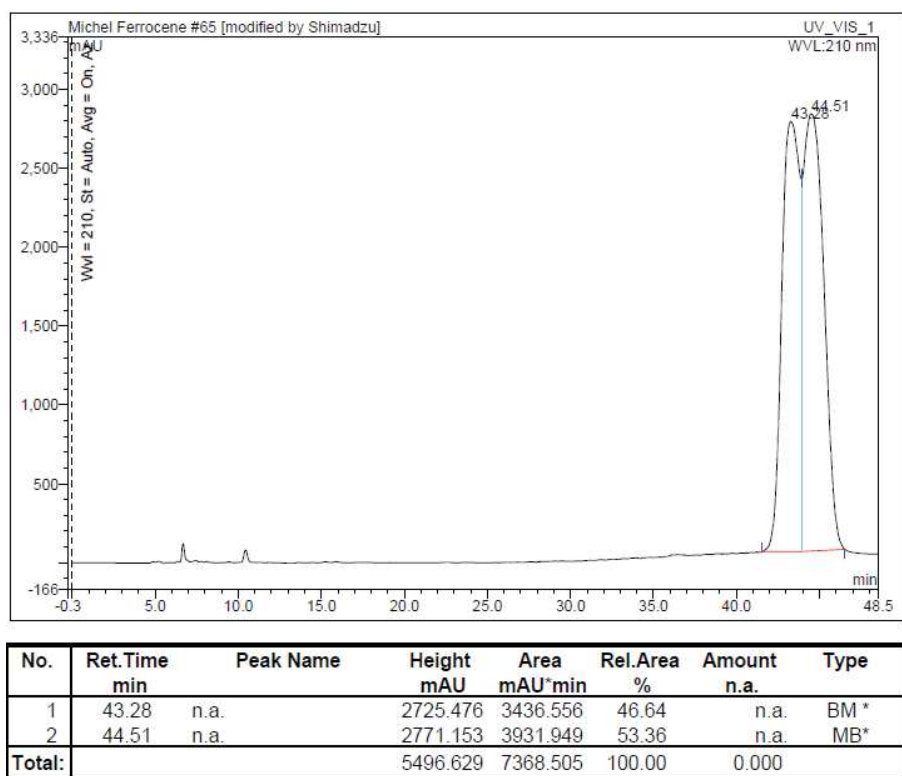


Figure 62 : Chiral HPLC of *rac*-20. Amylose 2 column, 50% MeCN in water, 1 mL.min⁻¹, monitored at 210 nm

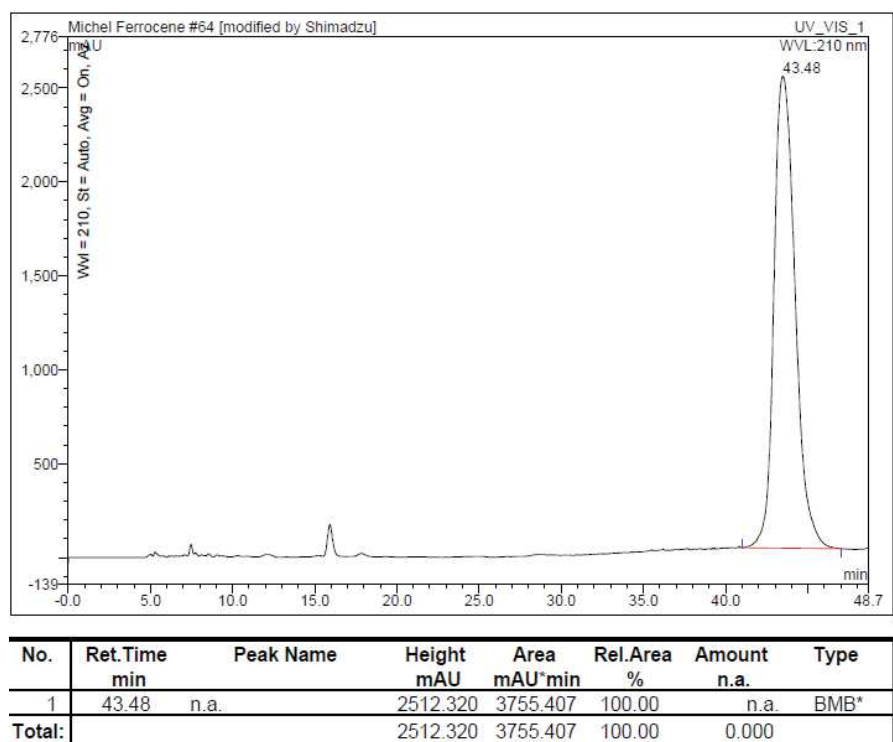


Figure 63: Chiral HPLC of (*R*)-20. Amylose 2 column, 50% MeCN in water, 1 mL.min⁻¹, monitored at 210 nm

Bi-functional Thiourea 21:

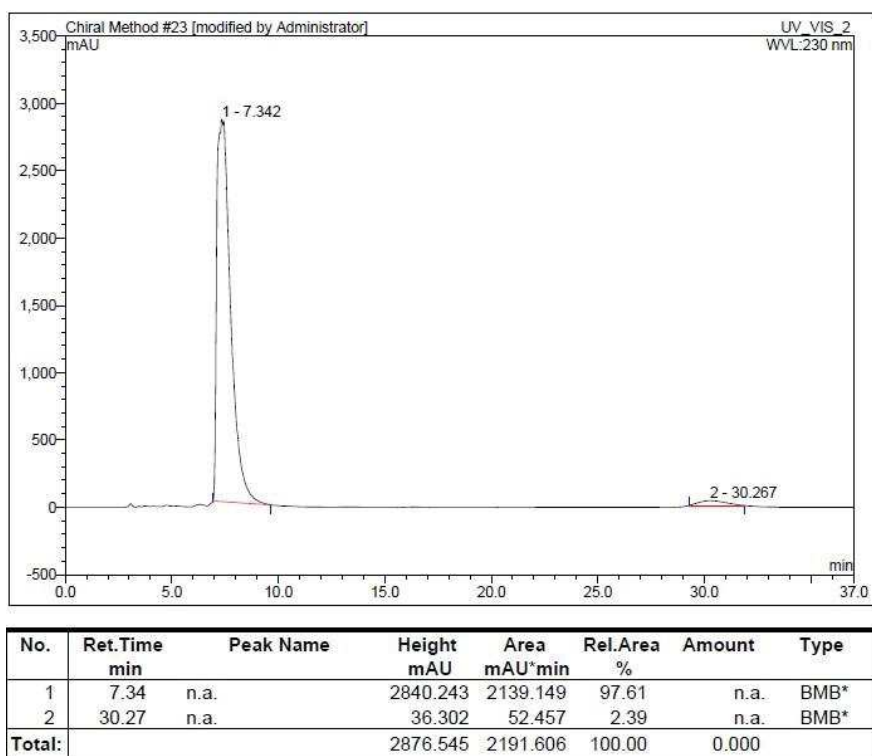


Figure 64: Chiral HPLC of (*R,Rp*)-21. OD column, 15% IPA in hexane, 1 mL.min⁻¹, monitored at 230 nm

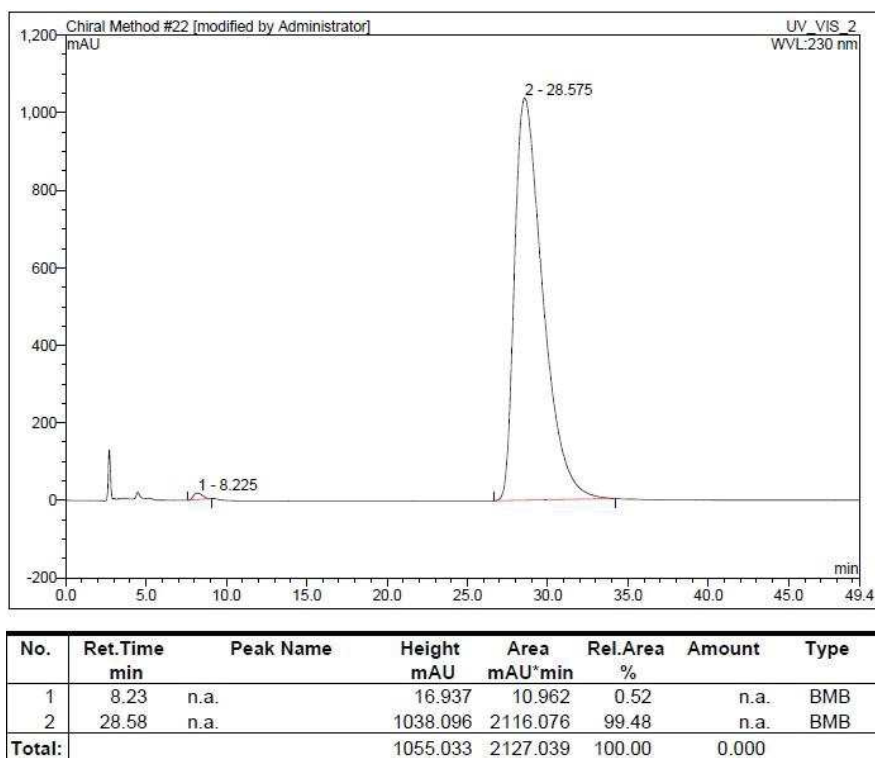


Figure 65: Chiral HPLC of (*S,Sp*)-21. OD column, 15% IPA in hexane, 1 mL.min⁻¹, monitored at 230 nm